



UNIVERSITEIT VAN PRETORIA  
UNIVERSITY OF PRETORIA  
YUNIBESITHI YA PRETORIA

**INVESTIGATING THE LIMITATIONS OF THE  
DISCHARGE-HEAD RELATIONSHIP OF  
COMPOUND CRUMP WEIRS EXCEEDING THEIR  
HYDRAULIC CAPACITIES**

**ASHLEY AMY MARITZ**

**A dissertation submitted in partial fulfilment of the requirements for the degree of  
MASTER OF ENGINEERING (WATER RESOURCES ENGINEERING)**

**In the**

**FACULTY OF ENGINEERING**

**UNIVERSITY OF PRETORIA**

**January 2020**

# DISSERTATION SUMMARY

## INVESTIGATING THE LIMITATIONS OF THE DISCHARGE-HEAD RELATIONSHIP OF COMPOUND CRUMP WEIRS EXCEEDING THEIR HYDRAULIC CAPACITIES

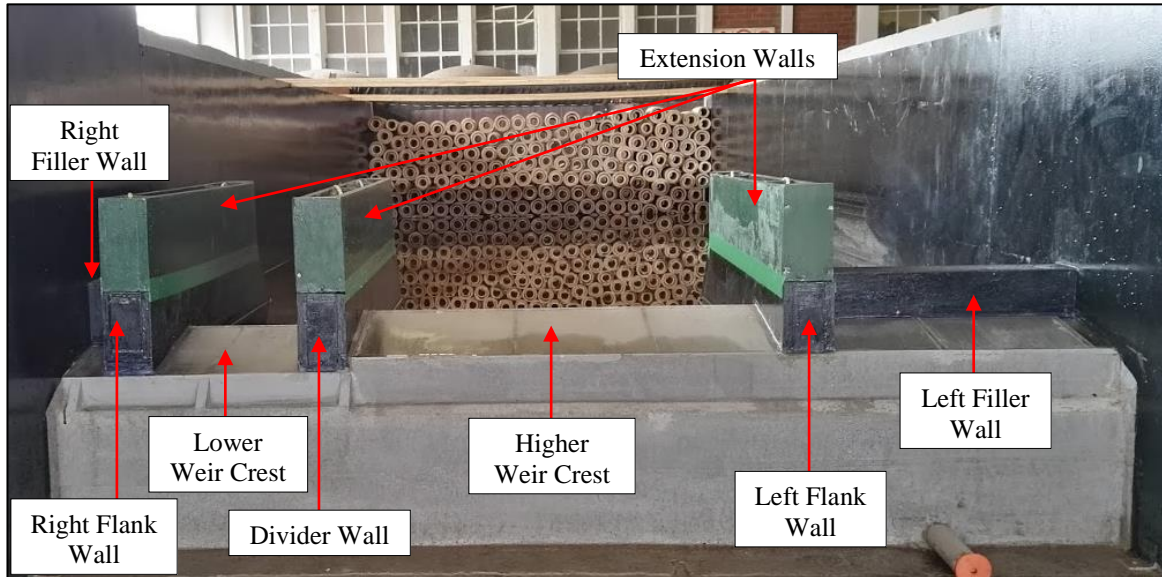
**ASHLEY AMY MARITZ**

<b>Supervisor:</b>	Professor S.J. van Vuuren
<b>Co-Supervisor:</b>	Doctor P. Wessels
<b>Department:</b>	Civil Engineering
<b>University:</b>	University of Pretoria
<b>Degree:</b>	Master of Engineering (Water Resources Engineering)

The implementation of compound weirs, in South Africa, is necessary owing to the abrupt and substantial changes in flow conditions experienced within rivers. The current discharge-head relationships, used for the calculation of flow rates over weirs, were developed with the assumption of parallel flow lines. The BSI ISO 14139 (British Standards Institution, 2000) requires the use of divider walls in the design of compound weirs, in order to ensure parallel flow. However, for flow rates that moderately exceed the hydraulic capacity of these weirs, three-dimensional flow lines are induced as a result of the divider walls disturbing the flow lines. Therefore, measuring flow rates within this flow regime is beyond the scope of the current, available discharge-head relationships. The measuring of these increased flow rates is of utmost importance for the efficient management of water resources and the design of infrastructure.

The study presented in this dissertation aims at investigating the limitations of the discharge-head relationship of compound Crump weirs during flow rates that moderately exceed the hydraulic capacity. A physical model of a compound Crump weir was built at the Department of Water and Sanitation (DWS) hydraulic laboratories and is shown below in **Figure 1**. The model consists of two Crump weir crests at different levels with a divider wall separating the crests and flank walls built on the outside of the two crests which are then connected to the channel walls using filler walls. When the flow rate over the model exceeds the hydraulic capacity, the divider and flank walls are overtopped. The flow over these flank walls can be calculated using the broad-crested weir

relationship due to their rectangular shape. The scope of the study does not include the improvement of the broad-crested weir discharge coefficient relationships and for consistency, the DWS discharge coefficient equations were used to quantify the portion of flow over the filler walls when the hydraulic capacity is exceeded.

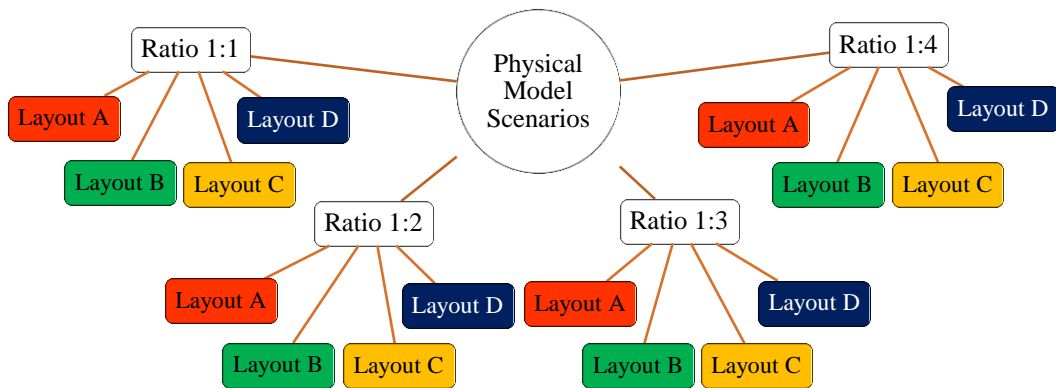


**Figure 1: The physical model of a compound Crump weir used in the study**

During the model study, the width of the lower Crump crest ( $B_L$ ) was kept constant while the width of the higher Crump crest ( $B_H$ ) was varied in order to model different  $B_H:B_L$  ratios. Four lower to higher Crump width ratios (1:4, 1:3, 1:2 and 1:1) were considered. The design head ( $H_d$ ) of the model was kept constant throughout the study, during higher flows, this design head was exceeded, resulting in the overtopping of the filler walls and cross-flow over the divider and flank walls. The extension walls indicated in green were used to prevent cross-flow over the divider and flank walls. They were then systematically removed with the anticipation of quantifying the influences of each component on the observed water levels. The model can thus be divided into four layouts, namely Layout A (with all of the extension walls present), Layout B (with the centre extension wall removed), Layout C (with the centre and left extension walls removed) and Layout D (with no extension walls). The physical model study thus included a total of 16 scenarios as shown in **Figure 2**.

Water level measurements upstream of the higher and lower Crump weir crests and the two filler walls were observed and used to calculate the flow over each component using the current discharge-head relationships. The total flow ( $Q_{\text{calculated}}$ ) was then taken as the sum of the calculated individual flow rates over each weir segment. The total flow ( $Q_{\text{calculated}}$ ) was then compared to the model input flow rate ( $Q_{\text{input}}$ ) in order to determine the accuracy of the current discharge-head relationships when the structure operates above the hydraulic capacity. Due to the complex nature of the flow over the

divider walls, they were not calculated for the total flow estimation but were rather considered to be part of the error induced due to operating above hydraulic capacity.



**Figure 2: The physical model scenarios**

The results indicated that the calculated flow rates were greater than the modelled input flow rates ( $Q_{\text{calculated}} > Q_{\text{input}}$ ). The largest difference was observed for lower to higher Crump width ratio 1:4 and gradually decreased from ratio 1:3 to ratio 1:1. The decrease in the difference between the modelled and calculated flow rates could be attributed to any combination of the following: the increasing length of the left filler wall functioning as a more prominent overflow structure during increased flow rates; and/or the reduction in the effective flow areas between divider walls whereby more flow is diverted over the structure and not between the divider and flank walls; and/or the potential influence of the exaggerated divider and flank wall widths in the model study. The systematic removal of the extension walls, used to simulate the increased capacity of the structure, indicated a reduction in the difference between the modelled and calculated flow rates which could indicate that the effective flow area is altered.

Furthermore, a numerical model study was performed to determine its use in calibration of weirs beyond hydraulic capacity. A three-dimensional model of the as-built physical model was made with computer-aided drawing (CAD) software, AutoCAD 2016 and imported into the modelling continua of the Computational Fluid Dynamics (CFD) software, STAR-CCM+ v.11.04. In contrast to the physical model results, the numerical model analyses under-estimated the calculated flow rate when using the same calculation procedure. Detailed investigation of the numerical model indicated that the flow lines in the body of water upstream of the structure appeared to be uniform with nominal cross-flow and minimal disturbances displayed at the surface interface in the vicinity of the flank and divider walls. This was also in contrast to what was observed during physical modelling. With the limited time and resources available for the investigation, no further attempts could be made to improve the comparability with the physical model. It is recommended that investigations using CFD are continued in order to improve the flow-gauging network.

## ABSTRACT

**Title:** Investigating the limitations of the discharge-head relationship of compound Crump weirs exceeding their hydraulic capacities

**Author:** A.A. Maritz

**Supervisor:** Professor S.J. van Vuuren

**Co-Supervisor:** Doctor P. Wessels

**Department:** Civil Engineering

**University:** University of Pretoria

**Degree:** Master of Engineering (Water Resources Engineering)

The variability of the South African (SA) climate results in abrupt changes in river discharge rates. Compound weirs have been implemented as an attempt to ensure accurate discharge calculations over an extended, but limited, range of flows. It would be financially and practically impossible to design compound weirs that can measure the entire range of flow rates that are experienced in SA rivers to the same degree of accuracy. Extensive research on the accuracy of weirs, within their intended hydraulic capacity, has been done over the years. However, when weirs operate above this capacity, three-dimensional flow is observed as a result of the presence of the divider and flank walls. The observed three-dimensional flow causes uncertainty in the application of the current discharge-head relationships, as these relationships were developed with the assumption of parallel flow lines. In this dissertation, a physical model study was done at the Department of Water and Sanitation hydraulic laboratories. The results indicated that the flow rates, calculated using the current discharge-head relationships, consistently over-estimates the input flow rates.

Additionally, a numerical model study using Computational Fluid Dynamics (CFD) software STAR-CCM+ was done. CFD proved to be a valuable tool for extending the domain of the study. A comparison of the physical model and numerical model results is shown with some comments on shortcomings identified in the user-defined volume mesh inputs that could not be addressed in this study due to time and resource limitations.

## DECLARATION

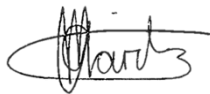
I, the undersigned with this declare that:

- I understand what plagiarism is and I am aware of the University's policy in this regard;
- the work contained in this dissertation is my original work;
- I did not refer to the work of current or previous students, lecture notes, handbooks or any other study material without proper referencing;
- where other people's work has been used this has been adequately acknowledged and referenced;
- I have not allowed anyone to copy any part of my dissertation;
- I have not previously in its entirety, or part submitted this dissertation at any university for a degree.

### DISCLAIMER:

The work presented in this report is that of the student alone. Students were encouraged to take ownership of their projects and to develop and execute their experiments with limited guidance and assistance. The content of the research does not necessarily represent the views of the supervisor or any staff member of the University of Pretoria, Department of Civil Engineering. The supervisor did not read or edit the final report and is not responsible for any technical inaccuracies, statements or errors. The conclusions and recommendations given in the report are also not necessarily that of the supervisor, sponsors or companies involved in the research.

**Signature of student:**



**Name of student:**

Ashley Amy Maritz

**Student number:**

10690515

**Date:**

30 January 2020

**Number of words in report:** 35 044 words

On average, one tree can be used to make 8 333.3 sheets of paper, thus printing this document uses 1.7 % of a tree. Be wise, recycle where possible.

## ACKNOWLEDGEMENTS

I gratefully acknowledge the admirable work done by the Department of Water and Sanitation (DWS) Career Management division in providing graduates (like me) with opportunities, resources, mentorship and encouragement to pursue their career goals for the uplifting of our country.

I want to express my appreciation for my supervisor, Prof S. J. van Vuuren for his patience and support throughout this study. His ongoing pursuit of academic excellence and caring nature has been of unmeasurable value for the study as well as my personal development. Furthermore, I am indebted to my co-supervisor, Dr P. Wessels who has worked assiduously to ensure the success of this study. His unprejudiced approach to mentorship and passion for education in engineering has taught me more than I can credit here.

Also, I wish to acknowledge Christiaan de Wet (Aerotherm), Charles Crosby (Centre of High Performance Computing) and Louis Coetzee for their assistance with the numerical modelling performed in this study. I would also like to thank Pieter Mynhardt, Vhahangwele Phophi and the DWS hydraulic laboratory staff for assisting with the physical model testing. Moreover, I gratefully acknowledge Louis Coetzee for the proofreading of this dissertation.

Lastly, I would like to thank my family for always believing in me and for devotedly listening to my presentations even though it was gibberish to them.

To God be all the glory.

## TABLE OF CONTENTS

TABLE OF CONTENTS .....	viii
LIST OF TABLES.....	x
LIST OF FIGURES .....	xi
LIST OF SYMBOLS .....	xiv
LIST OF ABBREVIATIONS.....	xvii
GLOSSARY .....	xviii
1 INTRODUCTION .....	1-1
1.1 Background.....	1-1
1.2 Motivation for study .....	1-6
1.3 Hypothesis and objectives of study .....	1-9
1.4 Scope of the study.....	1-10
1.5 Methodology of study.....	1-10
1.6 Organisation of the report.....	1-11
2 LITERATURE REVIEW.....	2-1
2.1 Introduction .....	2-1
2.2 Brief history of flow measuring in South Africa .....	2-3
2.3 Impacts of inaccurate flow measurements.....	2-5
2.4 Hydraulics of weirs.....	2-7
2.4.1 Basic flow equations.....	2-7
2.4.2 Discharge equation development.....	2-9
2.4.3 Froude number.....	2-10
2.4.4 Crump weirs .....	2-10
2.4.5 Compound weirs.....	2-13
2.4.6 Broad-crested weirs .....	2-15
2.4.7 Errors associated with compounded weirs.....	2-19
2.4.8 Minimum requirements for calibration.....	2-22
2.5 Theory of physical modelling .....	2-23
2.6 Computational fluid dynamics.....	2-25
2.6.1 Introduction .....	2-25
2.6.2 Modelling of multi-phase flows.....	2-26
2.6.3 Volume of Fluid (VOF) model .....	2-28
2.6.4 Overview of STAR-CCM+.....	2-29
2.6.5 Closing.....	2-34



3	EXPERIMENTAL WORK.....	3-1
3.1	Introduction .....	3-1
3.2	Model design and dimensions .....	3-2
3.3	Experimental procedure.....	3-8
3.4	STAR-CCM+ set-up.....	3-13
3.4.1	Generating model geometry .....	3-15
3.4.2	Selecting physics models, fluid properties and method for solving turbulence equations ...	3-16
3.4.3	Meshing of the flow domain.....	3-17
3.4.4	Set-up of necessary plots and monitors .....	3-18
3.4.5	Preparation of model for CHPC interaction .....	3-20
4	PRESENTATION AND DISCUSSION OF RESULTS .....	4-1
4.1	Presentation of physical model results.....	4-1
4.1.1	Physical model results for ratio 1:4 .....	4-3
4.1.2	Physical model results for ratio 1:3 .....	4-5
4.1.3	Physical model results for ratio 1:2 .....	4-7
4.1.4	Physical model results for ratio 1:1 .....	4-9
4.2	Discussion of physical model results.....	4-10
4.2.1	Overestimation of all layouts.....	4-11
4.2.2	Effect of cross-flow over the divider and flank walls.....	4-26
4.2.3	Effect of changing the lower to higher-Crump width ratio.....	4-28
4.3	Correction of errors seen in results .....	4-31
4.3.1	The implication of an additional error .....	4-31
4.3.2	Partial correction of overestimation error.....	4-33
4.3.3	Correction of error due to overtopping .....	4-35
4.4	Discussion of numerical model results .....	4-36
5	CONCLUSIONS AND RECOMMENDATIONS .....	5-1
5.1	Conclusions .....	5-1
5.2	Recommendations.....	5-3
6	REFERENCES.....	6-1

APPENDIX A

APPENDIX B

## LIST OF TABLES

Table 2.1: Percentage error made in discharge per unit crest length for an 18 mm overestimation in water level reading (Wessels, 1996) .....	2-6
Table 2.2: The various discharge coefficient calculation methods for broad-crested weirs .....	2-18
Table 2.3: Errors induced by compounding weirs .....	2-20
Table 2.4: Minimum requirements for the calibration of compound Crump weirs .....	2-23
Table 2.5: Summary of model laws in conformance of the similarity laws .....	2-25
Table 3.1: Dimensions of the physical model.....	3-4
Table 3.2: Thermo-physical properties of the water phase.....	3-16
Table 4.1: Physical model results for lower to higher Crump width ratio of 1:4 .....	4-3
Table 4.2: Physical model results for lower to higher Crump width ratio of 1:3 .....	4-5
Table 4.3: Physical model results for lower to higher Crump width ratio of 1:2 .....	4-7
Table 4.4: Physical model results for lower to higher Crump width ratio of 1:1 .....	4-9
Table 4.5: Photographs of flow lines observed as a result of eddy formation around the upstream ends of the extension walls for Layout A, B and C of Ratio 1:1 .....	4-27
Table 4.6: Comparing the error in calculated flow rates using a single-crest stage measurement with those using multi-crest stage measurements .....	4-32
Table 4.7: Water level adjustment values for the correction of contraction for Ratios 1:4, 1:3, 1:2 and 1:1 .....	4-34
Table 4.8: Water level adjustment values for the correction of overtopping for Ratios 1:4, 1:3, 1:2 and 1:1 .....	4-35
Table 4.9: Mesh cell count for the various flow rates modelled.....	4-36
Table 4.10: Visual comparison of the physical and numerical model .....	4-39

## LIST OF FIGURES

Figure 1: The physical model of a compound Crump weir used in the study .....	iii
Figure 2: The physical model scenarios .....	iv
Figure 1.1: Profile of a typical Crump weir (Maritz et al., 2015).....	1-1
Figure 1.2: Examples of compound Crump weirs in the field .....	1-2
Figure 1.3: Flooding of the Komati Weir in the Komatipoort River in the year 2000 .....	1-3
Figure 1.4: Upgraded Komati Weir in the Komatipoort River after the 2000 flood event.....	1-4
Figure 1.5: Determining design capacity for the Komati Weir using the percentage time occurrence criteria compared to using the percentage volume contribution criteria.....	1-5
Figure 1.6: Four operating phases of the Oranje Draai Weir, Orange River .....	1-7
Figure 1.7: Rating curve for the Oranje Draai Weir, Orange River.....	1-8
Figure 1.8: Definition sketch of 2014 UP model study (Maritz et al., 2015) .....	1-9
Figure 2.1: Chapter overview .....	2-1
Figure 2.2: Mean flow rate over the hydrological year for the entire record at station A2H012 in the Krokodil River at Kalkheuwel.....	2-2
Figure 2.3: Types of weirs in South African rivers (Wessels & Rooseboom, 2009 (a)) .....	2-3
Figure 2.4: Number of operational gauging stations in SA by weir type for 2018.....	2-5
Figure 2.5: Relative reservoir size required to meet a yield of 50, 60, 70 and 80% of the MAR (Wessels, 1996).....	2-7
Figure 2.6: Truncated Crump weir with dimensions .....	2-11
Figure 2.7: Definition sketch of the Crump weir profile under modular flow conditions .....	2-12
Figure 2.8: Definition sketch for Crump weir during non-modular conditions.....	2-13
Figure 2.9: Flow lines over compound weirs (A) without and (B) with divider walls .....	2-14
Figure 2.10: Definition sketch of a broad-crested weir with an isometric view of the weir showing the Crump crest in relation to the flak and filler walls .....	2-14
Figure 2.11: Discharge coefficients for broad-crested weirs resulting from various investigations before 1957 (Tracey, 1957; Govinda Rao & Muralidhar, 1963) .....	2-15
Figure 2.12: Discharge coefficients for broad-crested weirs using the upstream water level (h) versus the upstream energy level (H) (Tracey, 1957; Govinda Rao & Muralidhar, 1963).....	2-17
Figure 2.13: Definition sketch for correction factors of compound Crump weirs with divider walls (Wessels & Rooseboom, 2009 (b)).....	2-20
Figure 2.14: Definition sketch for correction factors of compound Crump weirs without divider walls (Wessels & Rooseboom, 2009 (b)).....	2-21
Figure 2.15: Divider wall dimension requirements .....	2-22
Figure 2.16: Two-phase flow examples applicable to hydraulic engineering .....	2-27
Figure 2.17: Definition sketch for the $y+$ wall treatment.....	2-31

Figure 2.18: Prism layer meshing of Crump weir boundary .....	2-31
Figure 2.19: Normalised Variable Diagram (NVD) (STAR-CCM+, 2017).....	2-32
Figure 3.1: Allocated model space for the University of Pretoria .....	3-2
Figure 3.2: Physical model components .....	3-3
Figure 3.3: The four layouts being modelled.....	3-3
Figure 3.4: Photos of physical model layout .....	3-5
Figure 3.5: Physical model dimensions .....	3-6
Figure 3.6: Design of removable extension walls.....	3-7
Figure 3.7: Photograph of stilling well and point gauge.....	3-8
Figure 3.8: Calibration weir at DWS hydraulic laboratory.....	3-8
Figure 3.9: Calibration of the magnetic flow meter.....	3-9
Figure 3.10: Flow chart of the experimental procedure followed.....	3-10
Figure 3.11: Photographs of the physical model layouts for lower to higher Crump width ratio 1:4 operating at the DWS hydraulic laboratories.....	3-11
Figure 3.12: Photographs of the physical model layouts for lower to higher Crump width ratio 1:3 operating at the DWS hydraulic laboratories.....	3-12
Figure 3.13: Photographs of the physical model layouts for lower to higher Crump width ratio 1:2 operating at the DWS hydraulic laboratories.....	3-12
Figure 3.14: Photographs of the physical model layouts for lower to higher Crump width ratio 1:1 operating at the DWS hydraulic laboratories.....	3-13
Figure 3.15: A generic method for setting up a numerical model in STAR-CCM+ (STAR-CCM+, 2017).....	3-14
Figure 3.16: Model geometry in STAR-CCM+.....	3-15
Figure 3.17: Volumetric mesh grid with refinement volumes .....	3-18
Figure 3.18: User-defined refinement of volumetric mesh grid with refinement volumes .....	3-18
Figure 3.19: Example of Residuals Plot .....	3-19
Figure 3.20: Example of Water Level Head Plot.....	3-20
Figure 3.21: Example of Volume Flow Rate Plot.....	3-20
Figure 3.22: Scaling results for a 16-million cell STAR-CCM+ simulation (Hedges, 2016) .....	3-21
Figure 3.23: A generic example of the script needed to run a STAR-CCM+ job (simulation) on the CHPC (Crosby, 2018).....	3-23
Figure 4.1: Calculation procedure for flows above the physical model capacity .....	4-2
Figure 4.2: Graph of physical model results for lower to higher Crump width ratio of 1:4 .....	4-4
Figure 4.3: Graph of physical model results for lower to higher Crump width ratio of 1:3 .....	4-6
Figure 4.4: Graph of physical model results for lower to higher Crump width ratio of 1:2 .....	4-8
Figure 4.5: Graph of physical model results for lower to higher Crump width ratio of 1:1 .....	4-10
Figure 4.6: Schematic of the flow lines as observed for Ratio 1:4 Layout A.....	4-12

Figure 4.7: Total energy head (H) at each measuring point for Ratio 1:4 Layout A.....	4-13
Figure 4.8: Differences in energy levels at each measurement point relative to the upstream point for Ratio 1:4 Layout A .....	4-14
Figure 4.9: Schematic of the flow lines as observed for Ratio 1:1 Layout A.....	4-15
Figure 4.10: Total energy head (H) at each measuring point for Ratio 1:4 Layout A.....	4-16
Figure 4.11: Differences in energy levels at each measurement point relative to the upstream point for Ratio 1:1 Layout A .....	4-17
Figure 4.12: Schematic of the flow lines as observed for Ratio 1:4 Layout D.....	4-18
Figure 4.13: Total energy head (H) at each measuring point for Ratio 1:4 Layout D.....	4-18
Figure 4.14: Differences in energy levels at each measurement point relative to the upstream point for Ratio 1:4 Layout D .....	4-19
Figure 4.15: Schematic of the flow lines as observed for Ratio 1:1 Layout D.....	4-20
Figure 4.16: Total energy head (H) at each measuring point for Ratio 1:1 Layout D.....	4-20
Figure 4.17: Differences in energy levels at each measurement point relative to the upstream point for Ratio 1:1 Layout D .....	4-21
Figure 4.18: Photograph of 3-dimensional flow phenomena observed during physical modelling ..	4-24
Figure 4.19: Vortex formation evident over Crump crest.....	4-25
Figure 4.20: Vortex formation upstream of Crump crest (Wessels, 1996).....	4-25
Figure 4.21: Graph of physical model results for Layout A.....	4-29
Figure 4.22: Graph of physical model results for Layout D.....	4-30
Figure 4.23: Graph of adjusted physical model results to account for contraction for Ratio 1:4 .....	4-34
Figure 4.24: Results of the numerical model analysis ( $Q_{\text{calc\_numerical}}$ ) in comparison with the physical model results ( $Q_{\text{calc\_physical}}$ ) for Ratio 1:4 Layout D.....	4-37
Figure 4.25: Comparing the results of the numerical model with surface interface refinement of 2.5 mm ( $Q_{\text{calc\_2.5mm\_refinement}}$ ) in comparison with a surface interface refinement of 1 mm ( $Q_{\text{calc\_1mm\_refinement}}$ ).....	4-38
Figure 4.26: Streamlines around the divider wall showing the velocity magnitude.....	4-40
Figure 4.27: Streamlines around the entire structure showing the velocity magnitude.....	4-41
Figure 4.28: Results of the numerical model analysis ( $Q_{\text{calc\_numerical}}$ ) in comparison with the physical model results ( $Q_{\text{calc\_physical}}$ ) as well as the physical model results adjusted for contraction ( $Q_{\text{adjusted\_physical}}$ ).....	4-42

## LIST OF SYMBOLS

### International System of Units

m = metre

mm = millimetre

s = second

kg = kilogram

N = Newton ( $\text{kg m/s}^2$ )

### Hydraulics of weirs

u = velocity in the main flow direction (m/s)

p = pressure ( $\text{N/m}^2$ )

$\gamma$  = unit weight of water ( $\text{kg/m}^3$ )

z = height above datum (m)

$\mu$  = dynamic viscosity ( $\text{N s/m}^2$ )

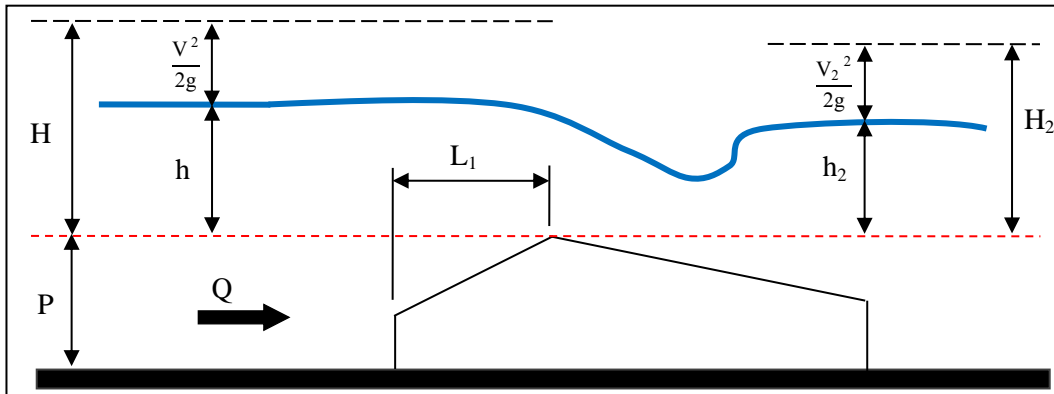
$\rho$  = fluid density ( $\text{kg/m}^3$ )

$\nu$  = kinematic viscosity ( $\mu/\rho$ ) ( $\text{m}^2/\text{s}$ )

$C_d$  = discharge coefficient

Fr = Froude number

$k_h$  = constant with unit length



### Definition sketch for Crump weirs

$Q$  = discharge ( $\text{m}^3/\text{s}$ )

$b$  = width of crest perpendicular to flow (m)

$P$  = pool depth below crest

$h$  = measured water level upstream relative to the weir crest (m)

$H$  = total energy head upstream relative to the weir crest (m)

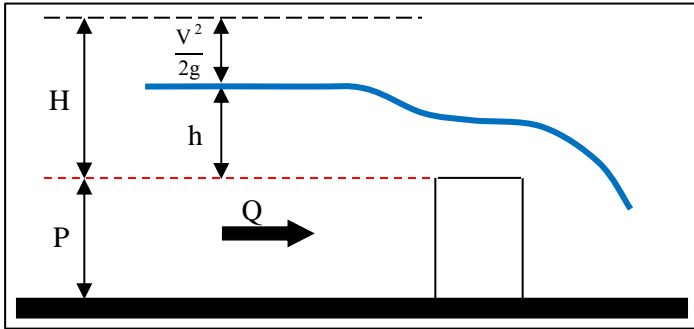
$V$  = approach velocity (m/s)

$h_2$  = measured water level downstream relative to the weir crest (m)

$H_2$  = downstream energy head relative to the Crump weir crest

$V_2$  = downstream velocity (m/s)

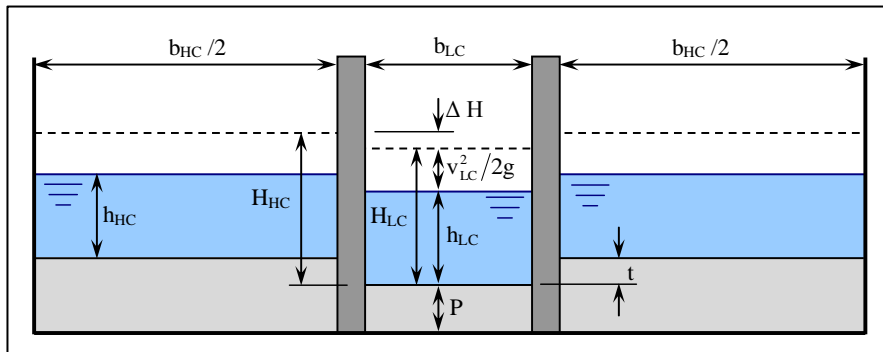
$h_v$  = velocity head (m)



**Definition sketch for broad-crested weirs**

$C$  = discharge coefficient from  $H$  ( $\sqrt{\text{m/s}^2}$ )

$\bar{C}$  = discharge coefficient from  $h$  ( $\sqrt{\text{m/s}^2}$ )



**Definition sketch for correction factors of compound Crump weirs with divider walls (Wessels & Rooseboom, 2009 (b))**

$b_{HC}$  = width of higher crest perpendicular to flow (m)

$b_{LC}$  = width of lower crest perpendicular to flow (m)

$\Delta H$  = entrance loss (m)

$h_{HC}$  = measured water level upstream of higher weir crest (m)

$H_{HC}$  = total energy head upstream of higher weir crest (m)

$H_{LC}$  = total energy head upstream of lower weir crest (m)

$h_{LC}$  = measured water level upstream of lower weir crest (m)

$V_{LC}$  = approach velocity upstream of lower weir crest (m/s)

$t$  = step height between the lower and higher crests (m)

$k_{Cm}$  = correction factor for entrance losses

### **Computational fluid dynamics (CFD)**

$V_i$  = volume of phase i

$\alpha_i$  = volume fraction of phase i

$S_{\alpha_i}$  = source/sink of the  $i^{\text{th}}$  phase

$\frac{D \rho_i}{Dt}$  = material derivatives of the phase densities

$\Delta t$  = solution time step

$\Delta x$  = length of the interval (or cell size)

$Cu$  = Courant number

$C_{max}$  = Maximum Courant number

CAD = Computer Aided Drawing

### **Physical Modelling**

$P_L$  = lower Crump weir pool depth

$P_H$  = higher Crump weir pool depth

$FW_R$  = right filler wall width

$H_d$  = design head

$B_L$  = lower Crump weir crest width

$B_H$  = higher Crump weir crest width

$FW_L$  = left filler wall width

$y$  = correction factor

$Q_{Mag\ Flow}$  = flow rate measured by the magnetic flow meter

$Q_{input}$  = calibrated model input flow rates as per pumps (l/s)

$Q_{calculated}$  = flow rate calculated using measured water levels upstream of the model (l/s)

$E$  = percentage difference between  $Q_{input}$  and  $Q_{calculated}$  (%)

$\Delta h_c$  = water level adjustment value correcting for contraction (m)

$Q_{adjusted}$  = calculated flow rate adjusted to account for the error induced by contraction (l/s)

$\Delta h_o$  = water level adjustment value correcting for overtopping (m)



## LIST OF ABBREVIATIONS

<b>SA</b>	South Africa
<b>DWS</b>	Department of Water and Sanitation
<b>CFD</b>	Computational Fluid Dynamics
<b>CAD</b>	Computer Aided Design
<b>MAR</b>	Mean Annual Runoff
<b>VOF</b>	Volume of Fluid
<b>RANS</b>	Reynolds-Averaged Navier-Stokes
<b>HRIC</b>	High-Resolution Interface Capturing
<b>CD</b>	Central Differencing
<b>LUD</b>	Linear Upwind Differencing
<b>NVD</b>	Normalised Variable Diagram
<b>DD</b>	Downwind Differencing
<b>UD</b>	Upwind Differencing
<b>HPC</b>	High-Performance Computing
<b>CHPC</b>	Centre for High Performance Computing
<b>VNC</b>	Virtual Network Computing

## GLOSSARY

<b>Flow rate</b>	(also known as volumetric flow rate, volume flow rate, rate of fluid flow, volume velocity or discharge) is the volume of fluid which passes a particular point per unit time; usually represented by the symbol $Q$ with SI unit $\text{m}^3/\text{s}$ (cubic metres per second).
<b>Flow measuring structures</b>	generally, act as hydraulic controls in open channels, such as rivers, in order to provide a unique relationship between the upstream head and the flow rate.
<b>Weir</b>	is a type of flow measuring structure, usually in the form of a low head dam, placed across a river that alters the flow characteristics of the water and usually results in a change in the upstream water level. There are several profile designs for a weir that allows water to flow freely over the top of the weir crest before flowing down to a lower level.
<b>Compound weir</b>	is any weir that comprises multiple weir crests (could be the same or varying profiles) constructed in parallel at different levels into one structure in order to measure varying flow rates more accurately.
<b>Divider walls</b>	are walls that run parallel with the river flow, used to separate the crests that make up a compound weir in order to prevent the presence of three-dimensional flow caused by the step difference between the crests of a compound weir.
<b>Flank walls</b>	are walls that border the edges of a weir and which support the river banks on either side of the structure.
<b>Filler walls</b>	tie the structure into the riverbank, extending from the flank walls into the river bank usually to rock level.
<b>Hydraulic capacity</b>	is the amount of water that can pass through a hydraulic structure before exceeding the flank wall levels.
<b>Gauging station</b>	a specifically selected location on a river that is equipped and operated to provide continuous water level readings that can be used to determine the discharge in a river, observations of biota and water quality may also be made.
<b>Flow-gauging network</b>	group of gauging stations.

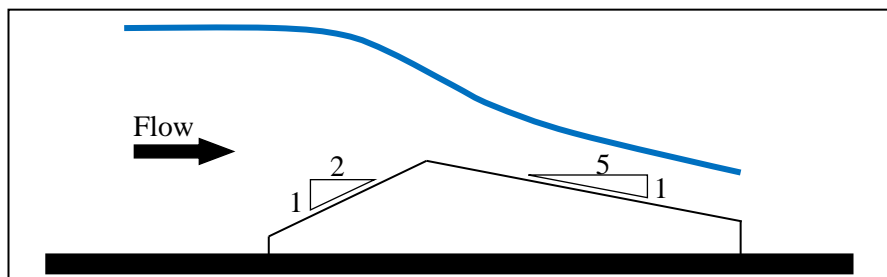
# 1 INTRODUCTION

## 1.1 BACKGROUND

The supply of water in South Africa (SA) is restricted, disproportionately distributed, and negatively influenced by climate change, pollution, and the spread of alien plant species. Water rationing schedules and water conservation strategies have become a necessity in the country's ever-growing economy. In 2004, the Department of Water and Forestry, now known as the Department of Water and Sanitation (DWS), stated that SA would have a 1.7% water deficit by the year 2025. Agriculture and forestry consume 65% of the country's available surface water. Therefore, the dangerous combination of increasing development and climate change has obvious implications for food security, irrigation methods and land reforms (Blignaut & van Heerden, 2009).

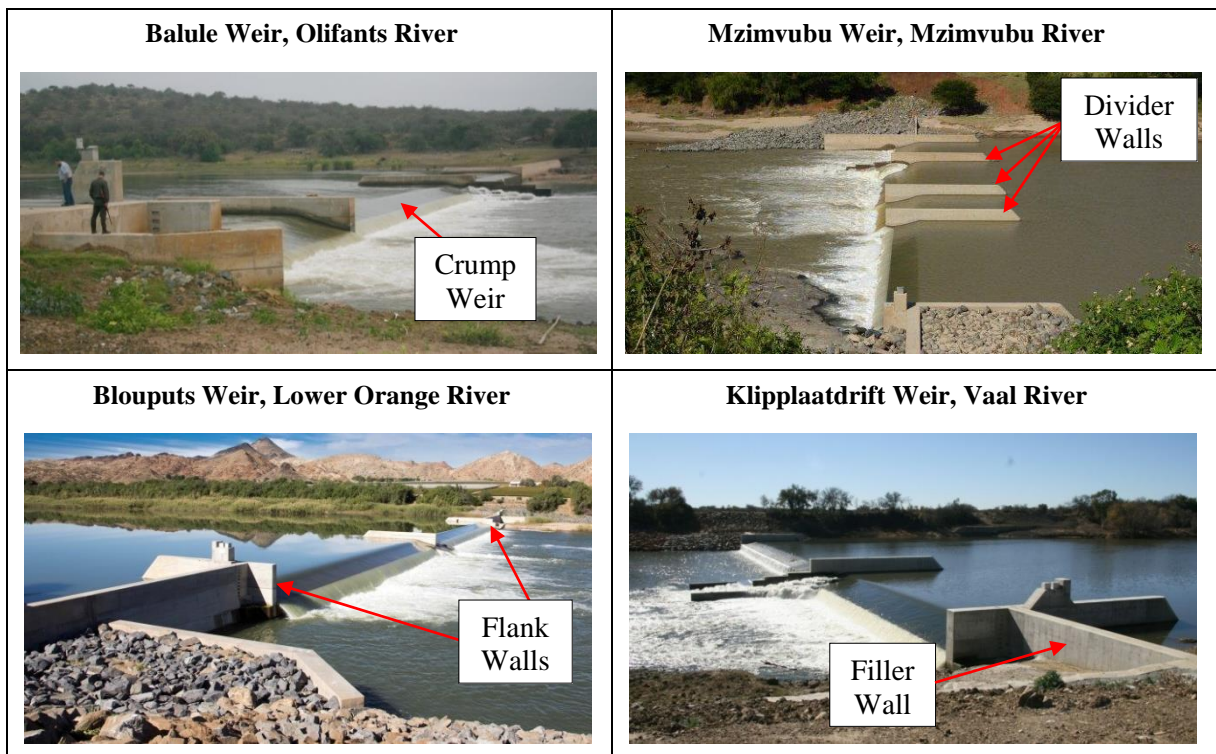
According to the Centre for Research on the Epidemiology of Disasters (2015) floods were the most frequent type of natural disaster worldwide and had affected a total of 2.4 billion people of which 160 000 have died while leaving 66 million houses damaged during the period 1994 to 2013. The measuring of flow rates for the early prediction of the magnitude of flood events is essential for the prevention of these calamities.

Flow measuring structures, such as weirs, have two main functions: (1) measuring flow rates in rivers and (2) the early prediction of flood events (Rickard et al., 2003). Various types of weir profiles exist, each with its own set of relationships for calculating the flow rate. The Crump weir is most often used in SA because of its robustness against structural damage of the weir crest caused by floating tree trunks during flood events or high flow conditions. A typical Crump weir consists of a triangular profile with an upstream slope of 1:2 and a downstream slope of 1:5 as shown in **Figure 1.1**.



**Figure 1.1: Profile of a typical Crump weir (Maritz et al., 2015)**

Compound weirs consist of multiple crests at different levels clustered together in parallel to measure varying flow rates more accurately. The implementation of compound weirs is essential in SA due to the abrupt and substantial changes in flow conditions experienced in rivers (Wessels & Rooseboom, 2009 (b)). The current discharge head relationships were developed with the assumption of parallel flow lines over the weir crest. Divider walls are used to separate the crests that make up a compound weir, in order to prevent the presence of three-dimensional flow. It is a requirement of the BSI ISO 14139 (British Standards Institution, 2000) to include divider walls in the design of compound weirs. **Figure 1.2** shows examples of compound Crump weirs operating in various rivers throughout SA.

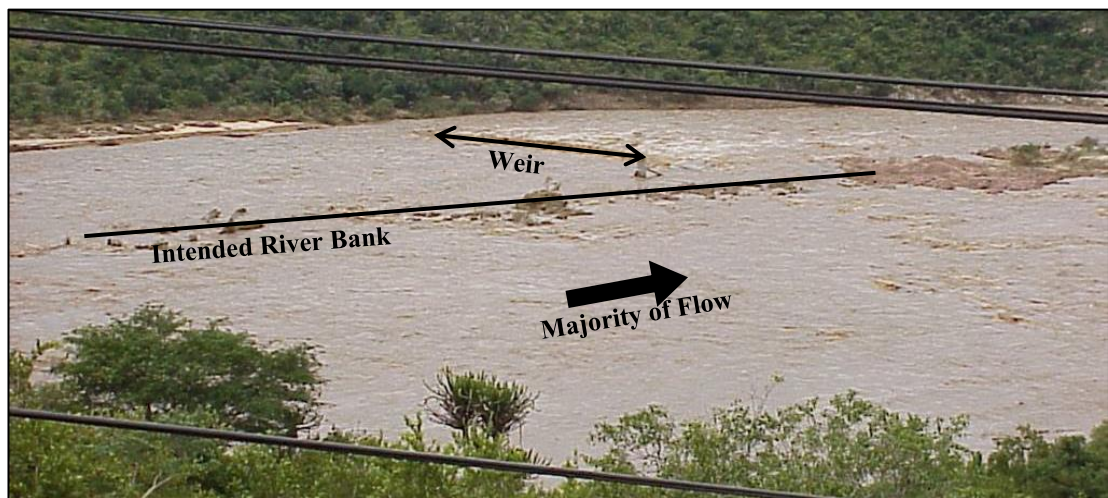


**Figure 1.2: Examples of compound Crump weirs in the field**

It would be financially and practically impossible to design compound weirs that can measure the entire range of flow rates that may occur in the river to the same degree of accuracy. To accurately measure high flows in rivers, large and expensive structures are required. However, limits to the hydraulic capacity of a compound weir must be applied in order to save costs. The DWS has adopted the approach suggested by van Heerden et al. (1985) to determine the hydraulic capacity of these weirs which was later questioned by Wessels (2016) based on specific in-field observations (described below). Van Heerden et al. (1985) and Wessels (2016) agreed that cost-benefit analyses should be performed to determine the most economical layout without compromising accuracy at high or low flow rates; and

furthermore, the impact of the weir on upstream water levels should be limited to prevent an increase in the risk of flooding the surrounding development and scouring of the riverbanks. Van Heerden et al. (1985) also suggested that the structures be designed to measure flow rates that occur 80% of the time in the river channel, this Wessels (2016) questioned. In SA rivers low flow rates are experienced for most of the year with abrupt flow rate changes during the rainy seasons. This results in low design flow rates for an 80%-time-occurrence criteria. Weirs would thus be frequently damaged during rainy seasons when the flow rate rapidly increases. Wessels (2016) thus suggests that weirs be designed for flow rates that make up 80% of the flow volume passing through the river over a historical hydraulic year.

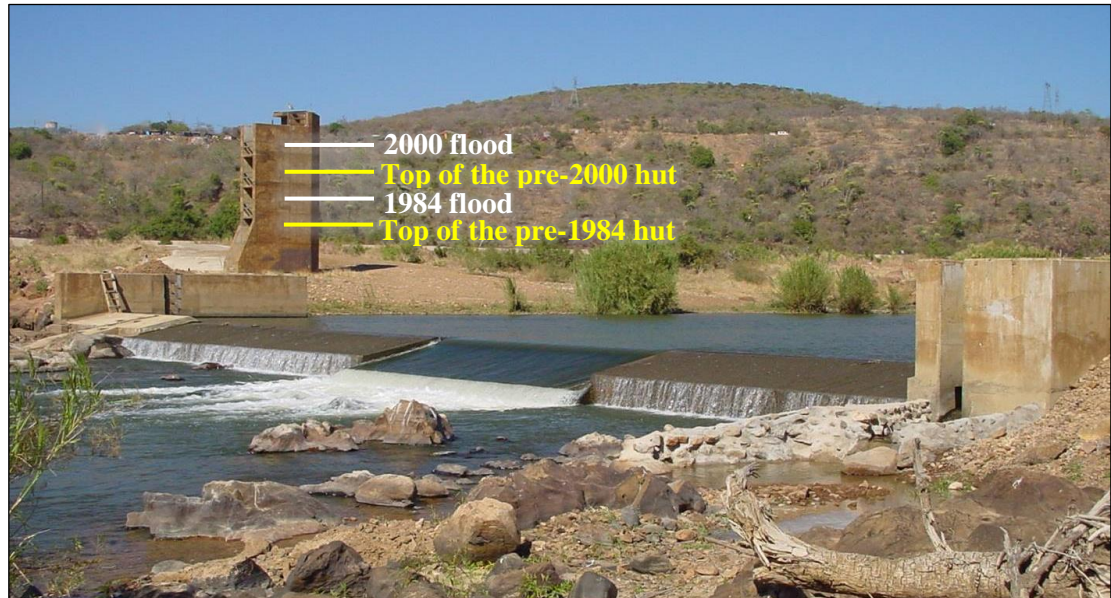
Consider the Komati Weir in the Komatipoort River that was constructed by DWS in 1982 with a hydraulic capacity of  $55 \text{ m}^3/\text{s}$ . In 1984, the Komatipoort River experienced high flow rates that caused damage to the original instrumentation hut. The hut was then rebuilt to 5 m higher than the original hut in order to prevent damage during future flooding. In the year 2000, severe flooding occurred, damaging the weir and instrumentation hut once again. **Figure 1.3** shows the Komati Weir operating well above its hydraulic capacity during the severe flood that occurred in 2000. At the moment that the photograph was taken, the water level was still on the rise reaching an estimated flood peak of  $19\,000 \text{ m}^3/\text{s}$ , close to the calculated RMF flood event. The weir position is visible due to surface waves and the majority of the flow in the river bypassed the weir on the right-hand side. The instrumentation hut was completely drowned at the flood peak level.



**Figure 1.3: Flooding of the Komati Weir in the Komatipoort River in the year 2000**

Due to the importance of measuring flow rates in rivers, the instrumentation hut had to be reconstructed for the second time. The weir was upgraded to a hydraulic capacity of  $299 \text{ m}^3/\text{s}$

at a design head of 2.3 m. **Figure 1.4** shows the final upgraded Komati weir as well as the 1984 and 2000 flood levels along with the tops of the measuring huts before these floods. The instrumentation hut was, however, constructed above the 2000 flood line due to the high-cost component of the gauging instrumentation.

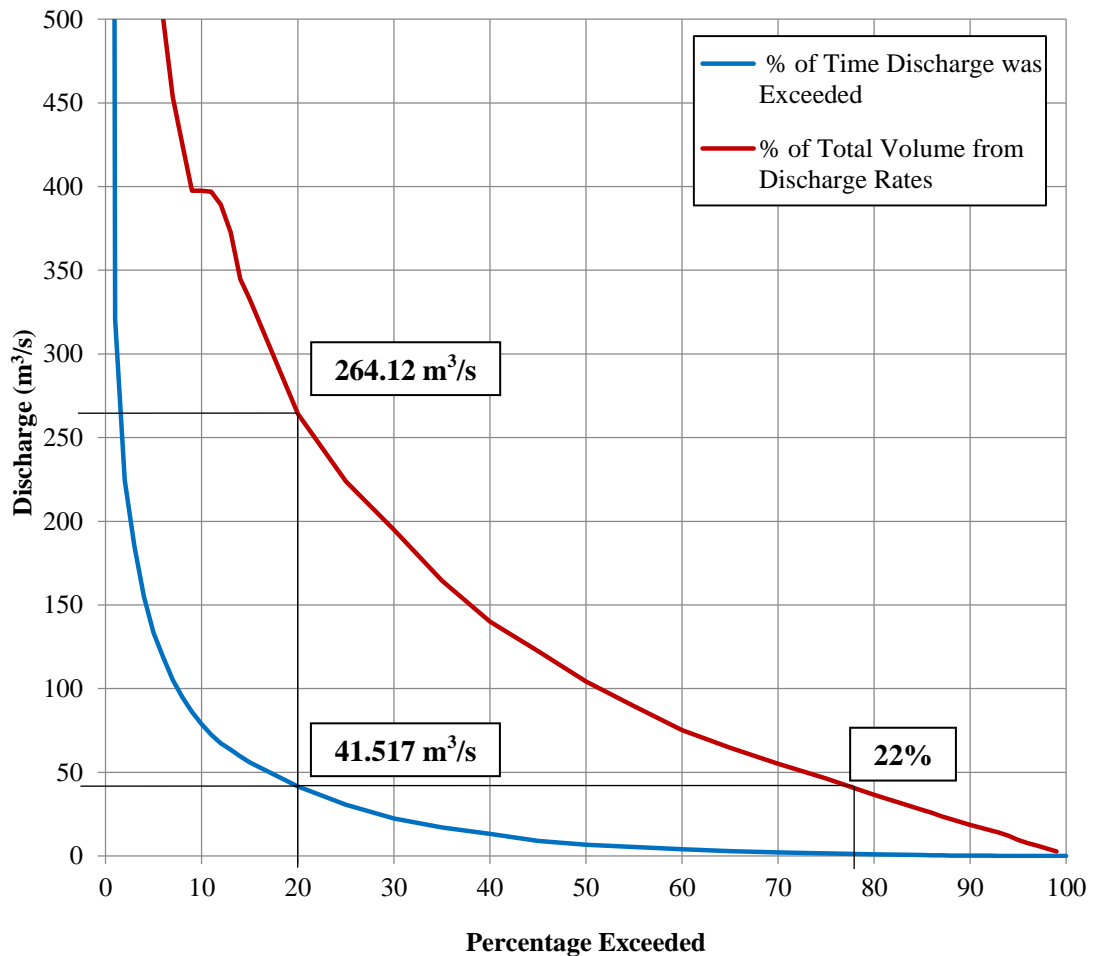


**Figure 1.4: Upgraded Komati Weir in the Komatipoort River after the 2000 flood event**

The difference in the hydraulic capacity based on a percentage time occurrence and a percentage volume contribution is shown in **Figure 1.5**. The Figure shows that the original hydraulic capacity of  $55 \text{ m}^3/\text{s}$  lies above the required discharge of  $41.5 \text{ m}^3/\text{s}$  for the 80%-time occurrence criteria. However, the flood events that occurred in 1984 and 2000 shows that the 80%-time-occurrence criteria cannot be implemented in the design of this weir due to the high risk of damage to instrumentation during flood events. The risk at high flow rates can be significantly reduced by using the 80%-volume-contribution criteria for the hydraulic design of the weir. **Figure 1.5** shows the 80%-volume-contribution discharge to be  $264.12 \text{ m}^3/\text{s}$ . The upgraded Komati Weir has a design capacity of  $299 \text{ m}^3/\text{s}$ , falls above the 80%-volume-contribution criteria.

Therefore, if the site conditions favour high flow measurements, the 80%-volume-contribution criteria should be used as the hydraulic capacity instead of the 80%-time occurrence criteria used in the past. The cost implication to construct a weir that can measure higher discharges should always be weighed against the incremental gain in the hydraulic capacity of a structure and the 80%-time-occurrence criteria should be considered the

minimum possible design capacity for rivers that do not experience significant variations in flow rates (Wessels, 2016).



**Figure 1.5: Determining design capacity for the Komati Weir using the percentage time occurrence criteria compared to using the percentage volume contribution criteria**

On further investigation of **Figure 1.5**, it can be seen that for Komati Weir, a design flow rate of  $41.517 \text{ m}^3/\text{s}$  only caters for flow rates up to 22% of the flow volume contribution. It thus follows that the flow rates that make up 78% of the flow volume contribution would be above hydraulic capacity and would not be measured with confidence. An over- or underestimation of the flow rate would thus skew the flow-gauging record resulting in unreliable recurrence flow rates used in the design of sensitive infrastructures such as dams, bridges and culverts. Unfortunately, many weirs were designed with the 80%-time-occurrence criteria and therefore investigating the rating of weirs above hydraulic capacity is of utmost importance for the improvement of the flow record.

## 1.2 MOTIVATION FOR STUDY

The study is motivated by the limits implemented on the hydraulic capacities of weirs. The measuring of flow rates beyond the hydraulic capacity of these structures is still of utmost importance for the efficient management of water resources and the design of infrastructure. Wessels and Rooseboom (2009 (a); 2009 (b)) have done extensive research on the accuracy of weirs that operate within their hydraulic design capacity. However, when the structures operate above their hydraulic capacities the presence of three-dimensional flow resulting from the influence of the divider walls is beyond the scope of the current discharge head relationships for weirs.

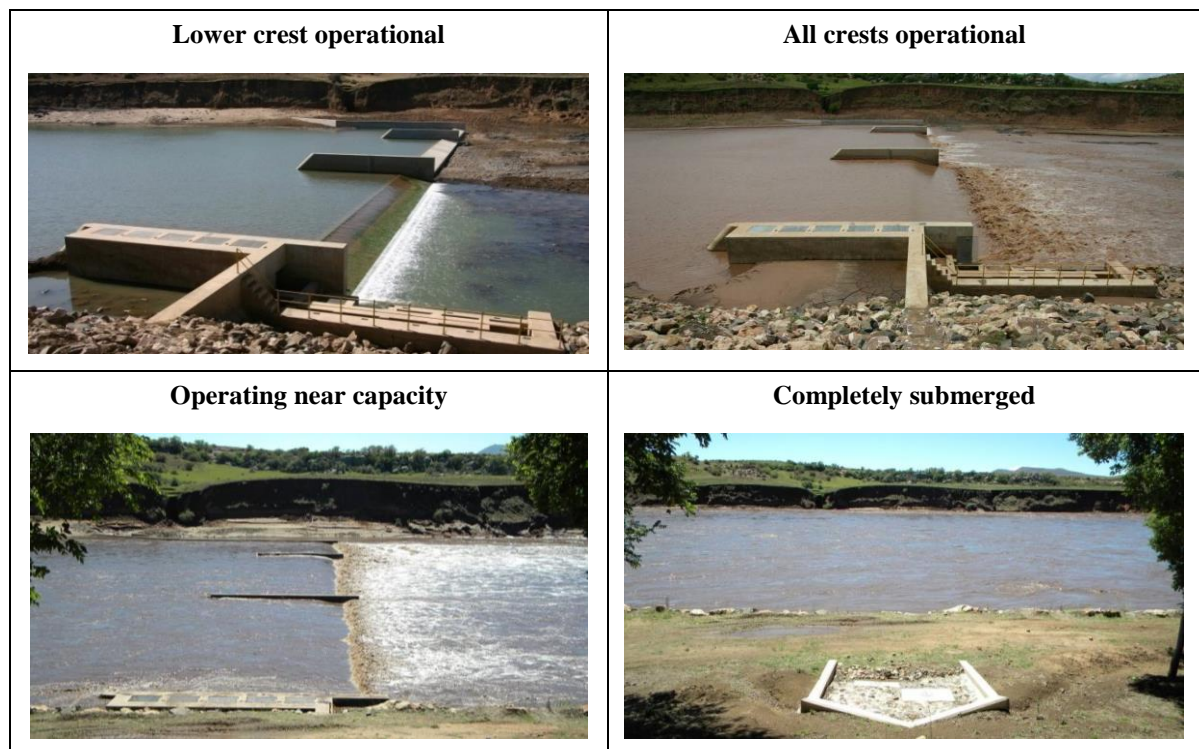
The general philosophy of designing a compound Crump weir is to ensure that the structure becomes fully submerged at high flow regimes (beyond its hydraulic limit) in order to prevent damage to the structure due to scouring of the riverbanks. Submergence is measured using the modular limit defined as the ratio of the downstream total head level and the upstream total head level ( $H_{DS}/H_{US}$ ). The range of the modular limit is 0.74 to 0.78; therefore it can be said submergence occurs when the downstream total head level is between 74 and 78% of the upstream total head level (Ackers et al., 1978). Wessels (2016) suggested the following techniques for rating weirs that exceed their design capacities under high-submergence conditions:

- The theory developed for rating highly submerged structures, using water levels upstream and downstream of a weir, should be applied with caution.
- Backwater calculations such as the standard- or direct-step method or indirectly using the slope-area method with water levels estimated using flood water marks along the river bank, a survey of two or more river cross-sections, and by estimating the river roughness coefficient, could be used to determine peak flow of the event. This flow rate can then be linked to the peak head measurements at the weir.
- Comparing flow volumes and flood peaks of a specific flood event between two weirs in a river where little to no inflow or loss of flow volume occurs between the two structures during the event. This method, however, requires one of the structures to be accurately rated over the full discharge range of the event.

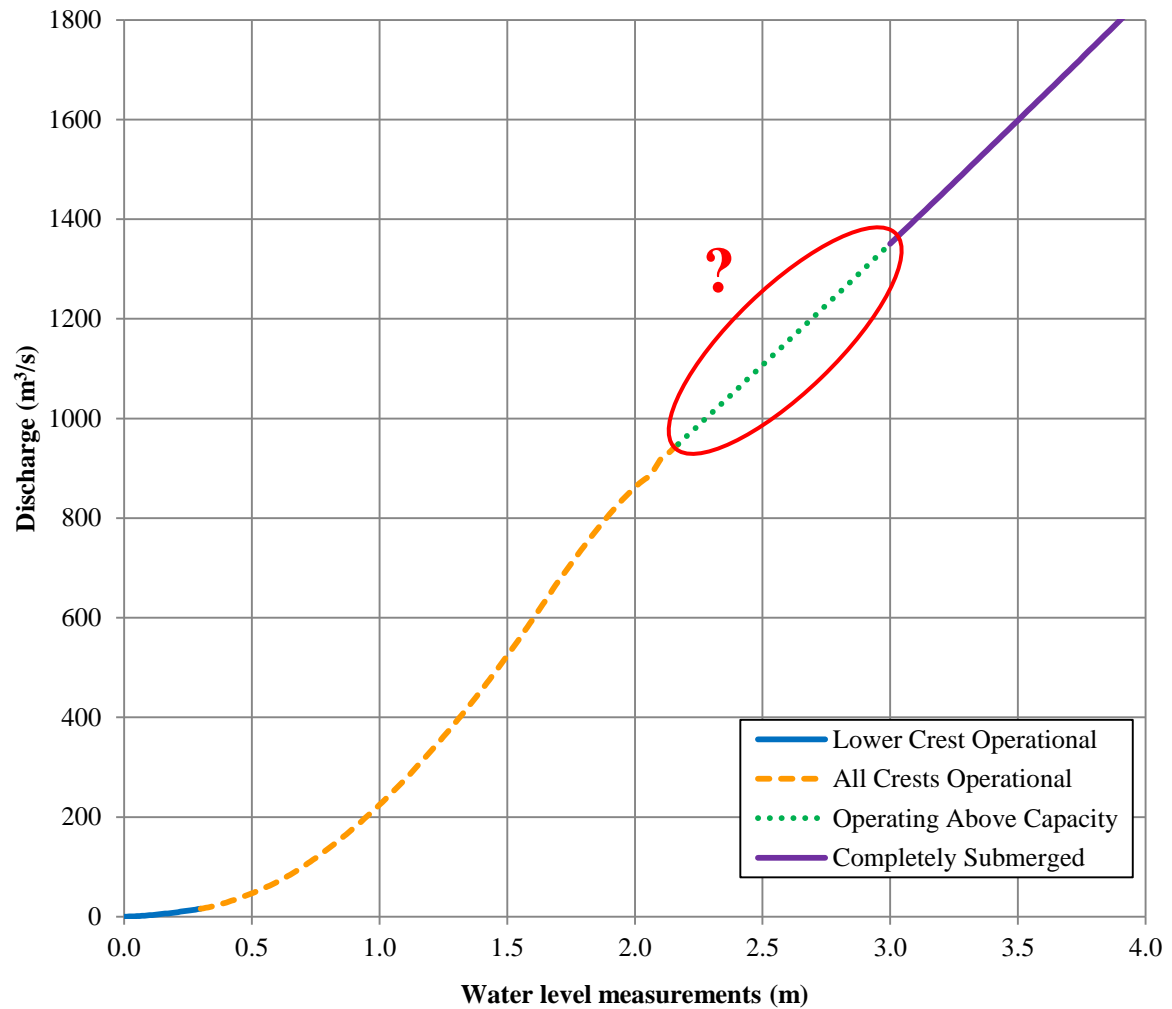
These techniques are commonly referred to as indirect methods and are used to calculate discharge above the hydraulic capacity of weirs. **Figure 1.6** shows the four operating phases of the Oranje Draai Weir in the Orange River. The structure consists of three crests at increasing heights of 300 mm with a design capacity of 950 m<sup>3</sup>/s. The Figure shows the weir



operating at  $4.2 \text{ m}^3/\text{s}$  (lower crest operational),  $48 \text{ m}^3/\text{s}$  (all crests operational),  $945 \text{ m}^3/\text{s}$  (operating near capacity) and  $3400 \text{ m}^3/\text{s}$  (completely submerged). The Oranje Draai Weir often operates above its design capacity, but due to financial constraints, confinement of the main river channel and highly corrosive riverbanks a higher weir could not have been built. The rating curve of the Oranje Draai Weir is plotted in **Figure 1.7**. The structure was rated up to hydraulic capacity using the discharge-head relationships (blue and orange curves) and then the indirect methods were used to estimate the flow rates during overtopping of the structure (green and purple curve). The structure becomes fully submerged when the discharge is between  $1107 \text{ m}^3/\text{s}$  and  $1350 \text{ m}^3/\text{s}$ , after which the indirect methods can be applied. The results obtained from the indirect methods can only be trusted if the transition between rating at hydraulic capacity and complete submergence is accurately estimated. However, uncertainties exist in the rating of structures during flow rates that fall between hydraulic capacity and 100% submergence (circled in red). The study discussed in this dissertation focuses on determining the nature of the error made in this region of uncertainty.

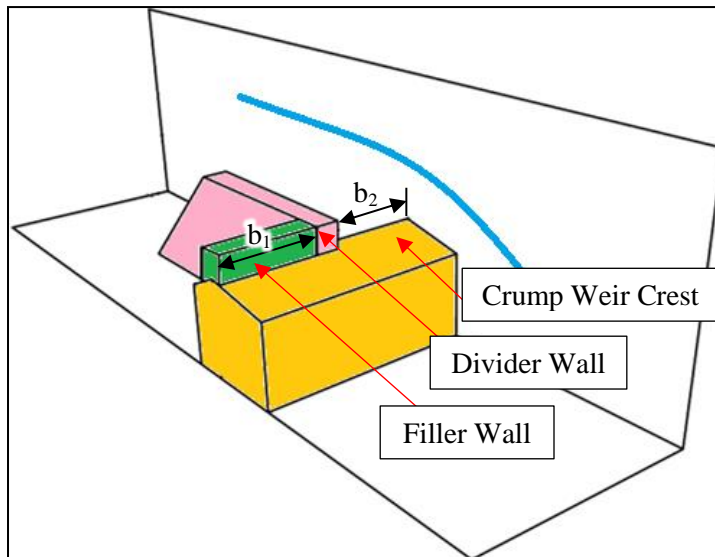


**Figure 1.6: Four operating phases of the Oranje Draai Weir, Orange River**



**Figure 1.7: Rating curve for the Oranje Draai Weir, Orange River**

In 2014, the University of Pretoria (UP) conducted a pilot study to determine whether the discharge-head relationships for Crump weir structures with divider and filler walls were accurately predicting the flow rates when the hydraulic capacity of the structure was exceeded. Maritz, et al. (2015) investigated a section of a standard Crump weir consisting of one weir crest with a divider and filler wall as shown in **Figure 1.8**. Three different weir width ( $b_1$ ) to filler-wall length ( $b_2$ ) ratios were modelled, namely; 1:0.57, 1:0.94 and 1:2.8. The study concluded that for ratios 1:0.57 and 1:0.94 ( $b_1/b_2$ ) the flow in the channel was overestimated during overtopping of the divider and filler wall. However, for ratio 1:2.8 the influence of the divider wall was predominant, leading to the underestimation of flow in the channel. The conclusions of this pilot study indicate that the current Crump weir discharge-head relationships needed to be improved if they were to be used for determining the flow rates of weir structures operating above their hydraulic capacities.



**Figure 1.8: Definition sketch of 2014 UP model study (Maritz et al., 2015)**

Computing the effects of three-dimensional flow lines induced by the overtopping of divider and filler walls of compound Crump weirs is possible due to the developments in numerical modelling techniques. Using physical modelling to verify numerical modelling allows the researcher to investigate multiple structure layouts simultaneously. Rating of compound weirs that operate above their designed capacity would lead to the construction of more cost-effective infrastructure and could advance the early prediction of flood events (Maritz et al., 2015).

### 1.3 HYPOTHESIS AND OBJECTIVES OF STUDY

It is hypothesised that when compound Crump weirs with divider walls, operate above their hydraulic design capacity, three-dimensional flow conditions influence the water level readings resulting in false flow rate calculation values. Therefore, the objectives of the study were to:

- demonstrate from experimental measurement, that flow rates above hydraulic design capacity bring about three-dimensional flow that influences the observed water levels;
- determine from experimental quantification of flow rates above hydraulic capacity, the validity of the current discharge-head relationships used for calculating flow rates over compound Crump weirs; and
- determine using Computational Fluid Dynamics (CFD) analyses of the modelled compound Crump weir, the capabilities of numerical modelling for the rating of weirs above their hydraulic design capacities.

## 1.4 SCOPE OF THE STUDY

The investigation was split into two phases, (1) the physical model study, done at the DWS hydraulic laboratories and (2) the numerical model study, executed using the computational fluid dynamics (CFD) software STAR-CCM+. The following physical model parameters were kept constant: pool depth, width and length of the divider walls, width and length of the filler walls, the width of the lower and higher Crump weirs, and the heights of the two weirs as well as the flow condition (modular flow). The pumping capacity at the DWS laboratories limited the maximum flow to 220 l/s.

## 1.5 METHODOLOGY OF STUDY

Research and experimental work aimed at investigating the limitations of the discharge-head relationship of modelled compound Crump weirs during high flow regimes was done during the study. An extensive review of the available literature concerning modelling of compound weirs and the current discharge-head relationships as well as numerical modelling using CFD software was used to define the scope and objectives of the study. The experimental procedure was then designed according to the literature review in order to achieve the defined objectives. The experimental procedure divides into two sections: (1) the physical model study and (2) the numerical model study.

A physical model representing a compound Crump weir structure was built at the DWS hydraulic laboratories. Water level measurements, upstream of the various components (Crump weir crests, divider walls, and filler walls), were taken in order to calculate the flow rate over the structure. The current Crump weir discharge-head relationship was used for these calculations and was compared to the laboratory flow meter. The flow meter in the laboratory was calibrated using a standardised Crump weir in order to adjust for any discrepancy between the actual flow and that measured by the flow meter.

The numerical model study was set-up in the CFD software, STAR-CCM+ version 12.04.009 for Windows 64. The physical model built in the DWS laboratories was constructed in AutoCAD and imported as a volume into STAR-CCM+. The structure was then analysed in order to determine whether the CFD model and the physical model correspond with one another. After the results were collected and analysed, conclusions and recommendations were made.

## **1.6 ORGANISATION OF THE REPORT**

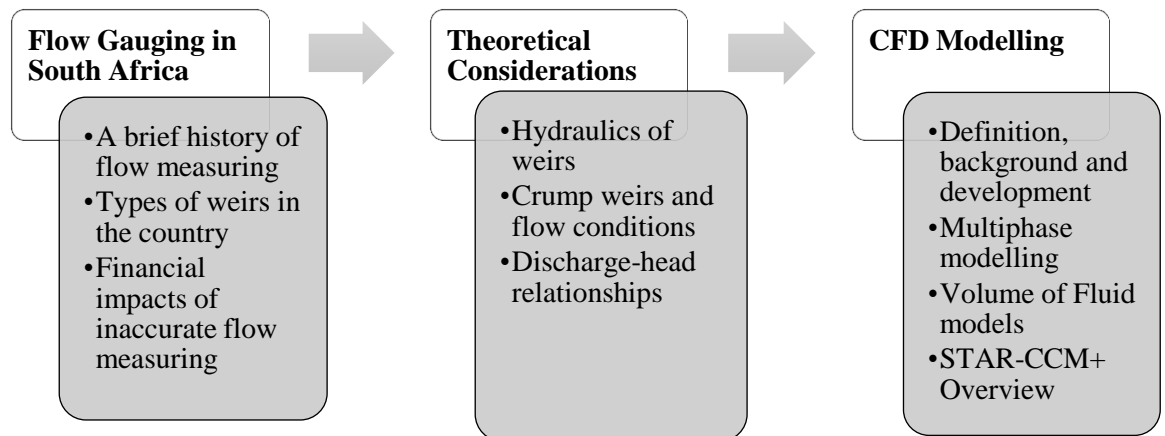
The chapters and appendices that make up the dissertation can be described as follows:

- Chapter 1 serves as an introduction to the study and describes the reasons motivating the study. The study objectives, scope, and methodology are also discussed.
- Chapter 2 contains a technical review of the available literature concerning measuring structures and focusing specifically on compound Crump weirs and their limitations.
- Chapter 3 explains the physical model study as well as the CFD study. This chapter also discusses the data collection, and result processing procedure followed.
- Chapter 4 discusses the comparison of the experimental results for the physical and CFD study. The observations noted throughout the study are addressed in this chapter.
- Chapter 5 discusses the conclusions to the objectives set out for the study and provides recommendations for future studies and designs of compound Crump weirs operating beyond their capacity.
- Chapter 6 reflects the list of references used in the study.
- The study appendices are provided at the end of the report.

## 2 LITERATURE REVIEW

In this chapter, a thorough review of the available literature on flow measuring in general and specifically on the use of compound Crump weirs is presented. A brief history of flow measuring in South Africa (SA), the financial impacts of inaccurate flow measuring and an overview of the type of weirs in the country are discussed. Details of the Crump weir hydraulics within its capacity are given as well as the limitations of the current discharge-head relationship being used.

The chapter also includes a description of Computational Fluid Dynamics (CFD) modelling, its history, and use in SA. The use of CFD modelling software and its advantages are also discussed along with a brief description of the computational methodologies involved. An overview of the chapter is given in **Figure 2.1**.



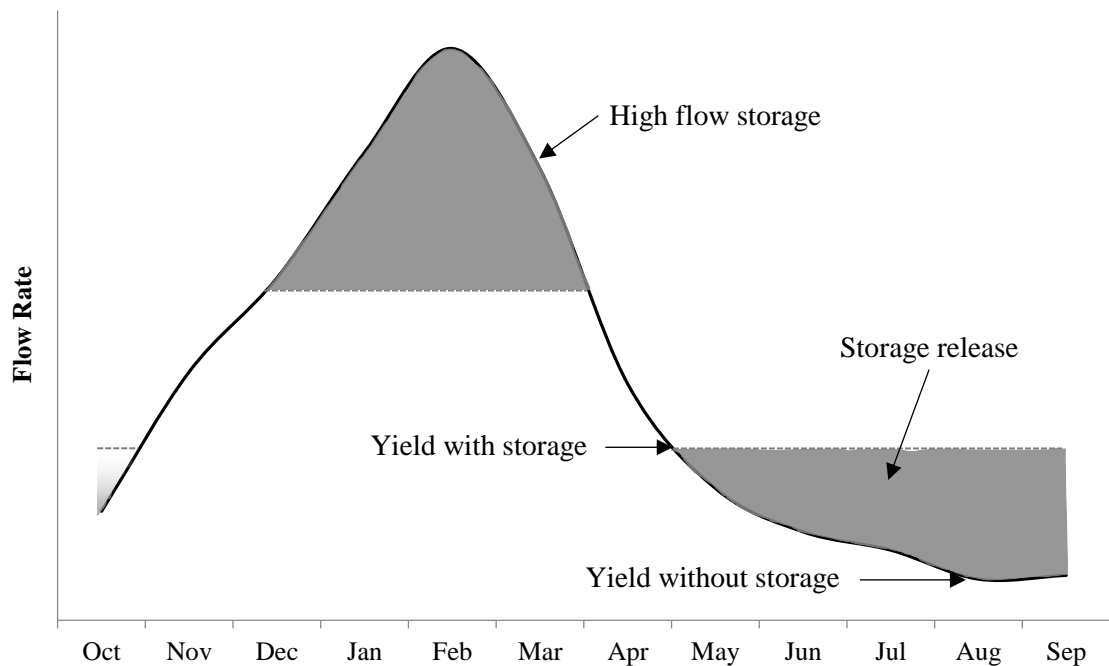
**Figure 2.1: Chapter overview**

### 2.1 INTRODUCTION

In a semi-arid, developing country like South Africa (SA), the management of available water resources is of utmost importance. Knowing the quantity of water available in the country is the first step in the effective and efficient management of water resources for current and future development (Ackers et al., 1978).

The average yearly rainfall experienced in SA is 450 mm; this is just more than half the 860 mm world average rainfall per year. It has been estimated that by 2025, the water demand in SA will exceed the country's available freshwater resources that are economically obtainable. A continuing trend in the urbanisation of the population places further pressure on SA's water resources. The added complexity of large fluctuation in monthly streamflow

experienced in the country's rivers, as shown in **Figure 2.2** (a mean flow rate plot over the entire record for station A2H012 in the Krokodil River at Kalkheuwel), emphasises the need for effective planning and management of resources. If adequate knowledge of streamflow data is available, water can be stored in dams during high flow periods to be used in dry hydrological cycles as indicated by the shaded areas in **Figure 2.2**.

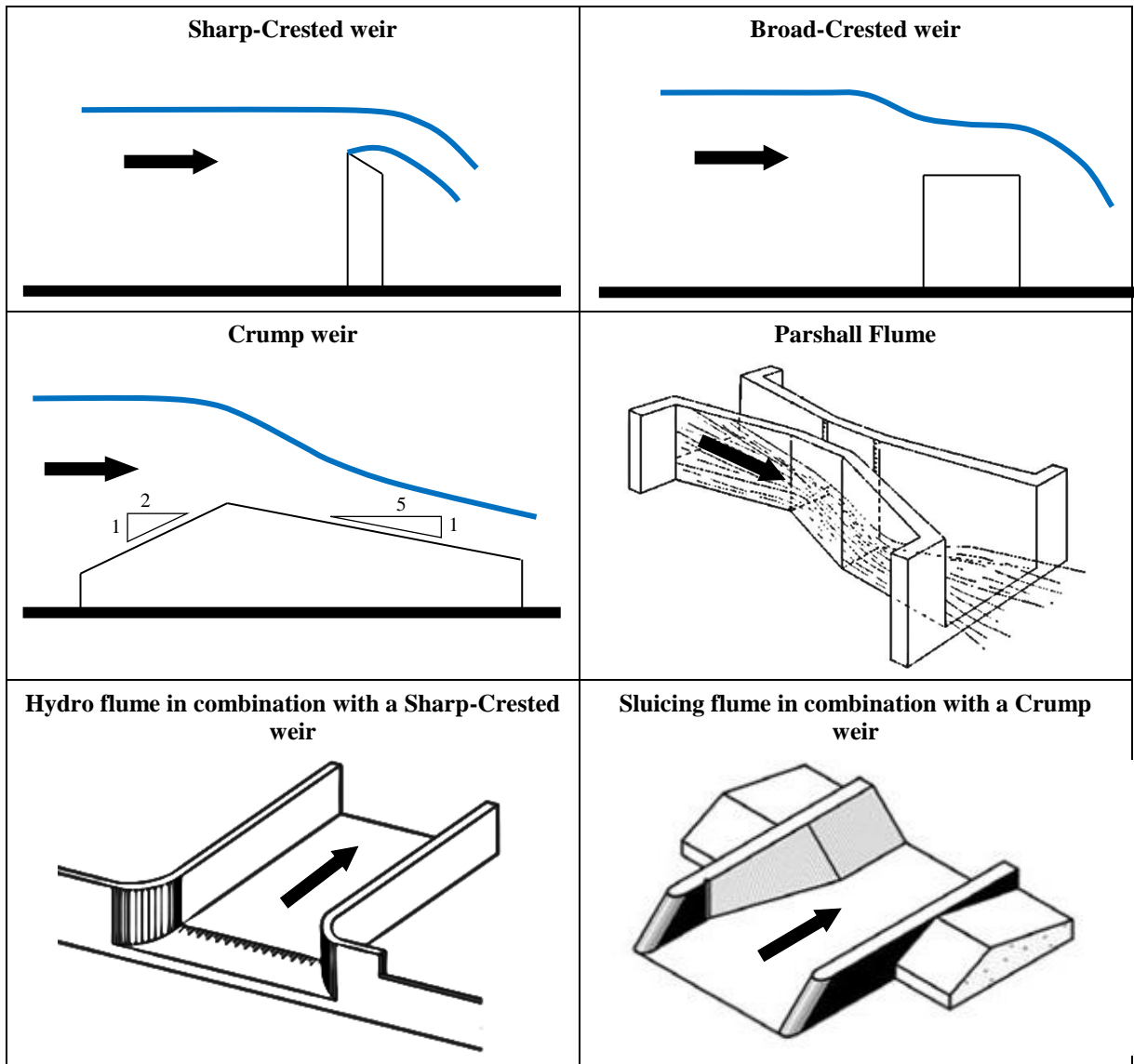


**Figure 2.2: Mean flow rate over the hydrological year for the entire record at station A2H012 in the Krokodil River at Kalkheuwel**

Engineers typically use hydrological data, such as calculated runoff or streamflow to size spillways, reservoirs and culverts, determine the height of a bridge or a low water crossing and even predict the inundation of developed areas. Runoff is a function of rainfall and rainfall intensity as well as catchment size and characteristics. The streamflow information (discharge or water level readings) is generally used to determine the runoff of catchments. It is thus essential to establish and maintain an extensive flow-gauging network (Wessels, 1996).

A flow-gauging network is made up of several gauging stations that can be defined as a specifically selected location on a river that is equipped and operated to provide continuous water level readings that can be used to determine the discharge in a river. The relationship between water levels and discharge depends on the cross-sectional properties of the site; the cross-section is often altered using flow measuring structures such as weirs (Lambie, 1978).

The various types of weirs shown in **Figure 2.3** have been used in South Africa's extensive flow-gauging network (Wessels & Rooseboom, 2009 (a)).



**Figure 2.3:** Types of weirs in South African rivers (Wessels & Rooseboom, 2009 (a))

## 2.2 BRIEF HISTORY OF FLOW MEASURING IN SOUTH AFRICA

The measuring of flow rates in SA rivers started in the year 1859 in the Olifants River. Those recordings were only utilised for the management of water resources when the Department of Water and Sanitation (DWS) officiated the responsibility of these measurements in 1909. Wessels (1996) stated that the first documented flood event took place on the 22<sup>nd</sup> of July 1652, at the Cape of Good Hope. Extreme rainfall caused the rivers in the area to flood destroying vegetable gardens and crops. In 1822, another flood event was documented, this time in the Olifants River near Clanwilliam in the Western Cape. The water level rose to 9 m



above the average water levels experienced in the river. Discharge observations were, however, not yet recorded. A peak discharge of  $710 \text{ m}^3/\text{s}$  was estimated for the flood event that occurred on the 18th of May 1859. Furthermore, daily flow observations in the Kariega River in the Eastern Cape were documented from December 1860 up to the drying up of the river in 1880. In the Vaal River near Kimberly in the Northern Cape, the Kimberly Water Works Company established the first gauging station for the documentation of long-term daily water level readings from July 1885. In 1909, the Department of Water and Sanitation (DWS) took over the recordings of these water levels until 1917 when the gauging station was closed down (Wessels, 1996).

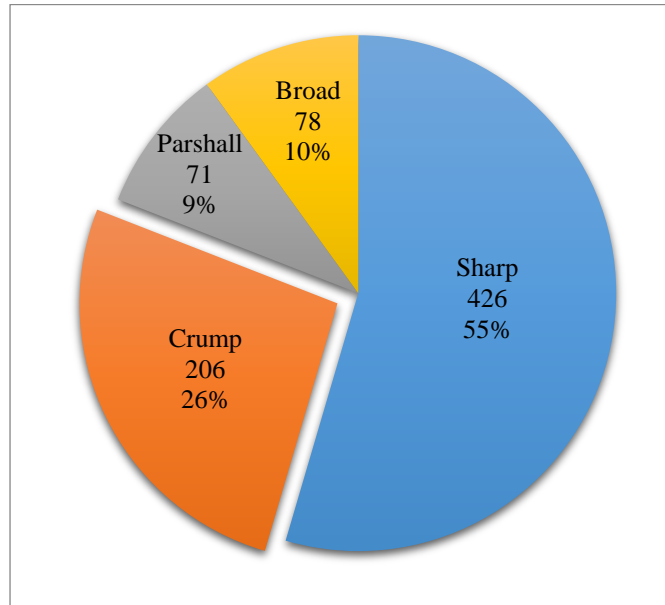
In December 1900, the first mechanical water level recorder was installed in the Vaal River near Vereeniging in Gauteng and was operational until the 30th of September 1922. On the 1st of March 1905, the oldest functioning mechanical recorder was installed in the Pienaars River near Klipdrift (Wessels, 1996). Weirs, used to measure flow, were constructed from 1904 to 1912 in the old Transvaal province (now known as, Limpopo, North West, and Gauteng). According to Wessels (1996) at least 17 weirs, that were measured using mechanical recorders, were constructed by the start of the First World War. The Rand Water Board constructed several other structures in 1915, and another 11 were functional across South Africa.

At the end of the Second World War there was a rapid increase in the number of weirs until reaching an optimal number (about 800) by the early 1970s. In October 1977, the first compound Crump weir was operational, and by March 1995, 25% of all 818 gauging stations were compound Crump weirs (Wessels, 1996).

In the early 1990s, DWS opted to improve the flow-gauging network by closing down almost 90 weirs that did not comply with the departmental standards. By the end of 2007, the number of operational weirs across South Africa stood at 782 of which 35% were compound Crump weirs. The remaining 65% of gauging stations are sharp-crested weirs, broad crested weirs, dams and velocity-area stations (Wessels & Rooseboom, 2009 (a)). According to DWS, there are 980 gauging stations across the country today, of which 781 are currently in operation. The number of gauging stations per weir type in SA is shown in **Figure 2.4**; this data was collected from DWS. Of the 781 operational gauging stations, 26% are compound Crump weirs.

Wessels and Rooseboom (2009 (a)) reported that velocity-area gauging stations are not extensively used in South African rivers due to the lack of skilled labour, difficulty reaching

sites and large variations in flood events resulting in changes in the cross-sectional area of the river. This method is often used in conjunction with other gauging weirs or at established abstraction weirs.



**Figure 2.4: Number of operational gauging stations in SA by weir type for 2018**

### 2.3 IMPACTS OF INACCURATE FLOW MEASUREMENTS

The development of a flow record should be carried out as accurately as possible within acceptable financial constraints. The cost of the individual steps involved in collecting flow data should thus not exceed the potential benefit of the flow record. Assessment of the potential benefit of a flow record is difficult to determine since the number of current- and future users of the record are undefined and the benefits of the record to these users is hard to quantify. It is thus useful to investigate the effects of errors in compiling a flow record and in quantifying these errors regarding infrastructure costs (Wessels, 1996).

The accuracy of flow measurements is directly influenced by the quality of the water level reading upstream of the weir. False gauge plate readings, digitising errors, incorrect pen settings, uncertainty in the gauge zero, graph processing and mechanical recorder errors are some of the causes for uncertainty in flow measurements. Mistakes in the derivation of flow from the water level readings and variations in pool depth due to sediment build-up also influence the accuracy of the flow record (Wessels, 1996).

According to Ackers et al. (1978), the total uncertainty in the water level readings using old mechanical recorders was approximately  $\pm 18$  mm. This error considered uncertainties in the gauge plate zero and readings, graph processing and mechanical equipment. **Table 2.1** shows the influence of this estimated uncertainty in water level readings on the accuracy of the calculated discharge over a Crump weir of unit length and unit pool depth. Due to the influences of human error in the development of flow records, improved accuracy in the calibration theory, especially during high flow applications, is required. The justification of these improvements can only be based on the relative potential impacts of error in the flow record as a whole (Wessels, 1996).

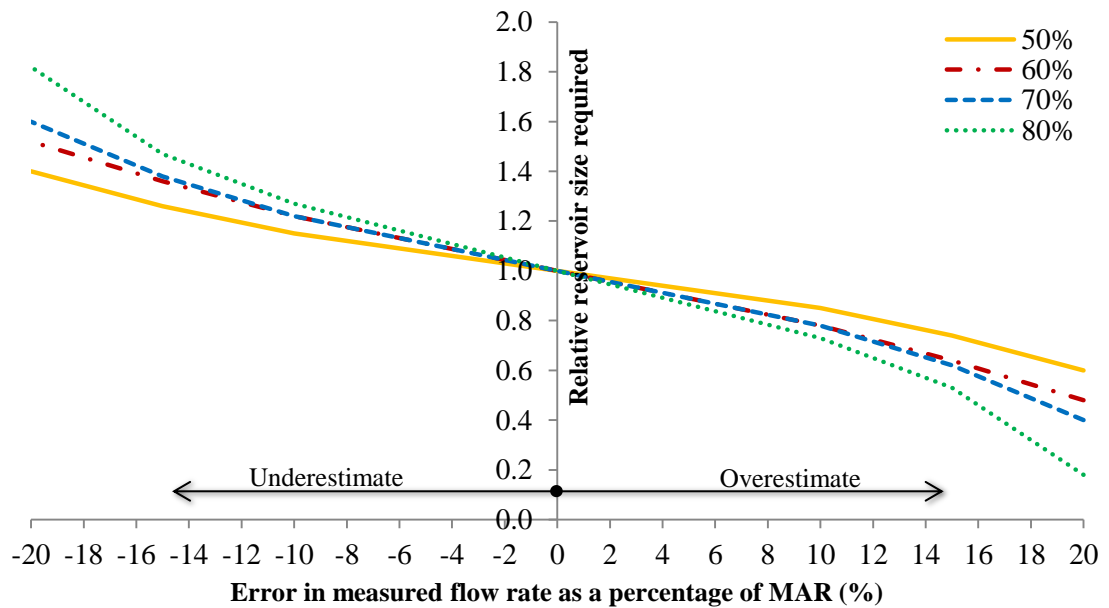
**Table 2.1: Percentage error made in discharge per unit crest length for an 18 mm overestimation in water level reading (Wessels, 1996)**

Actual Water Level, $h$ (m)	Actual Discharge, $Q$ (m <sup>3</sup> /s)	Overestimated Water Level, $h + 18$ mm (m)	Overestimated Discharge, $Q$ (m <sup>3</sup> /s)	% Error
0.10	0.063	<b>0.118</b>	0.080	<b>28.4</b>
0.20	0.178	<b>0.218</b>	0.203	<b>14.0</b>
0.30	0.331	<b>0.318</b>	0.362	<b>9.3</b>
0.40	0.514	<b>0.418</b>	0.550	<b>7.0</b>
0.50	0.726	<b>0.518</b>	0.767	<b>5.6</b>
0.75	1.368	<b>0.768</b>	1.420	<b>3.8</b>
1.00	2.161	<b>1.018</b>	2.224	<b>2.9</b>

Wessels (1996) did a study on the impacts of errors in flow-data on the sizing of a reservoir. Flow records at various sites around SA were used to calculate the reservoir size that would be required. Errors were then applied to the flow data to determine the impact on the sizing of reservoirs to meet yields of 50, 60, 70 and 80% of the mean annual runoff (MAR). The effects of varying locations and catchment sizes were accounted for by ignoring evaporation and rainfall data. **Figure 2.5** shows the results obtained. In SA nearly 90% of the available surface water is currently being utilised, therefore most reservoirs are sized to a yield of 80% of the MAR. To determine the size of a reservoir that is to yield 80% of the MAR for the case of making a 10% underestimation error in the flow data, a reservoir of 1.27 times the required size is found. In contrast, an overestimation error of 10% would result in a reservoir that is only 0.73 of the required size that is to yield 80% of the MAR.

The study concluded that an underestimation in flow rate results in the construction of unnecessarily large reservoirs causing an increase in the capital costs. The overestimation of flow rates, however, leads to the construction of smaller reservoirs that could result in

considerable losses due to shortfalls in supply (Wessels, 1996). The economic implications of this study can be extended to other infrastructures such as bridges, culverts, and dams.



**Figure 2.5: Relative reservoir size required to meet a yield of 50, 60, 70 and 80% of the MAR (Wessels, 1996)**

## 2.4 HYDRAULICS OF WEIRS

### 2.4.1 Basic flow equations

Weirs are most commonly designed to act as a control in the river channel. The flow conditions in such a river are dependent on the geometry of the structure, the approach channel and the physical properties of the water. Critical flow conditions exist at this control, and a unique discharge-head relationship occurs (Ackers et al., 1978). The phenomena of flow may be explained by three basic principles namely, the conservation of mass, energy, and momentum (Ojha et al., 2013).

**The conservation of mass:** For a controlled incompressible fluid volume, the rate of mass inflow minus the rate of mass outflow is equal to the rate of change of mass within the controlled volume. For steady, incompressible flow the mass of the fluid within the controlled volume must remain fixed. This then implies that the change of mass is zero. This is commonly referred to as the equation of continuity and can be expressed as follows:

$$\rho A_1 V_1 = \rho A_2 V_2 \quad (2.1)$$

where:

$\rho$  = density of fluid ( $\text{kg/m}^3$ )

$A_1$  = inlet area ( $\text{m}^2$ )

$V_1$  = velocity of fluid at inlet ( $\text{m/s}$ )

$A_2$  = outlet area ( $\text{m}^2$ )

$V_2$  = velocity of fluid at outlet ( $\text{m/s}$ )

**The conservation of energy:** The total energy head along a streamline that is equal to the energy per unit weight of water (the sum of the pressure, velocity, and datum heads) is constant. For ideal flow, the Bernoulli equation is applied to get the total energy head (H) as:

$$H = \frac{p}{\gamma} + \frac{V^2}{2g} + z \quad (2.2)$$

where:

$p$  = pressure ( $\text{N/m}^2$ )

$\gamma$  = unit weight of water ( $\text{kg/m}^3$ )

$V$  = velocity ( $\text{m/s}$ )

$z$  = height above datum (m)

$g$  = gravitational acceleration ( $9.81 \text{ m/s}^2$ )

The derivation of the Bernoulli equation for real flow problems depends on the information available concerning the frictional work as done by the fluid. In many practical situations, real flow problems can be analysed with the help of a modified form of Bernoulli's equation as follows:

$$\frac{p_1}{\gamma} + \frac{V_1^2}{2g} + z_1 = \frac{p_2}{\gamma} + \frac{V_2^2}{2g} + z_2 + h_L \quad (2.3)$$

where:

$h_L$  represents the secondary work done (the work done against the fluid friction and any other additional work) per unit weight of the flow while moving from position 1 to 2 along a streamline, because of fluid friction or viscosity, in the direction of flow. For an inviscid flow  $h_L = 0$ , and the total energy is constant along a streamline.

**The conservation of momentum:** When the losses in the energy equation cannot be defined, the linear momentum equation is applied and can be expressed as follows:

$$-\frac{\partial p}{\partial x} = \rho u \frac{\partial u}{\partial x} \quad (2.4)$$

where:

$p$  = pressure ( $\text{N/m}^2$ )

$x$  = distance (m)

$\rho$  = density of fluid ( $\text{kg/m}^3$ )

$u$  = velocity in the main flow direction (m/s)

## 2.4.2 Discharge equation development

Simple weirs, such as broad-crested weirs make use of the Bernoulli equation to derive an equation for the discharge over the structure. However, the discharge over irregularly shaped weirs, such as the Crump weir, cannot be determined directly from theory. The discharge equations of these weirs can be determined from the theory of dimensions by using experimental studies. It is assumed that the discharge is a function of the total head ( $H$ ), gravitational acceleration ( $g$ ), the density of water ( $\rho$ ), dynamic viscosity ( $\mu$ ), surface tension ( $\sigma$ ) and the geometric dimensions of the crest ( $x_1, x_2, x_3$ , etc.) as follows (Ackers et al., 1978):

$$Q = f(H, g, \rho, \mu, \sigma, x_1, x_2, x_3, \dots) \quad (2.5)$$

By dimensional analysis the equation can be expressed as follows:

$$C_d = \frac{Q}{\sqrt{g} H^{3/2}} = f\left(\frac{\nu}{\sqrt{g} H^{3/2}}, \frac{\sigma}{\rho g H^2}, \frac{x_1}{H}, \frac{x_2}{H}, \frac{x_3}{H}, \dots\right) \quad (2.6)$$

where:

$\nu$  = kinematic viscosity ( $\mu/\rho$ ) ( $\text{m}^2/\text{s}$ )

$C_d$  = dimensionless discharge coefficient

The second term, on the right of the relationship, depends only on the temperature of the water and can be expressed as follows:

$$\frac{\sigma}{\rho g^{1/3} \nu^{4/3}} = \text{constant}$$

The first term on the right of the relationship is the only term that includes the scale of flow and is the inverse of the Reynolds number. We know that the Reynolds number has the most significant influence during low heads and therefore we can assume the expression as follows:

$$\frac{Q}{\sqrt{g} H^{3/2}} = \left[ 1 - \left( \frac{\nu}{\sqrt{g} H^{3/2}} \right)^n \right] f\left(\frac{x_1}{H}, \frac{x_2}{H}, \frac{x_3}{H}, \dots\right)$$

If  $r$  is a constant and  $n = 2/3$  then:

$$\frac{Q}{\sqrt{g}(H-k_h)^{3/2}} = f\left(\frac{x_1}{H}, \frac{x_2}{H}, \frac{x_3}{H}, \dots\right)$$

where:

$$k_h = \frac{2}{3} \left( r^2 \frac{v^2}{g} \right)^{1/3} = \text{constant}$$

For the Crump weir, the term  $f$  is merely a constant determined by the slopes of the upstream and downstream faces (Ackers et al., 1978).

### 2.4.3 Froude number

When the velocity head becomes significant with respect to the flow depth, the discharge coefficient of the weirs varies. The Froude number ( $Fr$ ) is a dimensionless parameter that can be used to describe this ratio. For a rectangular channel with parallel flow, the Froude number can be expressed as follows:

$$Fr = \frac{V}{\sqrt{g D}} \quad (2.7)$$

where:

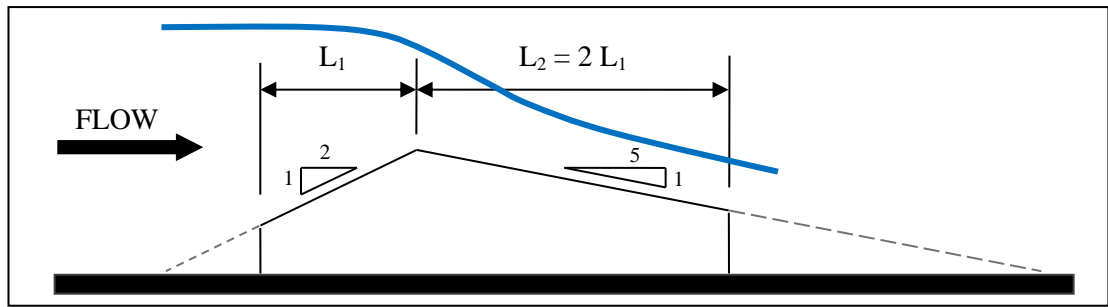
$V$  = mean flow velocity in channel (m/s)

$g$  = gravitational acceleration (9.81 m/s<sup>2</sup>)

$D$  = hydraulic depth (m)

### 2.4.4 Crump weirs

The Crump weir was developed at the Hydraulics Research Laboratory in Wallingford, England and was named after E.S. Crump who published a paper on the new type of triangular profile weir in 1952 (Ackers et al., 1978). The Crump weir has a triangular profile with an upstream slope of 1:2 and a downstream slope equal to 1:5 as shown in **Figure 2.6**. The Crump weir is a straightforwardly constructed, robust structure that is usually truncated as indicated in **Figure 2.6** to save on material costs without influencing the discharge calculations (Wessels & Rooseboom, 2009 (b)).



**Figure 2.6: Truncated Crump weir with dimensions**

The calibration of a Crump weir is formulated due to the unique relationship that exists for a Crump weir, between discharge ( $Q$ ) and the total energy head ( $H$ ). The total energy head is defined as the combination of the measured upstream water level ( $h$ ) and the velocity head component  $\left(\frac{V^2}{2g}\right)$ . There are, however, two different types of flow conditions, namely:

**Modular Flow (not submerged):**

Modular flow occurs when the upstream water level is uninfluenced by the water level downstream of the Crump crest. It is, therefore, possible to determine the flow over the weir by taking a single measurement upstream of the crest. The discharge-head relationship used to determine flow rate over a Crump weir for modular flow conditions is as follows:

$$Q = C_d \frac{2}{3} \sqrt{\frac{2}{3}} g b H^{3/2} \quad (2.8)$$

where:

$$C_d = 1.163 \left(1 - \frac{0.0003}{h}\right)^{3/2}$$

$$H = h + \frac{V^2}{2g}$$

The formulae and definition sketch parameters, shown in **Figure 2.7** are as follows:

$C_d$  = modular discharge coefficient

$b$  = width of crest perpendicular to flow

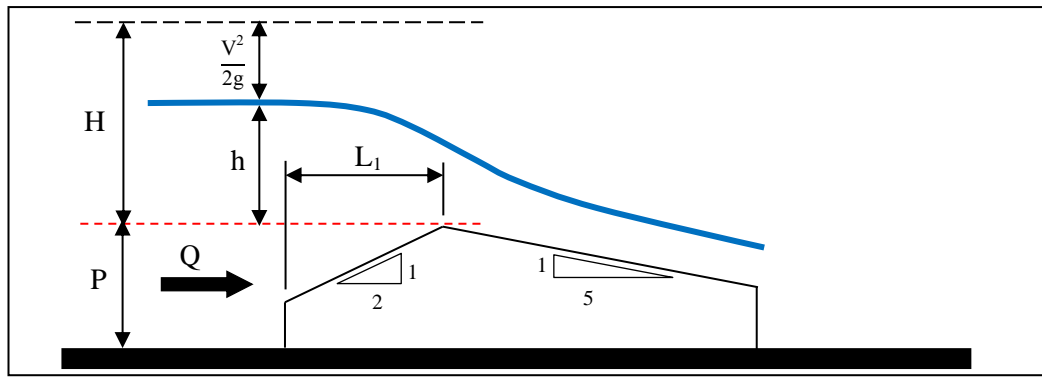
$H$  = total energy head upstream relative to the weir crest

$h$  = measured water level upstream relative to the weir crest

$V$  = approach velocity

$P$  = pool depth below crest





**Figure 2.7: Definition sketch of the Crump weir profile under modular flow conditions**

During modular flow conditions, the water upstream of the Crump weir crest flows sub-critically, obeying the fundamental relationship of cross-sectional area multiplied by the channel mean velocity. The flow approaching the weir increases in velocity due to the decrease in cross-sectional area and then flows over the crest, converting potential energy to kinetic energy. The downstream water level decreases as the water accelerates under gravity resulting in supercritical flow conditions (Beach, 1984).

**Non-Modular Flow (submerged):**

Non-modular flow occurs when the downstream water level rises above the crest level, influencing the upstream water level, see **Figure 2.8**. The discharge calculation for non-modular conditions is corrected by applying a dimensionless flow-reduction factor ( $f$ ) to the discharge-head relationship described for modular flow conditions. This factor is a function of the ratio between the total downstream energy head ( $H_2$ ) and the total upstream energy head ( $H$ ). Therefore, measuring of both the upstream and downstream water levels is necessary in order to determine the discharge over the Crump weir (Sileshi, 2009). The flow-reduction factor can be determined using the following equations:

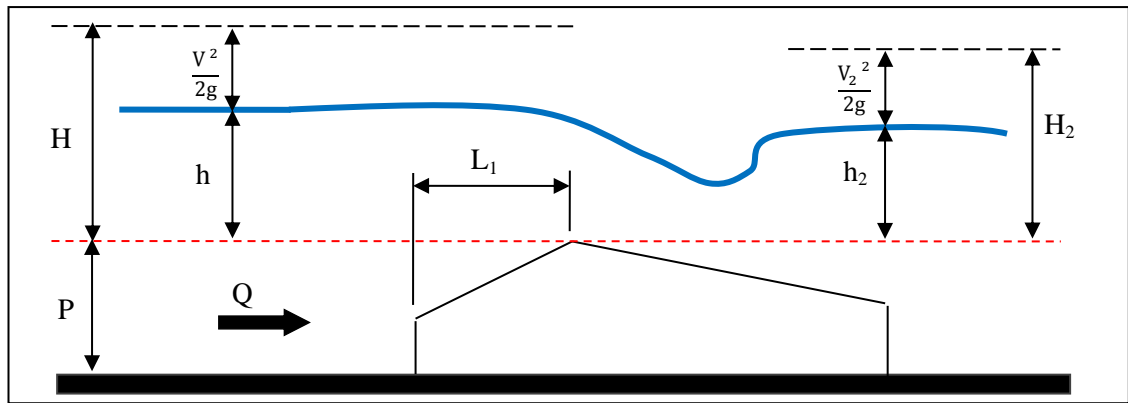
$$f = 1.00 \text{ if } \frac{H_2}{H} \leq 0.75$$

$$f = 1.035 \left[ 0.871 - \left( \frac{H_2}{H} \right)^4 \right]^{0.0647} \text{ if } 0.75 < \frac{H_2}{H} \leq 0.93$$

$$f = 8.686 - 8.403 \left( \frac{H_2}{H} \right) \text{ if } 0.93 < \frac{H_2}{H} \leq 0.985$$

where:

$H_2$  = downstream energy head relative to the Crump weir crest



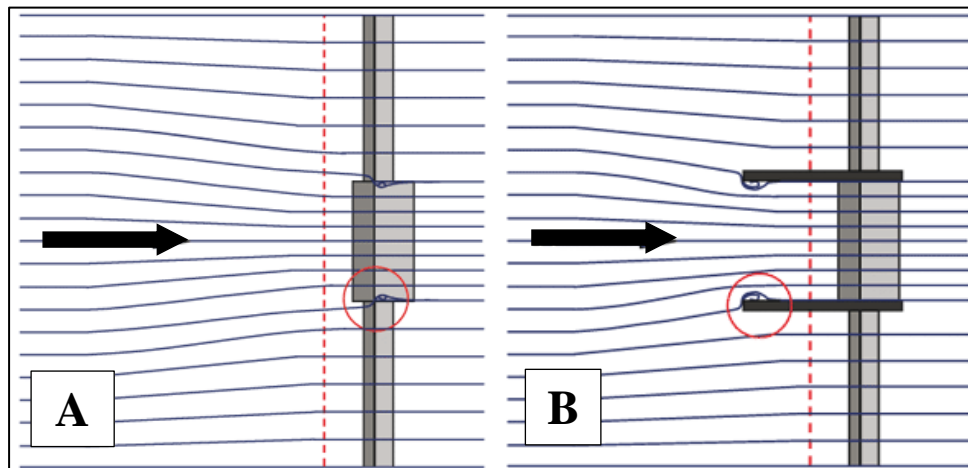
**Figure 2.8: Definition sketch for Crump weir during non-modular conditions**

The primary advantage of the Crump weir is that the discharge coefficient remains constant for modular flow conditions and is relatively insensitive to non-modular flow conditions if the downstream energy level is less than 75% of the upstream energy level (also known as the modular limit of the structure).

#### 2.4.5 Compound weirs

The SA climate results in the abrupt changes in river discharge rates varying between very high and shallow flows. The use of compound weirs has been implemented as an attempt to ensure accurate discharge calculations over a range of flow rates. Compound weirs consist of two or more weirs at different heights in parallel, built perpendicularly to the flow along a river stream. The structures are designed to allow the lower discharges to flow over the lowest weir and as discharge increases, the adjacent higher weirs systematically start operating. This allows for measuring a wide range of flow rates without significantly raising the upstream water levels (Wessels & Rooseboom, 2009 (b)).

According to the BSI 3680 standards, compound weirs are to be constructed with divider walls. Since the discharge-head relationship for Crump weirs was developed for two-dimensional flow conditions, each weir must operate independently without being influenced by adjacent weirs. The divider walls ensure parallel flow lines across the weir section where the water level is measured. When compared to compound weirs without divider walls, the flow lines are distorted across the weir section adjacent to where the weirs meet downstream of the measuring point as shown in **Figure 2.9** (water level measuring location indicated by dashed red line) (Wessels & Rooseboom, 2009 (b)).



**Figure 2.9: Flow lines over compound weirs (A) without and (B) with divider walls**

Weirs are commonly built within the known river section, with divider walls separating the different weir crests and flank walls built on the outside of the two outer crests which are then connected to the extended riverbanks using filler walls. When the flow in the river section exceeds the hydraulic capacity of the weir, the divider, flank and filler walls start to overtop, resulting in three-dimensional flow lines and flow over the filler walls. The filler walls have a rectangular cross-sectional profile, as shown in **Figure 2.10**. The flow over the filler walls is thus calculated using the discharge-head relationship for broad-crested weirs described in more detail in the subsequent section and can be defined as follows:

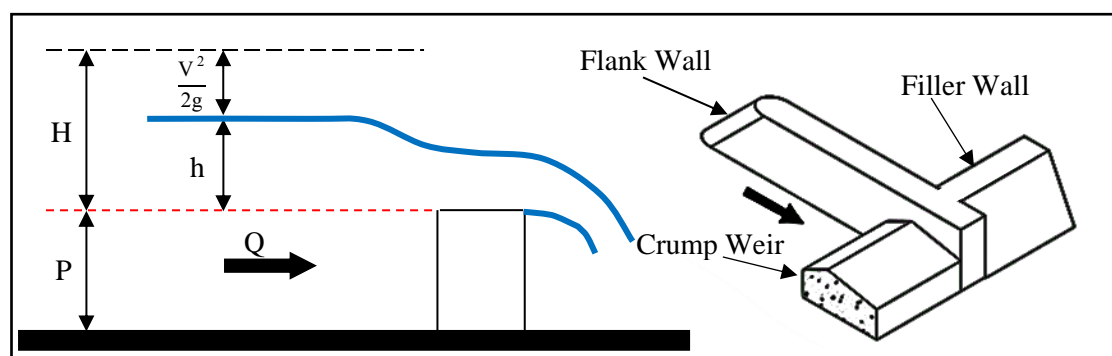
$$Q = C b H^{3/2} \quad (2.9)$$

where:

$C$  = discharge coefficient ( $\sqrt{\text{m/s}^2}$ )

$b$  = width of crest perpendicular to flow (m)

$H$  = total energy head upstream relative to the weir crest (m)



**Figure 2.10: Definition sketch of a broad-crested weir with an isometric view of the weir showing the Crump crest in relation to the flank and filler walls**

### 2.4.6 Broad-crested weirs

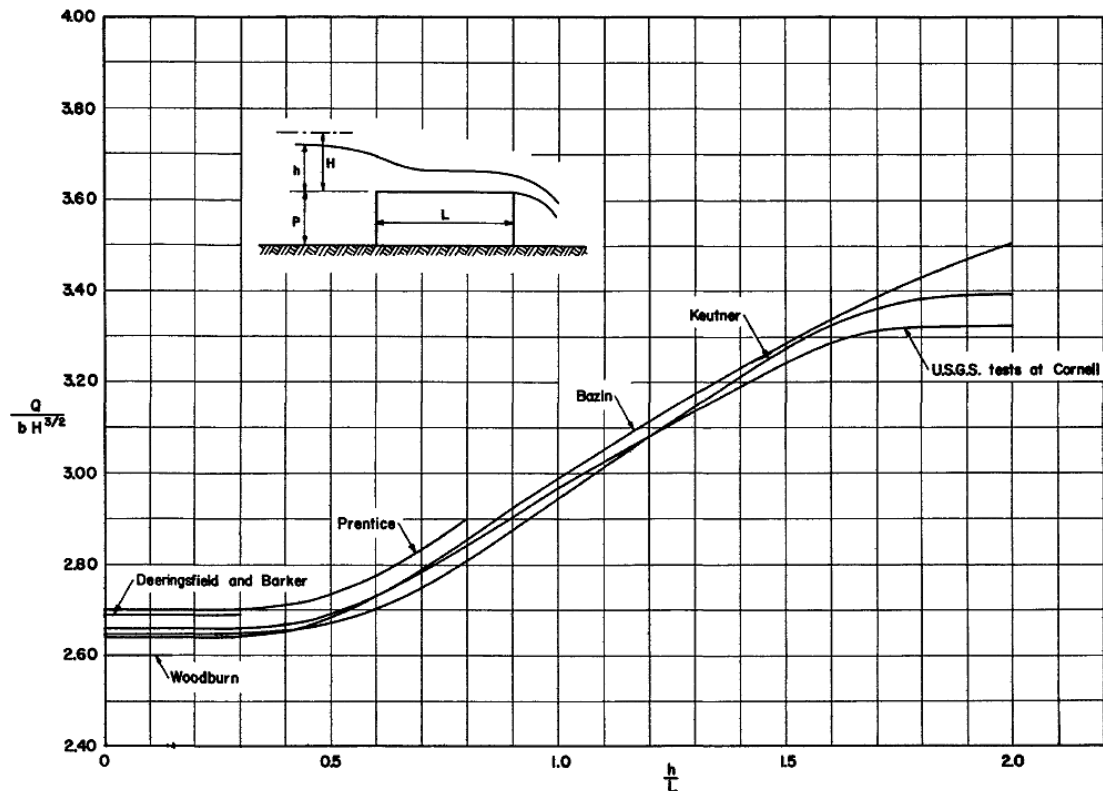
Broad-crested weirs have been researched for the past 140 years or so, which has led to a large variety of discharge calculation methods, mainly due to the disadvantage of a variable coefficient of discharge and the uncertainty of the upstream head application in various research attempts. It has been speculated that some researchers neglect the additional energy head resulting from the velocity in the channel section. Ackers et al. (1978) conducted a thorough review of the literature available by 1994. He noted the discharge coefficient as a function of various non-dimensional ratios including  $h/L$  and  $h/P$ . They indicated that Tracy (1957) and Govinda Rao and Muralidhar (1963) plotted the discharge coefficient against  $h/L$  and found no effects due to  $h/P$ . Tracy (1957) and Govinda Rao and Muralidhar (1963) looked at work done by various researchers at the time, formulating a comparison as shown in **Figure 2.11**, with:

$$C = \frac{Q}{b H^{3/2}} = C_d \sqrt{2g}$$

where:

$C_d$  = discharge coefficient

$g$  = gravitational acceleration ( $m/s^2$ )



**Figure 2.11:** Discharge coefficients for broad-crested weirs resulting from various investigations before 1957 (Tracey, 1957; Govinda Rao & Muralidhar, 1963)

Govinda Rao and Muralidhar (1963) tried to explain the variations in the results of the different investigations by looking at the influence of using the upstream water level ( $h$ ) versus the upstream energy level ( $H$ ) in calculating the discharge coefficient (see **Figure 2.12**). The problem with using the upstream energy head was that an iterative process was required since the velocity in the channel is not measured in practice. The wide disagreement between the different investigations is explained when comparing **Figure 2.11** and **Figure 2.12**.

Govinda Rao and Muralidhar (1963) then conducted their experimental tests by considering only the upstream water level in order to overcome the iterative process. They studied broad-crested weirs with a square upstream face, with  $h/L$  ratios between 0.02 and 1.9, and  $h/P$  ratios between 0.1 and 0.9. Their results plotted consistently higher in comparison with the other investigations (namely; Bazin, Keutner, Woodburn, Doeringsfield and Baker, and U.S.G.S tests at Cornell plotted in **Figure 2.11**). The discharge-head relationship used in their study can be defined as follows:

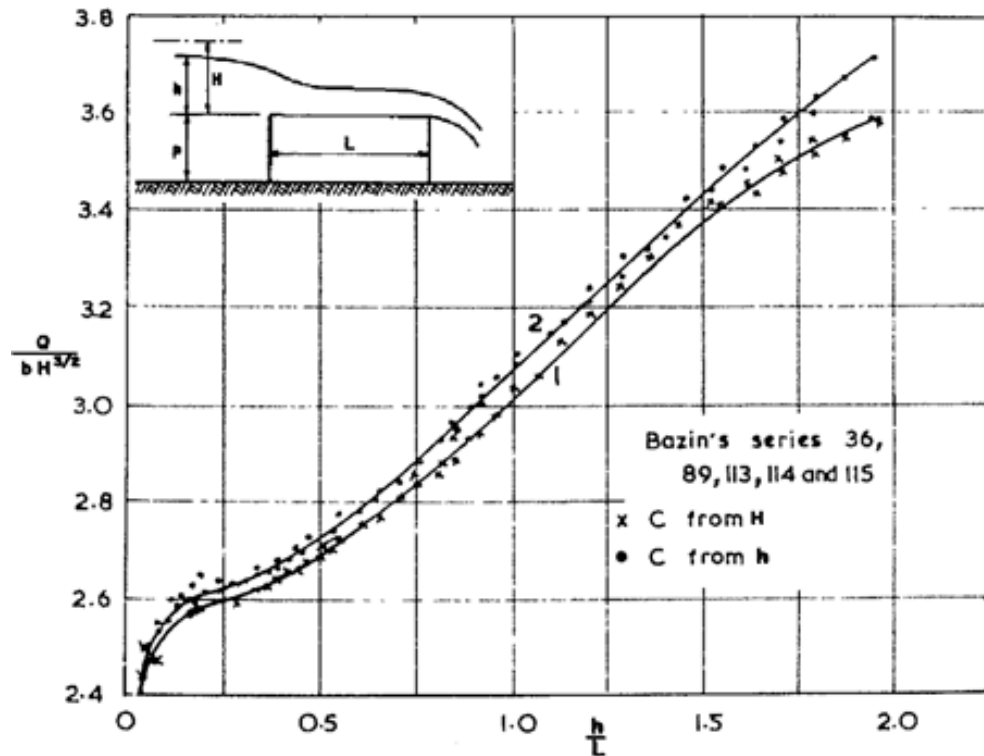
$$Q = \bar{C} b h^{3/2} \quad (2.10)$$

where:

$\bar{C}$  = discharge coefficient derived from using  $h$  ( $\sqrt{m/s^2}$ )

$b$  = width of crest perpendicular to flow (m)

$h$  = upstream water level relative to the weir crest (m)



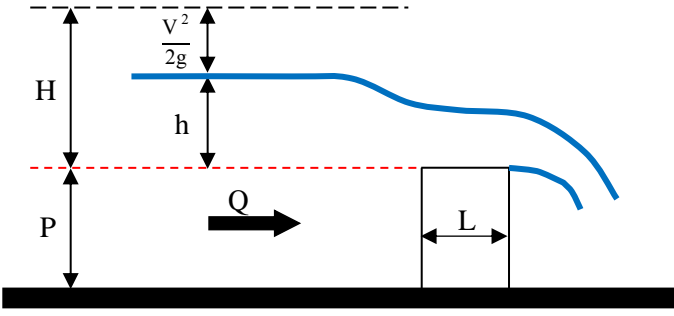
**Figure 2.12: Discharge coefficients for broad-crested weirs using the upstream water level ( $h$ ) versus the upstream energy level ( $H$ ) (Tracey, 1957; Govinda Rao & Muralidhar, 1963)**

The discharge coefficient in **Eq. 2.9** is not the same as in **Eq. 2.10**, since they are derived with different head components in the discharge-head relationship. In **Table 2.2**, a summary of the various discharge coefficient calculation methods is given, along with a definition sketch explaining the difference in the head component used by various researchers.

Govinda Rao and Muralidhar (1963) used **Eq. 2.10** to derive the discharge coefficients, **Eqs. 2.11-2.13**; they suggested that the discharge-head relationship for sharp-crested weirs be used for  $h/L$  values greater than 1.5 to 1.9. Bing (1991) compiled a guideline for the calibration of gauging stations at the DWS. He used a combination of previous research along with laboratory testing to develop the discharge coefficients, **Eqs. 2.14-2.15** with  $h/L$  values between 0 and 1.48. These equations were derived using **Eq. 2.9** and thus a single-step iteration process is required to calculate the discharge over the structure. Bing (1991) also suggested an additional correction factor for structures with shallow pool depth, namely  $H/P > 0.27$ . Hager (IAHR AIRH, 1994) also used **Eq. 2.9** to derive the discharge coefficient **Eq. 2.16** for  $H/L$  values less than 2. Since **Eq. 2.16** contains the total energy head component, a two-step iteration process is required to determine the discharge over the structure since both  $Q$  and  $H$  contain the unknown velocity component. Azimi and Rajaraatnam (2009)

derived the discharge coefficients, **Eqs. 2.17-2.19** by taking the average of the experimental observations by Bazin, Tison, Woodburn, Wakhlu, Keutner, Ramamurthy, Minnesota, Johnson and Washington (1896-2002). For  $h/L$  values less than 0.4, they found that  $\bar{C}$  was independent of  $h/L$  but varied regarding  $[h/(h+P)]$ . In contrast,  $h/L$  values between 0.4 and 2.0 were found to vary with  $h/L$  and not with  $[h/(h+P)]$ .

**Table 2.2: The various discharge coefficient calculation methods for broad-crested weirs**

Broad-Crested Weir General Equation and Definition Sketch			
$Q = C b H^{3/2} \quad (\text{Equation 2.9})$ $Q = \bar{C} b h^{3/2} \quad (\text{Equation 2.10})$ 			
Researcher	Discharge Coefficients	Equation Number	Limits
<b>Govinda Roa &amp; Muralidhar</b> (1963)	$\bar{C} = 1.656 (h/L)^{0.022}$	(2.11)	$0 < h/L \leq 0.1$
	$\bar{C} = 0.0828 (h/L) + 1.557$	(2.12)	$0.1 \leq h/L \leq 0.4$
	$\bar{C} = 0.3533 (h/L) + 1.452$	(2.13)	$0.4 < h/L \leq 1.5 \text{ to } 1.9$
<b>DWS</b> (Bing, 1991)	$C = 1.448$	(2.14)	$h/L < 0.36$
	$C = 0.2896 (h/L) + 1.347$	(2.15)	$0.36 \leq h/L \leq 1.48$
<b>Hager</b> (IAHR AIRH, 1994)	$C = 0.42 \sqrt{2g} \left[ 1 - \frac{2}{9(1+H/L^4)} \right]$	(2.16)	$0 < H/L < 2.0$
<b>Azimi &amp; Rajaraatnam</b> (2009)	$\bar{C} = 1.739 [h/(h+P)]^{0.12}$	(2.17)	$0 < h/L < 0.1$
	$\bar{C} = 1.620 \left( \frac{h}{h+P} \right)^2 - 0.6479 \left( \frac{h}{h+P} \right) + 1.517$	(2.18)	$0.1 < h/L < 0.4$
	$\bar{C} = 0.3666 (h/L) + 1.308$	(2.19)	$0.4 < h/L < 2.0$

The scope of the study presented in this dissertation does not include the improvement of the broad-crested weir discharge coefficient relationships. However, filler walls extend, perpendicularly to the direction of flow, from the flank walls to the riverbanks on either side of the structure. When the discharge in the river exceeds the hydraulic capacity, these flank walls are overtopped, and thus the flow over the wall can be calculated using the broad-crested weir relationship. In this study, the DWS discharge coefficient equations were used to quantify the portion of flow over the filler walls when the hydraulic capacity is exceeded.

### 2.4.7 Errors associated with compounded weirs

Due to the large variations of flow rates experienced in SA rivers, the DWS usually designs weirs to be compounded in order to improve the accuracy of flow measurements over a wide range of flows, compared to a single crest weir. Almost all the compound weirs, before 1988 were constructed without divider walls in order to reduce costs and prevent the adverse effects of debris being trapped in divider walls. This, however, deviates from the BSI 3680 standards, raising doubts about the accuracy of the flow measurements for these structures. After 1988, divider walls were included in the design of compound weirs. In 1996, Wessels conducted a study to test the accuracy of discharge calculations for compound weirs with- and without divider walls. Three-dimensional flow conditions near the measuring points, upstream of the compound weir, was found to affect the accuracy of the flow measurements. Wessels and Rooseboom (2009 (b)) developed correction factors for the observed errors. The following parameters cause three-dimensional flow conditions to occur (Wessels & Rooseboom, 2009 (b)):

- differences in adjacent weir heights;
- relative flow depths over adjacent weirs;
- length of adjacent weirs relative to one another; and
- flow velocities upstream of each weir.

These four parameters are influenced by one another and were thus varied in the tests in order to determine the influences on discharge accuracy. Modular flow conditions were studied, and each model configuration was tested with- and without divider walls. A summary of the results for 88 tests executed in this study are shown in **Table 2.3**; the discharge over the compound Crump weir model was calculated using the sum of the flow rates over each weir ignoring the effects of three-dimensional flow due to compounding. It was found that the models with divider walls underestimated the discharge by 4.3% because the energy loss occurs upstream of the water level measuring points, around the entrances of the divider walls, seen in **Figure 2.9**. The calculated discharge over the compound Crump weir models was overestimated for the test conditions where divider walls were omitted, see **Table 2.3**. The overestimation is as a result of the energy losses experienced downstream of the water level measuring points, where the adjacent weirs meet as shown in **Figure 2.9**.

It should be noted that the study conducted by Wessels and Rooseboom (2009 (b)) is limited to hydraulic capacity and did not take into account structures that are compounded with

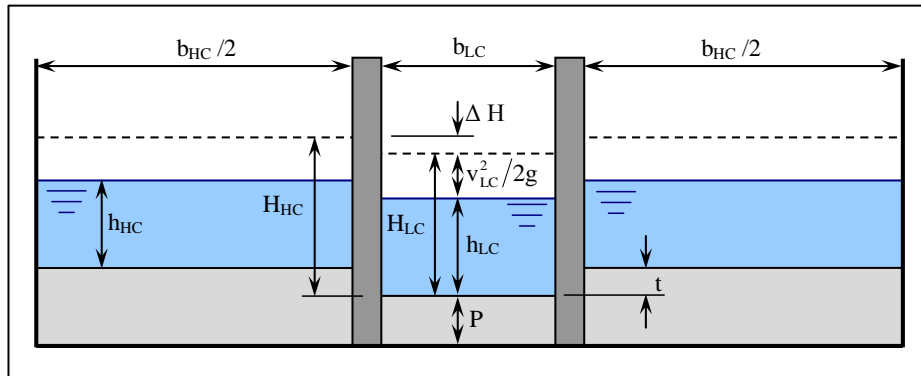


different weir shapes (i.e. broad-crested weirs in combination with Crump weirs). The study also neglects the entrance losses experienced due to the flank walls.

**Table 2.3: Errors induced by compounding weirs**

Test Condition	Nature of Error	Percentage Error	Standard Deviation
With divider walls	Underestimated	-4.3 %	-4.8 %
Without divider walls	Overestimated	+2.8 %	+2.2 %

The errors in discharge underestimation, induced by compounding with divider walls, can be corrected using the formulae developed from the study (Wessels, 1996) as shown below. **Figure 2.13** shows the definition sketch for the correction factors of compound Crump weir with divider walls.



**Figure 2.13: Definition sketch for correction factors of compound Crump weirs with divider walls (Wessels & Rooseboom, 2009 (b))**

Total discharge over the compound weir:

$$Q_T = Q_{LC} + Q_{HC} \quad (2.20)$$

where:

Discharge over the lowest weir,

$$Q_{LC} = C_d \frac{2}{3} \sqrt{\frac{2}{3}} g b_{LC} H_{LC}^{3/2} \quad (2.21)$$

Discharge over the higher weirs providing for entrance loss ( $\Delta H$ ),

$$Q_{HC} = C_d \frac{2}{3} \sqrt{\frac{2}{3}} g b_{HC} (H_{LC} - t + \Delta H)^{3/2} \quad (2.22)$$

$$\text{for, } \Delta H = k_{Cm} \left( \frac{v_{LC}^2}{2g} \right)$$

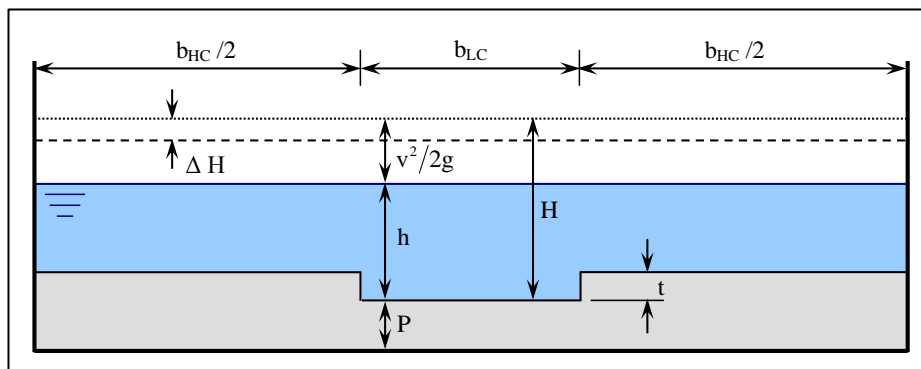
Correction factor for entrance losses,

$$k_{Cm} = -1.6465 (H_{LC}/t) + 3.156 \quad \text{if } 1 < H_{LC}/t \leq 1.75; \quad t/P \geq 0.8 \text{ and } b_{HC}/b_{LC} \geq 2.8$$

$$k_{Cm} = -0.3661 (H_{LC}/t) + 0.9153 \quad \text{if } 1 < H_{LC}/t \leq 2.5$$

$$k_{Cm} = 0 \quad \text{if } H_{LC}/t > 2.5$$

Wessels (1996) also developed the formulae for correcting the discharge overestimation errors, induced by compounding without divider walls, from the study results as shown below. **Figure 2.14** shows the definition sketch for the correction factors of compound Crump weir without divider walls.



**Figure 2.14: Definition sketch for correction factors of compound Crump weirs without divider walls (Wessels & Rooseboom, 2009 (b))**

Total discharge over the compound weir:

$$Q_T = Q_{LC} + Q_{HC} \quad (2.23)$$

where:

Discharge over the lowest weir providing for entrance loss ( $\Delta H$ ),

$$Q_{LC} = C_d \frac{2}{3} \sqrt{\frac{2}{3} g} b_{LC} (H - \Delta H)^{3/2} \quad (2.24)$$

Discharge over the higher weirs,

$$Q_{HC} = C_d \frac{2}{3} \sqrt{\frac{2}{3} g} b_{HC} (H - t - \Delta H)^{3/2} \quad (2.25)$$

for,

$$\Delta H/H = 0.0172 \quad \text{if } 0 < H/t \leq 1$$

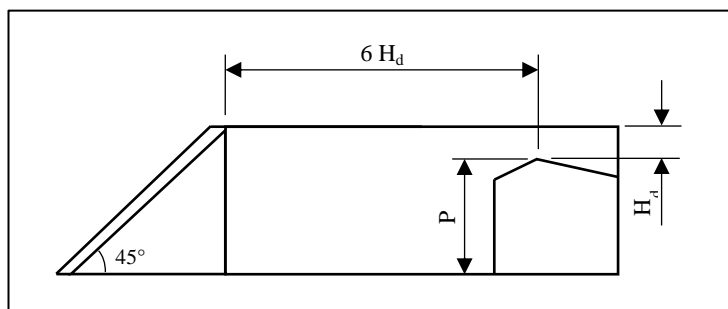
$$\Delta H/H = -0.0132 (H/t) + 0.0304 \quad \text{if } 1 < H/t \leq 2.3$$

$$\Delta H/H = 0 \quad \text{if } H/t > 2.3$$

### 2.4.8 Minimum requirements for calibration

A summary of the minimum requirements of the Froude number, divider wall dimensions, pool depth, compounding and tapping positions, is given in **Table 2.4**. Stable flow conditions upstream of the weir are achieved by limiting the Froude number to 0.4. This limit minimises variations in the approach velocity that could result in inaccurate water level readings (van Heerden et al., 1985).

The compound weir should be built with divider walls that extend upstream of the water level measuring point in order to ensure parallel flow lines (BSI 3680). Wessels and Rooseboom (2009) established the DWS standards for divider walls and suggested that they extend horizontally at a  $90^\circ$  angle upstream of the weir crest for a minimum distance of six times the design head ( $H_d$ ), which is the height of the highest measurable water level resulting from the design flow. The walls should then extend at a  $45^\circ$  angle until it reaches the floor, as shown in **Figure 2.15**, the edge of this extension should be semi-circular. A 1 m wall thickness should be used in order to avoid losses due to abrupt changes in flow lines at the entrances.



**Figure 2.15: Divider wall dimension requirements**

The discharge-head relationship for the Crump weir was developed with the upstream and downstream slopes extending to the floor of the river. Due to truncation, a minimum pool depth of  $H_d/2$  is required to ensure accurate flow measuring. The pool length should extend upstream to at least 5 times the top water-surface width ( $B$ ) of the weir section when the upstream water level equals the total design head of the structure. In order to limit the effects of compounding, the step height difference between adjacent weirs ( $t$ ) must be less than 0.5 m according to the BSI 3680 standards. The DWS, however, suggests a more conservative value of 0.3 m difference in step heights. The ratio of total energy head over the lower weir section

( $H_{LC}$ ) to the step height ( $t$ ) must be less than 2.5; otherwise, the correction factors, described above, should be applied in order to compensate for entrance losses caused by the divider walls.

According to Ackers et al. (1978), the tapping positions for the water level measurements upstream of the weir crests should be at the minimum distance of the following; (a) six times the low crest pool depth, (b) twice the total design head, or (c) twice the total head at the modular limit. In South Africa, the large river systems result in relatively high structures, therefore, the general criteria becomes twice the total design head as stated by Wessels and Rooseboom (2009 (a)).

**Table 2.4: Minimum requirements for the calibration of compound Crump weirs**

Requirements	Details
<b>Froude number</b> (van Heerden et al., 1985)	$Fr < 0.40$
<b>Divider wall dimensions</b> (Wessels & Rooseboom, 2009 (b))	-Extend horizontally at a $90^\circ$ angle -Length upstream of the weir crest $\geq 6 H_d$ -Upstream end extends at a $45^\circ$ angle until reaching the floor -1m thickness -Edge of the divider wall should be semi-circular
<b>Pool depth</b> (Wessels & Rooseboom, 2009 (b))	$P \geq \frac{H_d}{2}$ -Length of the pool should extend at least 5 times $B$ at $H_d$
<b>Compounding</b> (Wessels & Rooseboom, 2009 (b))	$t \leq 0.3 \text{ m}$ $H_{LC}/t > 2.5$
<b>Tapping position</b> (Ackers et al., 1978; Wessels & Rooseboom, 2009 (a))	$2 H_d$

## 2.5 THEORY OF PHYSICAL MODELLING

The aid of model studies has relevance in hydraulic engineering problems due to the complexity of boundary conditions and the characteristics of water that are often difficult to solve analytically. In practice, hydraulic projects are often optimised to the most efficient design by making use of model studies. The model represents a full-scale design that, known as the prototype, and can be larger, same size or smaller than the prototype. It is most common for the model to be smaller than the prototype and often, only the section being studied is model if sectioning of the prototype does not change the flow conditions. The accurate interpretation of the model study results depends on a thorough understanding of the theory of physical modelling. The laws of hydraulic similarity govern the relationship between the model and the prototype. It is, however, impossible to avoid discrepancies in

extrapolating the model results to the prototype application. These errors are referred to as scale effects and can be minimised by making use of larger physical models (Weber, 1971).

The results obtained from the physical model study can be transferred to the prototype if the two flow systems are hydraulically similar regarding geometry, kinematics, and dynamics. The following relationships are applicable (Weber, 1971):

**Geometric similarity:** This is dimensional homogeneity that can be described as the ratio of any two dimensions in the model study is the same as the corresponding ratio in the prototype, i.e.

$$\frac{(L_1)_{\text{model}}}{(L_2)_{\text{model}}} = \frac{(L_1)_{\text{prototype}}}{(L_2)_{\text{prototype}}}$$

This follows that the linear scale of the model is  $1:x$ , the scale for the model area is  $1:x^2$  and the model volume scale is  $1:x^3$ . Geometric similarity includes the scaling of boundary roughness to  $1:x$ , this is, however, difficult to achieve due to factory finishes of the materials used to construct the models. Discrepancies in this factor are often tolerated depending on the aim of the study and if the roughness in the model has the same effect on the flow conditions as that of the prototype (Weber, 1971).

**Kinematic similarity:** This involves the similarity of motion involving vector quantities and a time factor. The velocity of the water in the model at any corresponding point and time in the prototype has the same ratio, i.e.

$$\frac{(V_1)_{\text{model}}}{(V_2)_{\text{model}}} = \frac{(V_1)_{\text{prototype}}}{(V_2)_{\text{prototype}}}$$

The boundary geometry determines the patterns of the flow lines for any ideal fluid thus geometric similarity is a prerequisite to achieve kinematic similarity (Weber, 1971).

**Dynamic similarity:** The forces at any given point in the model have the same ratio and direction as the prototype, i.e.

$$\frac{(F_1)_{\text{model}}}{(F_2)_{\text{model}}} = \frac{(F_1)_{\text{prototype}}}{(F_2)_{\text{prototype}}}$$

Dynamic similarity has the same implications as hydraulic and kinematic similarity meaning that geometric similarity is the governing factor and cannot be compromised (Weber, 1971).

**Table 2.5** summarises the implications of these relationships regarding the Euler, Froude, Reynolds and Weber laws along with their scalar relationships (Weber, 1971).

**Table 2.5: Summary of model laws in conformance of the similarity laws**

Model Law	Relationship
Euler: $\left(E = \frac{V}{\sqrt{2 \Delta P / \rho}}\right)$	$\frac{V_p}{V_m} = \frac{\sqrt{\Delta P_p} \sqrt{\rho_m}}{\sqrt{\Delta P_m} \sqrt{\rho_p}}$
Froude: $\left(Fr = \frac{V}{\sqrt{g L}}\right)$	$\frac{V_p}{V_m} = \frac{\sqrt{g L_p}}{\sqrt{g L_m}}$
Reynolds: $\left(R = \frac{V L}{\nu}\right)$	$\frac{V_p}{V_m} = \frac{\nu_p L_m}{\nu_m L_p}$
Weber: $\left(W = \frac{V}{\sqrt{\sigma / L \rho}}\right)$	$\frac{V_p}{V_m} = \frac{\sqrt{\sigma_p} \sqrt{\rho_m} \sqrt{L_m}}{\sqrt{\sigma_m} \sqrt{\rho_p} \sqrt{L_p}}$

A physical model study should not be considered as a calculating machine or computer that can produce precise solutions based on the data given to them. The success of a model study depends on the skills of the person building the structure and the ingenuity used in interpreting the results. According to Weber (1971), model studies cannot compete with analytical methods and that analytical methods should be used where possible. Recent advancements in the field of mathematical models have made it possible for computers with large storage capacities to calculate the motion of fluid in a volume accurately (Weber, 1971). Model studies are generally used as a form of calibration for mathematical models.

## 2.6 COMPUTATIONAL FLUID DYNAMICS

### 2.6.1 Introduction

Computational Fluid Dynamics (CFD) is a computer-based tool that uses numerical methods to describe and analyse fluid flow, heat transfer and chemical reaction systems. CFD modelling started in the 1950s with the aim of developing an alternative for physical modelling. From the late 1960s, the development and application of CFD modelling in all forms of fluid dynamics increased exponentially thanks to the aerospace industry that profited from its use for the design and manufacturing processes of aircraft (Nshuti Kanyabujinja, 2015).

In hydraulic engineering, modelling in one-, two- or three-dimensions that use various equations and discretisation techniques has been developed for different applications. One-dimensional models are limited and cannot be used for structures with curved surfaces,

junctions, steep slopes or changes in size or shape of the channel. Two- and three-dimensional models, however, allow for the variability of flows caused by curved obstacles, obstructions, wall boundaries or other complex geometries (Nshuti Kanyabujinja, 2015). Numerical models are based on a set of partial differential equations that include the conservation of mass, momentum, and energy also known as the Navier-Stokes equation that can be simplified as follows:

$$\rho \left[ \frac{\partial \mathbf{V}}{\partial t} + (\mathbf{V} \cdot \nabla) \mathbf{V} \right] = -\nabla P + \rho \mathbf{g} + \mu \nabla^2 \mathbf{V} \quad (2.26)$$

where:

$\frac{\partial \mathbf{V}}{\partial t}$  = change in velocity over time

$\rho$  = density of fluid ( $\text{kg/m}^3$ )

$\mathbf{g}$  = gravitational acceleration ( $9.81 \text{ m/s}^2$ )

$\nabla P$  = pressure gradient ( $\text{N/m}^2$ )

$\mu$  = fluid viscosity ( $\text{kg/m}\cdot\text{s}$ )

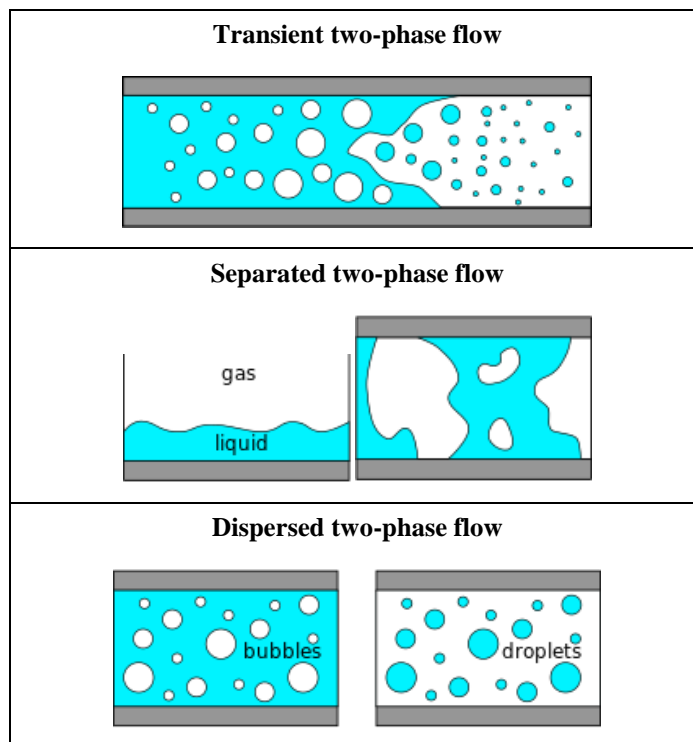
The Navier-Stokes equation describes the motion of viscous fluids in a volume and arises from applying Newton's second law of fluid motion. The first term on the left-hand side of the equation described a change in velocity with time and the second term accounts for the convective acceleration of the fluid. The right-hand side of the equation has three terms, namely; pressure term (fluid flows in the direction of the most substantial change in pressure), external forces that act of the fluid term and the velocity diffusion term that is controlled by the fluid viscosity (Chorin, 1968).

## 2.6.2 Modelling of multi-phase flows

Multi-phase segregated flow modelling refers to the modelling of the flow and interaction between different phases within the same continua, in hydraulic engineering applications, two-phase flow models are investigated (see **Figure 2.16**). A phase may be defined as a quantity of matter within a system that has its own physical properties, which is different from other phases within the same system. Different modelling approaches are applied to the various multi-phase scenarios encountered in engineering. The choice of modelling approach depends on the flow regimes and the physical properties of the phases involved. The two main multi-phase flow models approaches are the Euler-Lagrange and Euler-Euler approaches (Jesudhas, 2016).

The **Euler-Lagrange** modelling approach is used for dispersed flows such as bubbles or droplets, schematically shown in **Figure 2.16**. The continuous phase is solved using the Euler formulation (Navier-Stokes equations), and the dispersed phase is solved using the Lagrange formulation (equations of motion of individual particles). The particle trajectory and size distribution are calculated for each particle as well as the mass transfer between particles. This approach also allows for the modelling of the particle-particle and particle-phase interaction by making use of additional force terms in the motion equations. This large amount of details requires significant computing power, restricting the approach to smaller particle concentrations (Jesudhas, 2016).

The **Euler-Euler** modelling approach solves each phase with the Euler formulation of the conservation of energy, mass, and momentum. Separated two-phase flow problems are solved using this approach; the volume fraction of each phase is calculated individually using a single pressure field for both phases. This approach accounts for the mixing and separating of the phases. However, a very fine mesh is required for capturing individual particles. Unfortunately, the particle trajectory, size distribution, and interactions cannot be directly modelled. Since each phase is individually solved, this approach also requires significant computing power (Jesudhas, 2016). The need for reducing computational costs resulted in the development of the Volume of Fluid (VOF) model that was first proposed by Hirt and Nichols in 1981.



**Figure 2.16: Two-phase flow examples applicable to hydraulic engineering**



### 2.6.3 Volume of Fluid (VOF) model

The Volume of Fluid (VOF) model was developed for multi-phase flow scenarios where the phases do not interpenetrate. Each phase in the model occupies a certain volume fraction in each computational cell. The sum of the volume fractions of all the phases in each cell is one (1). Therefore, the following three conditions are possible for each cell (Fluent Inc., 2001):

- $\alpha_i = 1$ , the cell is full of the  $i^{\text{th}}$  phase;
- $\alpha_i = 0$ , the cell is empty; and
- $0 < \alpha_i < 1$ ; the cell contains a free-surface (interface between the  $i^{\text{th}}$  phase and other fluids).

The variables and properties of each cell represent a volume-averaged value and thus depend on the volume fraction of each phase in the cell (Fluent Inc., 2001). This volume-averaged value is calculated as follows:

$$V_i = \int_V \alpha_i dV \quad (2.27)$$

where:

$$\sum_{i=1}^n \alpha_i = 1$$

$V_i$  = volume of phase  $i$

$\alpha_i$  = volume fraction of phase  $i$

Additionally, all phases in the computational cell share the same velocity and pressure field. Therefore, a single set of transport equations is used to describe the mass and momentum of all the phases (Spence, 2014). This variation of the Euler-Euler multi-phase flow model significantly reduces the computing power required to solve numerical models without compromising the engineering accuracy of the models (Jesudhas, 2016). For a two-phase model example, with subscripts 1 and 2 and if the second phase is being monitored, the density of each computable cell is calculated as follows:

$$\rho = \alpha_2 \rho_2 + (1 - \alpha_2) \rho_1 \quad (2.28)$$

All other fluid properties are also calculated in the same way (Fluent Inc., 2001). A more generic calculation of the volume-averaged value for density and viscosity of the  $i^{\text{th}}$  phase are as follows:

$$\rho = \sum_i \rho_i \alpha_i \quad \text{and} \quad \mu = \sum_i \mu_i \alpha_i$$

The conservation equation is solved for the volume fraction as follows:

$$\frac{\partial}{\partial t} \int_V \alpha_i dV + \int_S \alpha_i \mathbf{u} \cdot \mathbf{n} dA = \int_V \left( S_{\alpha_i} - \frac{\alpha_i D \rho_i}{\rho_i} \frac{D}{Dt} \right) dV \quad (2.29)$$

where:

$S_{\alpha_i}$  = source/sink of the  $i^{\text{th}}$  phase

$\frac{D \rho_i}{Dt}$  = material derivatives of the phase densities

The standard discretisation schemes of the convective term ( $\int_S \alpha_i \mathbf{u} \cdot \mathbf{n} dA$ ) results in the smearing of the interface between the phases (Jesudhas, 2016). A compression term, called the sharpening factor ( $C_\alpha$ ) is introduced to reduce the numerical diffusion of the simulation. This compression term is added to the volume fraction equation as follows:

$$\nabla \cdot [v_{c_i} \alpha_i (1 - \alpha_i)]$$

where:

$$v_{c_i} = C_\alpha |u| \frac{|\nabla \alpha_i|}{|\nabla \alpha_i|}$$

The sharpening factor is a value between zero and one ( $0 < C_\alpha < 1$ ) and  $u$  is the velocity of the fluid being monitored. If the sharpening factor is zero (0), no reduction in numerical diffusion is seen, however, if the value is one (1), the reduction in numerical diffusion results in a very sharp interface between the phases. The compression term is only applied to a thin region close to the interface between the phases. The solution is thus unaffected by this factor outside of the free surface but should be applied with caution to prevent non-physical alignment of the interface (Jesudhas, 2016).

#### 2.6.4 Overview of STAR-CCM+

The STAR-CCM+ software is used in this study to perform the numerical analyses of some of the physical model layouts (explained later). CD-Adapco initially developed the software as an attempt to allow users to develop simulations using lightweight computers (laptops or small desktops) and then doing the computationally expensive math on a remote supercomputer. The STAR-CCM+ software was released in 2004 and in 2006, STAR-CCM+ became part of the Siemens PLM family. Commercially available software has proprietary source code requiring the user to verify the results using a physical model study. The user rarely has the capabilities of modifying the source code to benchmark the simulation, so this cannot be a limitation (Spence, 2014).

The STAR-CCM+ software provides multiple options for solving the Navier-Stokes equations. For free surface flow models, the Reynolds-Averaged Navier-Stokes (RANS) method is used. Other methods include the Large Eddy Simulations method, the Detached Eddy Simulations method, and the inviscid potential flow method. The three classes of **Turbulence Modelling** available in STAR-CCM+ are the Spalart-Allmaras, K-Epsilon and K-Omega models. For free surface flow modelling, the K-Epsilon (**k-ε**) model, as introduced by Jones and Launder (1972), is used. Two transport equations are solved for the two turbulence quantities. The transport equation for **k** is as follows:

$$\frac{\overline{D}k}{\overline{D}t} = \nabla \cdot \left( \frac{v_T}{\sigma_k} \nabla k \right) + \overline{P} - \varepsilon \quad (2.30)$$

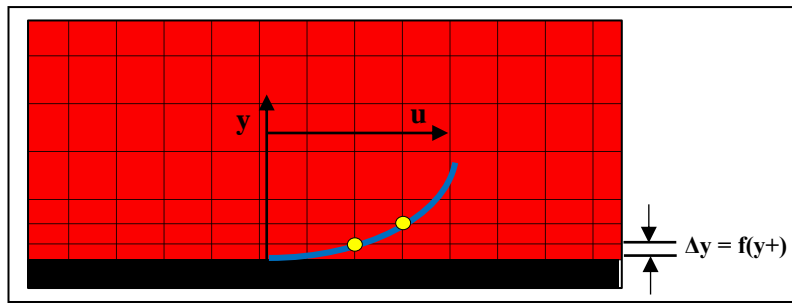
Moreover, the transportation equation for  $\varepsilon$  is:

$$\frac{\overline{D}\varepsilon}{\overline{D}t} = \nabla \cdot \left( \frac{v_T}{\sigma_\varepsilon} \nabla \varepsilon \right) + C_{\varepsilon 1} \frac{\overline{P}_\varepsilon}{k} - C_{\varepsilon 2} \frac{\varepsilon^2}{k} \quad (2.31)$$

where the turbulent viscosity is:

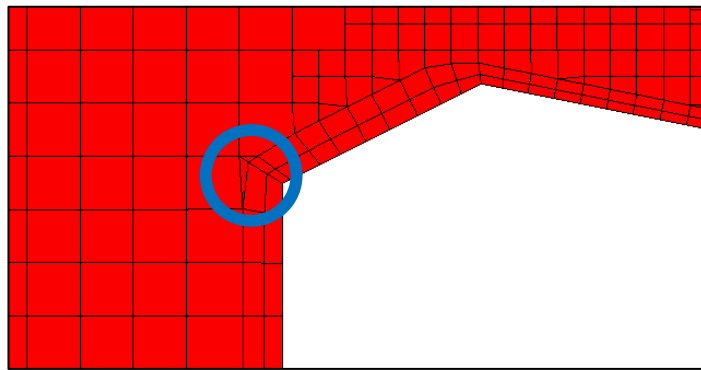
$$v_T = \frac{C_\mu k^2}{\varepsilon} \quad (2.32)$$

STAR-CCM+ combines the **k-ε** model with the two-layer approach, allowing the model to be applied in the sub-layer. The turbulent dissipation rate ( $\varepsilon$ ) and the turbulent viscosity ( $\mu$ ) are functions of wall distance in the layer next to the wall. The turbulent dissipation rates in the near-wall layer are blended smoothly with the values computed far from the wall. This is achieved by considering the  $y^+$  values. The  **$y^+$  value** is a non-dimensional distance from the wall to the first mesh node, as shown in **Figure 2.17**. To use a wall treatment approach for a specific turbulence model, the  $y^+$  values need to be within a certain range. Flows with very high Reynolds numbers (typically aircraft, ships, etc.) will experience a logarithmic boundary layer that extends to several thousand  $y^+$  values, whereas flows with a low Reynolds number (turbine blades) may have upper limit  $y^+$  values of as little as 100 (LEAP Australia, 2014). The turbulence approach used for free surface flow models is the "realizable k-epsilon two-layer" model approach that allows for an all  $y^+$  wall treatment. The all  $y^+$  wall treatment attempts combine the high  $y^+$  wall treatment for high Reynolds numbers and the low  $y^+$  wall treatment for low Reynolds number.



**Figure 2.17: Definition sketch for the  $y^+$  wall treatment**

The software also provides the user with various meshing topologies, namely; polyhedral, cylindrical, trimmed-hexahedral and tetrahedral. STAR-CCM+ uses the **Prism Layer Mesher** as a single tool to solve for the boundary layer near non-slip walls regardless of the type of volume mesh topology chosen (Spence, 2014). **Figure 2.18** shows the resulting cells from trimming a tetrahedral volume mesh around the boundary layer of a Crump weir using the prism layer mesher.



**Figure 2.18: Prism layer meshing of Crump weir boundary**

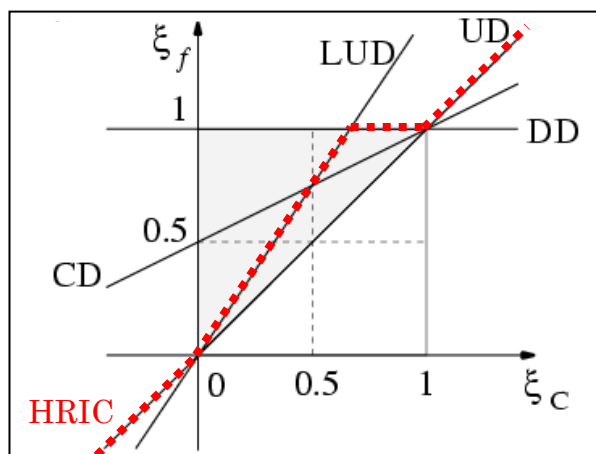
The software allows for local refinement of the mesh by making use of specified refinement volumes that range from cylinders to quadrilaterals and even arbitrary shapes imported in a suitable CAD format. The software automatically meshes the volume surrounding the user-specified refinement, saving a significant amount of time when compared to manual meshing approaches (Spence, 2014).

The **Trimmer Mesher** approach, used in the software, easily accommodates arbitrary geometry in free-surface flow modelling to produce a high-quality mesh. However, in some cases, the combination of geometry, volume mesh, and prism layer thickness results in the trimming of outer volume cells and causes a jump in cell size (see trimmed cells circled in blue in **Figure 2.18**). The trimmer mesher requires a mesh base size that is a power of two (2)

of the cell size specified around the free surface. The cell size within the refined volume will be a factor of two of the base size nearest to the specified value. The trimmer only permits the increasing and decreasing of cell sizes by a factor of two thus the aspect ratio is limited to a power of two (Spence, 2014).

STAR-CCM+ uses the VOF model for solving free surface flows. The VOF model assumes that the various fluid phases are immiscible. An essential quality of immiscible fluid phase mixtures, such as air and water, is that a sharp interface always separates the phase components. The software makes use of the **High-Resolution Interface Capturing (HRIC)** scheme to mimic the convective transport of the phase components suitable for tracking sharp interfaces. Simple higher-order schemes, such as the central differencing (CD) or linear upwind differencing (LUD) schemes, fail to approximate large spatial discrepancies of phase volume fractions, which are best represented by the unit step function (Heaviside). **Figure 2.19** shows the normalised variable diagram (NVD) for analysing the limit properties of the LUD, CD, downwind differencing (DD), and upwind differencing (UD) schemes. The HRIC scheme (dashed and highlighted in red) is based on the NVD shown in **Figure 2.19**. The normalised face value ( $\xi_f$ ) for the HRIC scheme is calculated as follows:

$$\xi_f = \begin{cases} \xi_C & \text{if } \xi_C < 0 \\ 2\xi_C & \text{if } 0 \leq \xi_C < 0.5 \\ 1 & \text{if } 0.5 \leq \xi_C < 1 \\ \xi_C & \text{if } 1 \leq \xi_C \end{cases}$$



**Figure 2.19: Normalised Variable Diagram (NVD) (STAR-CCM+, 2017)**

The normalised face value ( $\xi_f$ ) is corrected to consider the amount of one fluid that can be transferred from one cell to the next, during a time-step. The amount of one fluid available in the receiving cell should always be less than or equal to the amount available in the donor

cell; this is known as the availability criterion (STAR-CCM+, 2017). The correction to  $\xi_f$  is made by calculating the local convective Courant number as follows:

$$Cu = \Delta t \sum_{i=1}^n \frac{u_{xi}}{\Delta x_i} \leq C_{\max} \quad (2.33)$$

where:

$u$  = velocity of the fluid

$\Delta t$  = solution time step

$\Delta x$  = length of the interval (or cell size)

$C_{\max} = 1$  (this is so that less than or all the available fluid in the donor cell can be transferred to the receiving cell within one time-step without jumping cells)

The upper ( $Cu_u$ ) and lower ( $Cu_l$ ) limit of the Courant number are by default 1 and 0.5 respectively. These limits are introduced to control the blending of the HRIC and UD schemes depending on the Courant number. STAR-CCM+ uses the HRIC scheme for Courant numbers less than the lower limit, a blend of the HRIC and UD schemes for Courant numbers between the limits and the UD scheme for Courant numbers higher than the upper limit. This correction is applied to the normalised face value as follows:

$$\xi_f^* = \begin{cases} \xi_f & \text{if } Cu < Cu_l \\ \xi_C + (\xi_f - \xi_C) \frac{Cu_u - Cu}{Cu_u - Cu_l} & \text{if } Cu_l \leq Cu < Cu_u \\ \xi_C & \text{if } Cu_u \leq Cu \end{cases}$$

Blending is done in cases experiencing a considerable time variation of the free surface shape for a time-step that is too large to determine the details of the free surface. Smaller values of  $Cu_u$  and  $Cu_l$  help to converge the solution for these cases by activating the UD scheme sooner and stabilising the calculations. The interface is, however, less sharp in regions with large  $Cu$  numbers. For steady-state solution problems, the  $Cu_u$  and  $Cu_l$  values should be large to ensure the use of the HRIC scheme regardless of the time-step selected (STAR-CCM+, 2017).

The STAR-CCM+ software provides the user with a wide range of **post-processing** tools to analyse and visualise the simulation results. These include point and line probes, cutting planes, 2D line plots, 2D vector plots, and 3D scalar plots. Comparisons with other simulations, such as physical models are achieved by importing reference data from the STAR-CCM+ simulation in tabular form. It is also possible to create user-defined variables and field functions for the monitoring and recording of these variables at each time step. This allows the user to observe the convergence of the defined variables throughout the simulation without needing to save the entire flow field at every time step (Spence, 2014).

### 2.6.5 Closing

Over time, CFD simulating has developed from a mathematical tool to a multi-disciplinary tool that branch into almost every field of fluid dynamics. It assists in the analysis of fluid mechanics and its impacts on the structures over which water flows and is used in the engineering to optimise new designs before they are implemented. CFD modelling gives insight into flow patterns, mass and heat transfer, flow separation, and air entrainment improving the general understanding of the hydraulics field. It can also be used to reveal complex features that could not be achieved by physical modelling and extends the modelling capabilities to dangerous experiments without increasing the risk of injury. CFD modelling is a useful tool for the design of hydraulic structures; however, caution has to be taken when applying the results without some form of validation.

Numerical and physical model studies should not be considered capable of producing precise solutions since the output is directly based on the accuracy of the data input. Physical model studies are generally used as a form of calibration for numerical modelling. The purpose of using numerical modelling in this study is highlighted by the complexity of quantifying the effects of three-dimensional flow lines induced by the overtopping of the divider and flank walls. This study aims to determine to what extent numerical modelling can be used to investigate different compound Crump weir layouts.

### 3 EXPERIMENTAL WORK

This chapter discusses the experimental work that was undertaken for the study. The physical model and experimental procedure are described in detail along with an explanation of the calibration of the flow rate readings given by the magnetic flow meter. The numerical model set-up in the computational fluid dynamics software (CFD), STAR-CCM+ is also discussed.

#### 3.1 INTRODUCTION

Compound Crump weirs are rated up to hydraulic capacity using the discharge-head relationships that are currently available in the literature. Indirect methods for determining discharge during high flow rates are then used to rate the structure beyond its capacity. The results obtained from the indirect methods at high flow rates can only be trusted if the transition from the rating of the structure within its capacity to the rating during complete submergence, is accurately estimated. The uncertainties that exist in the rating of structures during flow rates beyond the hydraulic capacity of a compound Crump weir is addressed in this study.

The current discharge-head relationships of Crump weirs assume parallel flow lines are maintained within the confinement of the channel. However, during the overtopping of the structure (or flow rates exceeding the hydraulic capacity), three-dimensional flow lines are present due to the influence of the divider walls. It can be assumed that when the structure is completely submerged, the influence of the structure becomes insignificant and parallel flow lines are nearly fully restored.

To investigate the limitations of the discharge-head relationship of the Crump weir when compounded and operating under high flow regimes, a physical model representing a typical compound Crump weir had to be constructed. The model was built at the Department of Water and Sanitation (DWS) hydraulic laboratory situated in Pretoria West, South Africa. The minimum requirements for the calibration of weirs were set out in **Section 2.4.8** and were adhered to when designing the compound Crump weir model, to maintain consistency with previous studies. Due to the complex nature of designing weirs to measure discharge in rivers, the physical model design is site-specific, accounting for laboratory limitations.



The critical limitation of the DWS hydraulic laboratory is the flow rate and flow volume that can be supplied by the centrifugal pumps. A 100 m<sup>3</sup> underground sump limits the flow rate and stability of flow being supplied by the pumps. The laboratory has three centrifugal pumps that pump water to a six-metre-high constant head tank and can deliver a maximum constant flow rate of 220 l/s. The constant head tank is fitted with a 300 mm steel discharge pipe that diverts the excess water from the constant head tank to the underground sump. A 250 mm steel pipeline supplies water from the constant head tank to the physical model. The flow rate to the model is then regulated using butterfly valves and verified by a magnetic flow meter fitted to the supply pipe. A 60 m<sup>2</sup> area in the laboratory is reserved for the University of Pretoria to conduct model testing, shown in **Figure 3.1**.

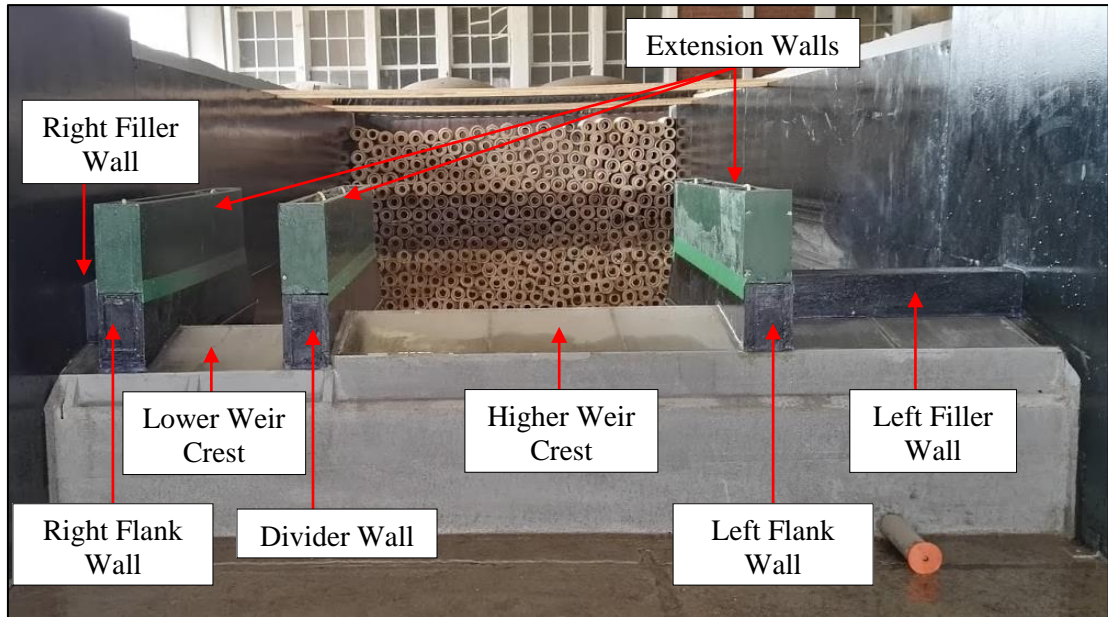


**Figure 3.1: Allocated model space for the University of Pretoria**

### 3.2 MODEL DESIGN AND DIMENSIONS

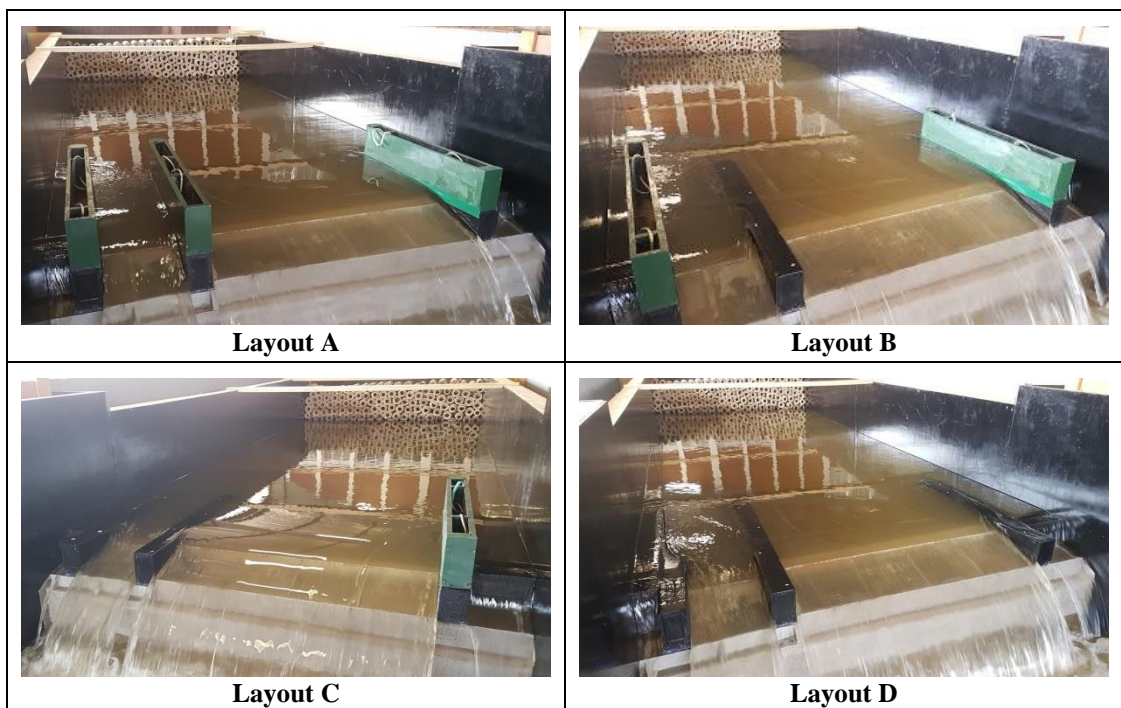
Due to the limited flow capacity of the laboratory, it was decided to model a typical compound Crump weir, consisting of two Crump weir crests (a lower and a higher crest) with a divider wall between the two crests, flank walls on the outside of the crests and filler walls extending to the channel walls, as shown in **Figure 3.2**.

The width of the lower Crump ( $B_L$ ) was kept constant while the width of the higher Crump ( $B_H$ ) was varied in order to model different  $B_H:B_L$  ratios. The design head ( $H_d$ ) of the model was kept constant throughout the study, during higher flows, this design head is exceeded, resulting in the overtopping of the filler walls and cross-flow over the divider and flank walls. The model was designed with a limited hydraulic capacity, to allow for sufficient overtopping of the divider, flank and filler walls. It was thus decided to limit the hydraulic capacity so that the water levels above the divider walls would be at least  $1 \times H_d$  (design head) at the maximum flow rate.



**Figure 3.2: Physical model components**

The extension walls indicated in green in **Figure 3.2** were used to prevent cross-flow over the divider and flank walls. They were then systematically removed with the anticipation of quantifying the influences of each component on the observed water levels. The model can thus be divided into four layouts, namely Layouts A, B, C and D shown in **Figure 3.3**. In Layout D all the extension walls are removed resulting in a model similar to the natural occurrence in the field.



**Figure 3.3: The four layouts being modelled**

**Figure 3.4** shows photographs of the constructed physical model along with the various components required for the experimental work. The allocated model space consists of a 3 m wide channel that had to be reduced in order to meet the design head requirements of the model. Shutter boards were used to reduce the channel size to 1.865 m, as shown in **Figure 3.4**. The centrifugal pumps (shown in the left corner) supplies the flow rates required for the experiment and are in the pump room behind the model. Shown in the right corner are the flow-stabilising pipes that help to dissipate the excessive turbulence produced by delivering the flow rate to the model. This dissipation of energy allows parallel flow lines to enter the model testing space and to achieve a uniform cross-sectional velocity distribution.

**Table 3.1** shows the dimensions of the physical model and compares them with that of the prototype (real-world dimensions). The physical model dimensions are shown in the construction drawings (side and top views) in **Figure 3.5** and should be considered in conjunction with **Table 3.1**.

**Table 3.1: Dimensions of the physical model**

Component	Symbol	Model Dimensions	Real-World Dimensions
Lower Crump weir pool depth	$P_L$	427 mm	4.27 m
Higher Crump weir pool depth	$P_H$	457 mm	4.57 m
Divider and flank wall widths	-	100 mm	1.00 m
Right filler wall width	$FW_R$	97 mm	0.97 m
Design head	$H_d$	118 mm	1.18 m
Lower Crump weir crest width	$B_L$	308 mm	3.08 m
<b><math>B_L:B_H = 1:4.1</math></b>			
Higher Crump weir crest width	$B_H$	1266 mm	12.66 m
Left filler wall width	$FW_L$	235 mm	2.35 m
<b><math>B_L:B_H = 1:3.0</math></b>			
Higher Crump weir crest width	$B_H$	925 mm	9.25 m
Left filler wall width	$FW_L$	575 mm	5.75 m
<b><math>B_L:B_H = 1:2.0</math></b>			
Higher Crump weir crest width	$B_H$	612 mm	6.12 m
Left filler wall width	$FW_L$	890 mm	8.90 m
<b><math>B_L:B_H = 1:1.0</math></b>			
Higher Crump weir crest width	$B_H$	310 mm	3.10 m
Left filler wall width	$FW_L$	1193 mm	11.93 m

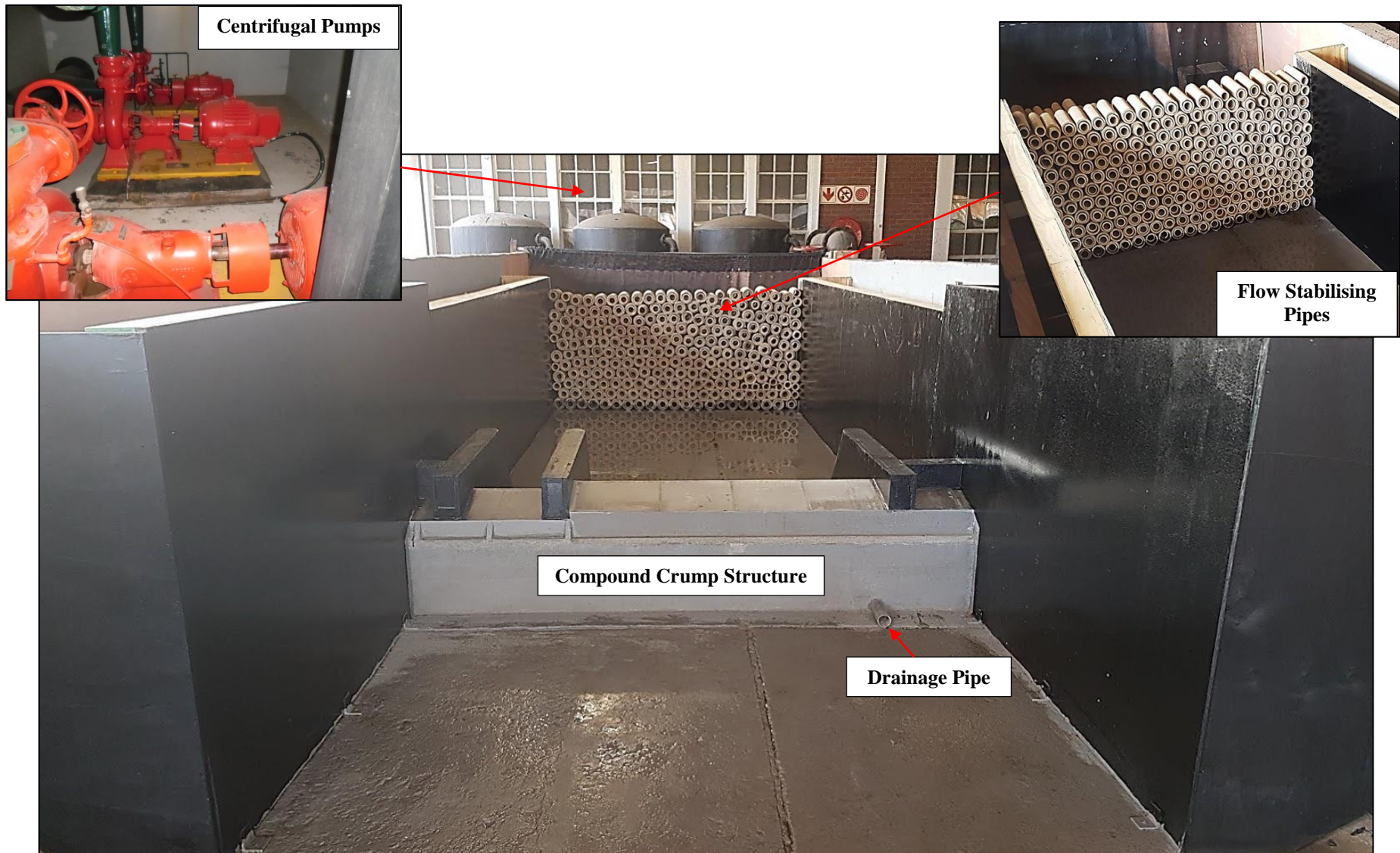


Figure 3.4: Photos of physical model layout

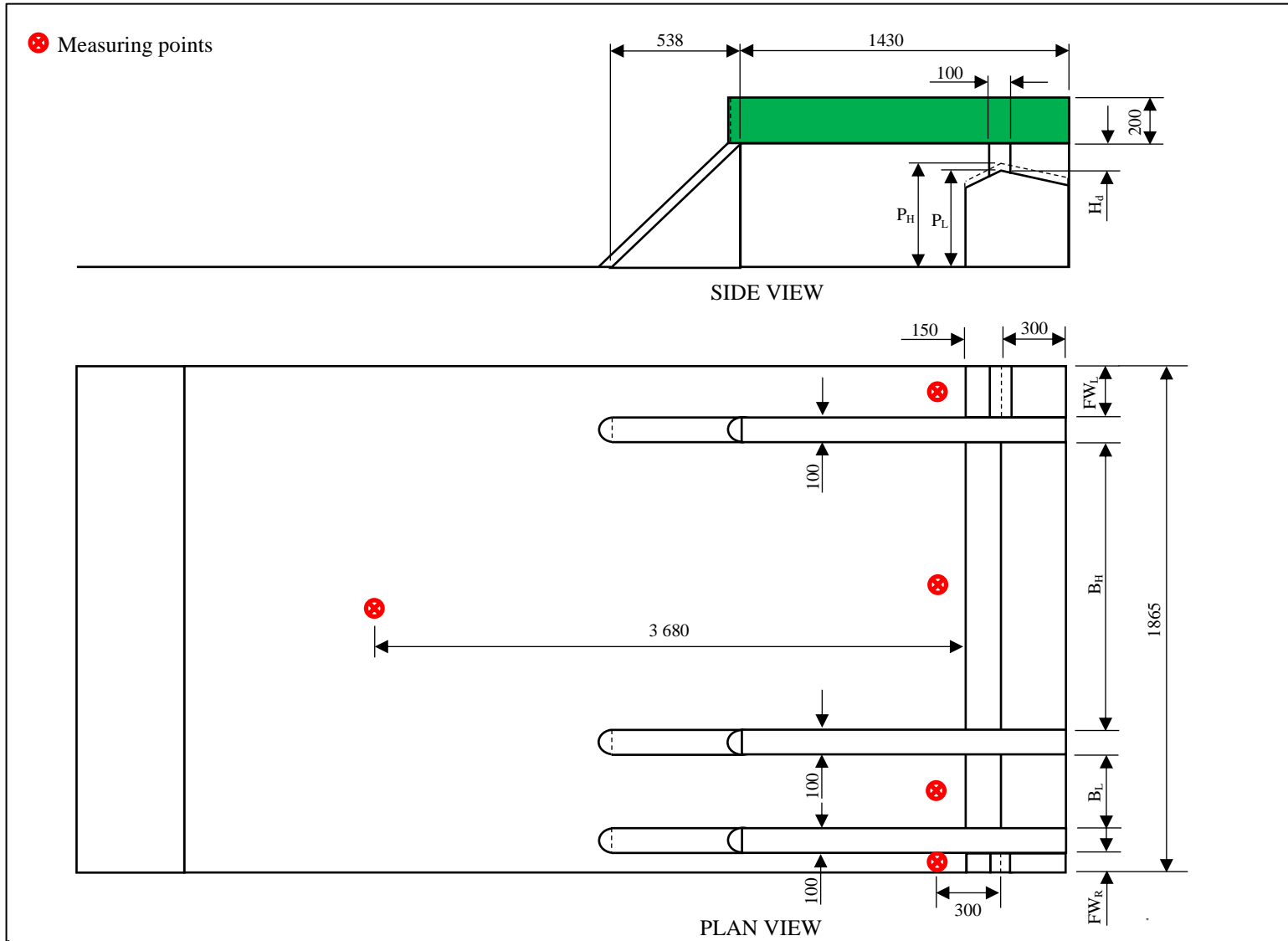
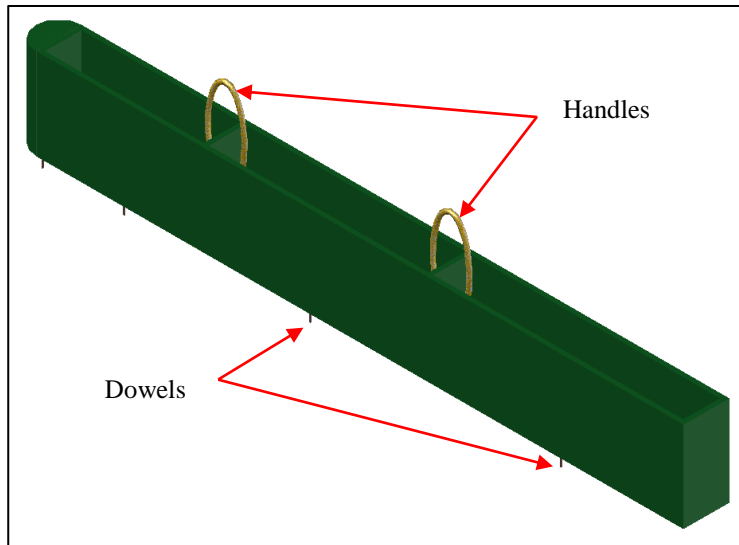


Figure 3.5: Physical model dimensions

The extension walls were designed to be hollow in order to create space for handles, which would be used to remove the walls for the different layouts easily. Inner wall spacers were used to keep the box shape and doubled as the base for the handles. Holes were then drilled through the spacers and ropes were strung through the holes functioning as handles, as seen in **Figure 3.6**. The extension walls were designed to be kept in place (on top of the divider and flank walls) by using dowels that would match with drilled holes on the divider and flank walls.



**Figure 3.6: Design of removable extension walls**

Point gauges are used to measure the water levels in a model study. If the layout of the model requires more than one measuring point, the point gauges are coupled with stilling wells. These wells are installed on the outside of the modelled river channel; a hole is then drilled through the channel wall to feed a pipe from the stilling well to the intended point of measurement. The water in the stilling well rises to the same level as the predetermined measuring point. It is also recommended that the connecting pipe be  $<4\%$  the diameter of the stilling well in order to compensate for water level fluctuations over time, if this is not possible, multiple point gauge readings should be taken over a short time interval and the average of these readings should be used in the results evaluation phase (USBR, 1997).

**Figure 3.7** shows a photograph of the point gauge and stilling well combination that was used in the model study. The point gauges have an accuracy of 0.1 mm and consist of a ruler bar, an adjustment knob, a zero indicator and a scale section. The point gauge in the photograph on the right reads 561.6 mm.



**Figure 3.7: Photograph of stilling well and point gauge**

### 3.3 EXPERIMENTAL PROCEDURE

The experimental procedure consisted of two main parts, the calibration of the model input flow rates and the execution of the physical model study. At the DWS laboratories, the flow supplied by the centrifugal pumps is measured using a magnetic flow meter. Additionally, a standardised Crump weir is available for the calibration of the flow meter. The calibration weir, shown in **Figure 3.8** is 547.5 mm wide with a design head of 400 mm, allowing for the measurement of the full range of flows supplied by the centrifugal pumps. The flow rate over the calibration weir is calculated using an upstream water level measurement.



**Figure 3.8: Calibration weir at DWS hydraulic laboratory**

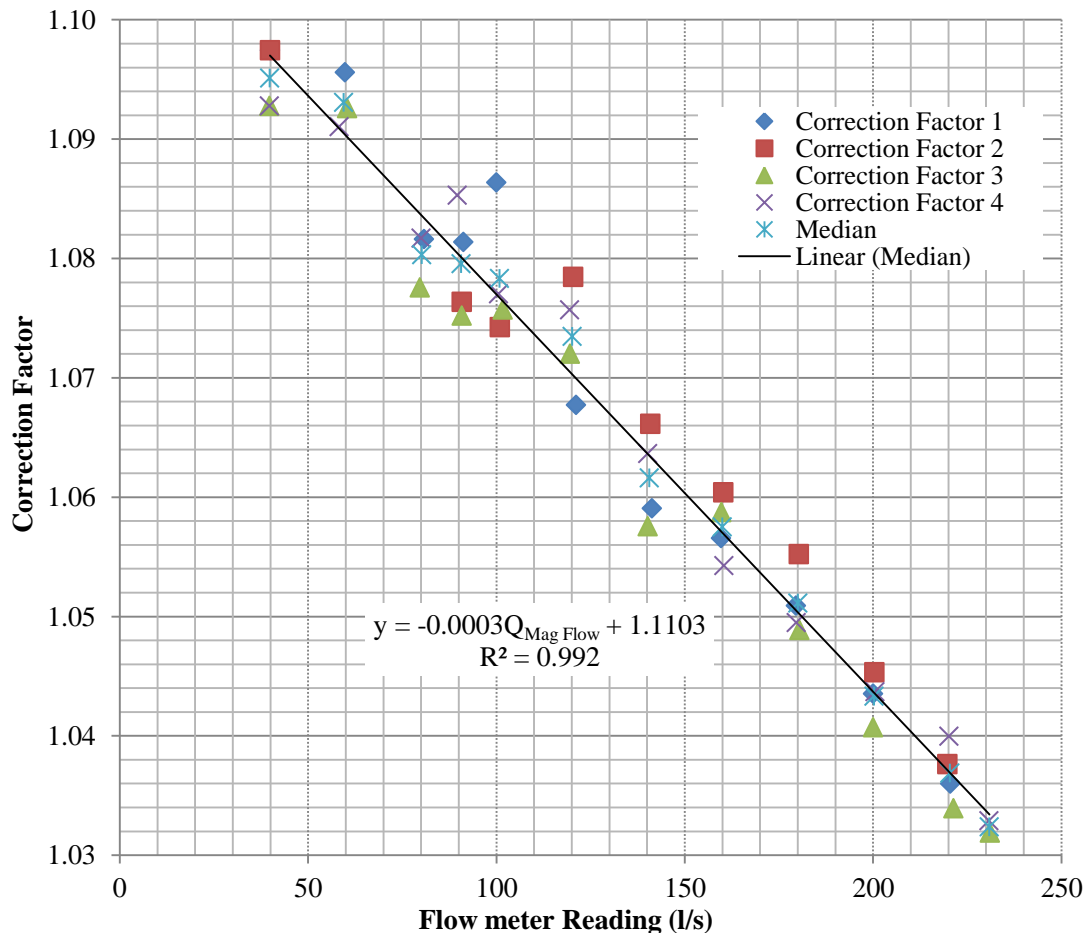
The results of the calibration of the DWS hydraulic laboratory's magnetic flow meter are indicated in **Figure 3.9**. Four water level readings per flow-rate were taken to compensate for any fluctuations over time. The average water level reading was then used to calculate the flow rate over the calibration weir, using the theory discussed in **Section 2.4.4** of this dissertation. The magnetic flow meter readings vary over time due to turbulence in the flow stream passing the measuring point. Twelve flow rate readings from the magnetic flow meter were thus recorded and averaged for every flow rate being calibrated, namely; 39.8, 59.5, 80.2, 90.6, 100.8, 120.1, 140.6, 160.0, 180.0, 200.2, 220.4 and 230.9 l/s. The results show that the magnetic flow meter underestimates the calculated flow rate values. The values obtained during the experimental phase should thus be adjusted using the following equation:

$$y = -0.0003 Q_{\text{Mag Flow}} + 1.1103 \quad (3.1)$$

where:

$y$  = correction factor

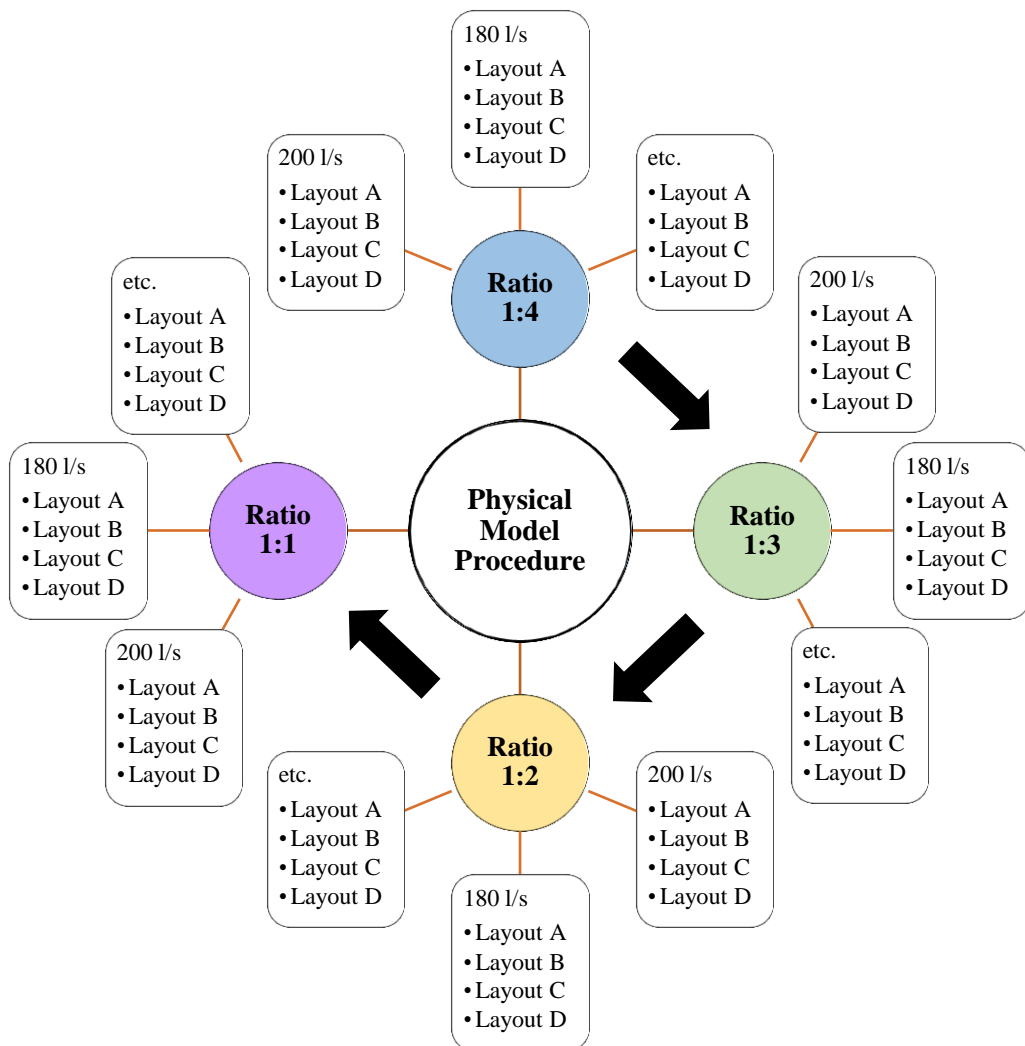
$Q_{\text{Mag Flow}}$  = flow rate measured by the magnetic flow meter



**Figure 3.9: Calibration of the magnetic flow meter**



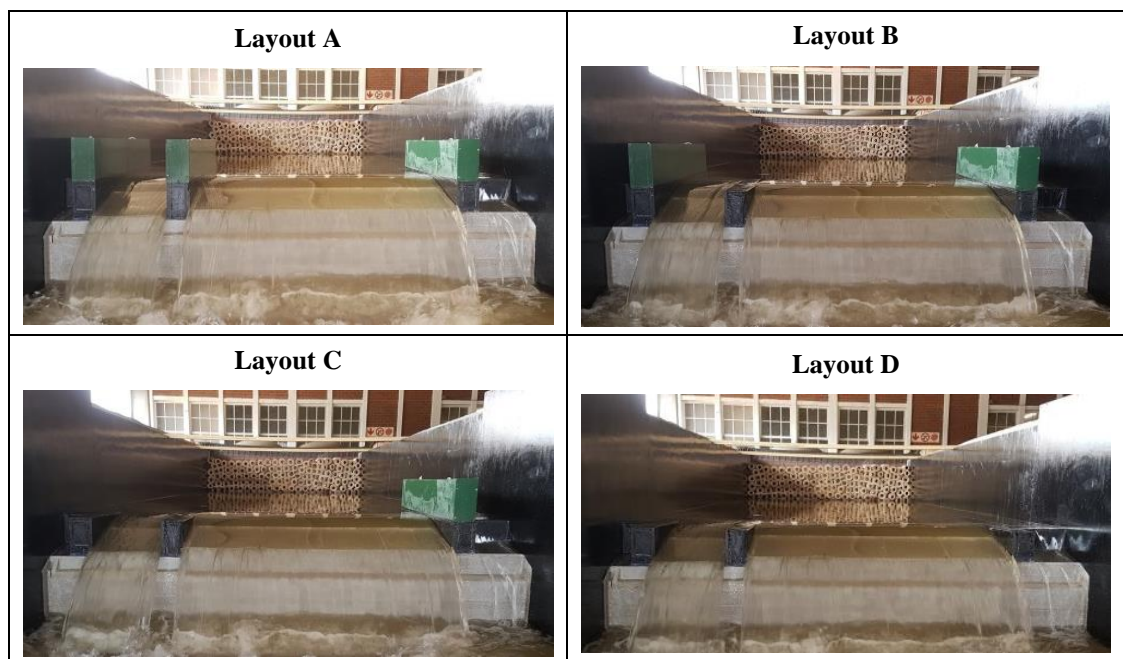
The flow rate supplied to the physical model is controlled by a butterfly valve with no means of setting the flow rate to an exact value. Multiple flow rate readings are thus taken and averaged to determine the flow value at the current valve setting. It is thus challenging to repeat the same valve setting on separate occasions. This limitation resulted in the flow rate being kept constant while the Layouts were changed as shown in **Figure 3.10**. Photographs of the physical model layouts (A, B, C and D) for the various lower to higher Crump width ratios (1:4, 1:3, 1:2 and 1:1) operating at the DWS hydraulic laboratories are shown in **Figure 3.11**, **Figure 3.12**, **Figure 3.13**, and **Figure 3.14**, respectively. The photographs were taken downstream of the entire model to show each component clearly, the extension walls, shown in green, were mounted to the black divider and flank walls and were systematically removed. The filler walls, on either side of the flank walls, were fixed onto the two Crump weirs and acted as broad-crested weirs during overtopping.



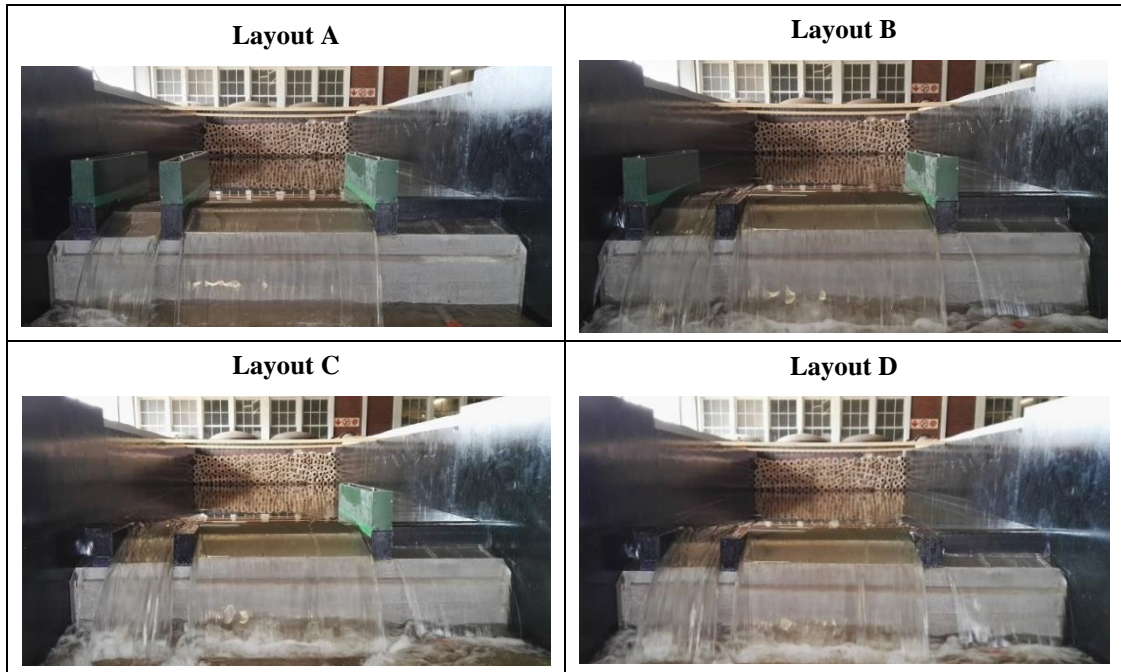
**Figure 3.10: Flow chart of the experimental procedure followed**

The model was first built to represent a lower to higher Crump width ratio of 1:4 ( $B_L:B_H = 308:1266$  mm, as shown in **Figure 3.11**) and was initially set-up as Layout A, described in the previous section. The valve setting was then adjusted in order to supply the desired flow rate to the model. The model was allowed to fill-up and reach a steady-state which takes between 30- and 60 minutes per flow-rate change. Water level readings were then recorded (four readings over 5 minutes) for each well. While keeping the flow rate running and constant, the model layout was changed to Layout B. The flow rate was then allowed to settle for about 20 minutes, after which the water level readings at each well were taken. These steps were then repeated for Layouts C and D. The model was then set-up to represent Layout A for the next flow rate, systematically changing to Layouts B, C and D.

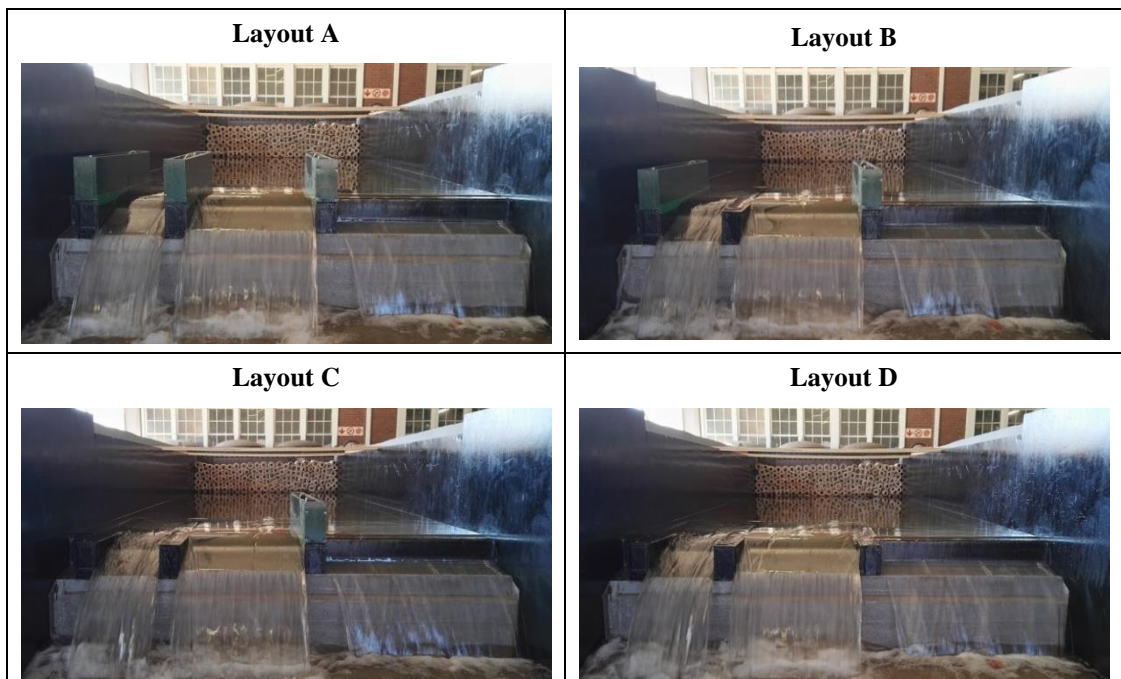
After all the flow rates were run, the model was emptied and allowed to dry completely. The model was then adjusted to represent a lower to higher Crump width ratio of 1:3 ( $B_L:B_H = 308:925$  mm, **Figure 3.12**), repeating the process of systematically changing the layouts for each flow rate. The process was also followed for lower to higher Crump width ratio 1:2 ( $B_L:B_H = 308:612$  mm, **Figure 3.13**) and ratio 1:1 ( $B_L:B_H = 308:310$  mm, **Figure 3.14**). Due to the need for a constant flow rate, water had to be continually flowing while changing the layouts. Therefore, caution had to be taken when entering the model since super-critical flow downstream of the model could result in serious injury.



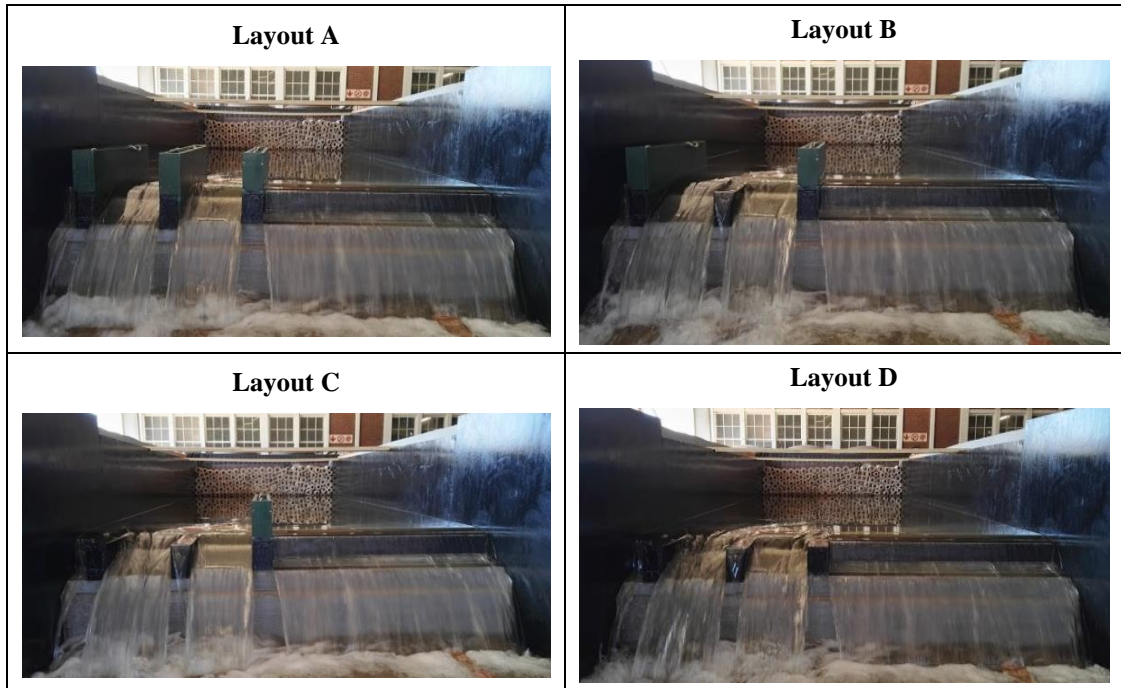
**Figure 3.11: Photographs of the physical model layouts for lower to higher Crump width ratio 1:4 operating at the DWS hydraulic laboratories**



**Figure 3.12: Photographs of the physical model layouts for lower to higher Crump width ratio 1:3 operating at the DWS hydraulic laboratories**



**Figure 3.13: Photographs of the physical model layouts for lower to higher Crump width ratio 1:2 operating at the DWS hydraulic laboratories**



**Figure 3.14: Photographs of the physical model layouts for lower to higher Crump width ratio 1:1 operating at the DWS hydraulic laboratories**

### 3.4 STAR-CCM+ SET-UP

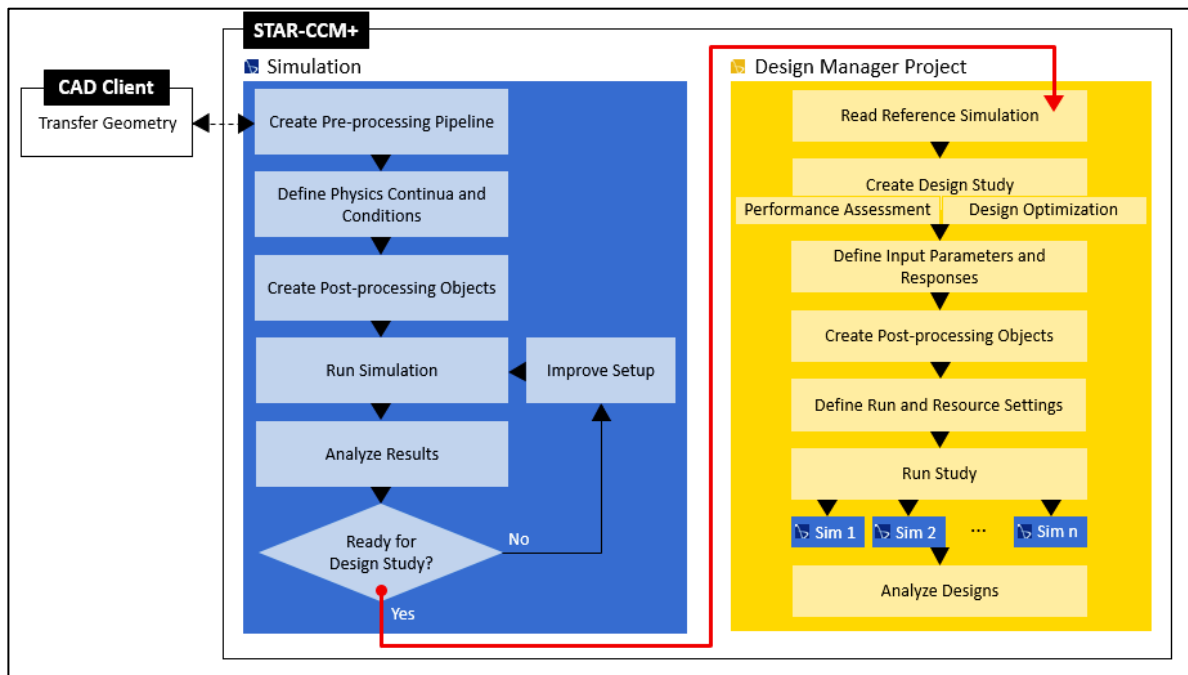
The computational fluid dynamics software (CFD), STAR-CCM+, was used in the investigation to perform the numerical analysis of the model study. The software was chosen for its user-friendly interface, automatic meshing features and its reputation for producing multi-phase flow simulation results comparable to the physical model results.

Simulation tools such as STAR-CCM+, allows the user to test solution designed under virtual conditions. The workflow followed when setting up a simulation in any CFD package is illustrated in **Figure 3.15**. Generally, the first step required is to generate the geometry that represents flow and no flow regions for the 3-dimensional flow domain. Then the physics models, fluid properties and method for solving the turbulence equations are chosen, representing the physics continuum. It is then necessary to set-up the post-processing objects by generating useful scenes to assist in visualising the flow domain in order to correctly set model boundaries, generate refinement areas for the mesh continuum, interpret the results, etc.

The next step is to construct a mesh continuum to generate an appropriate solving grid refined where high-resolution detail is required (usually the surface interface, around structural components, inlets, etc.). The user then defines the model boundary and initial conditions (mass flow rates through the model, upstream head, surface boundary conditions, etc.) before

running the solver. The solver is then set to run with an initial time-step value to compute the velocities and fluid volumes in each cell by using the initial conditions as specified. When the model converges, the user will run the solver with a smaller time-step value until convergence; the process is repeated until the desired time-step, for the most accurate solution, is achieved. Finally, post-processing of the results is performed to extract the desired information (Ho et al., 2003; STAR-CCM+, 2017).

In **Figure 3.15**, the ‘Design Manager Project’ program is introduced for the post-processing section of the workflow. STAR-CCM+ produced this program for the optimisation of designs, for example: maximising the flow through a system by changing the inlet geometry and reducing material costs. In this study, the physical model results are to be reproduced with the intention of improving the theory and thus, the Design Manager Project program would not be applicable. The post-processing was thus iteratively performed as described above.



**Figure 3.15:** A generic method for setting up a numerical model in STAR-CCM+ (STAR-CCM+, 2017)

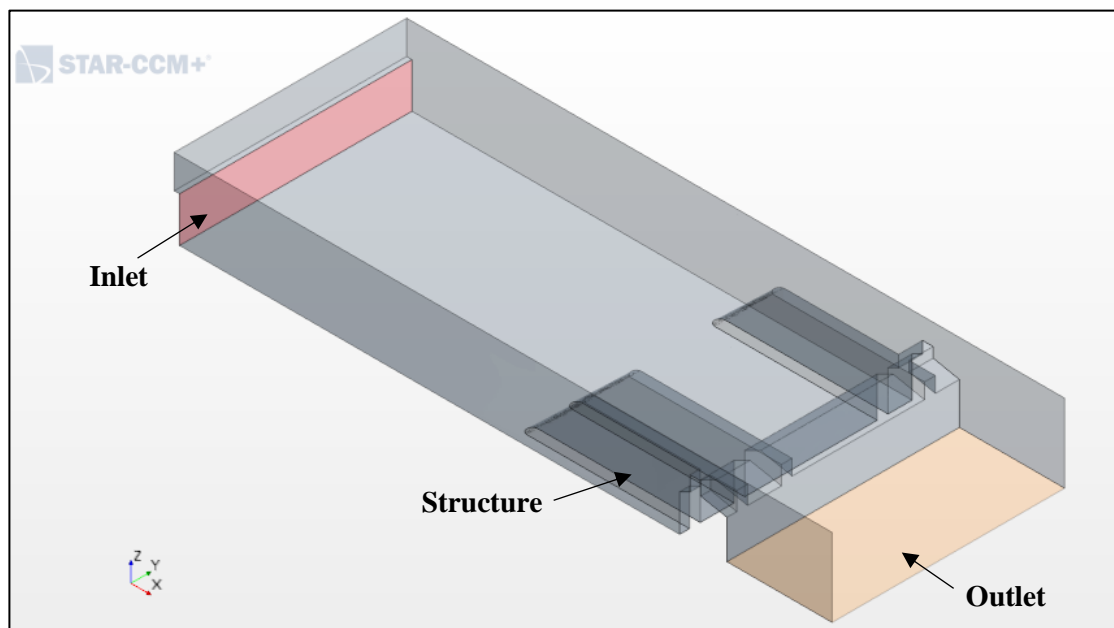
Based on the physical model results, it was decided to use Layout D (with no extension wall, allowing for cross-flow over all flank and divider walls) of the lower to higher Crump width ratio of 1:4 for the calibration of the numerical model. This layout and ratio were used due to the large Crump crest section compared to the filler wall section which ensures that the full three-dimensional flow effects are captured without the false improvement of the results due

to a long left-filler-wall, seen in the other ratios. The details of the numerical model set-up in STAR-CCM+ are given in the succeeding sections.

### 3.4.1 Generating model geometry

A CFD analysis requires geometric parts for which the spatial construction of the flow and no-flow regions can be defined. STAR-CCM+ allows users to create the geometry in a built-in 3D-CAD modeller but also provides for the importing of CAD from various software packages. For the study at hand, the as-built dimensions of the physical model, Layout D of the lower to higher Crump width ratio 1:4, was used to generate the model geometry of the numerical model in the AutoCAD 2016 student drawing package. The volume in which the fluid is to be computed was extracted as a STL file and imported into the STAR-CCM+ software. After that, it was necessary to split the volume into its various surface faces so that the flow boundaries could be set.

**Figure 3.16** shows the geometry of the model with the inlet boundary in light red and the drop outlet boundary in light orange. A drop outlet, where the flow over the structure exits the flow domain as it reaches the floor, was selected to reduce the cell count of the mesh continuum. Additionally, the model would be tested for modular flow, where the downstream water level does not influence the upstream water level, and thus the results would not be impacted by the drop outlet.



**Figure 3.16:** Model geometry in STAR-CCM+

### 3.4.2 Selecting physics models, fluid properties and method for solving turbulence equations

STAR-CCM+ provides the user with a wide range of physics models and simulation methods for multi-phase flow and other flow phenomena. The physics models define how physical phenomena in a continuum are represented; they define the simulation variables such as pressure, temperature, velocity, viscosity as well as the mathematical formulation needed to generate a solution. The Volume of Fluid (VOF) Multiphase Model (principles described in **Section 2.6.3**) was selected due to its numerical efficiency and suitability for simulations of flows where each phase constitutes a large structure with a relatively small contact area between the phases. The VOF model utilises a Eulerian framework in their formulation, and thus the simulation is set-up using distinct Eulerian phases namely; water and air. The thermo-physical properties of the water phase are given in **Table 3.2** below.

**Table 3.2: Thermo-physical properties of the water phase**

Parameter	Value
Density	997.561 kg/m <sup>3</sup>
Dynamic viscosity (at 20°C)	8.8871E <sup>-4</sup> Pa.s
Surface tension	0.074 N/m
Gravity constant	9.81 m/s <sup>2</sup>
Atmospheric pressure	101325.0 Pa

The STAR-CCM+ (2017) user manual suggests that, for moving free-surface flow problems, at least three mesh cells across the surface interface be provided to minimise modelling errors. The spatial distribution of each phase at any given time is defined by the volume fraction variable. These distributions are calculated, in STAR-CCM+, by solving a transport equation for the phase volume fraction (see **Section 2.6.3**) and make use of the Segregated Flow Model. The interface between phases (free-surface) in the simulation needs to be established in this study in order to determine the water levels at any given flow rate. To obtain a sharp interface, the 2<sup>nd</sup>-order discretisation scheme is to be used along with an appropriate sharpening factor of 0.2, an angle factor of 0.5 and lower and upper Courant number limits of 10 and 20, respectively (see **Section 2.6.4**).

Multi-phase fluid flow is generally characterised by irregular fluctuating flow quantities which occur at small scales and high frequency. Solving these fluctuations in time and space becomes computationally exhaustive if exact governing equations are to be solved. It is less expensive to solve for averaged quantities and to approximate the small fluctuating structures. Thus the Reynolds-Averaged Navier-Stokes (RANS) Model along with the K-Epsilon and

Two-Layer All  $y^+$  Wall Treatment Models were selected in this study to govern the transport of averaged flow quantities (see **Section 2.6.4** for details).

### 3.4.3 Meshing of the flow domain

A mesh is a discretised representation of the flow domain which is used by the physics solvers to provide the numeric solution. STAR-CCM+ provides meshing tools that can be used to generate high-quality, structured meshes on CAD geometry. A surface mesh must be produced before the volume mesh can be generated. Two meshing tools were used in the study, namely; the Surface Wrapper and the Surface Remesher. The Surface Wrapper is used when the CAD geometry is imported to ensure that the geometry represents the actual structure. It produces a closed surface which is used by the Surface Remesher as a starting point for re-triangulation in order to generate a high-quality surface mesh (STAR-CCM+, 2017).

In this study, the Trimmed Cell Mesher Tool was used to generate the volume mesh due to the robust and efficient production of a high-quality grid used for simple and complex mesh generation problems. The other advantages of this meshing tool are (1) predominantly hexahedral cells with minimal cell skewness; (2) mesh refinement is based on the surface mesh size, as well as user-defined refinement volumes; (3) independent of surface/CAD quality; and (4), can be aligned with a user-defined coordinate system. Furthermore, the Prism Layer Mesher Tool is used with a core volume mesh to produce orthogonal prismatic cells along the wall surfaces and boundaries, which improves the accuracy of the flow solution (STAR-CCM+, 2017).

The volumetric mesh grid for the numerical model study is shown in **Figure 3.17**; the pink blocks represent user-defined volume shapes for the refinement of the mesh. The mesh cell sizes for the initial conditions of the simulation were; Base Size: 80 mm, Volumetric Controls (Volume 1, 2 and 3) Absolute Size: 20 mm. The volume mesh was then systematically refined from a course to a fine mesh along the volume of fraction values of 0.05 to 0.95 (surface interface). **Figure 3.18** shows the volumetric mesh grid with refinement volumes and the user-defined refinement along the surface interface. The code necessary to produce a refinement of 5 mm along the surface interface and 2.5 mm along the measuring point of the surface interface is given below.

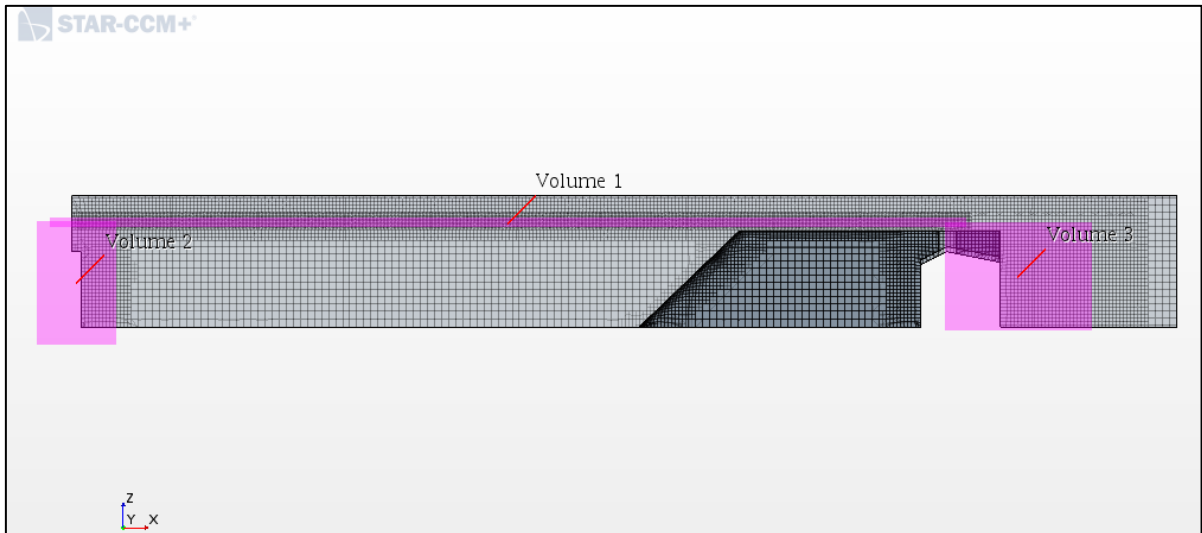


**Field function code for the refinement of the surface interface:**

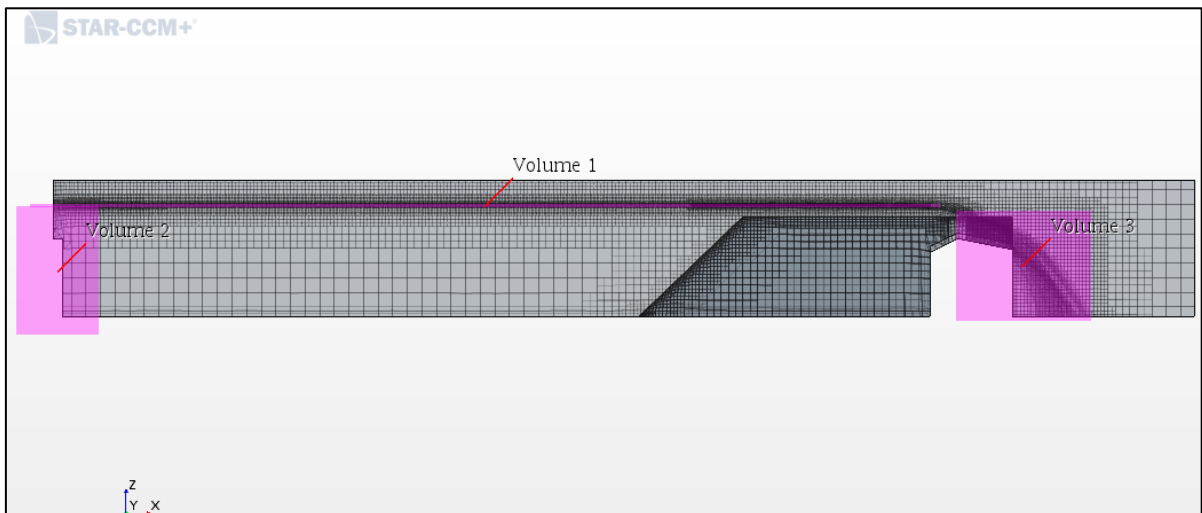
```

({VolumeFractionWater}<0.95 && {VolumeFractionWater}>0.05 && {{Centroid}[0]<3.5) ?
0.005 :({VolumeFractionWater}<0.95 && {VolumeFractionWater}>0.05 &&
{{Centroid}[0]>3.5 && {{Centroid}[0]<4.8) ? 0.0025 : ({VolumeFractionWater}<0.95 &&
{VolumeFractionWater}>0.05 && {{Centroid}[0]>4.8) ? 0.005 : 0

```



**Figure 3.17: Volumetric mesh grid with refinement volumes**



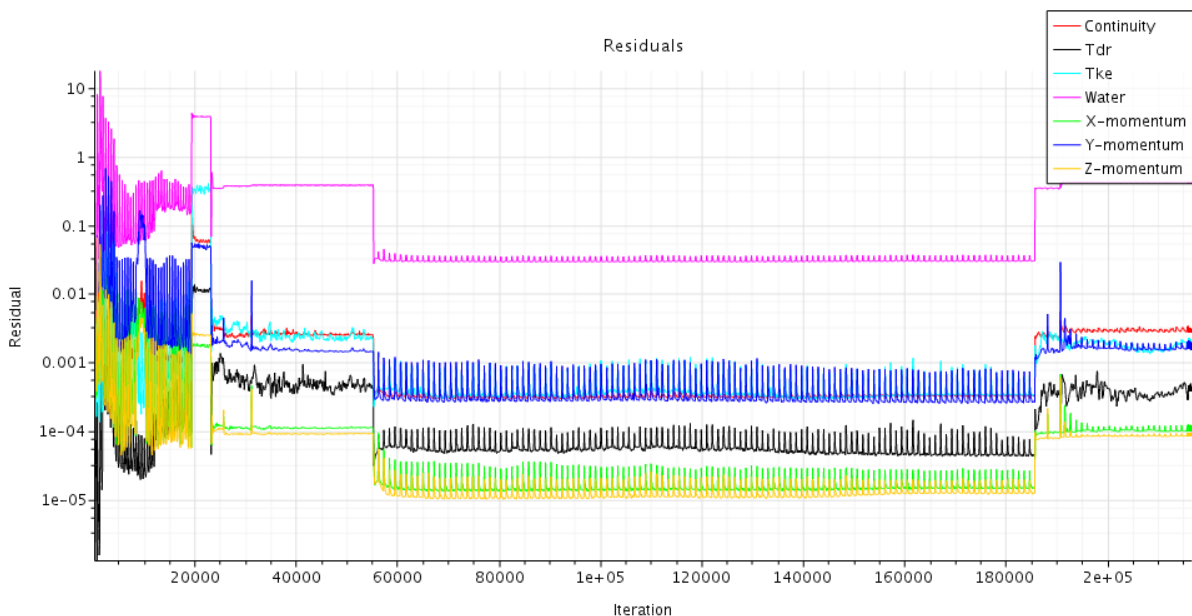
**Figure 3.18: User-defined refinement of volumetric mesh grid with refinement volumes**

### 3.4.4 Set-up of necessary plots and monitors

The setting-up of plots and monitors are required for the post-processing of results as well as monitoring the simulation as it runs. STAR-CCM+ provides raw data and data computed from the raw data by making use of Field Functions. These field functions are analysed by (1) creating reports of specific quantities; (2) visualising solution data in scalar and vector

scenes and (3) plotting of data sets extracted from the solution by creating monitors. These field functions need to be in place before simulating since the data is extracted and recorded by these field functions at each iteration. It is also necessary to select the part from which the data is to be extracted. These parts are generated by the user in the form of plane surfaces, boundaries and regions (STAR-CCM+, 2017).

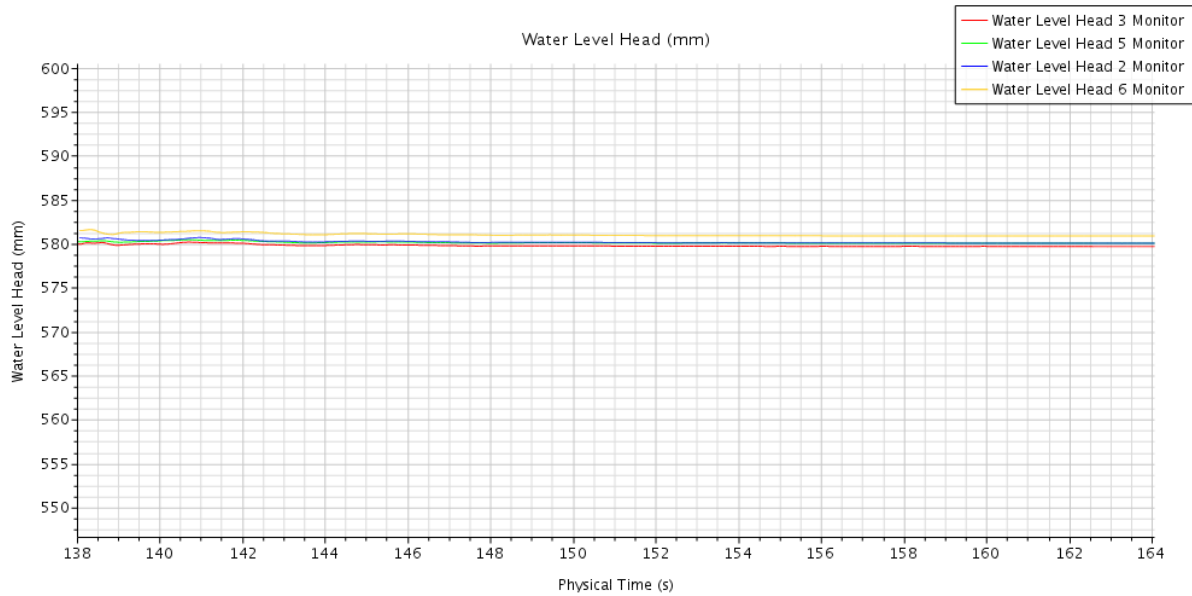
The residuals of a simulation represent the absolute error in the solution of the variable. It measures the degree to which the discretisation equation in each cell is satisfied. For a perfectly converged solution, the residual value in each cell would be equal to the machine precision. In STAR-CCM+, residual monitors keep a record of the global Root Mean Squared (RMS) value for each of the transport equations solved in the continua. A normalised value of the residuals is given by default so that the user can compare different residual values that vary widely. Since the study required a time-dependent solution (instead of a steady-state solution), the residuals are to be plotted for each time-step (see **Figure 3.19** for an example of the Residual Plots).



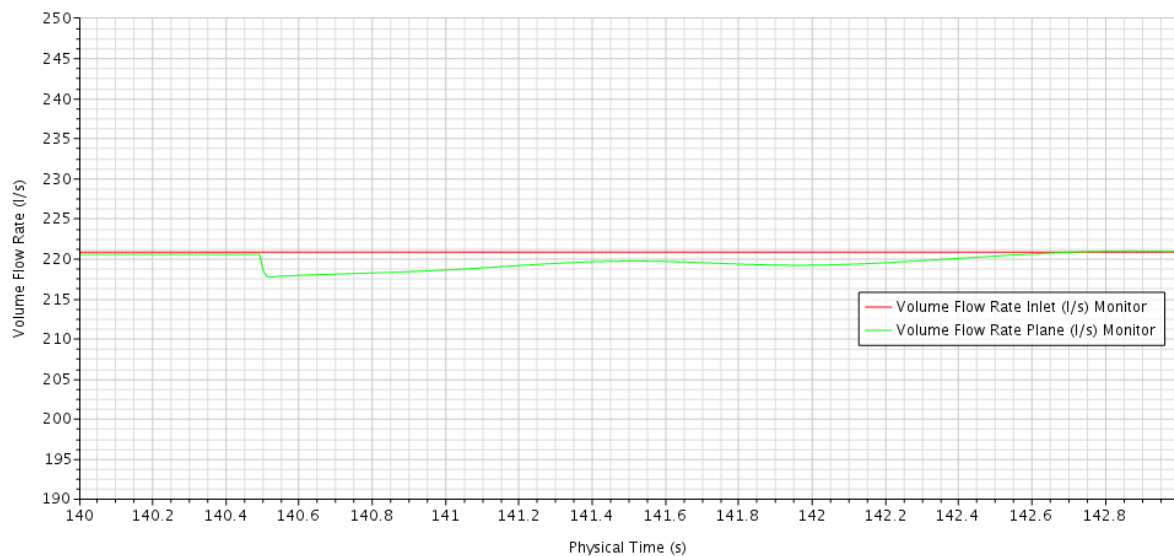
**Figure 3.19: Example of Residuals Plot**

In this study, the water levels upstream of each structural component (lower Crump, higher Crump, left filler and right filler walls) would need to be recorded in order to calculate the flow over the weir as done in the physical model study (see **Figure 3.20** for an example of the Water Level Head Plot, showing all four measuring points). Furthermore, the inlet and outlet flow volumes would need to be recorded in order to establish convergence (additional to the residuals check). A surface, perpendicular to the flow, was generated along the upstream

measuring points so that the extracted outflow values would correspond to the calculated values using the upstream water level head measurements. **Figure 3.21** shows an example of the Volume Flow Rate Plot.



**Figure 3.20: Example of Water Level Head Plot**



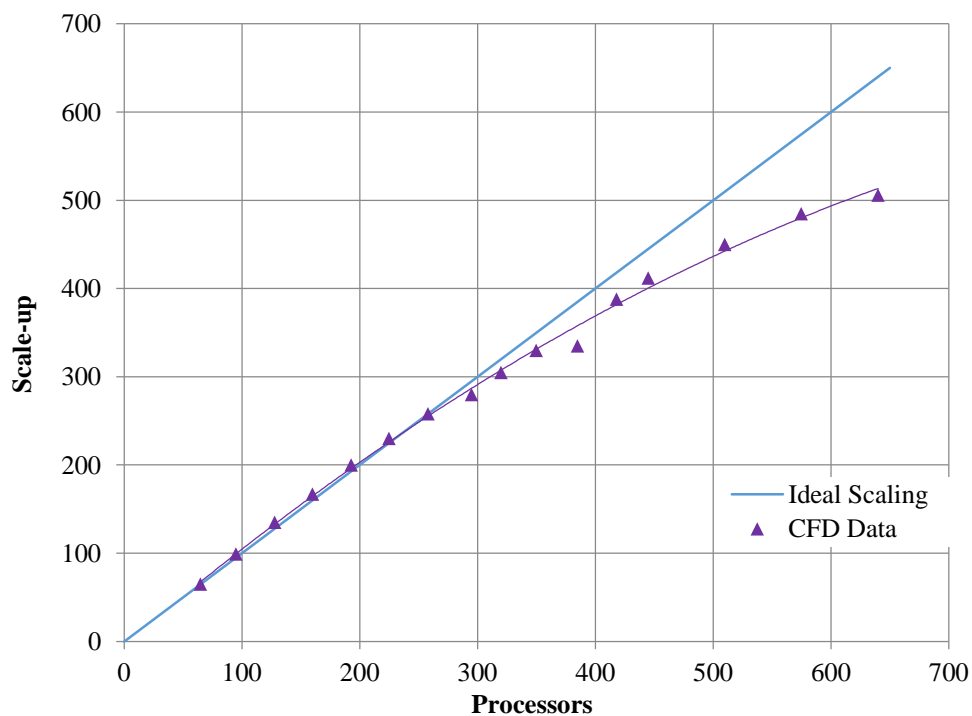
**Figure 3.21: Example of Volume Flow Rate Plot**

### 3.4.5 Preparation of model for CHPC interaction

UC Davis (2016) published an installation guideline providing the typical memory requirements for building and running a simulation in STAR-CCM+. The typical memory requirements (may vary significantly between models with different characteristics) for generating surface and volume meshes are approximately 0.5 GB per million surface triangles

and 0.5 GB per million trimmed cells, respectively. The memory requirements for solving a two-equation turbulence model with a trimmed cell volume mesh and segregated flow is approximately 0.5 GB per million cells.

In order to minimise computation time and improve simulation results, high-performance computing (HPC) can be used to run simulations using parallel computing resources. HPC applications, such as CFD, therefore depend greatly on the software's ability to scale compute tasks efficiently. Parallel performance is evaluated by determining the software's scale-up. Scale-up is a function of the number of cores/processors used in the computation and can be defined as the time it takes to complete a run on one core/processor, divided by the time it takes to complete the same run on the number of cores/processors used in parallel. For example, if a simulation reaches convergence in 32 hours when running on one processor and the same simulation takes 1 hour to converge on 32 processors, then the scale-up is equal to 32 on 32 processors. Similarly, if the same simulation took 8 hours to converge on 32 processors, it would have a scale-up of 4 on 32 processors. Scaling is considered excellent when the scale-up is approximately equal to the number of processors on which the simulation is run. The scale-up as a function of the number of processors running in parallel for a 16-million cell simulation in STAR-CCM+ is shown in **Figure 3.22**. The ideal scalability line is shown in blue with the actual scale-up shown in purple. Excellent scaling is observed until 300 processors, after which the scaling deviates from the ideal case (Hedges, 2016).



**Figure 3.22: Scaling results for a 16-million cell STAR-CCM+ simulation (Hedges, 2016)**

The Centre for High Performance Computing (CHPC), located in Cape Town, South Africa, hosts a supercomputer comprising of 1368 compute nodes with 24 cores and 128 GB of RAM each and five large memory (fat) nodes with 56 cores and 1 TB of RAM each. It is a Linux cluster and can be remotely connected to via the system's `ssh lengau.chpc.ac.za` with a username and password provided by the CHPC. On the CHPC cluster, simulations are submitted as jobs. Users can run 10 nodes with 24 cores each, for every job submitted, for a maximum wall-time of 48 hours. Jobs are submitted by running a specific script on the CHPC interface, an example of the script needed to run a STAR-CCM+ job is given in **Figure 3.23**. Unfortunately, the CHPC does not have direct access to the internet and therefore external licencing for the CFD package, used for the simulations, needs to be separately obtained by the user and connected to through ssh-tunnelling (Crosby, 2018).

Furthermore, it would be of the user's interest to monitor the solution as the simulation runs on the CHPC cluster. Since the cluster makes use of a Linux server, direct visualisation of the simulation is not possible. There are, however, different ways of remotely visualising the simulation, namely; X-forwarding using a VNC session and X-forwarding in two stages. Both these methods require specific coding that can be found on the CHPC wiki webpage – *how to STAR-CCM+* and would generally be used in cases where the volume mesh is to be constructed by the user and if frequent changes are to be made in-between simulation runs (Crosby, 2018).

For cases such as the study at hand, minimal changes to the simulation are required, and thus the monitoring of the simulation was achieved by generating a hard copy of the plots and scenes (discussed in **Section 3.4.4**) after each iteration. This can be set on the local server before uploading the simulation to the CHPC cluster. Any other changes to the simulation were achieved by running java scripts written in STAR-CCM+ using the macros function. For example, the time-step of the Implicit Unsteady Solver had to be changed after initial convergence, at a larger time-step was reached. In STAR-CCM+, the user would simply record a macro for changing the time-step and then run the file on the CHPC cluster as a submitted job. The same was done for the additional refining of the volume mesh at the surface interface in the vicinity of the measuring point from 2.5 mm to 1 mm.

```

#!/bin/bash
##### The following line will request 10 (virtual) nodes, each with 24 cores running 24 mpi processes for
##### a total of 240-way parallel.
#PBS -l select=10:ncpus=24:mpiprocs=24:nodetype=haswell_reg
#PBS -q normal
##### Supply YOUR programme code in the next line
#PBS -P MECH0000
#PBS -l walltime=1:00:00
#PBS -o /home/username/scratch/starccmtesting/star.out
#PBS -e /home/username/scratch/starccmtesting/star.err
##### The following two lines will send the user an e-mail when the job aborts, begins or ends.
#PBS -m abe
#PBS -M username@email.co.za
##### Set up path. Drop the "-R8" part if you want to use the single precision version of the code.
export PATH=/apps/chpc/compmech/CFD/CD-adapco/12.06.011-R8/STAR-CCM+12.06.011-R8/star/bin:$PATH
##### set up ssh-tunnels to your license server. Obviously, use the right port numbers and server IP.
##### The port numbers and server IP used here are for CD-Adapco's Power on Demand server. To use this you need a
valid account and PoD key, which gets entered on the command line.
##### lmgrd daemon
ssh -f username@chpclic1 -L 1999:flex.cd-adapco.com:1999 -N
##### vendor daemon port
ssh -f username@chpclic1 -L 2099:flex.cd-adapco.com:2099 -N
##### Tell solver where to look for the license.
##### localhost is correct here, it follows from the ssh-tunnelling. We are following a belts, braces and modest
##### underwear approach here by specifying the LM and CDLMD license files as well as giving a licensing path on the
command line.
export LM_LICENSE_FILE=1999@localhost
export CDLMD_LICENSE_FILE=1999@localhost
##### There is no -d option available under PBS Pro, therefore explicitly set the working directory and change to that.
export PBS_JOBDIR=/home/username/scratch/starccmtesting
cd $PBS_JOBDIR
nproc=`cat $PBS_NODEFILE | wc -l`
##### This is a minimal run instruction; it will run the solver until reaching the stopping criteria set in the sim file.
starccm+ -licpath 1999@localhost -batch run -power -podkey [your 22-character podkey] -mpi platform -fabric IBV -rsh
ssh -np $nproc -machinefile $PBS_NODEFILE simulationfilename.sim > run.out

```

**Figure 3.23: A generic example of the script needed to run a STAR-CCM+ job (simulation) on the CHPC (Crosby, 2018)**

## 4 PRESENTATION AND DISCUSSION OF RESULTS

This chapter gives an outline and detailed discussion of the results following the physical model study. Firstly, the specific calculation procedure used to produce the results is explained, and then the results are presented in tabular form as well as graphically to understand the trends observed better, this is followed by a discussion of the trends. The results of the numerical model, set-up in the computational fluid dynamics software (CFD), STAR-CCM+, are then discussed along with a comparison of the physical and numerical model results.

### 4.1 PRESENTATION OF PHYSICAL MODEL RESULTS

The physical model results were calculated using the procedure outlined in **Figure 4.1**. The equations expressed in the calculation procedure are the calibration equation (discussed in **Section 3.3**), the Crump weir equation for modular flow conditions (see **Section 2.4.4**) and the broad-crested weir equation (see **Section 2.4.6**), respectively. Water level readings were taken at five points upstream of the modelled compound Crump weir. These points are shown in **Figure 3.5** and were located upstream of each component namely; the lower and higher Crump crests, the left and right filler walls and upstream of the structure as a whole.

The important nomenclature used throughout this chapter (also see **Figure 4.1**) is as follows:

- $Q_{\text{input}}$  = input flow rate measured using the laboratory magnetic flow meter and calibrated against a standardised Crump weir
- $Q_{\text{calculated}}$  = sum of the flow rates calculated for each crest (flow over lower Crump crest + flow over higher Crump crest + flow over left filler wall + flow over right filler wall)
- $B_L:B_H$  = lower Crump crest width ( $B_L$ ) to higher Crump crest width ( $B_H$ ) ratio
- $FW_L$  = left filler wall crest width;  $FW_R$  = right filler wall crest width

The input flow rate, to the model, was measured using the magnetic flow meter and corrected using the calibration equation (corrected flow =  $Q_{\text{input}}$ ). An iterative process in Excel was used to calculate the discharge coefficients ( $C_{de}$ ) as well as the velocity head component ( $h_v$ ) for the total head ( $H$ ). These components were required to determine the flow rate over each crest (the lower Crump, higher Crump, left filler wall and right filler wall). The total flow rate over the weir ( $Q_{\text{calculated}}$ ) was then calculated by the summation of each crest section. Finally,  $Q_{\text{calculated}}$  was compared to  $Q_{\text{input}}$  to quantify the error observed in the water levels due to overtopping of the divider and flank walls.

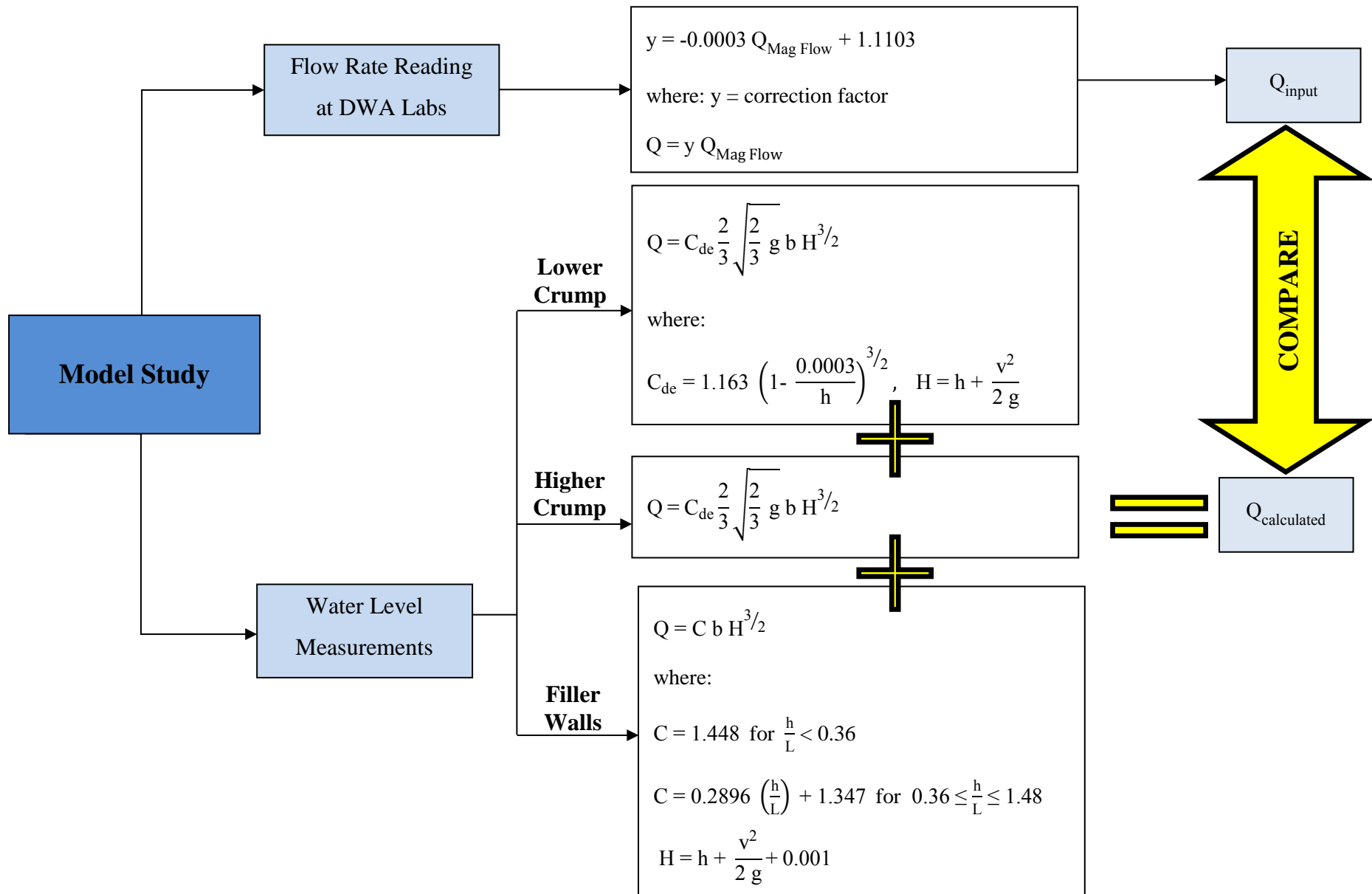


Figure 4.1: Calculation procedure for flows above the physical model capacity



#### 4.1.1 Physical model results for ratio 1:4

The results for the physical model representing a lower to higher Crump width ratio of 1:4 are shown in **Table 4.1** and **Figure 4.2**. The various configurations, Layouts A, B, C and D, were compared to understand the three-dimensional influence on the flow rates resulting from the removal of the extension walls. The hydraulic capacity of the model for  $B_L:B_H = 1:4$  (lower to higher Crump width ratio), when ignoring all energy losses, is 85.8 l/s and is indicated by the solid vertical black line in **Figure 4.2**. **Table 4.1** shows the model input flow rates ( $Q_{input}$ ), the calculated flow rates ( $Q_{calculated}$ ) and the error (E), expressed as the percentage difference between these two values for the various flow rates being modelled. The results indicate that the calculated flow rates over the hydraulic capacity of the weir, overestimate the modelled values for all four layouts when using the current discharge-head relationships. The error (E) increases as the model input flow rates increases until 209.1 l/s (possible indication of a limit being reached) and then decreases for flow rate 230.9 l/s.

**Table 4.1: Physical model results for lower to higher Crump width ratio of 1:4**

Model Input Flows, $Q_{input}$ (l/s)	Layout A		Layout B		Layout C		Layout D	
	$Q_{calculated\_A}$ (l/s)	E (%)	$Q_{calculated\_B}$ (l/s)	E (%)	$Q_{calculated\_C}$ (l/s)	E (%)	$Q_{calculated\_D}$ (l/s)	E (%)
<b>88.0</b>	89.7	1.86	89.7	1.86	89.7	1.86	89.7	1.86
<b>97.7</b>	101.5	3.87	101.5	3.90	101.8	4.17	102.2	4.63
<b>110.8</b>	115.9	4.61	115.9	4.62	116.0	4.73	116.5	5.18
<b>150.2</b>	159.4	6.10	158.2	5.33	159.1	5.93	159.3	6.05
<b>189.9</b>	205.8	8.38	203.0	6.87	203.0	6.88	202.5	6.61
<b>209.1</b>	228.3	9.18	224.4	7.31	223.9	7.07	222.9	6.58
<b>230.9</b>	251.7	8.99	247.5	7.16	245.9	6.47	244.7	5.96

**Note:** See **Figure 3.3** for details of Layouts A, B, C and D.

$Q_{input}$  = Calibrated model input flow rates as per pumps (l/s)

$Q_{calculated}$  = Flow rate calculated using measured water levels upstream of the model (l/s)

E = Percentage difference between  $Q_{input}$  and  $Q_{calculated}$  (%)

**Figure 4.2** expresses the results for ratio 1:4 graphically, comparing the four model layouts. For a better interpretation of the results,  $Q_{input}$  (representing a  $y=x$  line) was plotted in the figure, deviating from this identity line indicates unquantified energy losses experienced in the flow over the weir. For the model input flow rates 64.1 and 88.0 l/s, the discharge-head relationships tend to estimate the flow rates accurately. However, as the flow rates increase (97.7 to 230.9 l/s) the discharge-head relationships tend to overestimate the actual values. It is also important to note that up to 150.2 l/s the overestimation error of the four layouts are similar, after which Layouts B, C and D start to show a reduction in the error.

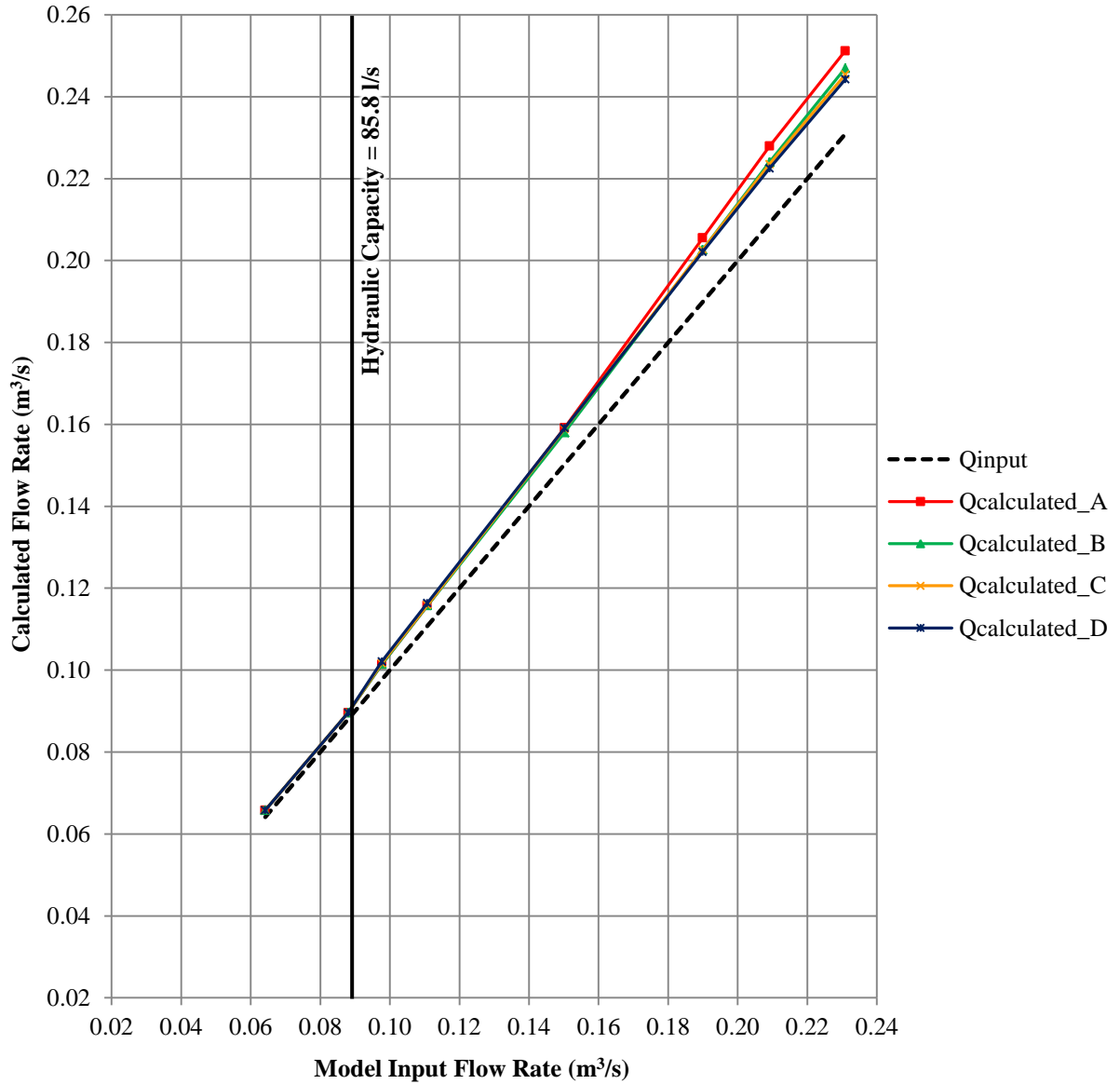


Figure 4.2: Graph of physical model results for lower to higher Crump width ratio of 1:4

#### 4.1.2 Physical model results for ratio 1:3

The physical model results for the lower to higher Crump width ratio of 1:3 are shown numerically in **Table 4.2** and graphically in **Figure 4.3**. The capacity of the model, when ignoring all energy losses, is 64.9 l/s and is once again indicated by the solid vertical black line. The results in **Table 4.2** indicate that, for model input flow rates ( $Q_{\text{input}}$ ) higher than the weir's capacity, the calculated flows ( $Q_{\text{calculated}}$ : calculated using the current discharge-head relationships), overestimate the actual values for all four layouts. The error (E) increases as the model input flow rate increases with no apparent limit being reached as seen in the results for ratio 1:4. However, the overestimation error is smaller when compared to ratio 1:4.

The error in Layout A becomes increasingly larger from 150.8 l/s compared to the observations from Layouts B, C and D. Layout B shows a lower overestimation compared to Layout A but shows an increase in the error from 190.0 l/s compared to Layouts C and D. Layouts C and D follow a similar trend with minimal differences, which are only evident from the numerical values shown in **Table 4.2**. Overall, the overestimation error for ratio 1:3 at lower flows tends to be greater than for ratio 1:4, at higher flows ratio 1:3 shows a decrease in the error made compared to ratio 1:4.

**Table 4.2: Physical model results for lower to higher Crump width ratio of 1:3**

Model Input Flows, $Q_{\text{input}}$ (l/s)	Layout A		Layout B		Layout C		Layout D	
	$Q_{\text{calculated\_A}}$ (l/s)	E (%)	$Q_{\text{calculated\_B}}$ (l/s)	E (%)	$Q_{\text{calculated\_C}}$ (l/s)	E (%)	$Q_{\text{calculated\_D}}$ (l/s)	E (%)
65.4	67.8	3.73	67.8	3.73	67.8	3.73	67.8	3.73
88.3	90.4	2.31	90.3	2.22	90.6	2.63	90.8	2.82
109.6	114.5	4.44	114.0	4.04	114.9	4.85	115.4	5.32
150.8	160.3	6.28	158.6	5.15	158.9	5.34	159.4	5.67
190.0	204.2	7.50	200.8	5.67	199.5	5.00	199.4	4.97
210.3	226.9	7.89	222.4	5.79	220.9	5.06	220.3	4.77
229.6	249.6	8.73	244.9	6.66	241.5	5.21	240.8	4.90

**Note:** See **Figure 3.3** for details of Layouts A, B, C and D.

$Q_{\text{input}}$  = Calibrated model input flow rates as per pumps (l/s)

$Q_{\text{calculated}}$  = Flow rate calculated using measured water levels upstream of the model (l/s)

E = Percentage difference between  $Q_{\text{input}}$  and  $Q_{\text{calculated}}$  (%)

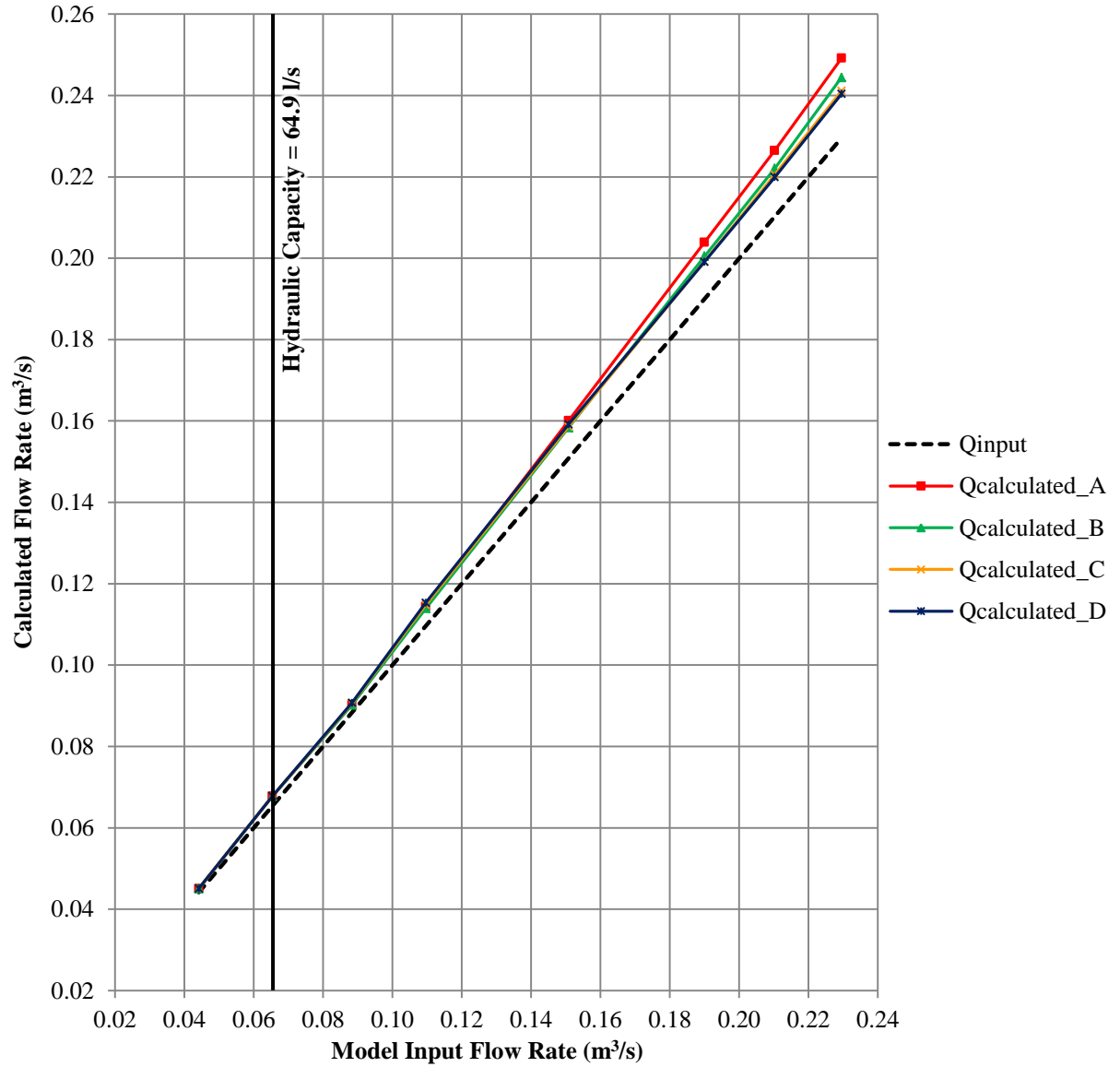


Figure 4.3: Graph of physical model results for lower to higher Crump width ratio of 1:3

### 4.1.3 Physical model results for ratio 1:2

The results for the lower to higher Crump width ratio of 1:2 are shown in **Table 4.3** and **Figure 4.4**. The capacity of the model, when ignoring all energy losses, is 50.7 l/s and is indicated by the solid vertical black line. **Table 4.3** shows that all four layouts overestimate the model input flow rates ( $Q_{input}$ ) for flows higher than the weir's capacity. The error (E) seen in Layout A increases as the model input flow rate increases with a sudden rise from 89.2 to 107.2 l/s of 3.98%. For Layouts B, C and D the average error at 66 l/s was 3.35%, the error then decreases for 89.2 l/s to 0.94% in Layout B, 1.61 % in Layout C and 2.07% in Layout D.

The graphical representation of the results in **Figure 4.4** shows a similar pattern to the results for ratio 1:4. The errors become more significant from 107.2 l/s with Layout A, noticeably higher in error than the other layouts. Layout B shows a lower overestimation compared to Layout A. Layout C shows a further decrease in the error and Layout D shows the lowest overestimation errors.

**Table 4.3: Physical model results for lower to higher Crump width ratio of 1:2**

Model Input Flows, $Q_{input}$ (l/s)	Layout A		Layout B		Layout C		Layout D	
	$Q_{calculated\_A}$ (l/s)	E (%)	$Q_{calculated\_B}$ (l/s)	E (%)	$Q_{calculated\_C}$ (l/s)	E (%)	$Q_{calculated\_D}$ (l/s)	E (%)
66.0	66.1	0.21	68.1	3.22	68.2	3.33	68.3	3.51
89.2	90.5	1.50	90.0	0.94	90.6	1.61	91.0	2.07
107.2	113.0	5.48	111.9	4.43	112.5	4.99	113.2	5.59
150.8	160.9	6.66	157.5	4.43	156.9	4.02	157.1	4.16
189.5	203.2	7.26	198.6	4.81	196.7	3.81	196.0	3.47
210.1	226.6	7.87	221.1	5.25	217.8	3.67	217.1	3.32
229.7	249.6	8.67	242.8	5.70	238.3	3.77	237.0	3.19

**Note:** See **Figure 3.3** for details of Layouts A, B, C and D.

$Q_{input}$  = Calibrated model input flow rates as per pumps (l/s)

$Q_{calculated}$  = Flow rate calculated using measured water levels upstream of the model (l/s)

E = Percentage difference between  $Q_{input}$  and  $Q_{calculated}$  (%)

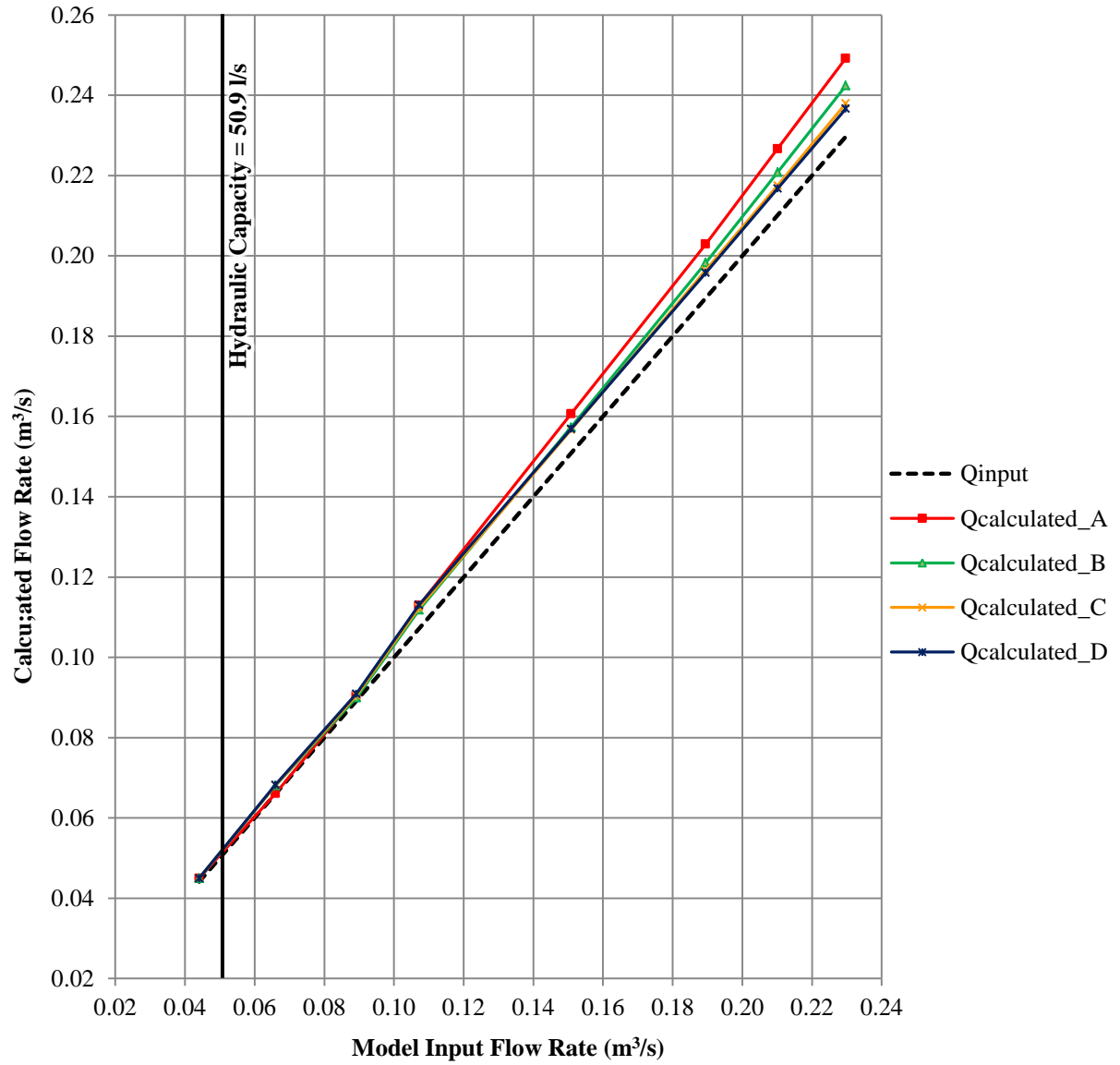


Figure 4.4: Graph of physical model results for lower to higher Crump width ratio of 1:2

#### 4.1.4 Physical model results for ratio 1:1

The physical model results, for the lower to higher Crump width ratio of 1:1, are shown in **Table 4.4** and **Figure 4.5**. The capacity of the model, when ignoring all energy losses, is 36.9 l/s and is indicated by the solid vertical black line. **Table 4.4** shows that all four layouts overestimate the model input flow rates ( $Q_{input}$ ) for flows higher than the weir's capacity. The error (E) seen in Layout A increases as the model input flow rate increases with a sudden rise from 89.2 to 107.2 l/s of 3.98%. For Layouts B, C and D the average error at 66 l/s was 3.35%, the error then decreases for 89.2 l/s to 0.94% in Layout B, 1.61 % in Layout C and 2.07% in Layout D. Layout B shows an increase in the error from 89.2 to 229.7 l/s. Layouts C and D also show an increase in the error from 89.2 l/s but reaches a limit at 150.8 l/s after which the error decreases.

The graph of the results in **Figure 4.5** shows a similar pattern to the results for ratios 1:4, 1:3 and 1:2. Layout A shows a consistently higher overestimation error than the other layouts, whereas, Layout D shows the lowest error in the calculated flow.

**Table 4.4: Physical model results for lower to higher Crump width ratio of 1:1**

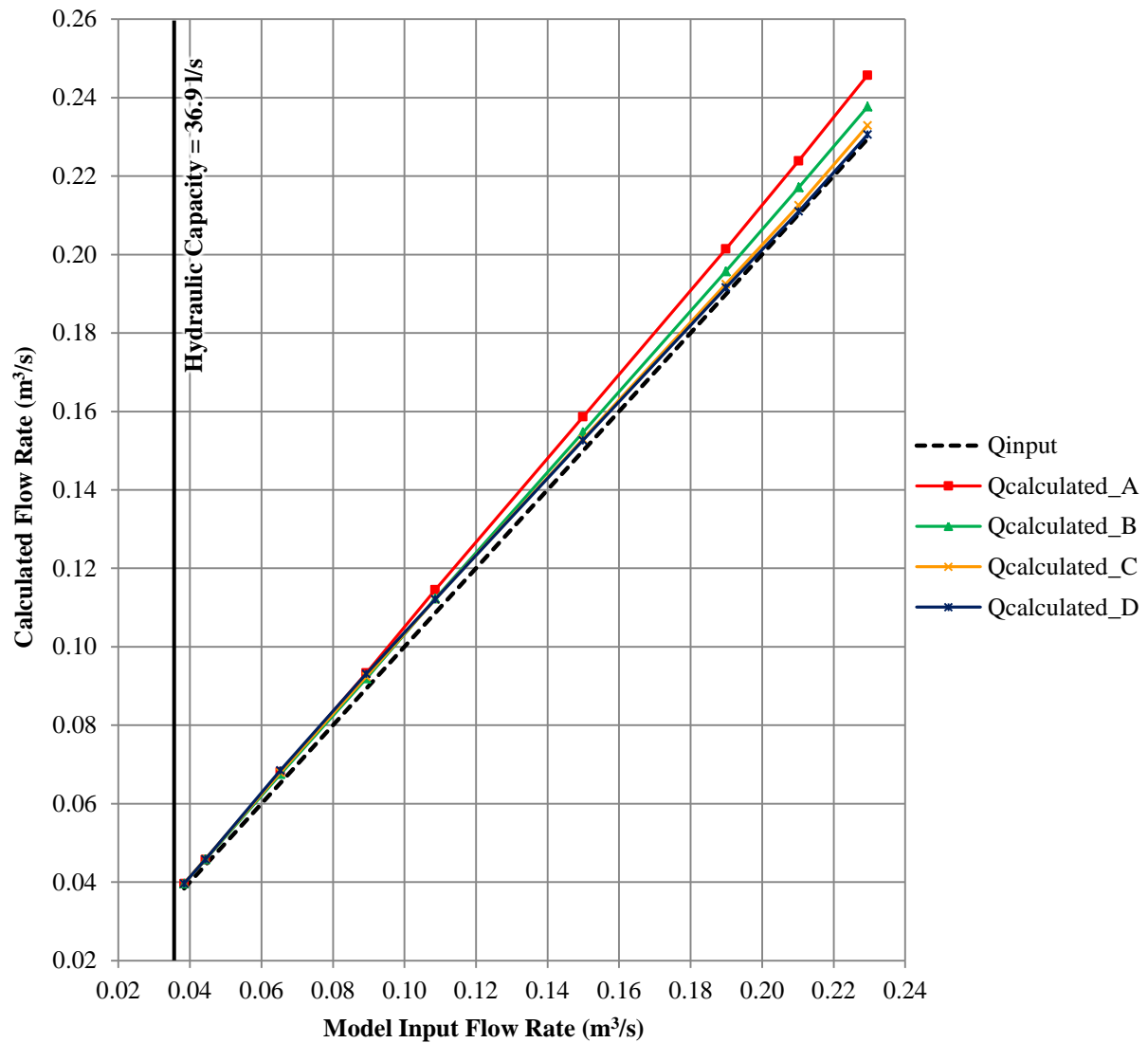
Model Input Flows, $Q_{input}$ (l/s)	Layout A		Layout B		Layout C		Layout D	
	$Q_{calculated\_A}$ (l/s)	E (%)	$Q_{calculated\_B}$ (l/s)	E (%)	$Q_{calculated\_C}$ (l/s)	E (%)	$Q_{calculated\_D}$ (l/s)	E (%)
44.3	45.7	3.15	45.8	3.31	45.9	3.50	45.8	3.37
65.3	68.0	4.24	67.5	3.45	68.0	4.12	68.5	4.93
89.3	93.3	4.45	91.9	2.96	92.5	3.56	93.1	4.31
108.6	114.5	5.46	112.3	3.46	112.1	3.28	112.2	3.31
149.9	158.6	5.80	154.8	3.24	153.0	2.09	152.7	1.88
189.9	201.4	6.06	195.9	3.16	192.6	1.45	191.7	0.97
210.2	223.9	6.49	217.3	3.36	212.7	1.19	211.2	0.46
229.5	245.7	7.07	237.9	3.68	233.1	1.59	230.8	0.57

**Note:** See **Figure 3.3** for details of Layouts A, B, C and D.

$Q_{input}$  = Calibrated model input flow rates as per pumps (l/s)

$Q_{calculated}$  = Flow rate calculated using measured water levels upstream of the model (l/s)

E = Percentage difference between  $Q_{input}$  and  $Q_{calculated}$  (%)



**Figure 4.5:** Graph of physical model results for lower to higher Crump width ratio of 1:1

## 4.2 DISCUSSION OF PHYSICAL MODEL RESULTS

The physical modelling was executed according to the experimental procedure described in **Section 3.3**, for each set-up (lower to higher Crump width ratio,  $B_L:B_H = 1:4, 1:3, 1:2$  and  $1:1$ ) the four model layouts (Layout A, B, C and D) were run for every one of the flow rates being considered. The total flow rate over the whole weir was calculated by the summation of the flow over the right filler wall, lower Crump crest, higher Crump crest and left filler wall using the theoretical equations as shown in **Figure 4.1**. This calculated flow value ( $Q_{\text{calculated}}$ ) was compared to the flow rate that was put into the model ( $Q_{\text{input}}$ ). The flow that occurs over the divider and flank walls, in Layouts B, C and D were quantified as part of the three-dimensional flow influence of each component. Defining an accurate water level above these walls would be based on various assumptions which should account for the cross-flow component that can only be approximated and was not included in the scope of this study.



The theory for calculating discharge over a Crump weir assumes (1) parallel flow lines throughout the channel with (2) near equal velocity distribution over the cross-sectional area and (3) a horizontal energy level perpendicular to the flow direction. The BSI ISO 14139 (British Standards Institution, 2000) suggests that compound weirs be built with divider walls that extend upstream of the water level measuring point to ensure the assumptions made in theory. Thus, the initial experimental assumption was that the divider walls would ensure parallel flow lines throughout the channel with near equal velocity distribution and a horizontal energy line perpendicular to the flow direction; however, this was not the case.

It was anticipated that the green extension walls, mounted onto the divider and flank walls, would extend the domain of parallel flow and that by systematically removing these walls, the effect of the divider and flank walls could be individually quantified. The results presented in **Section 4.1** indicate that the vertical extension walls do not improve the accuracy of the calculated flow rates. It is also important to note that the calculated flow rates for all the ratios and layouts were higher than the model input flow rates. To successfully understand the mechanisms at play, the problem needs to be separated into three distinct observations, namely:

- all layouts show an overestimation in the calculated flow rate values; and
- the systematic removal of the extension walls tends to result in improved accuracy of the calculated flow values;
- changes in the lower to higher Crump width ratio ( $B_L:B_H$ ) show an improvement in the calculated flow values from ratio 1:4 to 1:1.

The following subsections aim at developing an understanding of the flow mechanisms at play in the three results observations.

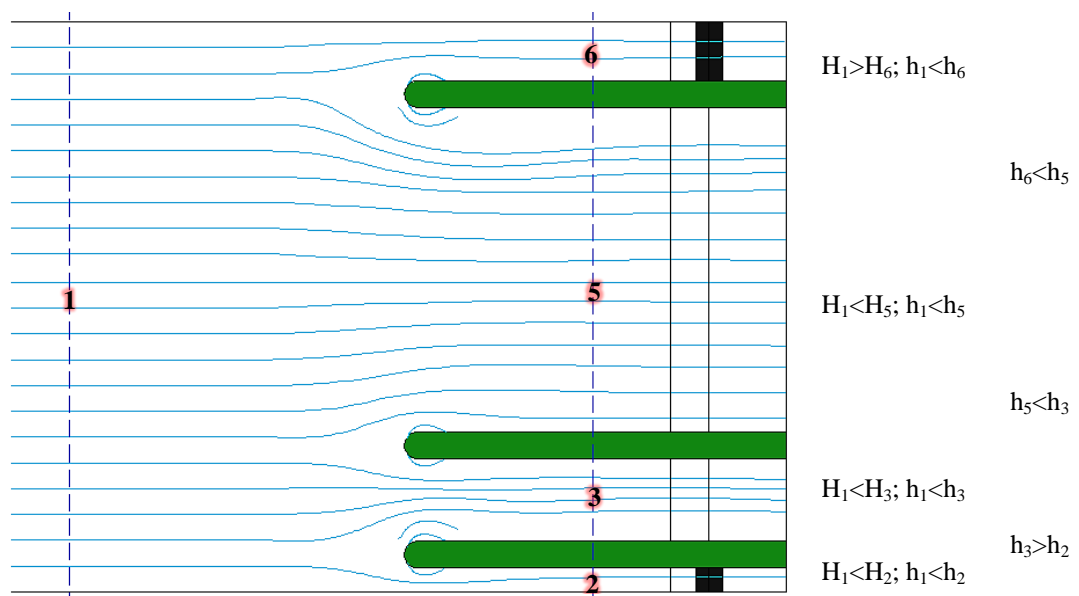
#### 4.2.1 Overestimation of all layouts

In the model design phase, the vertical extension walls were expected to prevent cross-flow over the divider and flank wall components, ensuring parallel flow lines throughout the channel with near equal velocity distribution over the cross-sectional area. Layout A, with the divider and flank walls raised, was thus anticipated to accurately estimate the model input flow rate since the three-dimensional flow lines were prevented.

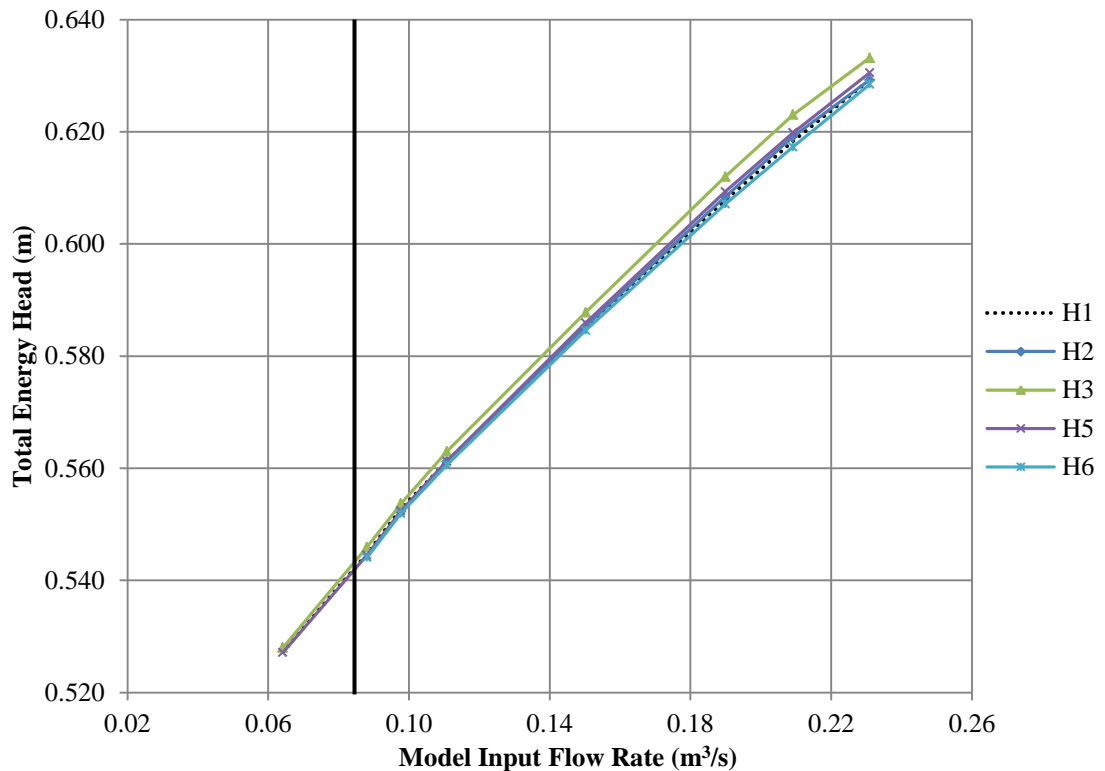
The results seen in **Figure 4.2** to **Figure 4.5** indicate a clear deviation from this expectation since Layout A showed the highest overestimation error compared to the other layouts.

Layout B, with the centre extension wall removed, resulting in some three-dimensional flow lines, shows a similar pattern to Layout A. However, at higher flow rates Layout B shows a lower error when compared to Layout A. The results for Layout C are similar to Layout B; both following the same trend as Layout A and then decreasing in error at higher flow rates. The removal of the right extension wall seems to have little effect on the results possibly due to the right filler wall being relatively short (98 mm wide) compared to the other structural components. The final layout with all extension walls removed, Layout D shows a similar trend to Layouts B and C with a relatively small decrease in the error made. The overestimation of the flow rates for Layout D shows that the predominant energy loss cannot be due to the cross-flow component over the divider and flank walls but instead due to some common factor throughout all the layouts.

Knowing that energy cannot be created nor destroyed (law of conservation of energy) it follows that the energy head from one upstream point ( $H_1$ ) should be equal to the next energy head at some point downstream ( $H_2$ ) if all energy loss components are accounted for. Therefore,  $H_1$  should be equal to  $H_2$  if the conservation of energy is maintained. In **Figure 4.6** below, a top view of the model along with the flow lines as observed during the physical modelling is schematically depicted for Layout A (with extension walls mounted onto the divider and flank walls shown in green) of Ratio 1:4. The figure also shows the relationship between the upstream energy level ( $H_1$ ) and the energy levels at the various measuring points upstream of each weir component ( $H_2$ ,  $H_3$ ,  $H_5$  and  $H_6$ ). The water level head relationships between the various points are also depicted. **Figure 4.7** shows the total energy head at each measuring point, clarifying the relationships shown in **Figure 4.6**.



**Figure 4.6: Schematic of the flow lines as observed for Ratio 1:4 Layout A**



**Figure 4.7: Total energy head (H) at each measuring point for Ratio 1:4 Layout A**

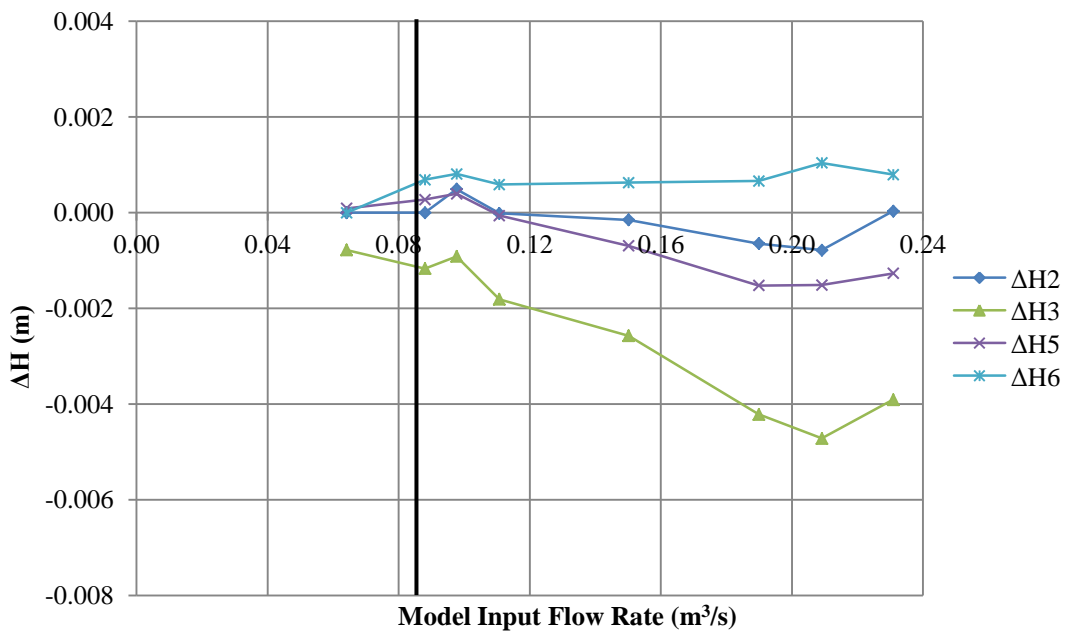
It is important to recall how each energy level depicted in the figure was calculated.  $H_1$  was determined by the summation of (1) the measured water level, and (2) the velocity head calculated from the measured input flow rate. The measured water levels at points 2 and 6 were used to calculate the energy levels  $H_2$  and  $H_6$  using an iterative process of the broad-crested weir equation for the determination of the velocity component. Similarly,  $H_3$  and  $H_5$  were calculated using the measured water levels along with an iterative process of the Crump weir equation.

For Layout A of Ratio 1:4, the energy level at point 1 is calculated to be lower than that of the downstream points 2, 3 and 5 but that the energy level at point 6 is lower than at point 1. According to the law of conservation of energy, an increase in the energy level downstream cannot be possible. **It thus follows that the discharge-head relationship does not hold and that one or more of the assumptions made in the development of the theory is not correct in the modelled case.** It can be concluded that the current discharge-head relationship for Crump weirs is **insufficient** for the determination of flow rate over the weir system in this specific layout.

Upon further investigation of the flow lines as depicted in **Figure 4.6**, it can be seen that eddies occur around the upstream ends of the divider and flank walls resulting in contraction

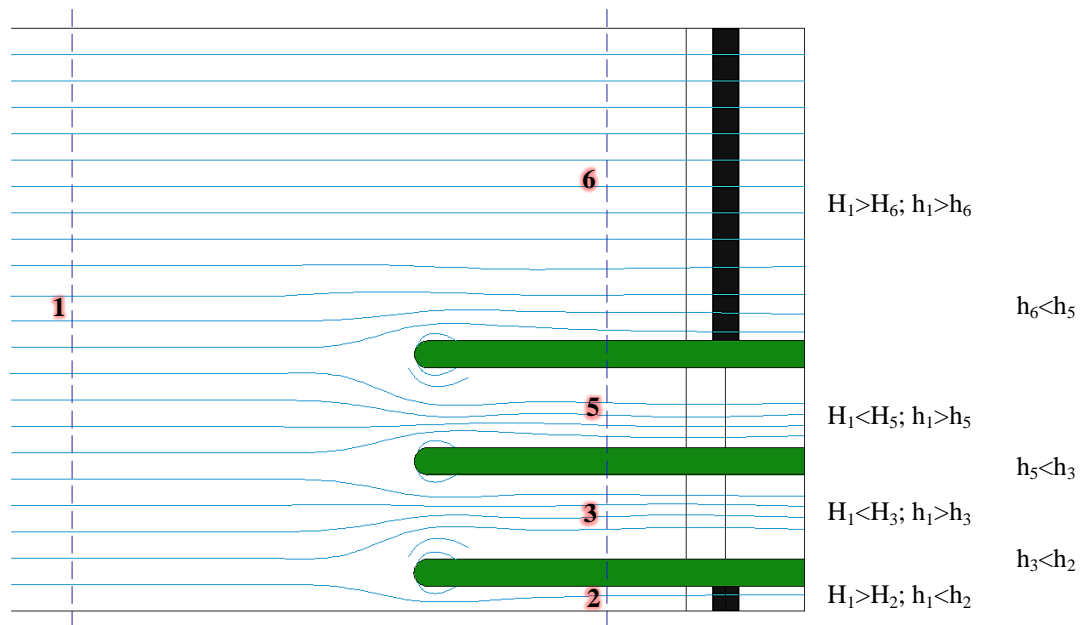
of the flow lines within the two Crump crest channels as well as additional rotational energy. This contraction ultimately results in a decrease in the effective width of each channel resulting in the perceived increase in water level. The narrowing effect along with the unaccounted for rotational energy would explain the overestimation error seen in the results in **Section 4.1**.

**Figure 4.8** shows the extent of the differences in energy levels of the measuring points upstream of each weir component relative to the most upstream energy level ( $H_1$ ). These differences are relatively small but seem to rise with an increase in flow rate. The differences in energy level from points 1 to 2 ( $\Delta H_2$ ) can be considered insignificant with the highest difference being 0.2 mm (recall measuring accuracy of point gauge: 0.1 mm, see **Section 3.2**). The differences between  $H_1$  and  $H_6$  ( $\Delta H_6$ ) can be averaged to around 0.7 mm. The differences in energy levels for the broad-crested weirs ( $\Delta H_2$  &  $\Delta H_6$ ) seem to remain constant whereas the differences in energy levels for the Crump weirs tend to increase with an increase in flow rate. The change in energy level for the higher Crump crest ( $\Delta H_5$ ) follows a similar pattern to that of the lower Crump crest ( $\Delta H_3$ ) but shows an error of half in magnitude. It is also possible that a limit in the errors exist as seen in this case at 209.1 l/s after which all the graphs tend to decrease towards 0.00 m. It might be that the significance of three-dimensional flow becomes less prominent with increased discharge head greater than 209.1 l/s over the structure because of the increased ratio of flow depth upstream of the structure versus the flow depth over the weir.

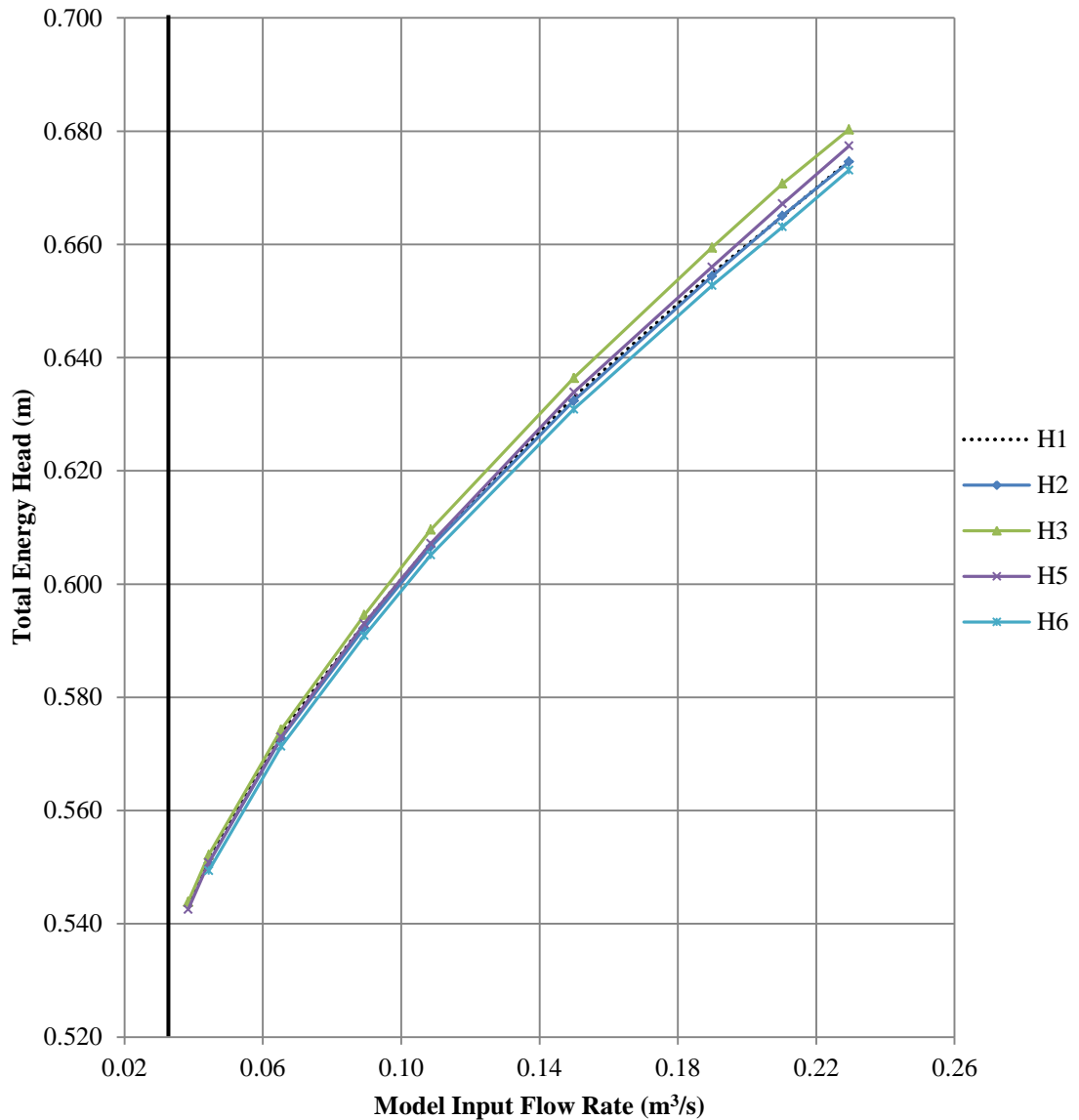


**Figure 4.8: Differences in energy levels at each measurement point relative to the upstream point for Ratio 1:4 Layout A**

**Figure 4.9** shows the flow lines as observed during the physical modelling of Layout A for Ratio 1:1. Similar to the flow lines observed in Layout A for Ratio 1:4, eddies occur around the divider and flank walls resulting in the contraction of flow lines within the two Crump crest channels as well as additional rotational energy. **Figure 4.10** shows the total energy head at each measuring point, clarifying the relationships shown in **Figure 4.9**. The energy level at point 1 is calculated to be lower than that of the downstream points 3 and 5, once again indicating the insufficiency of the discharge-head relationship for Crump weirs for this specific weir design. The flow lines over the left filler wall tend to become more parallel with the increase in width, resulting from the change in lower to higher Crump width ratio. The limitations of the broad-crested weir equation were also observed in this Layout since the energy level at point 1 was calculated to be higher than that of the downstream points 2 and 6 ( $H_2$  &  $H_6 < H_1$ ).

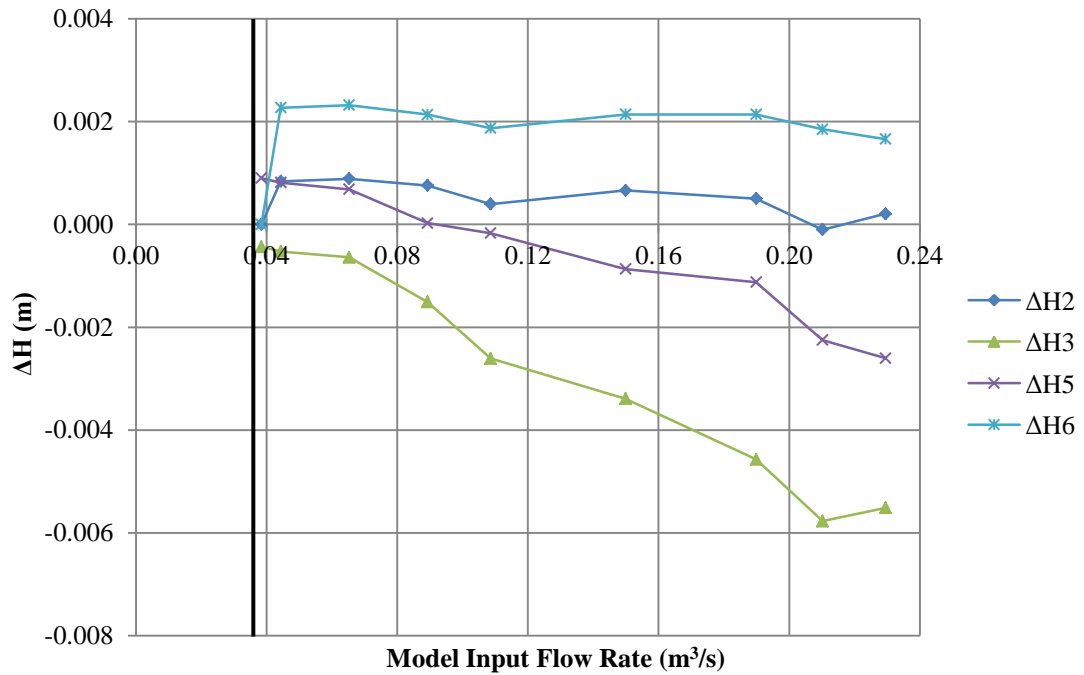


**Figure 4.9:** Schematic of the flow lines as observed for Ratio 1:1 Layout A



**Figure 4.10: Total energy head (H) at each measuring point for Ratio 1:4 Layout A**

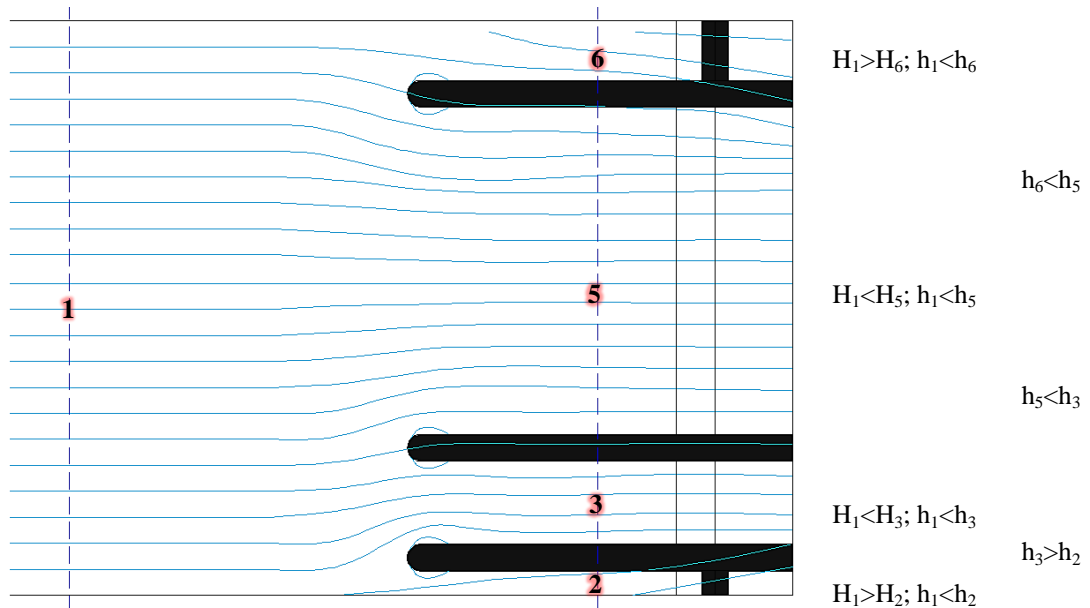
The extent of the differences in energy levels upstream of each weir component relative to the energy level at point 1 is shown in **Figure 4.11**. Like Ratio 1:4, the differences between  $H_1$  and  $H_2$  ( $\Delta H_2$ ) are small and tend to be more positive with the average being 0.5 mm. The differences between  $H_1$  and  $H_6$  ( $\Delta H_6$ ) can be averaged to around 2 mm which is higher than in Ratio 1:4. In both cases, the differences in energy levels for the broad-crested weirs seem to remain constant whereas the differences in energy levels for the Crump weirs tend to increase with an increase in flow rate. The most substantial difference is observed for the lower Crump crest ( $\Delta H_3$ ). A similar limitation in the errors exists at 209.1 l/s after which all the graphs tend to decrease towards 0.00 m.



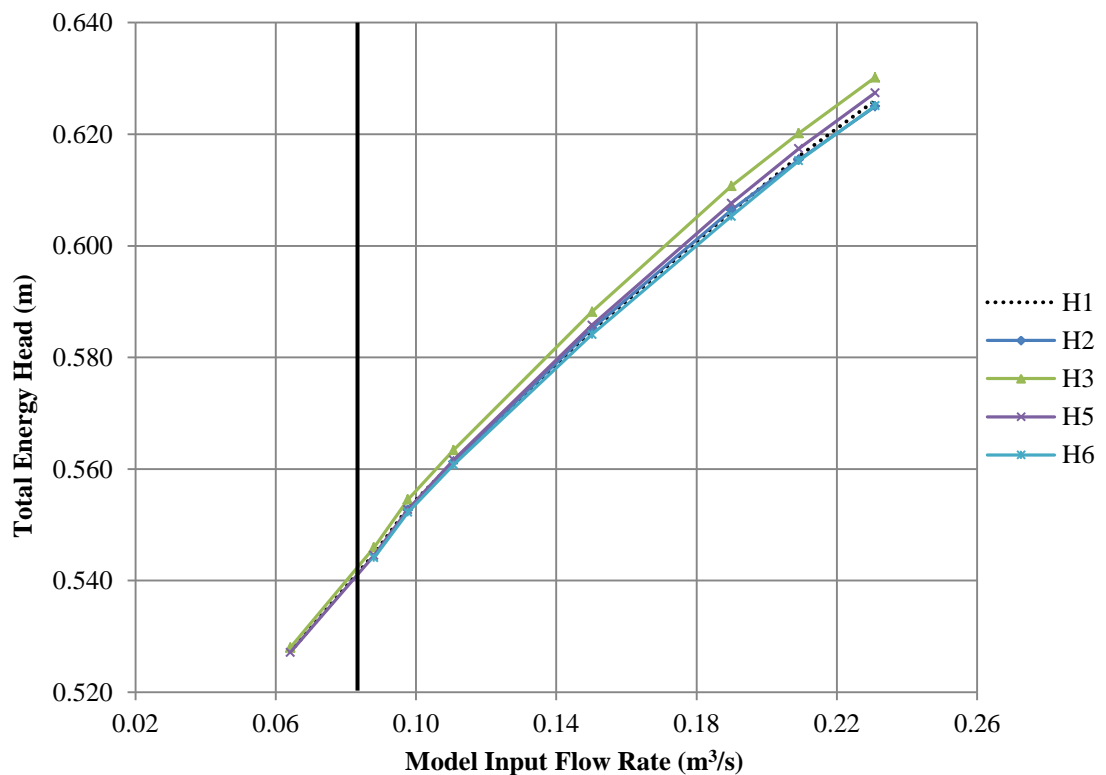
**Figure 4.11: Differences in energy levels at each measurement point relative to the upstream point for Ratio 1:1 Layout A**

**Figure 4.12** depicts the flow lines as observed during the physical modelling of Layout D (with no extension walls, representing the natural scenario) for Ratio 1:4. The relationship between the upstream energy level ( $H_1$ ) and the energy levels at the various measuring points upstream of each weir component ( $H_2$ ,  $H_3$ ,  $H_5$  and  $H_6$ ) along with the water level head relationships between the various points are shown in the figure. **Figure 4.13** shows the total energy head at each measuring point, clarifying the relationships shown in **Figure 4.12**.

Similar to Layout A for Ratio 1:4, the energy levels upstream of the two Crump weirs are calculated to be higher than the energy level at point 1 ( $H_3$  &  $H_5 > H_1$ ), once again confirming that the theoretical equation is insufficient in calculating the flow rate for this specific design. The energy level at point 1 is calculated to be higher than that of the broad-crested weirs (filler walls), which also indicates that the broad-crested weir equations may be insufficient for the weir design being modelled. It should be noted that in Layout A for Ratio 1:4, the energy level at point 2 is higher than at point 1 ( $H_2 > H_1$ ) but that in Layout D of Ratio 1:4 the energy level at point 2 is lower than at point 1 ( $H_2 < H_1$ ), the reason for this change in behaviour is unclear.



**Figure 4.12: Schematic of the flow lines as observed for Ratio 1:4 Layout D**

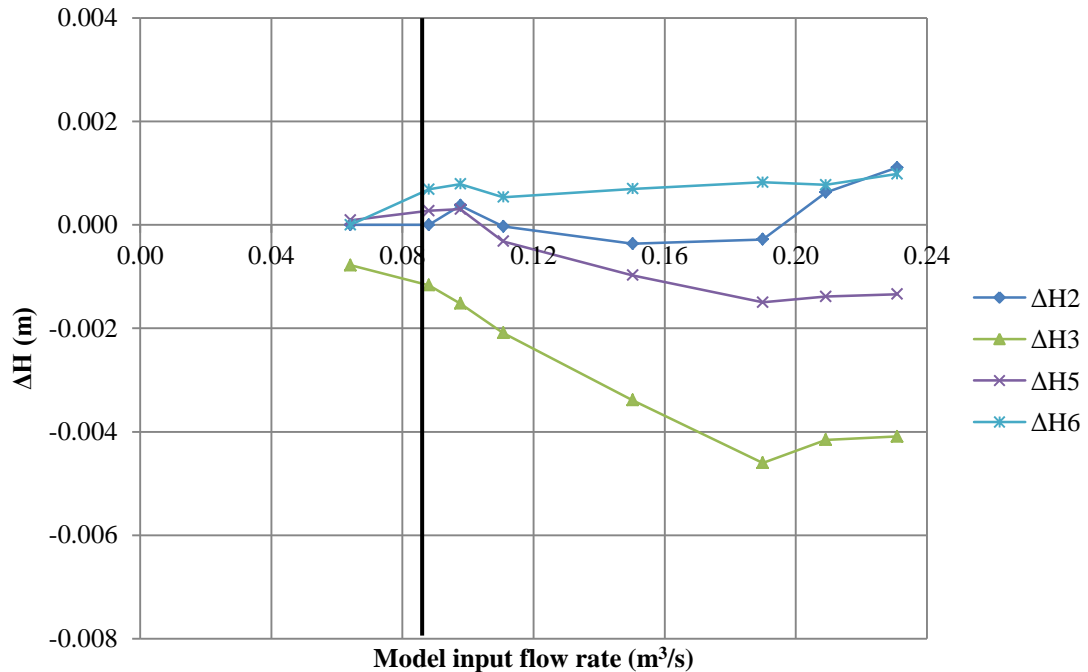


**Figure 4.13: Total energy head (H) at each measuring point for Ratio 1:4 Layout D**

The differences in energy levels upstream of each weir component relative to the energy level at point 1 are shown in **Figure 4.14**. The differences between  $H_1$  and  $H_2$  ( $\Delta H_2$ ) are positive and averages to a value of 0.8 mm. The differences between  $H_1$  and  $H_6$  ( $\Delta H_6$ ) are almost negligible up to 209.1 l/s where the error seems to be the same as for  $\Delta H_2$  but follows an



increasing trend. This pattern is also seen in Layout A for Ratio 1:4 (**Figure 4.8**). The difference in energy levels for the higher Crump weir ( $\Delta H_5$ ) increases up to 189.9 l/s after which a plateau of 0.13 mm is seen. A limit is also evident for the lower Crump crest ( $\Delta H_3$ ) starting at 189.9 l/s with a plateau of 4 mm.



**Figure 4.14: Differences in energy levels at each measurement point relative to the upstream point for Ratio 1:4 Layout D**

The flow lines, as observed during the physical modelling of Layout D for Ratio 1:1, are shown in **Figure 4.15** with the total energy head at each measuring point shown in **Figure 4.16**. Similar to Layout D for Ratio 1:4, the contraction of flow lines within the two Crump crest channels are observed with the addition of cross-flow into these channels. The cross-flow tends to favour the Crump crest channels possibly due to the higher flow velocities experienced. The insufficiency of the discharge-head relationship for Crump weirs for this specific weir design is seen by the calculated energy level at point 1 being lower than at the downstream points 3 and 5 ( $H_3$  &  $H_5 > H_1$ ). The flow lines over the left filler wall are also seen to be more parallel with the increase in width brought about by the change in lower to higher Crump width ratio. As before, the energy level at point 1 is calculated to be higher than that of the downstream points 2 and 6 ( $H_2$  &  $H_6 < H_1$ ).

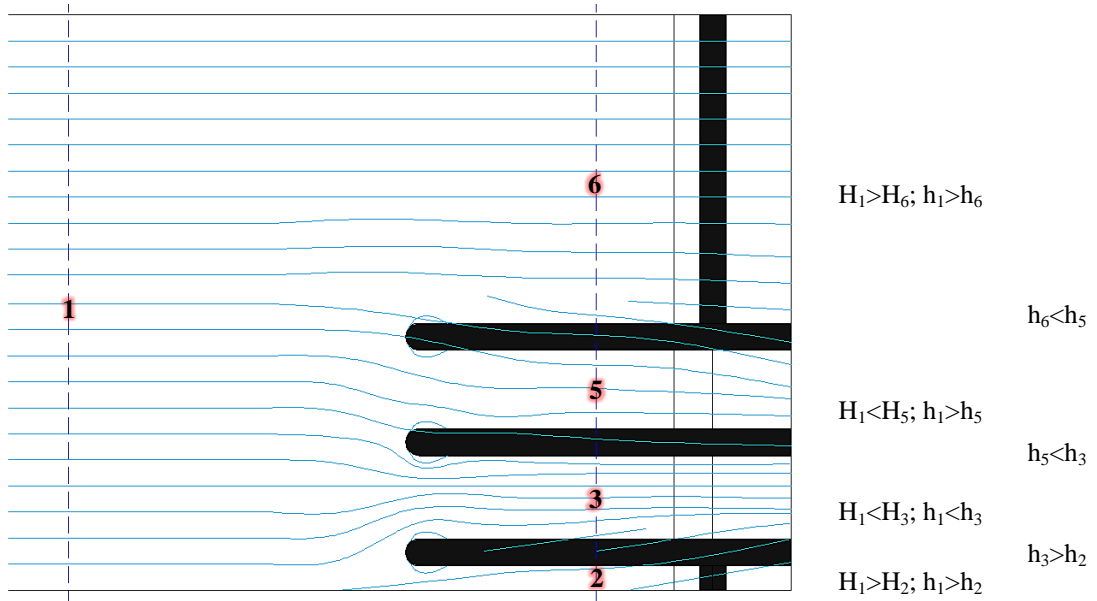


Figure 4.15: Schematic of the flow lines as observed for Ratio 1:1 Layout D

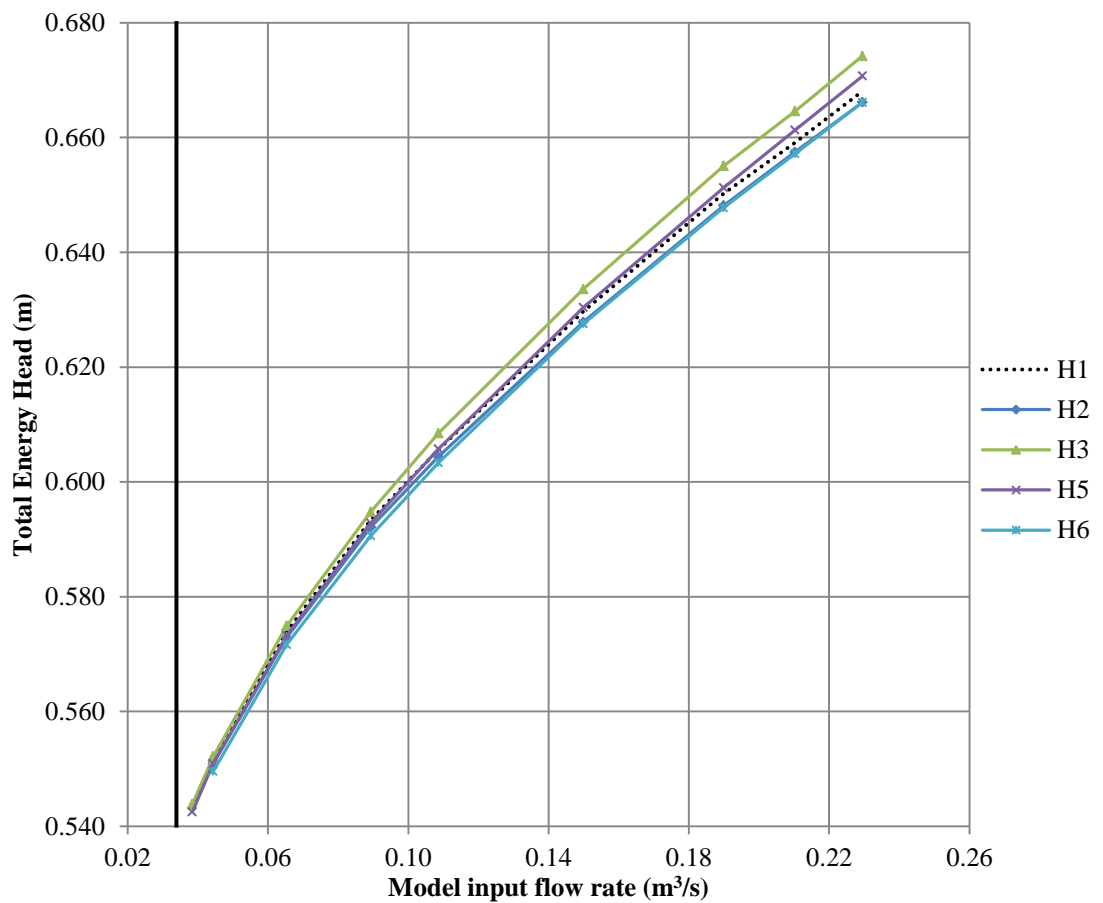
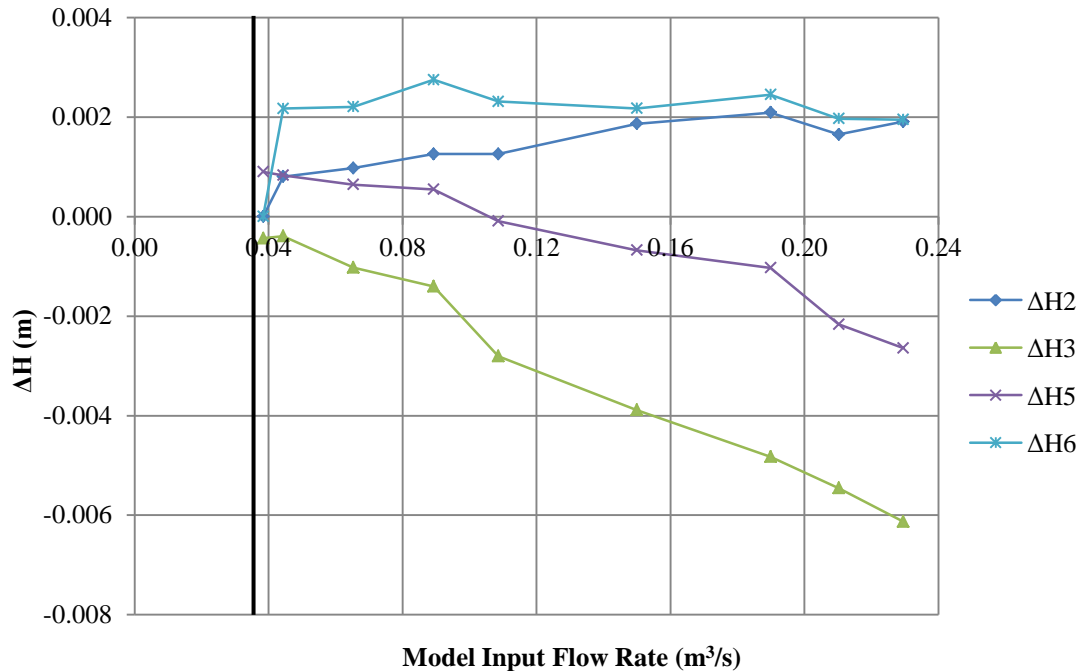


Figure 4.16: Total energy head (H) at each measuring point for Ratio 1:1 Layout D

Figure 4.17 shows the differences in energy levels upstream of each weir component relative to the energy level at point 1. The differences between  $H_1$  and  $H_2$  ( $\Delta H_2$ ) and between  $H_1$  and

$H_6$  ( $\Delta H_6$ ) tend toward one another, reaching the same value at 230.9 l/s. The differences can be averaged to around 2 mm similar to  $\Delta H_6$  in Layout A for Ratio 1:1 (**Figure 4.11**). As before, the differences in energy levels for the Crump weirs tend to increase with an increase in flow rate. No limitations in the errors can be noted indicating that a higher flow rate would need to be investigated if the values are to be fully accounted for in correction factors.

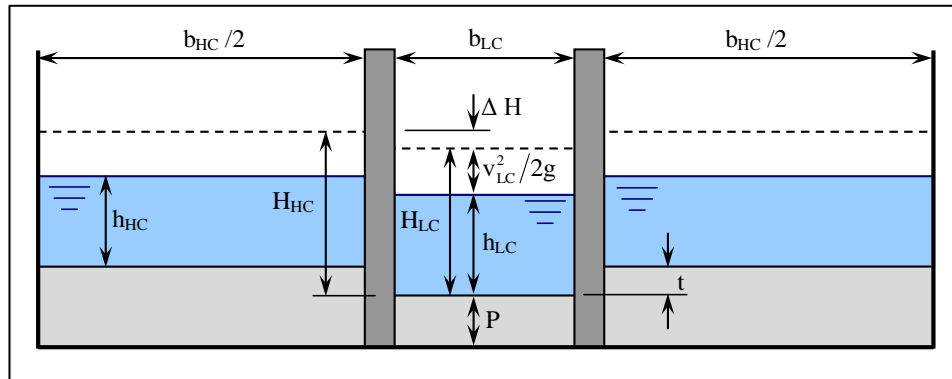


**Figure 4.17: Differences in energy levels at each measurement point relative to the upstream point for Ratio 1:1 Layout D**

For further detail of the observed flow lines and differences in energy levels at each measurement point relative the upstream point of all layouts for Ratios 1:3 and 1:2 as well as Layouts B and C for Ratios 1:4 and 1:1, refer to **Annexure A** at the end of the dissertation.

The flow line figures show that the water levels upstream of the lower Crump crest are higher than the water levels upstream of all of the other weir components ( $h_3 > h_2, h_5, h_6$ ). This, in turn, results in a higher total energy heads upstream of the low Crump crest,  $H_{LC}/H_3$ , than upstream of all of the other weir components ( $H_{LC} > H_2, H_5, H_6$ ). During his study of compounding weirs, Wessels (1996) found that for a very shallow pool and relatively short low crest, the total energy head upstream of the higher crests,  $H_{HC}$ , is  $\Delta H$  higher than the total energy head calculated from the measured water level upstream of the lower crest,  $H_{LC}$  ( $H_{HC} = H_{LC} + \Delta H$ ). He also found that for lower flow rates (all within the designed hydraulic limit) the calculated flows tend to underestimate the input flow value. He attributed this underestimation to three-dimensional flow conditions that were induced by the divider walls

upstream of the measuring point. He also suggested that the  $\Delta H$  value was induced due to the step height difference between the lower and higher crests. The correction factors derived from his finding were developed by Wessels and Rooseboom in 2009 and are described in **Section 2.4.7**. The definition sketch for these correction factors is shown below in repeated **Figure 2.13**.



**Figure 2.13 (repeated): Definition sketch for correction factors of compound Crump weirs with divider walls (Wessels & Rooseboom, 2009 (b))**

It is important to note that Wessels and Rooseboom (2009 (b)) considered compound weirs within hydraulic capacity. They also considered weirs with various different  $H_{LC}/t$  ratios. They came to the conclusion that the effects of compounding with divider walls were negligible for:

$$\frac{H_{LC}}{t} > 2.5$$

where:

$H_{LC}$  = total energy head upstream of the lower crest (m)

$t$  = step height between the lower and higher crests (m)

This limit of 2.5 is far exceeded in the study discussed in this dissertation with  $H_{LC}/t$  values all greater than 3.4 thus the effects of compounding were considered negligible.

The design of the model set-up was based on the conclusions made by Wessels (1996), namely; (1) the effects of compounding are negligible when  $H_{LC}/t > 2.5$ , and (2) at flow rates above hydraulic capacity of the weir (known as overtopping flow conditions), the cross-flow effect is the most significant contributor to errors observed in the flow rate calculations. The raising of the divider and flank walls were intended for the prevention of cross-flow, assuring parallel flow conditions and ultimately nullifying the errors induced by overtopping. The

study at hand, however, proved to contradict the conclusions made by Wessels (1996), since the layout with all extension walls raised, showed a more substantial overestimation error than any of the layouts with some or all of the extension walls removed. It thus follows that another aspect of the selected design contributes a more significant role in the disturbance of the flow lines than initially anticipated. That is: *the divider and flank wall thicknesses relative to the selected lower Crump crest width.*

The relative scale of the model was based on the pump capacity limitations experienced by the DWS Laboratories. The channel width had to be selected in such a way that at the maximum flow rate, the water level head would be at least  $1 \times H_d$  (design head) above the divider and flank walls. The step height between the lower and higher Crump crests was selected as 30 mm to ensure that the compounding effect would be accurately observed. The 30 mm step height then represents a 1:10 scale since the prototype structure requires a minimum step height difference of 0.3 m. It is common in practice to construct divider, flank and filler walls with a 1 m thickness. Therefore, for a 1:10 model scale, the thicknesses would need to be 100 mm. Wessels (1996) used divider wall thicknesses of 25 mm which is significantly thinner than the 100 mm used in the study at hand.

The model channel width of 1865 mm at a prototype scale of 1:10 is 18.65 m; it is likely that the designer would have selected one of the following options for flow measurements in the channel, depending on the site conditions:

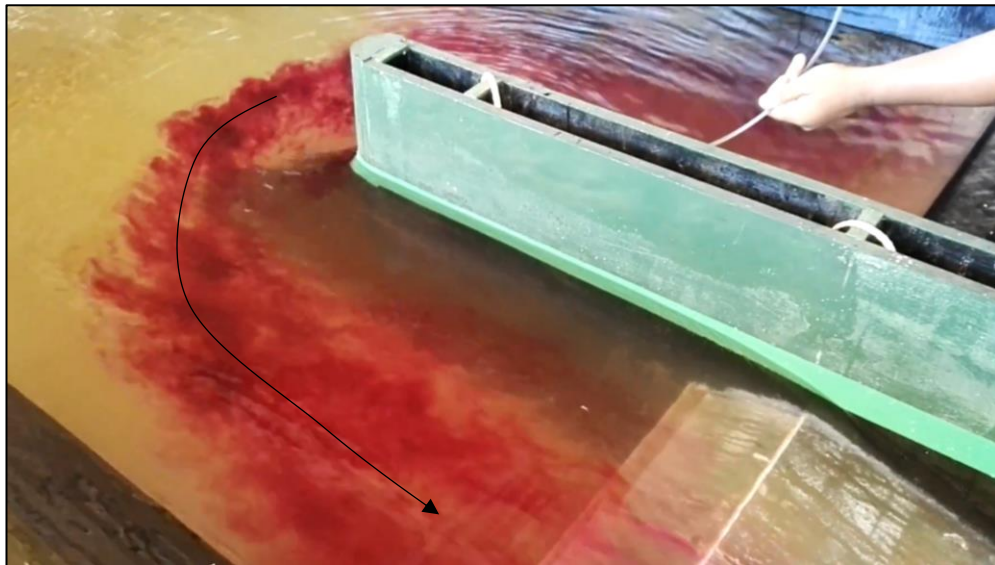
- a single crest set-up with flank and filler walls for narrowing of the channel; or
- a multi crest set-up with a divider wall, a low crest width of 6 or 9 m and filler walls extending to rock level.

However, due to the need for investigating multiple compound weir set-ups, it was decided to keep the low crest width constant at 309 mm (3 m in the prototype) while changing the higher crest width to model different lower to higher crest width ratios. If one considers the relative width of the divider and flank walls to that of the low crest (1:3), it could be possible that the divider and flank wall thicknesses had a more significant effect on the flow lines than initially anticipated, which may well explain the overestimation error seen in the results for all layouts.

Consider the photograph of the physical model in **Figure 4.18**, the right flank and extension walls resulted in eddy formation around the upstream ends of the walls, forcing the flow lines towards the left of the Crump crest as shown by the inserted dye. It was also evident that

three-dimensional flow was present within the upstream pool. As previously discussed, the divider and flank walls result in large-eddy formation around the upstream ends, narrowing the effective flow area over the Crump crests, even in the cases where the extension walls are removed. This narrowing effect is also indicated by the dye insert in **Figure 4.18** (flow near the wall is clear). These flow lines were also observed for ratios 1:1, 1:3 and 1:4, and seemed to be intensified with an increase in the flow rate.

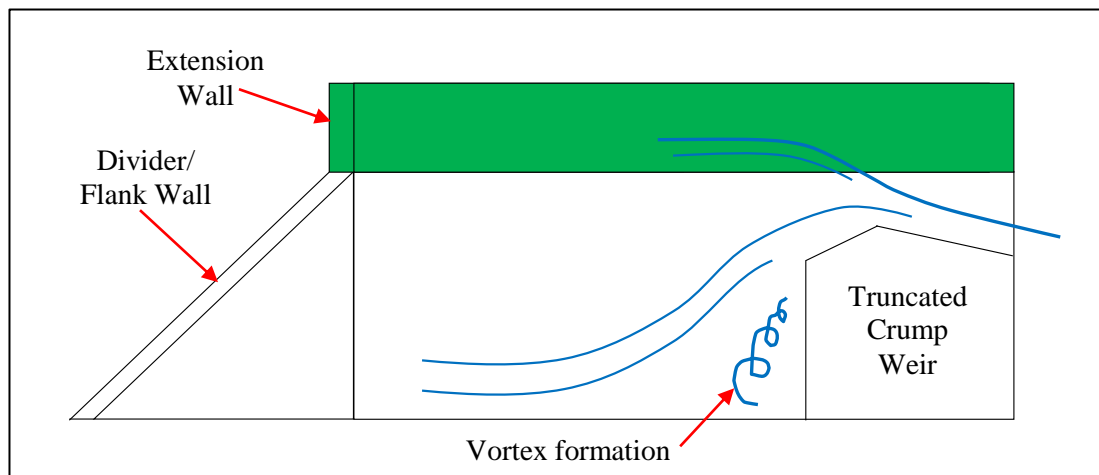
Additionally, the narrowing of the effective flow area due to eddies forming upstream may result in a vortex developing when the flow hits the truncation of the Crump weir, thereby increasing the rotational activity in the body of water, adding to increased water levels. The photograph of the model in **Figure 4.19** shows evidence of the vortex in the form of a depression line. This phenomenon was also observed by Wessels (1996) in his experimental modelling of sharp-crested weirs. A schematic of the flow lines within the body of water upstream of the Crump weir truncation is shown in **Figure 4.20**.



**Figure 4.18: Photograph of 3-dimensional flow phenomena observed during physical modelling**



**Figure 4.19: Vortex formation evident over Crump crest**



**Figure 4.20: Vortex formation upstream of Crump crest (Wessels, 1996)**

The influence of the divider and flank wall thicknesses relative to the lower Crump crest width is understood to have the most substantial influence on the overestimation error seen in the results. The increase in rotational energy and the narrowing of the effective flow area due to eddy formations upstream of these walls causes an increase in the measured water level which is unaccounted for in the current discharge-head relationship for Crump weirs. It is, however, useful to investigate the influences of cross-flow as well as the change in lower to higher Crump crest width ratio on the results. Further explanation is provided in the successive sections.



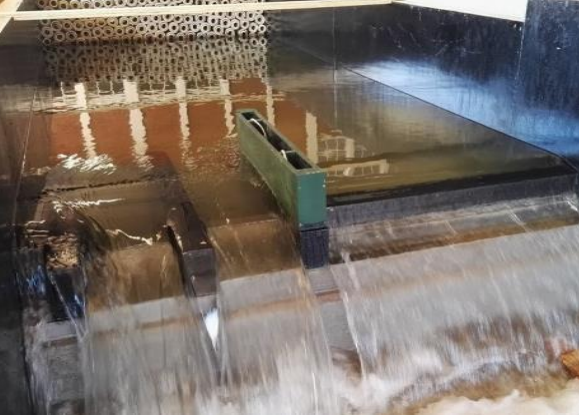

#### 4.2.2 Effect of cross-flow over the divider and flank walls

The green extension walls were used to prevent cross-flow over the divider and flank wall components. They were then systematically removed with the anticipation of quantifying the influences of each component on the observed water levels. The divider and both flank walls were raised for Layouts A, then in Layout B the centre extension wall was removed, for Layout C the right extension wall was also removed resulting in only the left flank wall being raised and finally Layout D had all of the extension walls removed resulting in a model similar to the natural occurrence in the field. This systematic removal of the extension walls caused the flow lines over the Crump crests to change as illustrated in **Table 4.5**.

In Layout A, the flow is confined to the filler walls and Crump crests, with no flow over the divider and flank walls. In Layout B the flow is no longer confined to the Crump crests but is seen to spill over the divider wall. The flow lines tend to move to the right of the lower Crump crest and the left of the higher Crump crest. For Layout C, only the right extension wall remains, resulting in diagonal flow lines over the lower Crump crest since the velocity in this region is higher than over any of the other crests. The flow over the left flank wall tends to favour the higher velocity zone resulting in the diagonal flow lines. Layout D showed cross-flow over the divider and flank walls, due to the lack of extension walls, resulting in three-dimensional flow lines over the Crump crests. Flow is observed over the divider wall but not over the filler walls. This is due to the larger flow area and higher flow velocity over the Crump crests resulting in diagonal flow over the filler walls into the Crump crest sections. It can also be seen that parallel flow lines occur over the left filler wall but that some disturbances are apparent in the flow lines over the right filler wall.



**Table 4.5: Photographs of flow lines observed as a result of eddy formation around the upstream ends of the extension walls for Layout A, B and C of Ratio 1:1**

Photograph	Problem Description
	<p><b><u>Model configuration:</u></b> Layout A</p> <p><b><u>Flow lines:</u></b> Flow confined to filler wall and Crump crests with no flow over the divider and flank walls. Three-dimensional flow lines are visible over Crump crests.</p>
	<p><b><u>Model configuration:</u></b> Layout B</p> <p><b><u>Flow lines:</u></b> The flow lines tend to move to the right for the lower Crump crest and to the left for the higher Crump crest.</p>
	<p><b><u>Model configuration:</u></b> Layout C</p> <p><b><u>Flow lines:</u></b> Diagonal flow lines over the lower Crump crest due to higher velocity.</p>
	<p><b><u>Model configuration:</u></b> Layout D</p> <p><b><u>Flow lines:</u></b> Flow over divider wall with diagonal flow over filler walls, due to larger flow area and higher velocity over Crump crests. Parallel flow lines occur over left filler wall, and some disturbances are apparent over the right filler wall.</p>

The previous section suggests that it is suspected that the size of the divider and flank walls may be resulting in higher water levels upstream of the filler walls and Crump crests due to the adverse effects of eddy formation upstream of the walls. The removal of the extension walls leads to an improvement in the accuracy of the calculated flow rates, as seen in **Section 4.1: Figure 4.2, Figure 4.3, Figure 4.4 and Figure 4.5**. It is suspected that the removal of the extension walls alleviates some of the contraction caused by the upstream eddies formed due to the presence of the divider and flank walls. This then results in fewer disturbances in the flow lines over the filler walls. The alleviation in contraction is evident in the results in **Section 4.1** since the overestimation of Layout D for all the model ratios tends to be lower than that of Layout A.

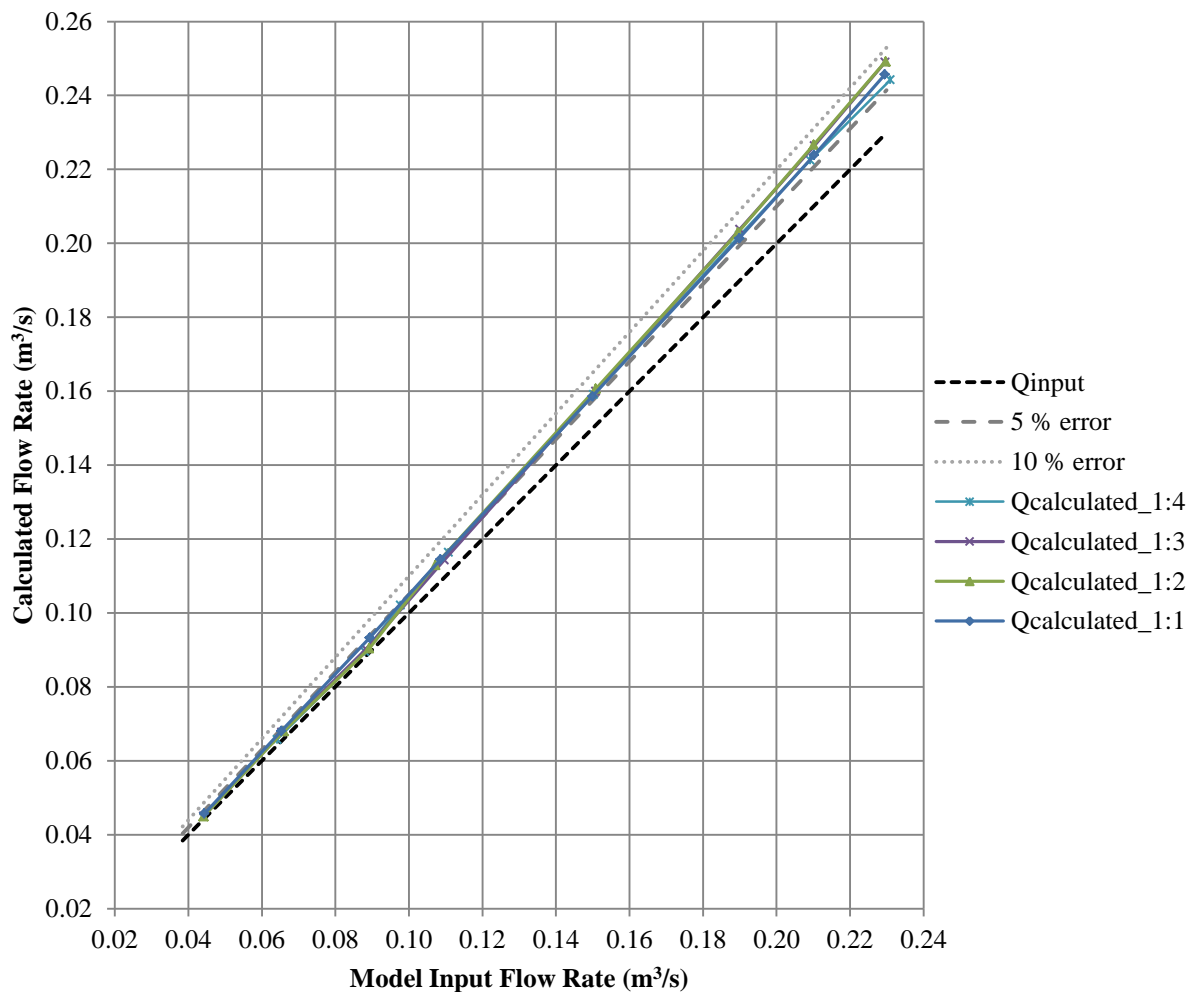
Additionally, the unaccounted flow over the divider and flank walls also contributes to the decrease in the overestimation error. **This omission of flow favours the results but should not mislead the reader into thinking that the discharge-head equation shows an improvement in estimating the flow when the extension walls are removed. This is not the case, the addition of the flow over the divider and filler walls could prove to increase the overestimation error seen in the results to a value closer to that of Layout A.**

### 4.2.3 Effect of changing the lower to higher-Crump width ratio

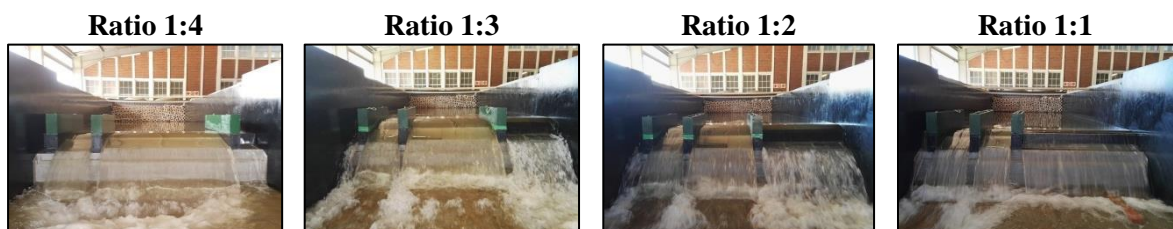
The effect of changing the lower to higher Crump width ratio is illustrated by comparing the various ratios for Layouts A and D in **Figure 4.21** and **Figure 4.22**, respectively. A pattern of improvement of the overestimation error from ratio 1:4 to 1:1 can be seen in the results. It is instinctive to assume that the improvement in the error is due to the lower to higher Crump crest width ratio decreasing and thus to conclude that a lower ratio would result in improved accuracy of the calculations. However, this improvement in accuracy can be attributed to the increase in the length of the left filler wall as the model ratio decreases. This then increases the left filler wall's portion of contribution to the total flow value. As seen from **Table 4.5**, the flow lines over the left filler wall tend to be more parallel in nature displaying fewer disturbances over the crest. Therefore, as the filler wall's contribution increases the total flow becomes more accurate thus decreasing the overestimation error.

The results for Layout A, for all four lower to higher Crump width ratios ( $B_L:B_H$ ) 1:1, 1:2, 1:3 and 1:4, are compared in **Figure 4.21** along with a 5% and 10% overestimation error line, for better interpretation of the results. The results indicate that all four ratios over-estimate the model input flow rates by less than 5% up to 110.8 l/s. All four ratios then increasingly over-estimate the flow rates by greater than 5% up to a maximum of 9.18% for Ratio 1:4 (see

**Table 4.1).** Ratio 1:3 displays a slight improvement of the overestimation error with a maximum of 8.73% at 229.6 l/s (see **Table 4.2**). The error improves to 8.67% at 229.7 l/s for ratio 1:2 as seen in **Table 4.3**. Ratio 1:1 shows the lowest overestimation error in the calculated flow rate with a maximum of 7.07% at 229.5 l/s as shown in **Table 4.4**. The results for Layout A showed a maximum overestimation error at the maximum model input flow rate with no apparent turning point being reached.



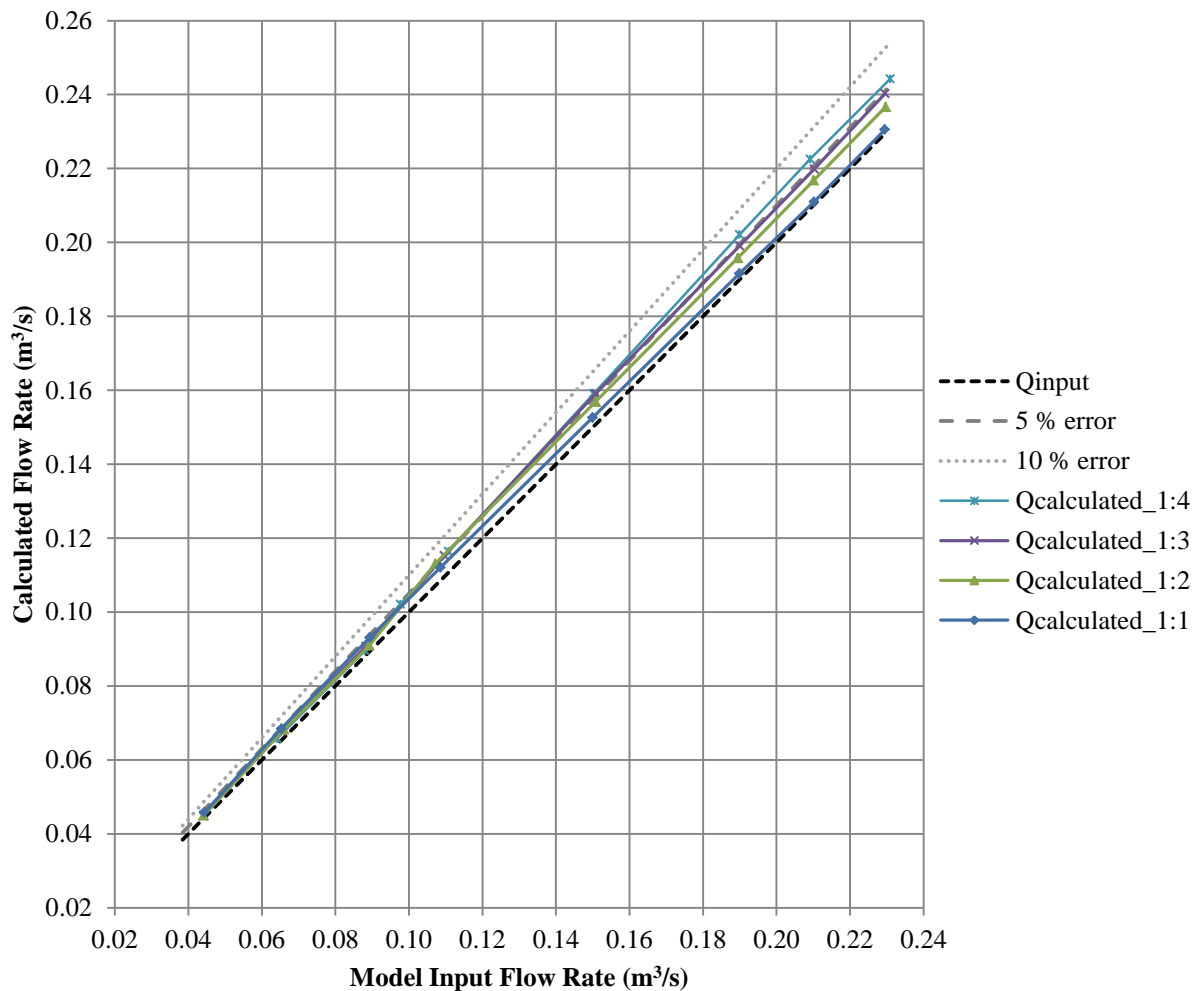
Note:



**Figure 4.21: Graph of physical model results for Layout A**

The results for Layout D, for all four lower to higher Crump width ratios, are compared in **Figure 4.22**. The results indicate that all four ratios overestimate the model input flow rates

by less than 5% up to 109 l/s. Ratio 1:4 then increasingly overestimates the flow rates by greater than 5% up to a maximum of 6.58% (see **Table 4.1**). Ratio 1:3 displays a slight improvement of the overestimation error with a maximum of 5.67% at 150.8 l/s after which the error decreases for higher flow rates (see **Table 4.2**). The turning point for ratio 1:2 is seen at 107.2 l/s with an error of 5.59% after which the error improves to 3.19% at 229.7 l/s (see **Table 4.3**). Ratio 1:1 shows the lowest overestimation error in the calculated flow rate with a maximum of 4.93% at 65.3 l/s after which the error improves to 0.57% at 229.5 l/s as shown in **Table 4.4**.



Note:

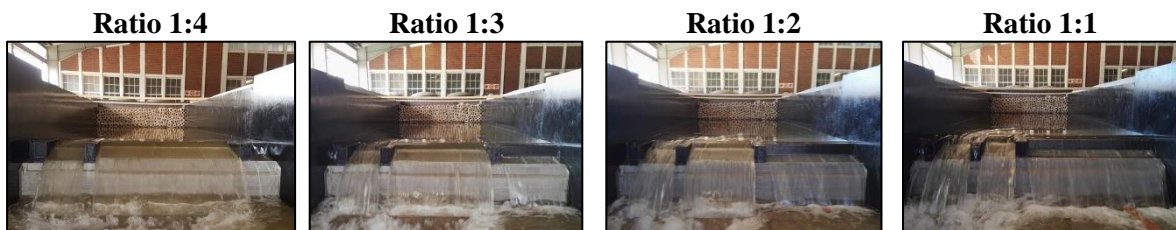


Figure 4.22: Graph of physical model results for Layout D

### 4.3 CORRECTION OF ERRORS SEEN IN RESULTS

#### 4.3.1 The implication of an additional error

Considering the results discussed above, it would be necessary to determine whether the error in the observed water level readings and resultant flow rate values is significant or not. When considering the general practices for the gathering of flow data at gauging stations in South Africa, some factors influence the accuracy of the calculated flow values, namely (Bing, 1991):

- incorrect application of theoretical discharge-head relationships;
- deviating from the standards for designing of gauging stations; and
- human error in gauge plate reading, surveying of elevation reference and checking of raw data.

In addition to the errors mentioned above, there are inherent flaws in the theoretical equations which are based on the accuracy with which the original experiments were done. Ackers et al. (1978) stated that the uncertainties, derived at a 95% confidence level for the Crump weir, is  $\pm(10 C_d - 9)\%$  and for broad-crested weirs is  $\pm 3\%$ .

Recall that:

$$C_d = 1.163 \left( 1 - \frac{0.0003}{h} \right)^{3/2}$$

where:

$C_d$  = modular discharge coefficient

$h$  = measured water level reading (m)

For standard design procedures, the incorrect application of the theory is inevitable since only a single water level measuring point is provided upstream of the lowest weir crest (if submergence is a concern, an additional downstream measuring point is provided in the form of a gauge plate which is manually recorded on inspection). The measured upstream water level is then used to calculate a total head which is assumed to be constant over the full width of the weir section ( $H_{HC} = H_{LC} - t$ ) as seen in **Section 2.4.7** (Wessels & Rooseboom, 2009 (b)). Furthermore, compound weirs designed without the proper use of divider walls or operated without applying the corrections for compounding would result in further inaccuracies in the resultant flow rate values. If the lower Crump crest values were used to calculate the total head over the full width of the section, a greater overestimation error in the

calculated flow rates would result. **Table 4.6** compares the error in flow rate calculated using total head values upstream of each crest with those calculated from the total head value upstream of the lower Crump crest (results for Layout D of Ratio 1:4). The table shows that a 6.61% error in the multi-crest flow calculation method ( $Q_{\text{calculated}_M}$ ) translates to a 9.36% error in the single-crest flow calculation method ( $Q_{\text{calculated}_S}$ ) using the water level at the lower Crump notch.

**Table 4.6: Comparing the error in calculated flow rates using a single-crest stage measurement with those using multi-crest stage measurements**

Model Input Flows, $Q_{\text{input}}$ (l/s)	Multi-crest stage measurements		Single-crest stage measurements	
	$Q_{\text{calculated}_M}$ (l/s)	E (%)	$Q_{\text{calculated}_S}$ (l/s)	E (%)
<b>64,1</b>	65,8	2,57	66,6	3,92
<b>88,0</b>	89,6	1,78	91,2	3,56
<b>97,7</b>	102,2	4,63	104,4	6,88
<b>110,8</b>	116,5	5,18	118,8	7,24
<b>150,2</b>	159,3	6,05	162,9	8,47
<b>189,9</b>	202,5	<b>6,61</b>	207,7	9,36
<b>209,1</b>	222,9	6,58	227,8	8,90
<b>230,9</b>	244,7	5,96	249,7	8,14

Other deviations from the standards include; negligence in selecting an appropriate upstream reach (resulting in high approach velocities), inappropriate width-of-crest to width-of-channel ratio, disregard for the minimum pool depth limits and inappropriate placing of gauge plates. According to Bing (1991), any combination of these errors could be as severe as  $\pm 4\%$  of the measured water levels which would translate to  $\pm 6.3\%$  in the calculated flow rate.

The significance of the overestimation error seen for higher flows over the hydraulic capacity of compound Crump weirs is better communicated regarding the mean annual runoff (MAR), used in sizing infrastructure such as reservoirs discussed in **Section 2.3**. Gauging stations are typically designed to measure up to 80% of the total volume contribution over the full length of the flow record. However, in rivers with large catchment areas, this would be unfeasible and impractical. Consequently, the gauging stations in large rivers are usually designed to measure only 50% of the total volume contribution. For the worst-case scenarios, 20 and 50% of the calculated MAR values would be overestimated for small and large catchments, respectively. For an overestimation error of 6.61% above hydraulic capacity with no indirect measurements implemented to improve high discharge ratings, the MAR for small catchments

could be overestimated by 1.3% resulting in a reservoir capacity that is 3.5% smaller than required to deliver a yield of 80% of the MAR. Similarly, for large catchments the MAR could be overestimated by 3.3% resulting in an 8.9% smaller reservoir on average, generating a significant shortfall in the supply.

### 4.3.2 Partial correction of overestimation error

Layout A is uninfluenced by cross-flow over the divider and flank walls because of the extension walls and therefore represents a model with infinite hydraulic capacity. It then follows that the only influence on the results is the excessive contraction and increased rotational energy within the body of water caused by the eddy formation upstream of the divider and filler walls. Correction factors can thus be applied to the results of Layout A in such a way that the overestimation error is reduced to zero. If these same correction factors are then applied to Layouts B, C and D then the only influence on the flow will be the effect of the cross-flow component since the effect of contraction and increased rotational energy is removed. This is, however, a simplified approach since the alleviation of the contraction due to the removal of the extension walls is unaccounted for.

The correction factor is subtracted from the total energy head using a water level adjustment, as follows:

$$H = (h - \Delta h_c) + \frac{V^2}{2g} \quad (4.1)$$

where:

H = total energy head upstream relative to the weir crest (m)

h = measured water level upstream relative to the weir crest (m)

$\Delta h_c$  = water level adjustment value correcting for contraction (m)

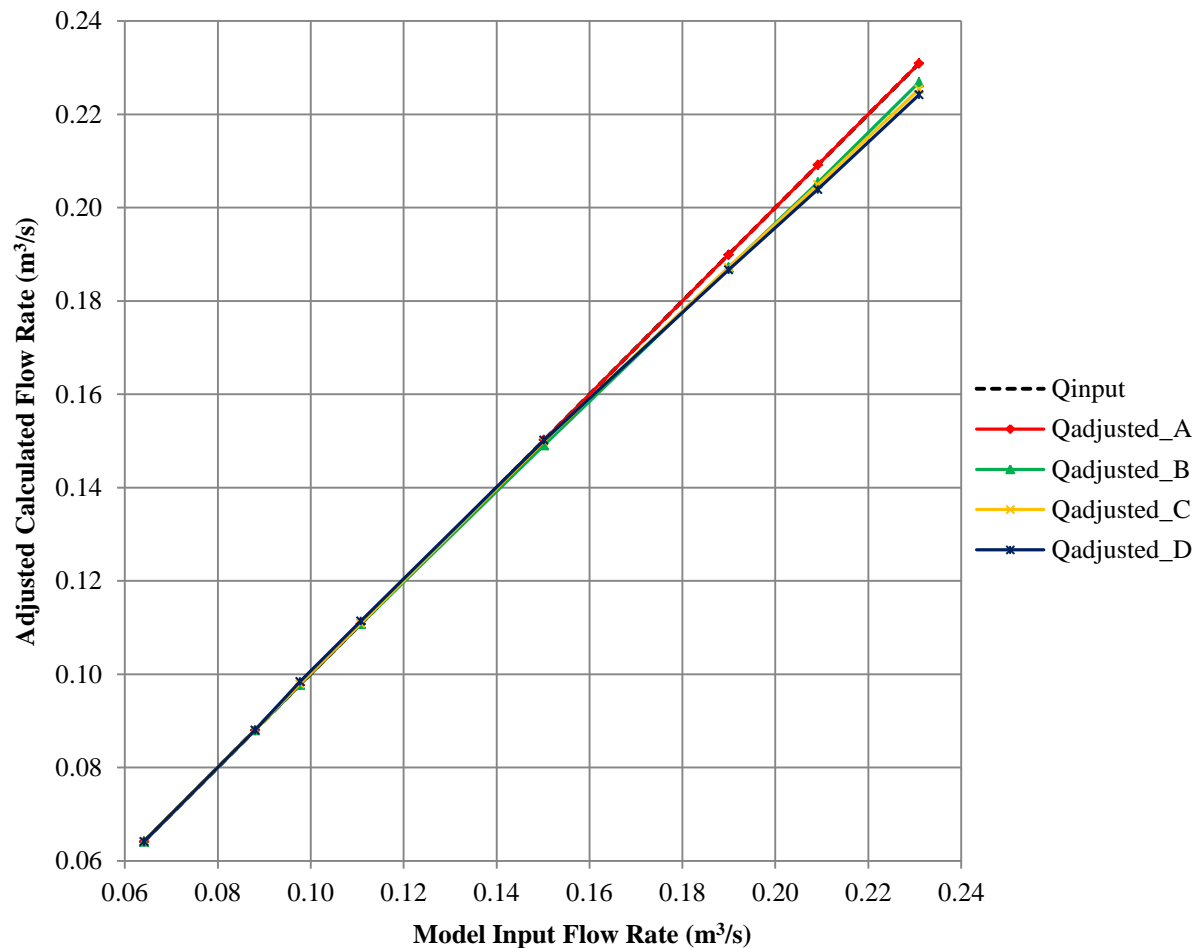
V = approach velocity (m/s)

g = gravitational acceleration ( $m/s^2$ )

The water level adjustment factors for the various model ratios are shown in **Table 4.7**. For flow rates above the hydraulic capacity for Ratio 1:4 (85.8 l/s) adjustment values were applied to the results for Layout A until no error was made. These adjustment percentages were then applied to Layouts B, C and D to illustrate a model with no contraction but with cross-flow. The adjusted graphs for ratio 1:4 are shown in **Figure 4.23**. The graphs for ratios 1:3, 1:2 and 1:1 are provided in Appendix B.

**Table 4.7: Water level adjustment values for the correction of contraction for Ratios 1:4, 1:3, 1:2 and 1:1**

$Q_{input}$ (l/s)	$\Delta h_{c1:4}$ (m)	$\Delta h_{c1:3}$ (m)	$\Delta h_{c1:2}$ (m)	$\Delta h_{c1:1}$ (m)
44	-	-	0.00106	0.00166
65	-	0.00215	0.00010	0.00241
89	0.00106	0.00140	0.00092	0.00284
110	0.00236	0.00302	0.00375	0.00381
150	0.00300	0.00502	0.00537	0.00473
190	0.00471	0.00677	0.00658	0.00555
210	0.00741	0.00752	0.00769	0.00626
230	0.00857	0.00872	0.00867	0.00711



**Figure 4.23: Graph of adjusted physical model results to account for contraction for Ratio 1:4**

It can be seen from **Figure 4.23** that an underestimation of the calculated flow rate is now perceived which corresponds to the findings of Wessels (1996). The assumption of contraction due to the oversized divider and flank walls would need to be confirmed by modelling of various thickness walls for the same model set-up.



### 4.3.3 Correction of error due to overtopping

Correction factors can be applied to the results of Layout D, after the above correction for contraction and rotation is applied, in such a way that the underestimation error, resulting from overtopping, is reduced to zero. These correction values were determined by adjusting the water levels at each measurement point for Layout D until no error was made. Layout D was used since this represents the natural occurrence in the field. It should be possible to determine the individual contribution to the error of each component, namely; the divider and each flank wall. However, this is only recommended once the contraction and rotational error has been fully defined, confirmed and accounted for.

The correction factor is added to the total energy head using a water level adjustment, as follows:

$$H = (h + \Delta h_o) + \frac{V^2}{2g} \quad (4.2)$$

where:

$\Delta h_o$  = water level adjustment value correcting for overtopping (m)

The water level adjustment factors for the correction of overtopping of the various model ratios are shown in **Table 4.8**.

**Table 4.8: Water level adjustment values for the correction of overtopping for Ratios 1:4, 1:3, 1:2 and 1:1**

$Q_{input}$ (l/s)	$\Delta h_{o1:4}$ (m)	$\Delta h_{o1:3}$ (m)	$\Delta h_{o1:2}$ (m)	$\Delta h_{o1:1}$ (m)
44	-	-	0.00000	0.00000
65	-	0.00000	0.00000	0.00000
89	0.00000	0.00000	0.00000	0.00013
110	0.00000	0.00000	0.00000	0.00154
150	0.00004	0.00049	0.00203	0.00326
190	0.00158	0.00230	0.00347	0.00473
210	0.00244	0.00300	0.00457	0.00590
230	0.00302	0.00386	0.00554	0.00663

Further investigation of different model set-ups is required to confirm that the results above are translatable over various weir configurations.

#### 4.4 DISCUSSION OF NUMERICAL MODEL RESULTS

The numerical model represented the physical model layout D of the lower to higher Crump width ratio 1:4. The water level measurements observed during the physical modelling were used as verification for the results obtained in the numerical model study. Flow rates 155.2, 178.2, 198.9 and 219.5 l/s were used as inputs, and the water level observations made in the physical model were used as the initial water level values as well as the initial zone for the refinement of the volume mesh at the surface interface. **Figure 4.1** in **Section 4.1** explains the calculation and comparison procedure followed during the interpretation of the physical model results, a similar approach is followed here. For the numerical model, the water levels upstream of the higher Crump, lower Crump, left filler wall and right filler wall, at an iso-surface of 0.5, were extracted from the simulation and used, along with the theoretical equations, to calculate the flow rate over the structure. These flow values were then compared to the corresponding flow rate extracted from STAR-CCM+ at the measuring points. The plane section, perpendicular to the flow, was used to determine the mass flow rate across the structure at an iso-surface value of 0.5.

The simulation was divided into three phases for each flow rate being modelled, namely;

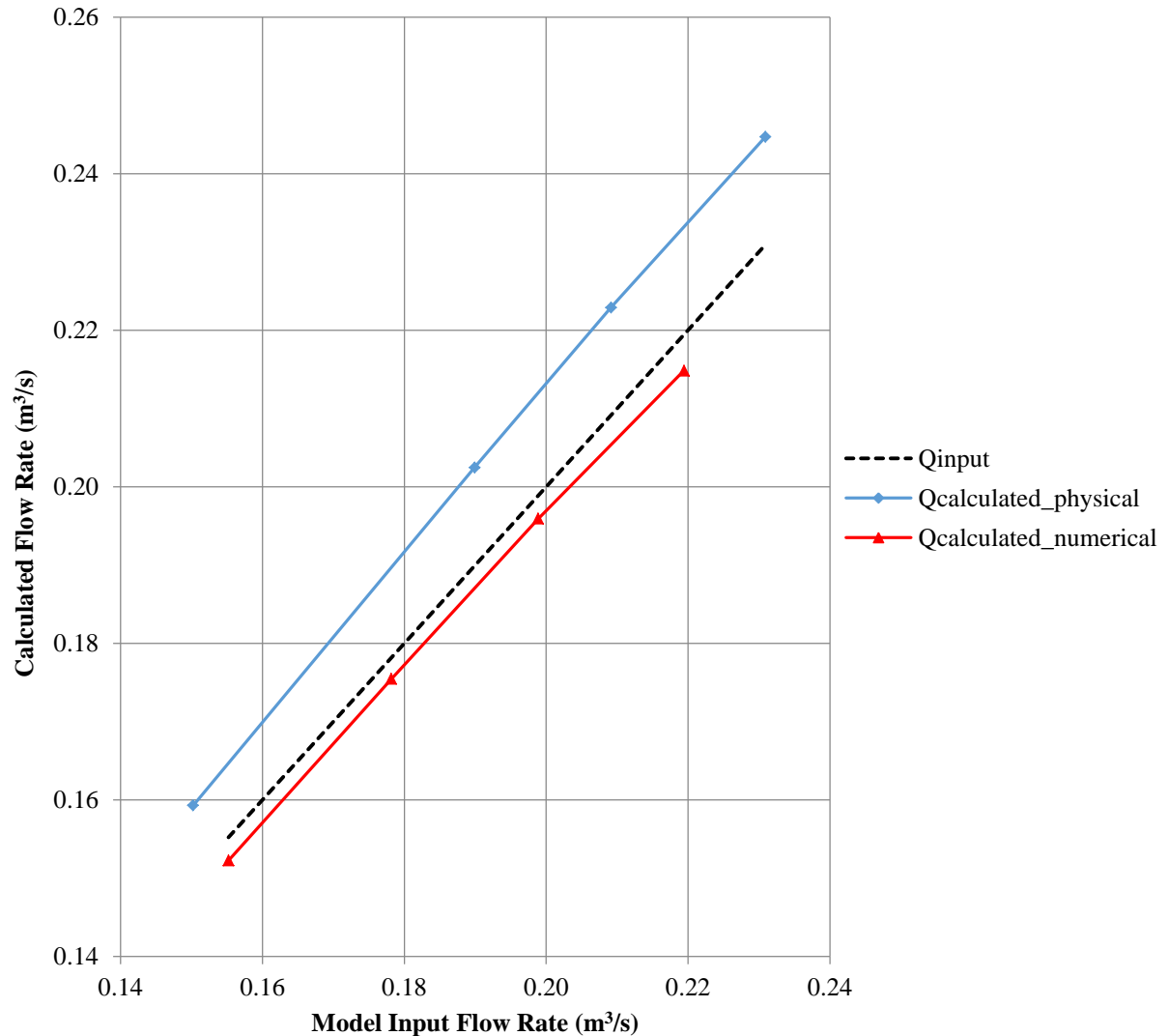
- 1) the initial run at a time-step of 0.1 s with mesh base size of 80 mm and volume refinements of 20 mm;
- 2) the secondary run at a time-step of 0.01 s with the user-defined mesh refinement of 5 mm at the interface and 2.5 mm at the water level measuring points; and
- 3) the final run at a time-step of 0.001 s with the user-defined mesh refinement of 5 mm at the interface and 2.5 mm at the water level measuring points.

This was done to reduce the computation time of the various simulations and to ensure that the surface interface was captured within an accuracy of  $\pm 2.5$  mm. The cell count for each of the flow rate models is given in **Table 4.9**.

**Table 4.9: Mesh cell count for the various flow rates modelled**

Flow Rate (l/s)	Surface Interface Refinement	
	2.5 mm	1.0 mm
155.2	4 850 176	69 374 699
178.2	4 367 132	-
198.9	4 837 518	-
219.5	5 723 198	68 417 577

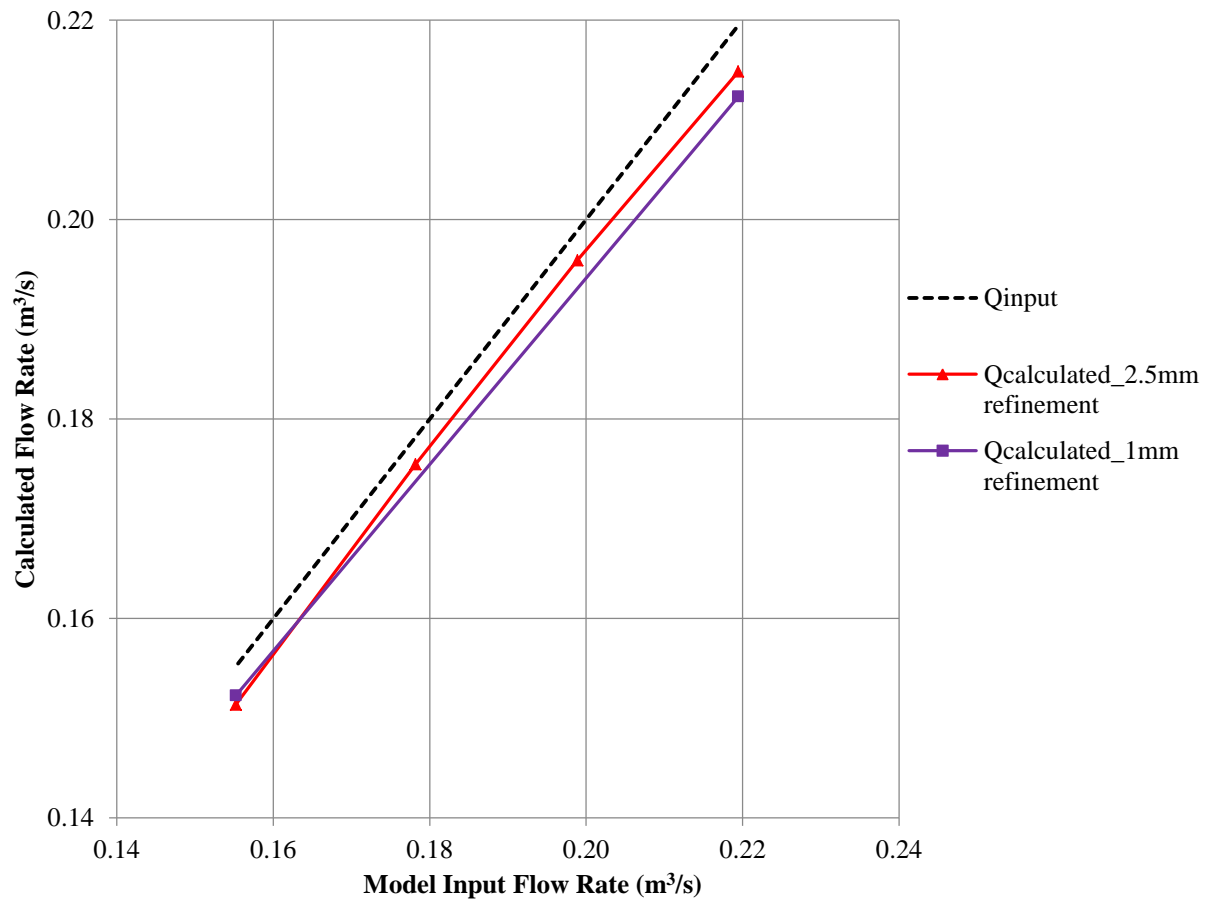
The results of the numerical model analysis in comparison with the physical model results are shown in **Figure 4.24**. The numerical model tends to underestimate the correct flow values and that, as discussed above the physical model overestimates the flow rates.



**Figure 4.24: Results of the numerical model analysis ( $Q_{\text{calc\_numerical}}$ ) in comparison with the physical model results ( $Q_{\text{calc\_physical}}$ ) for Ratio 1:4 Layout D**

Due to the large discrepancy between the physical model and the numerical model results, it was decided to refine the surface interface at the water level measuring points to 1.0 mm and perform an additional run first at 0.1 s and then at 0.001 s in order to improve the accuracy to  $\pm 1.0$  mm. Only models 155.2 l/s and 219.5 l/s were simulated with the additional refinement at the measuring points due to the large cell count produced when refining the mesh (see **Table 4.9**) for the increase in cell count when compared to a 2.5 mm refinement at the measuring point). The computation time increases significantly from a 4.8-million cell mesh to a 69.4-million cell mesh. It was thus decided first to evaluate whether the additional

refinement would significantly influence the results before testing models 178.2 l/s and 198.9 l/s.


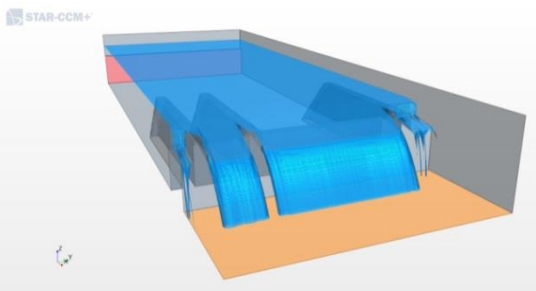

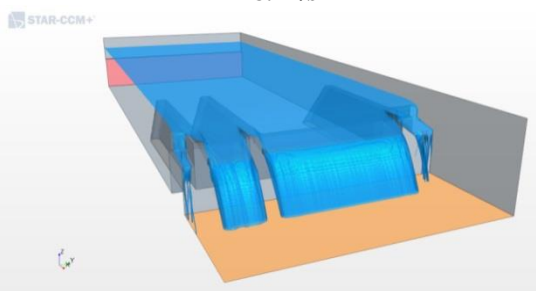

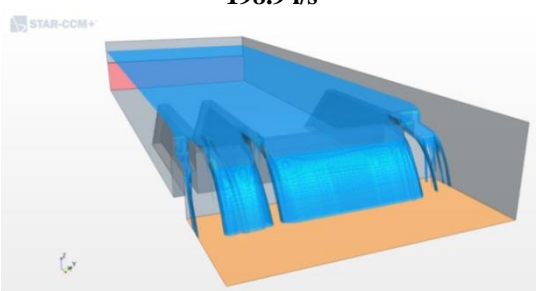

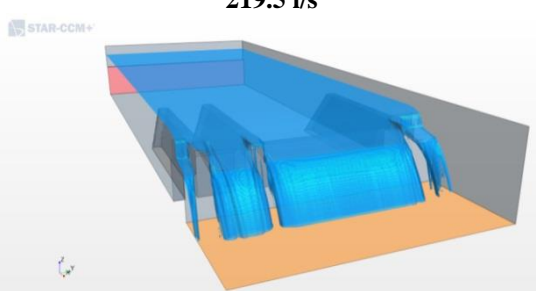


**Figure 4.25: Comparing the results of the numerical model with surface interface refinement of 2.5 mm ( $Q_{\text{calc}_2.5\text{mm refinement}}$ ) in comparison with a surface interface refinement of 1 mm ( $Q_{\text{calc}_1\text{mm refinement}}$ )**

It can be seen from **Figure 4.25** that the additional refinement of the surface interface at the measuring point, to a value of 1 mm, did not significantly change the resultant flow rate values and thus the analysis was continued using a refinement of 2.5 mm.

The dissimilarity between the calculated numerical model flow values and the correct flow values could be explained by the flow patterns observed in **Table 4.10**. A visual comparison between the physical model results and the numerical model results are shown for the various flow values. The flow patterns of the numerical models seem to be consistent with those of the physical model.

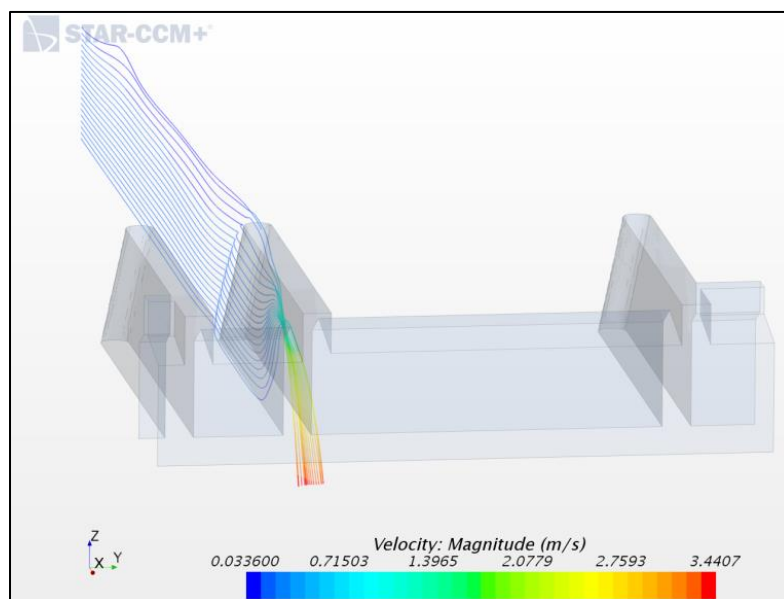
**Table 4.10: Visual comparison of the physical and numerical model**

Physical model	Numerical Model
<p style="text-align: center;"><b>150.2 l/s</b></p> 	<p style="text-align: center;"><b>155.2 l/s</b></p> 
<p style="text-align: center;"><b>189.9 l/s</b></p> 	<p style="text-align: center;"><b>178.2 l/s</b></p> 
<p style="text-align: center;"><b>209.1 l/s</b></p> 	<p style="text-align: center;"><b>198.9 l/s</b></p> 
<p style="text-align: center;"><b>230.9 l/s</b></p> 	<p style="text-align: center;"><b>219.5 l/s</b></p> 

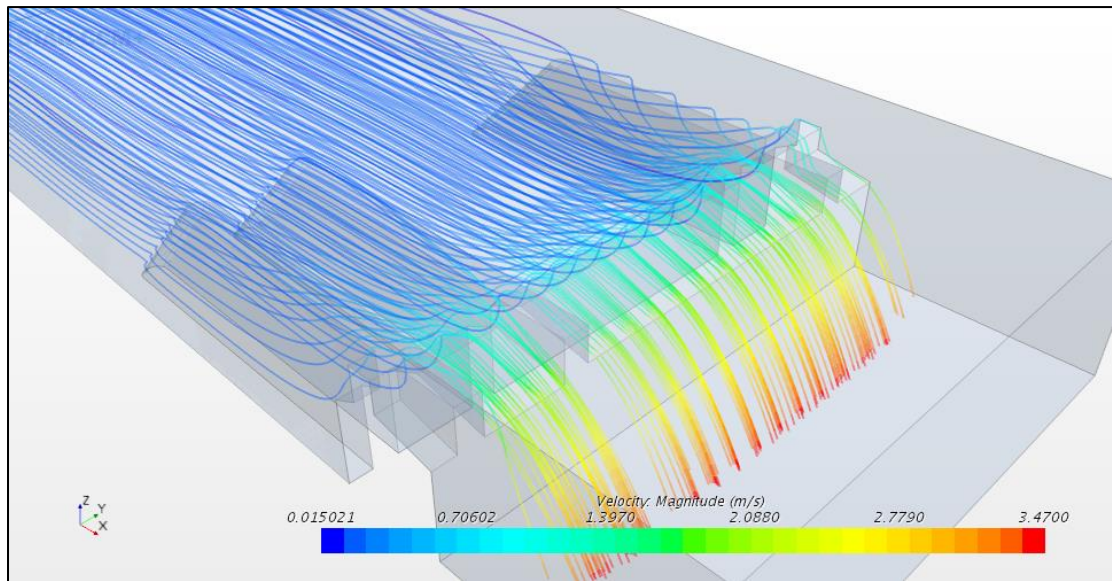
Further inspection of the flow lines within the body of water upstream of the weir is necessary in order to explain the underestimation error and discrepancy with the physical model results. **Figure 4.26** depicts a single row of streamlines flowing along the divider wall, parallel flow lines are observed with some evidence of cross-flow over the divider wall into the lower Crump weir section. The disturbance in the flow lines seems to occur upstream of the measuring point which could explain the underestimation seen in the results. When investigating the streamlines within the entire body of water upstream and in the vicinity of

the structure, as seen in **Figure 4.27**, predominantly parallel flow lines are observed. Near the surface of the water, cross-flow over the right and left flank walls are present with minimal disturbances over the divider wall. Some bending of the flow lines around the divider and flank walls can also be noted. This seems to stand in contrast to the large eddy formations (see evidence of vortex in **Figure 4.19**) observed in the physical model and could explain the discrepancy between the two results. In addition, the following user-dependent and software inherent aspects influence the comparability of the numerical model to the physical model:

- the numerical approximation of turbulence flow, the compressibility of fluids, physical properties of fluids, multi-phase flow, etc.;
- numerical errors included in the solving of equations, rounding errors that are present due to the finite realm available within the computer and truncation errors caused by approximations in the numerical models;
- the accuracy of the boundary conditions set to represent the physical model (such as roughness of the surfaces, accurate recreation of slight imperfections in the physical model, ignoring of turbidity of water in the physical model, etc.);
- the size of the mesh cells used to compute the volume fractions, limiting the accuracy at which the water level measurements can be taken; and
- the assumption made by the user regarding the representative iso-surface or volume fraction for the water level readings.



**Figure 4.26: Streamlines around the divider wall showing the velocity magnitude**



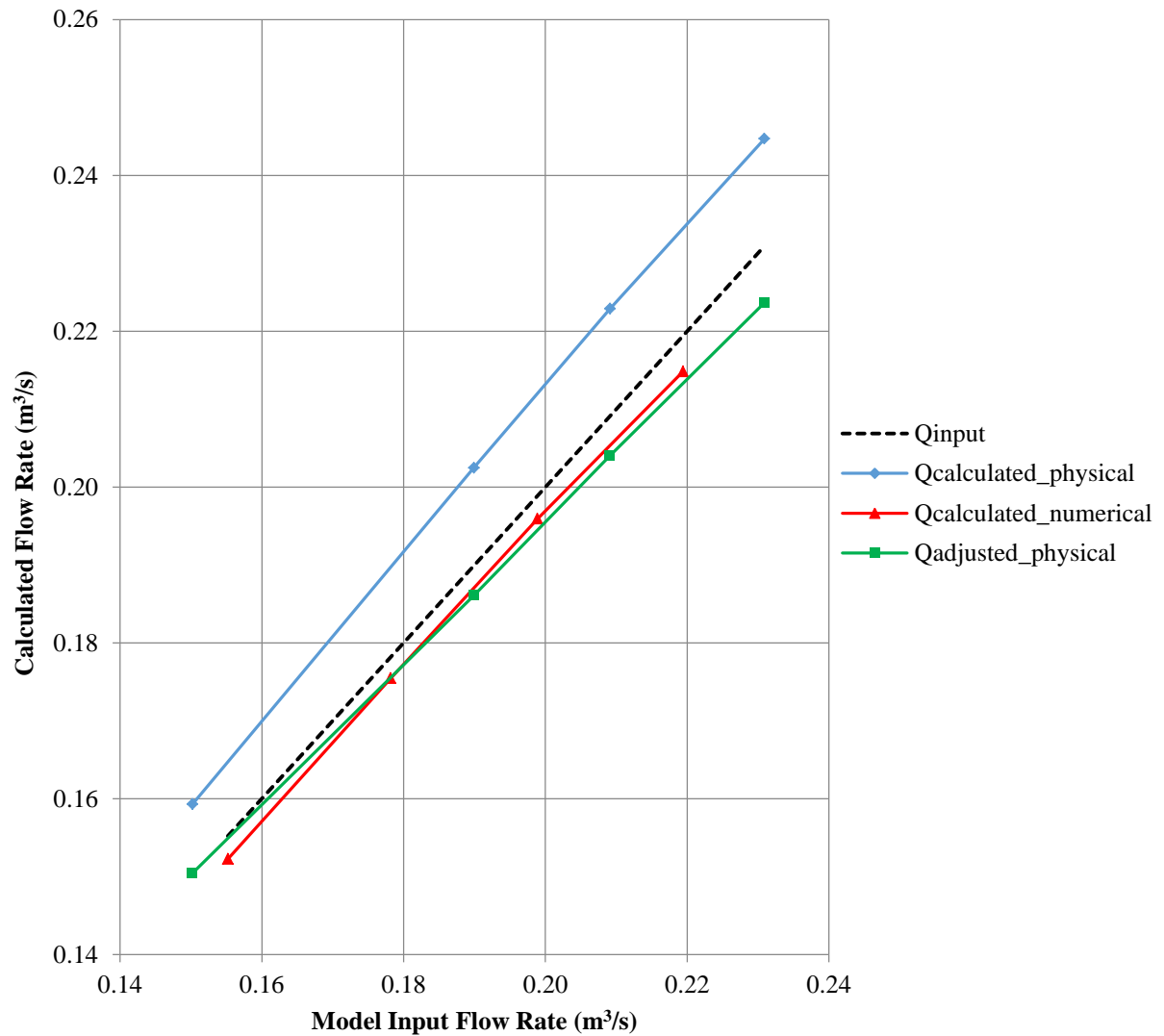
**Figure 4.27: Streamlines around the entire structure showing the velocity magnitude**

Recall from the physical model results that the influence of the divider and flank wall thicknesses relative to the lower Crump crest width had the most substantial influence on the overestimation error seen in the results (**Section 4.2.1**). The oversized divider and flank walls caused an increase in rotational energy and the narrowing of the effective flow area of each channel due to eddy formations upstream of these walls (this was evident due to the observed vortex formation in **Figure 4.19**). The correction factors introduced in **Section 4.3.2**, were derived from the reduction of the overestimation error, seen in the results for Layout A, to zero. Layout A is uninfluenced by cross-flow over the divider and flank walls because of the extension walls. It then follows that the only influence on the results is the contraction and increased rotational energy in each channel. The same correction factors were then applied to the results for Layouts B, C and D to account for contraction and increased rotational energy.

Since the volume mesh of the numerical model does not accurately capture the underlying contraction and rotational effects caused by the oversized divider and flank walls, it would be useful to compare the results from the numerical model to that obtained from adjusting the physical model to account for contraction and rotation. The results of the numerical model analysis in comparison with the physical model results as well as the physical model results adjusted for contraction are shown in **Figure 4.28**. The numerical model tends to agree with the adjusted physical model graph showing a similar underestimation error.

The similarity in the numerical model and adjusted physical model results improves the confidence of both the numerical model as well as the adjustments made to the physical model results to correct for contraction. This finding suggests that contraction is the limiting

factor in the physical model, resulting in large-eddy formations (vortex) and that the volume mesh in the numerical model is not fine enough throughout the body of water to accurately capture the contraction effects caused by the oversized divider and flank walls. This also verifies that CFD software is a useful tool in the modelling of hydraulic structures and that further investigations into the limitations of the discharge-head relationships of compound Crump-weirs using physical modelling can be performed in conjunction with numerical modelling.



**Figure 4.28: Results of the numerical model analysis ( $Q_{\text{calc\_numerical}}$ ) in comparison with the physical model results ( $Q_{\text{calc\_physical}}$ ) as well as the physical model results adjusted for contraction ( $Q_{\text{adjusted\_physical}}$ )**



## 5 CONCLUSIONS AND RECOMMENDATIONS

### 5.1 CONCLUSIONS

The study aimed at investigating the limitations of the discharge-head relationship of compound Crump weirs with divider walls for overtopping flow rates. The investigation was executed in two phases, (1) the physical model study, done at the DWS hydraulic laboratories and (2) the numerical model study using the computational fluid dynamics (CFD) software STAR-CCM+ (see **Chapter 3**). A compound Crump weir, consisting of two Crump sections at a step difference of 30 mm, separated by a 100 mm thick divider wall with a 100 mm thick flank wall on either side of the weirs and filler walls, connecting the flank walls to the channel sides, was modelled (see **Section 3.1**). The lower to higher Crump width ratios ( $B_L:B_H$ ) of 1:4, 1:3, 1:2 and 1:1 were studied with variable extension wall layouts (Layout A, B, C and D). Water level readings were taken at five points upstream of the modelled compound Crump weir in order to calculate the flow rate over each crest component. The flow rates were calculated using the Crump weir equation for modular flow conditions as well as the broad-crested weir equation for flow over the filler walls. The calculated values were then compared to the flow rate that was administered into the model and calibrated using the pump calibration equation (see **Section 3.2**).

Furthermore, the as-built dimensions of the physical model, representing the natural occurrence in the field (Layout D) for the lower to higher Crump width ratio 1:4, was used in the numerical model study. Phased refinement of the volume mesh and reduction in iteration time-step was implemented in order to improve the accuracy at which the surface interface could be captured. A plane section, upstream of the structure, perpendicular to the flow at the measuring point, was used to determine the mass flow rate at an iso-surface value of 0.5 and was also compared to the input flow rate (see **Section 4.4**).

For the physical model, the results indicated an overestimation for all modelled ratios and layouts (see **Figure 4.2**, **Figure 4.3**, **Figure 4.4** and **Figure 4.5**). The most severe overestimation error was observed for lower to higher Crump width ratio of 1:4 and gradually decreased from ratio 1:3 to 1:1. This improvement in flow estimation was attributed to the increasing length of the left filler wall. Layout A was expected to estimate the model input flow rate accurately since the three-dimensional flow lines were prevented by the addition of the extension walls. Instead, Layout A showed the most substantial overestimation errors for all ratios. This was due to the eddy formation around the upstream ends of the divider and filler walls resulting in the contraction of the flow lines within the cross-sectional area of the

Crump crests. Layouts B, C, and D followed the same trend as Layout A, but with a decrease in overestimation error. The decrease in error resulted from the alleviation in contraction due to the removal of the extension walls. The numerical model results showed an underestimation error in the calculated flow rate when the current discharge-head relationships were used (see **Figure 4.24**). On further investigation, the flow lines in the body of water upstream of the structure appeared to be uniform with some cross-flow and minimal disturbances displayed at the surface interface in the vicinity of the flank walls (see **Figure 4.26** and **Figure 4.27**).

A correction was made to the physical model results for the overestimation error stemming from the contraction of the flow lines due to the oversized divider and filler walls (see **Figure 4.23**). It was found that the adjusted physical model results agreed well with the numerical model showing a similar underestimation error (see **Figure 4.28**). It was demonstrated that three-dimensional flow developing from the overtopping of the divider and flank walls results in an underestimation of the calculated flow rate relative to the model input flow rate. Layout D with all extension walls removed was corrected in terms of the underestimation error resulting from overtopping. Adjustments of up to 6.63 mm in water level values, representing 66.3 mm in the prototype, had to be made in order to correct the underestimation error (see **Table 4.8**). This adjustment is significantly higher than an acceptable practical error allows and thus places substantial doubt in current streamflow data records. Further investigation of different model set-ups is required to confirm that the results above are translatable over various weir configurations.

In summary, the following conclusions can be drawn:

- the divider and flank wall thicknesses relative to the selected Crump crest widths contributed more significantly to the disturbance of the flow lines than initially anticipated, resulting in the contraction of the flow lines ultimately decreasing the effective width of each channel causing a perceived increase in water level which lead to an overestimation of the model input flow rates for all model layouts;
- after the correction for contraction due to the oversized divider and flank walls was applied, the resulting calculated flow rates underestimated the correct values as initially expected since the three-dimensional flow is observed during overtopping of the divider and flank walls; and
- the current discharge-head relationships, used for calculating flow rates over compound Crump weirs with divider walls, cannot be used to accurately calculate overtopping flow rates; and

- CFD software is a useful tool in the modelling of hydraulic structures and that further investigations into the limitations of the discharge-head relationships of compound Crump-weirs using physical modelling can be performed in conjunction with numerical modelling.

## 5.2 RECOMMENDATIONS

The study results indicate that caution should be taken when applying the current discharge-head relationships for the calculating of the flow rates over compound Crump weirs operating above capacity.

The reliability of the streamflow data is of significant concern for all designers involved in the design and maintenance of infrastructure. The sizing of dams and spillways, locating of housing and priority businesses, classification of road safety and the sizing of bridges and culverts are all directly influenced by the accuracy of streamflow data. It is thus recommended that further studies be conducted for the improvement of flow gauging data. These studies should focus on the development of correction factors aimed at improving the flow rate calculations of overtopping flows. The following recommendations for furthering the study are made:

- the physical model study should be re-evaluated for lower to higher Crump crest ratios 1:4, 1:3, 1:2 and 1:1 by keeping the total length of the Crump crest constant. The filler walls would need to be symmetrical and remain unchanged throughout the model study, while the lower and higher Crump widths are changed to adjust the ratio;
- the divider and flank wall thicknesses should be varied in order to determine the limiting thicknesses relative to the Crump crest widths;
- the use of extension walls should be disregarded, only evaluating the case where the divider, flank and filler walls overtop;
- changes in depth of the upstream pool should be included in the study;
- non-modular flow conditions should be investigated with varying modular limits; and
- the filler-wall length limits should also be determined.

It would be of great value to the study if the numerical model could be developed to compare well with the physical model results by using LES turbulence models. Due to volume and flow rate limitations at the DWS hydraulic laboratories extensive research using physical modelling cannot be performed for the development of correction factors. Numerical

modelling would allow for the extension of the model input flow rates and the number of layouts being considered. In order to stay within time constraints, resource limitations and cost implications for the improvement of the numerical model, the following suggestions are made:

- consider further refinement of the volumetric mesh around structural components and throughout the full depth of the water phase;
- due to the large mesh size, make use of the CHPC for running simulations;
- plan the mesh refinement and reduction in iteration time-step effectively before solving on the CHPC;
- perform the numerical calibration on a maximum of two extreme cases such as one flow within the hydraulic limit, and one well above the hydraulic limit;
- test a broad range of iso-surfaces between 0.4 and 0.6 and compare the results with the physical model; and
- include sensitivity analyses for surface roughness and slight changes in structural geometry.

## 6 REFERENCES

- [1] Ackers, P. White, W.R. Perkins, J.A. and Harrison, A.J.M. 1978. *Weirs and flumes for flow measurements*. John Wiley and Sons Ltd., Chichester.
- [2] Azimi, A.H. and Rajaratnam, N. 2009. Discharge characteristics of weirs of finite crest length. *Journal of Hydraulic Engineering*, Vol 135, No 12, pp 1081-85.
- [3] Beach, M. 1984. *Fish pass design-criteria for the design and approval of fish passes and other structures to facilitate the passage of migratory fish in rivers*. Ministry of Agriculture, Fisheries and Food. Fisheries Research Technical Report No. 78. Lowestoft.
- [4] Bing, G. 1991. *Guidelines for the calibration of flow gauging stations*. Department of Water Affairs. Pretoria.
- [5] Blignaut, J. and van Heerden, J. 2009. The impact of water scarcity on economic development initiatives. *Water SA*, Vol 35, No 4, pp 415-20.
- [6] British Standards Institution 2000. Compound gauging structures. *Flow measurements in open channels using structures*. BS ISO 14139. London.
- [7] Chorin, A.J. 1968. Numerical solution of the Navier-Stokes equations. *Mathematics of Computation*, Vol 22, No 104, pp 745-68.
- [8] CRED 2015. *The human cost of natural disasters – A global perspective*. Centre of Research on the Epidemiology of Disasters. Brussels.
- [9] Crosby, C. 2018. *STAR-CCM+ - CHPC Wiki*, 1 August 2018, <<http://wiki.chpc.ac.za/howto:starccm>>.
- [10] Department of Water and Sanitation (DWS) 2011. Chapter 1: Overview of the SA Water Sector. *Governing Board Induction Manual*. Pretoria, pp 3-14.
- [11] Fluent Inc. 2001. *FLUENT 6.0 User's Guide: Volume 4*. Fluent Inc.
- [12] Govinda Rao, N.S. and Muralidhar, D. 1963. Discharge characteristics of weirs of finite-crest width. *Houille Blanche*, Vol 18, No 5, pp 537-45.
- [13] Hedges, L. 2016. *Real World AWS Scalability*. 6 August 2018, <<https://aws.amazon.com/blogs/compute/real-world-aws-scalability/>>.

- [14] Hirt, C.W. and Nichols, B.D. 1981. Volume of Fluid (VOF) Method for Dynamics of Free Boundaries. *Journal of Computational Physics*, Vol 39, pp 201-25.
- [15] Ho, D.K.H. Boyes, K.M. Donohoo, S.M. and Cooper, B.W. 2003. Numerical flow analysis for spillways, *43rd ANCOLD Conference, Hobart, Australia, November 2003*.
- [16] IAHR AIRH 1994. Broad crested weirs/spillways. *Hydraulic Structures Design Manual, Discharge Characteristics*. Ed D.S. Miller. Taylor and Francis, New York, pp 27-30.
- [17] Jesudhas, V. 2016. *Modelling of free-surface flows with air entrainment*. University of Windsor.
- [18] Jones, W. and Launder, B. 1972. The prediction of laminarization with a two-equation model of turbulence. *International Journal of Heat and Mass Transfer*, Vol 15, No 2, pp 301-14.
- [19] Lambie, J.C. 1978. *Measurement of flow - velocity area methods*. John Wiley and Sons, Chichester.
- [20] LEAP Australia 2014. *LEAP Australia Computational Fluid Dynamics blog (CFD)*, 20 September 2017, <<https://www.computationalfluidynamics.com.au/tips-tricks-turbulence-wall-functions-and-y-requirements/>>.
- [21] Maritz, A.A. van Vuuren, S.J. and Wessels, P. 2015. Modelling of composite type variation of the Crump weir. *SAICE Magazine*, August, pp 36-45.
- [22] Nshuti Kanyabujinja, P. 2015. *CFD modelling of Ogee spillway hydraulics and comparison with physical model tests*. MEng Thesis. Stellenbosch University.
- [23] Ojha, C.S.P. Berndtsson, R. and Chandramouli, P.N. 2013. *Fluid Mechanics and Machinery*. 1st ed. Oxford University Press, New Delhi.
- [24] Rickard, C. Day, R. and Purseglove, J. 2003. *River Weirs - Good Practice Guide*. Environment Agency, Bristol.
- [25] Sileshi, R. 2009. *Flow over a Crump weir*. The University of Alabama.
- [26] Spence, S. 2014. *Numerical investigation of free surface flows*. Norwegian University of Science and Technology.

- [27] STAR-CCM+ 2017. *User Guide Version 12.02*. Siemens PLM Software. Melville.
- [28] Tracey, H.J. 1957. *Discharge characteristics of broad-crested weirs*. United States Department of the Interior: Geological Survey, Washington, D. C.
- [29] UC Davis 2016. *STAR-CCM+ Installation Guide*, 6 August 2018, <[http://stats.cse.ucdavis.edu/InstallationGuide\\_11.04.012\\_01.html](http://stats.cse.ucdavis.edu/InstallationGuide_11.04.012_01.html)>.
- [30] USBR 1997. Chapter 6 - Measuring and Recording Water Stage or Head. *USBR Water Measurement Manual*. Ed T. Hovland. 3rd ed. U.S. Government Printing Office, Washington, pp 6.9-6.10.
- [31] van Heerden, J.J. van der Spuy, D. and le Roux, P.J. 1985. *Manual for the planning, design and operation of river gauging stations*. Department of Water Affairs Directorate of Hydrology. Technical Report (TR) 126. Pretoria.
- [32] Weber, N.B. 1971. Hydraulic Models. *Fluid Mechanics for Civil Engineers*. Chapman and Hall Ltd., New York, pp 297-323.
- [33] Wessels, P. 1996. *The calibration of compound Crump and sharp-crested gauging weirs in South Africa*. PhD Thesis. University of Stellenbosch.
- [34] Wessels, P. 2016. Floods exceeding gauging capacity at weirs. *Flood Hydrology Course*. University of Stellenbosch.
- [35] Wessels, P. and Rooseboom, A. 2009 (a). Flow-gauging structures in South African rivers Part 1: An Overview. *Water SA*, Vol 35, No 1, pp 1-10.
- [36] Wessels, P. and Rooseboom, A. 2009 (b). Flow-gauging structures in South African rivers Part 2: Calibration. *Water SA*, Vol 35, No 1, pp 11-19.

## APPENDIX A

The figures below are to be studied in reference to **Section 4.2.1**. Each figure shows a top view of the model along with the flow lines as observed during the physical modelling (with extension walls mounted onto the divider and flank walls shown in green). The figures also show the relationship between the upstream energy level ( $H_1$ ) and the energy levels at the various measuring points upstream of each weir component ( $H_2$ ,  $H_3$ ,  $H_5$  and  $H_6$ ). The water level head relationships between the various points are also depicted.

### FURTHER INVESTIGATION OF RESULTS FOR LAYOUT A

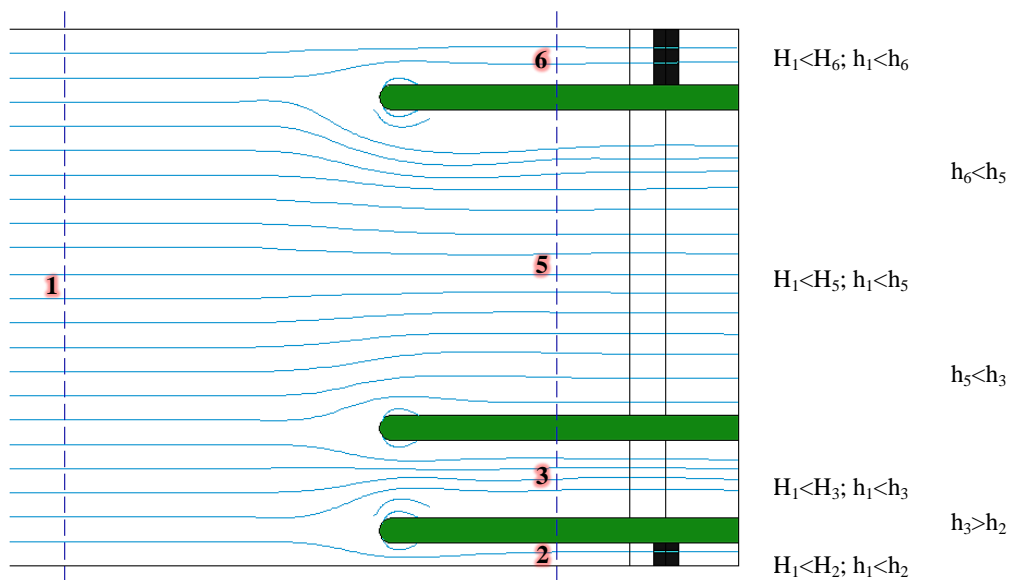


Figure A.1: Flow lines as observed for Ratio 1:4 Layout A

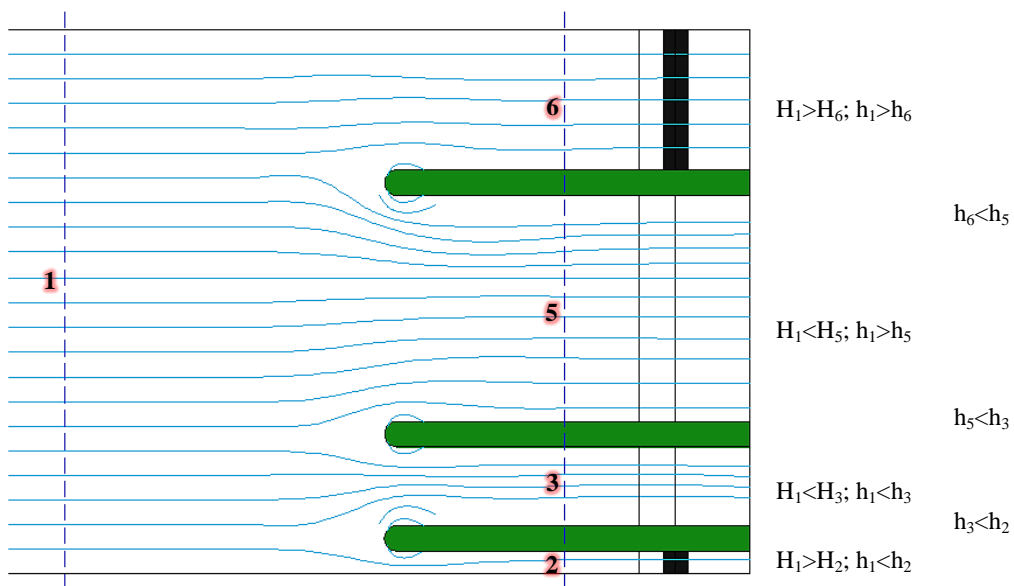


Figure A.2: Flow lines as observed for Ratio 1:3 Layout A



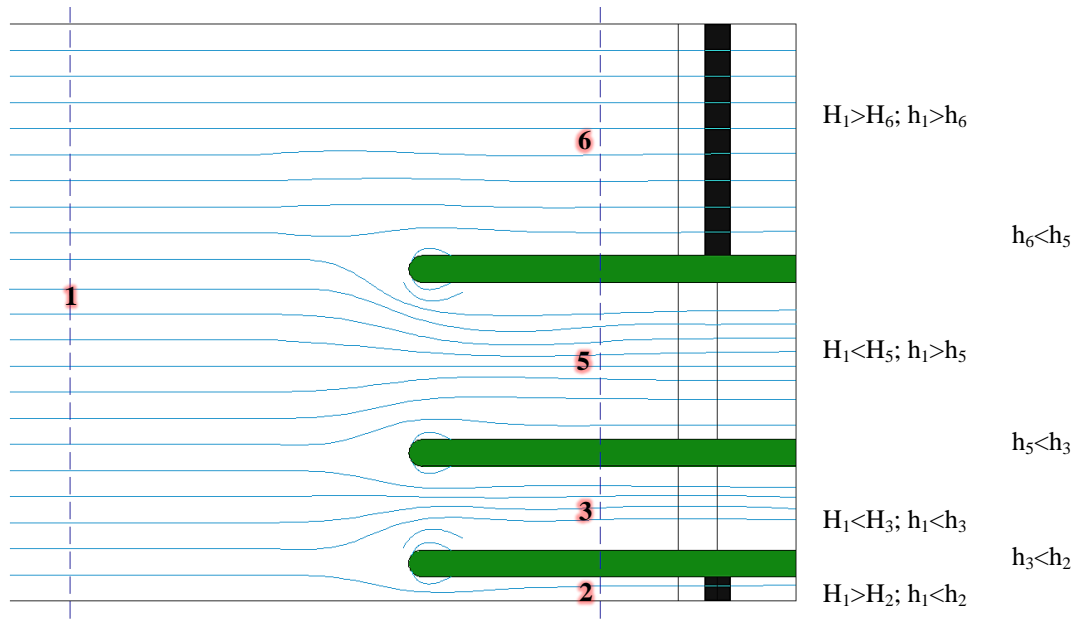


Figure A.3: Flow lines as observed for Ratio 1:2 Layout A

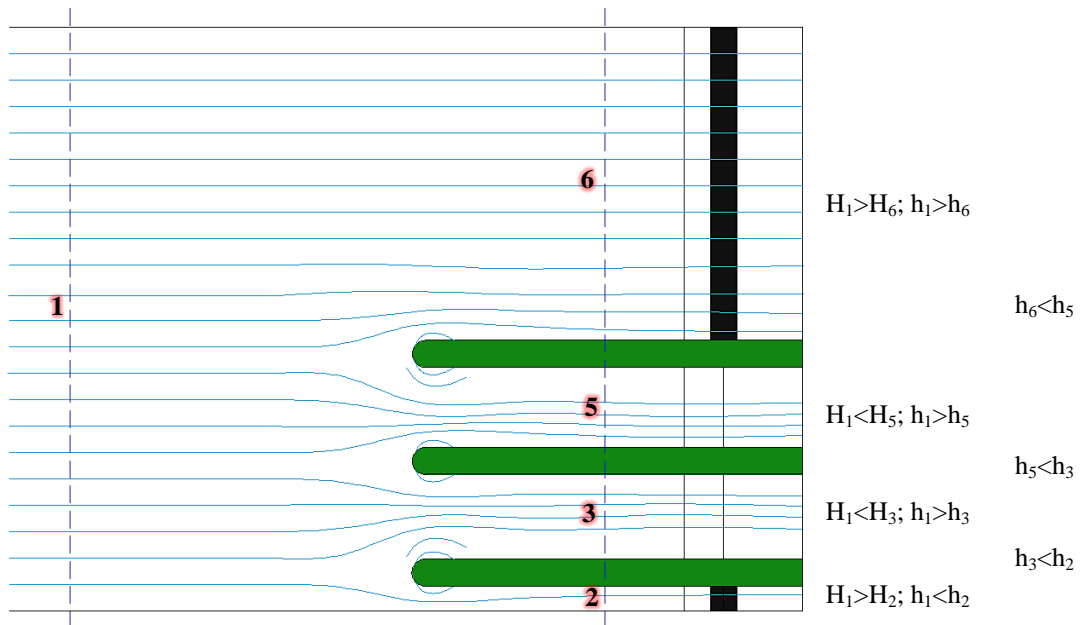
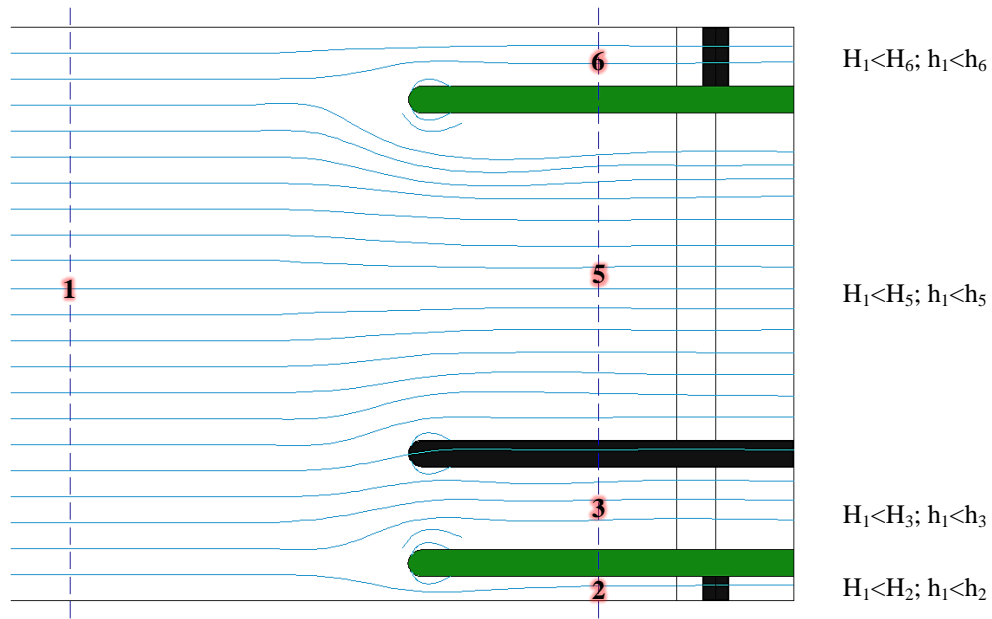
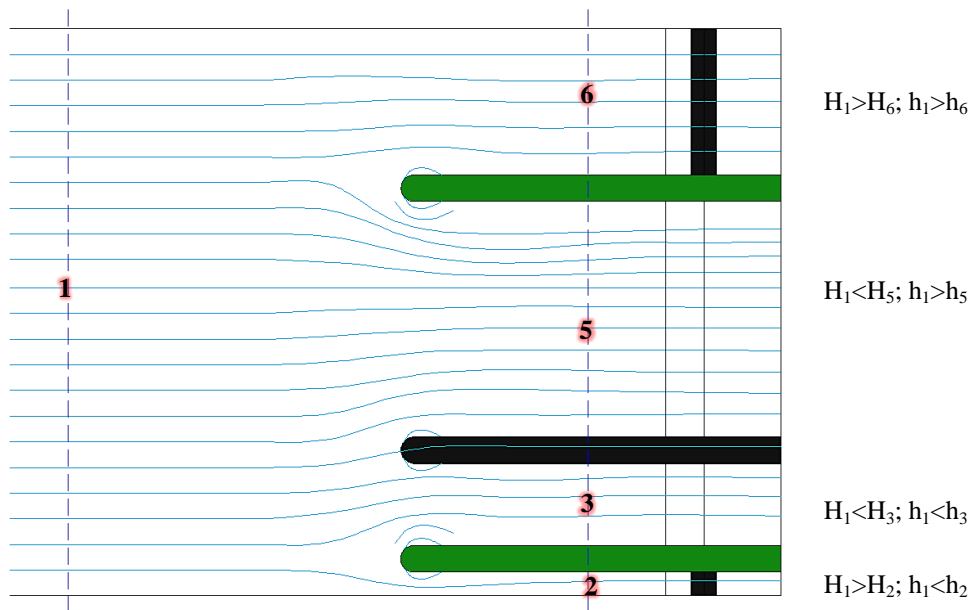


Figure A.4: Flow lines as observed for Ratio 1:1 Layout A

**FURTHER INVESTIGATION OF RESULTS FOR LAYOUT B**



**Figure A.5: Flow lines as observed for Ratio 1:4 Layout B**



**Figure A.6: Flow lines as observed for Ratio 1:3 Layout B**

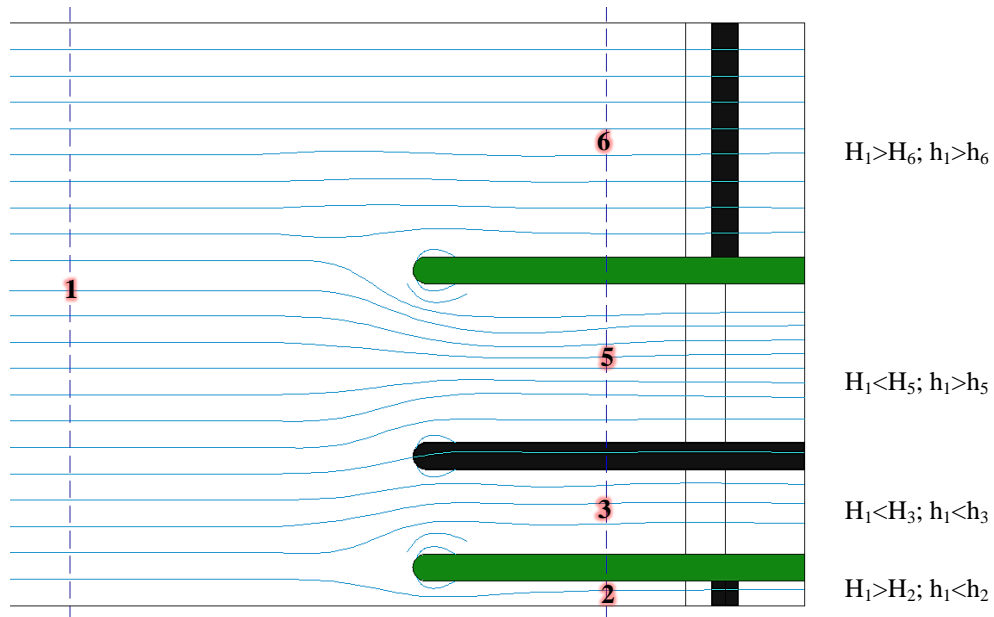


Figure A.7: Flow lines as observed for Ratio 1:2 Layout B

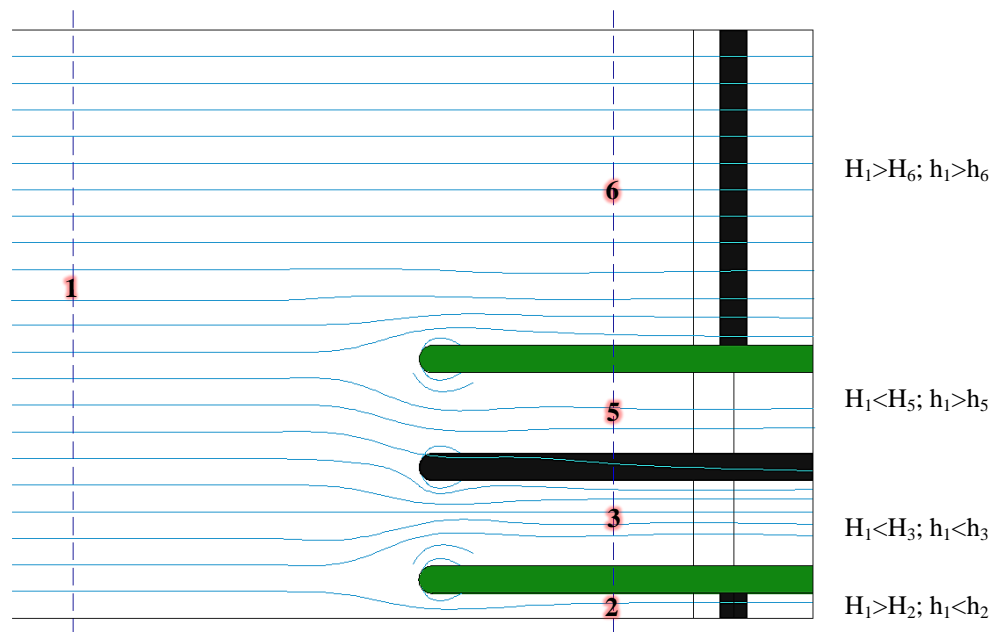
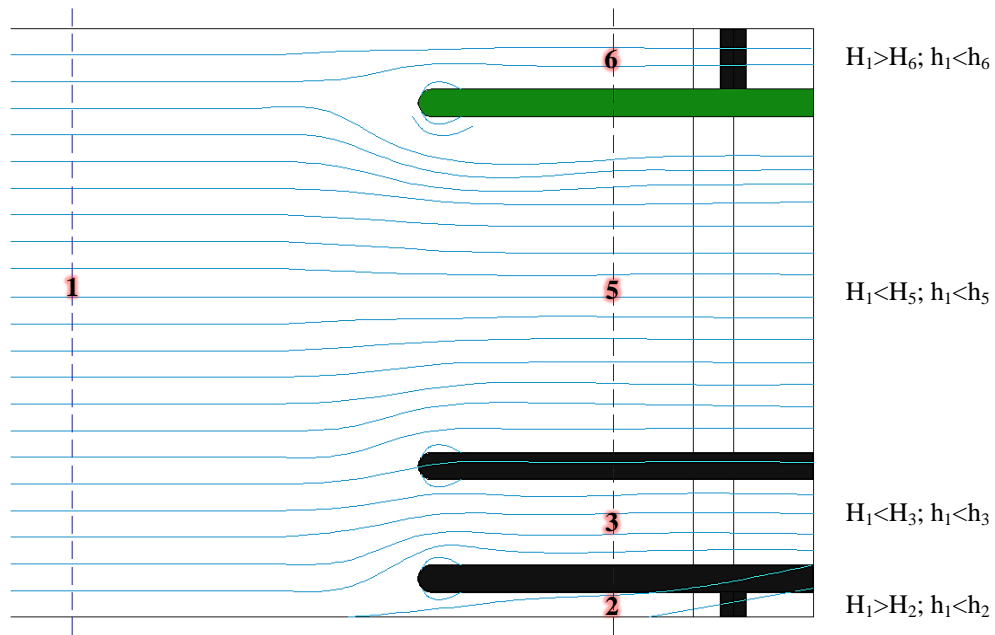
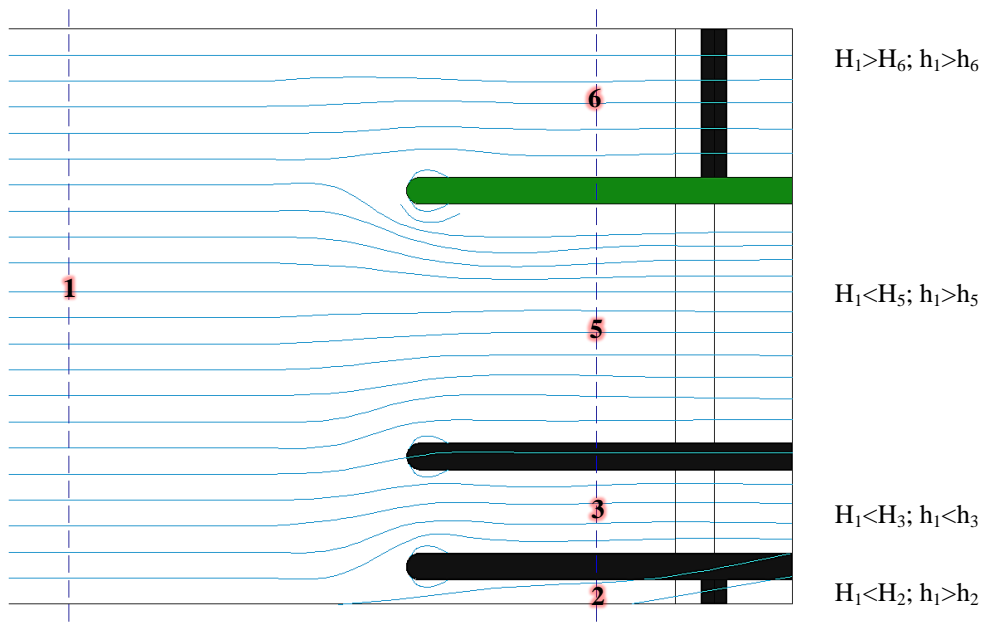


Figure A.8: Flow lines as observed for Ratio 1:1 Layout B

**FURTHER INVESTIGATION OF RESULTS FOR LAYOUT C**



**Figure A.9: Flow lines as observed for Ratio 1:4 Layout C**



**Figure A.10: Flow lines as observed for Ratio 1:3 Layout C**

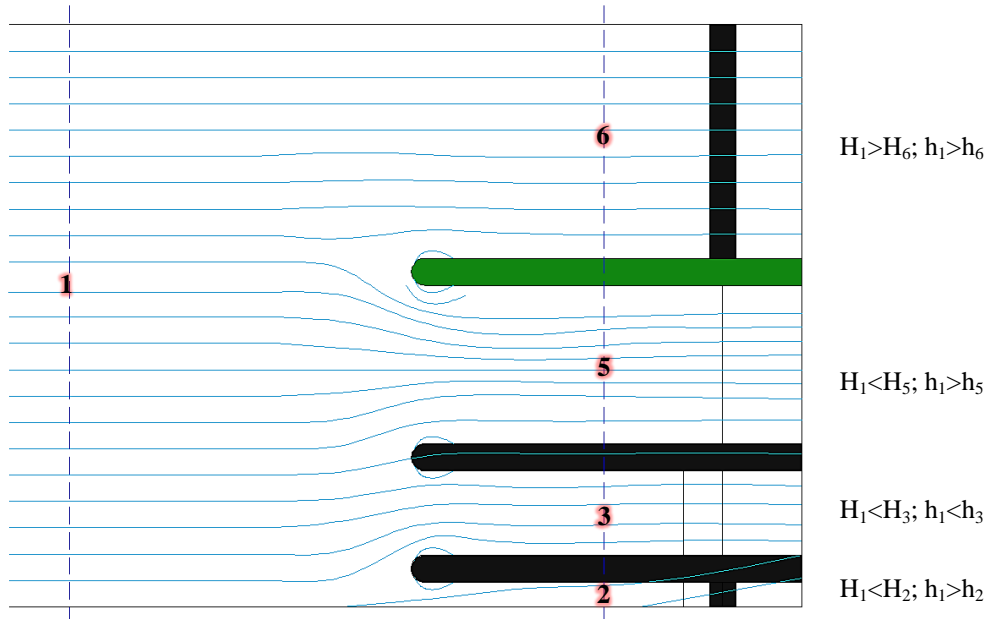


Figure A.11: Flow lines as observed for Ratio 1:2 Layout C

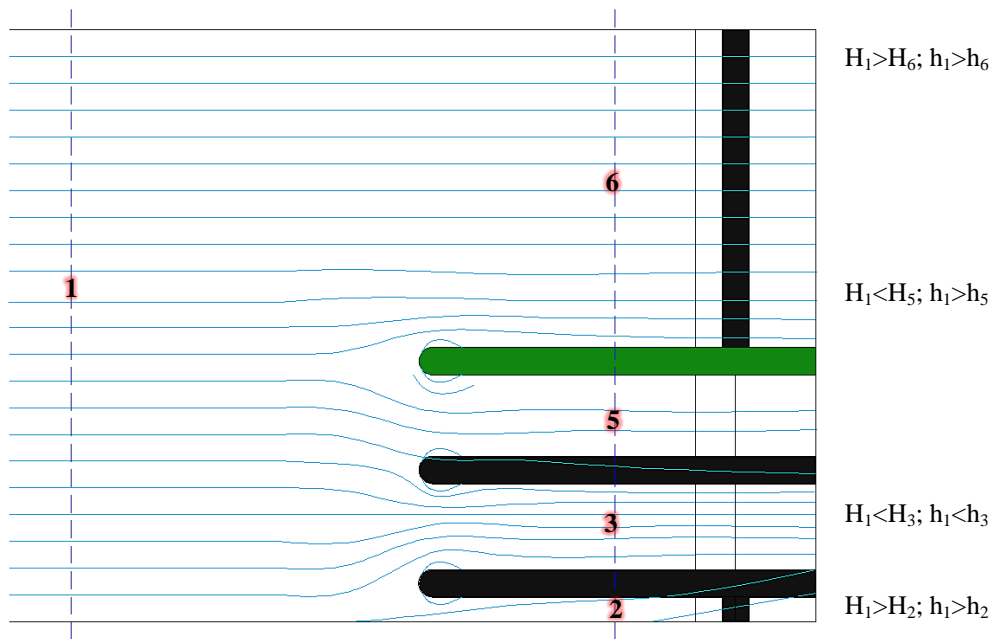
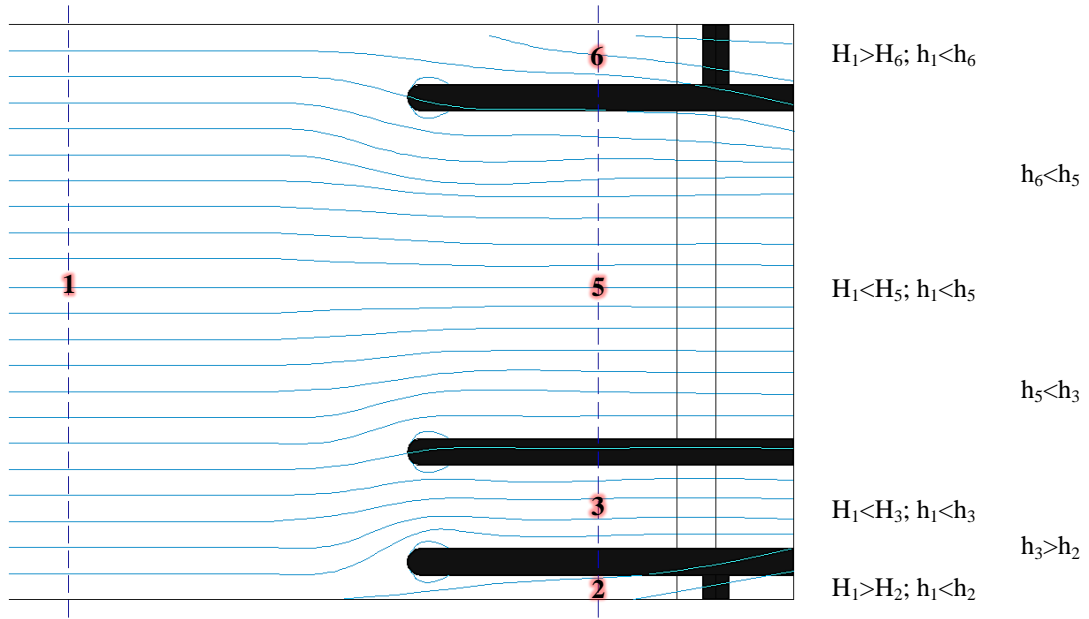
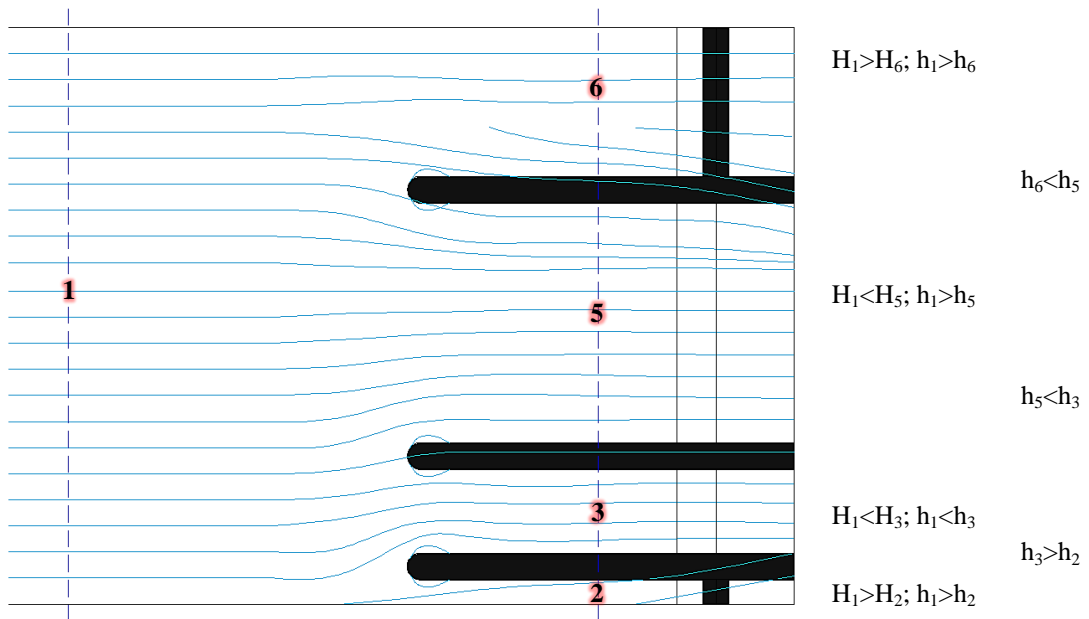


Figure A.12: Flow lines as observed for Ratio 1:1 Layout C

**FURTHER INVESTIGATION OF RESULTS FOR LAYOUT D**



**Figure A.13: Flow lines as observed for Ratio 1:4 Layout D**



**Figure A.14: Flow lines as observed for Ratio 1:3 Layout D**

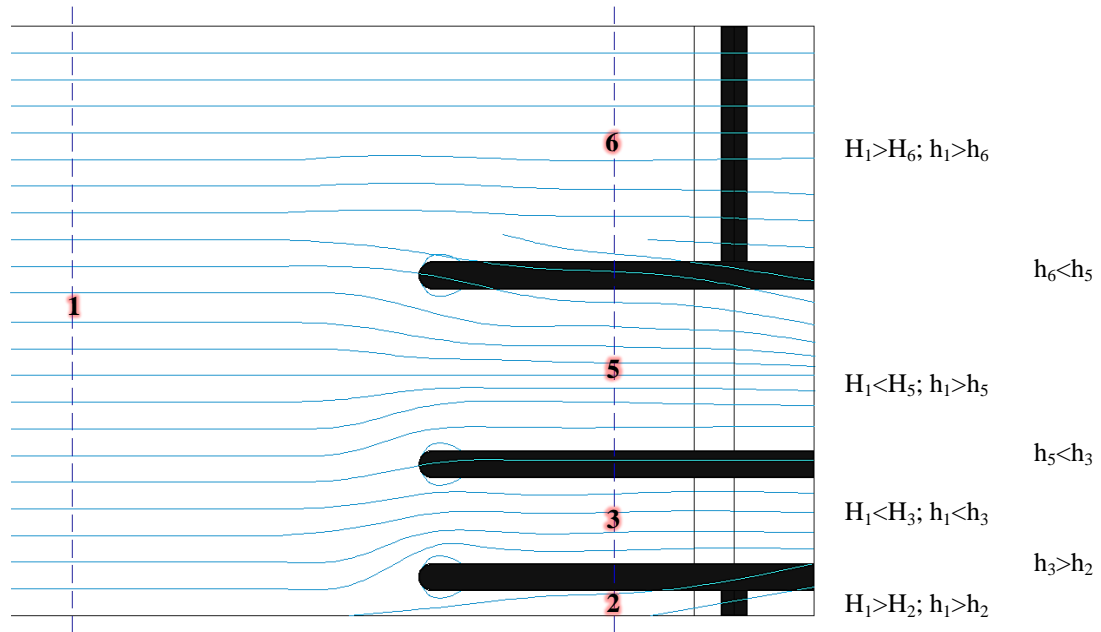


Figure A.15: Flow lines as observed for Ratio 1:2 Layout D

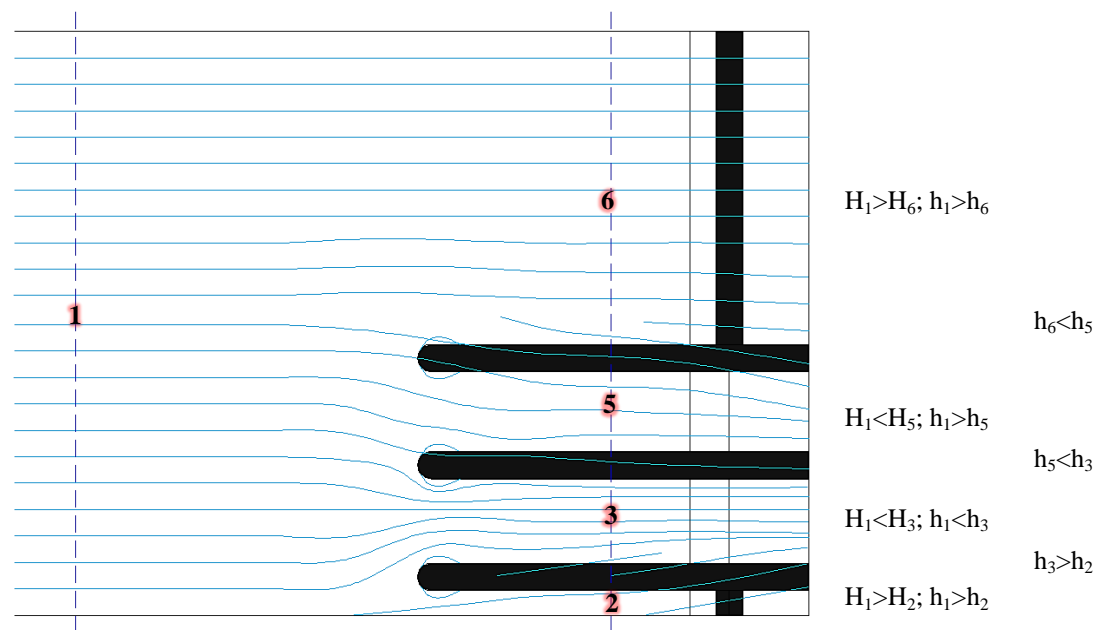
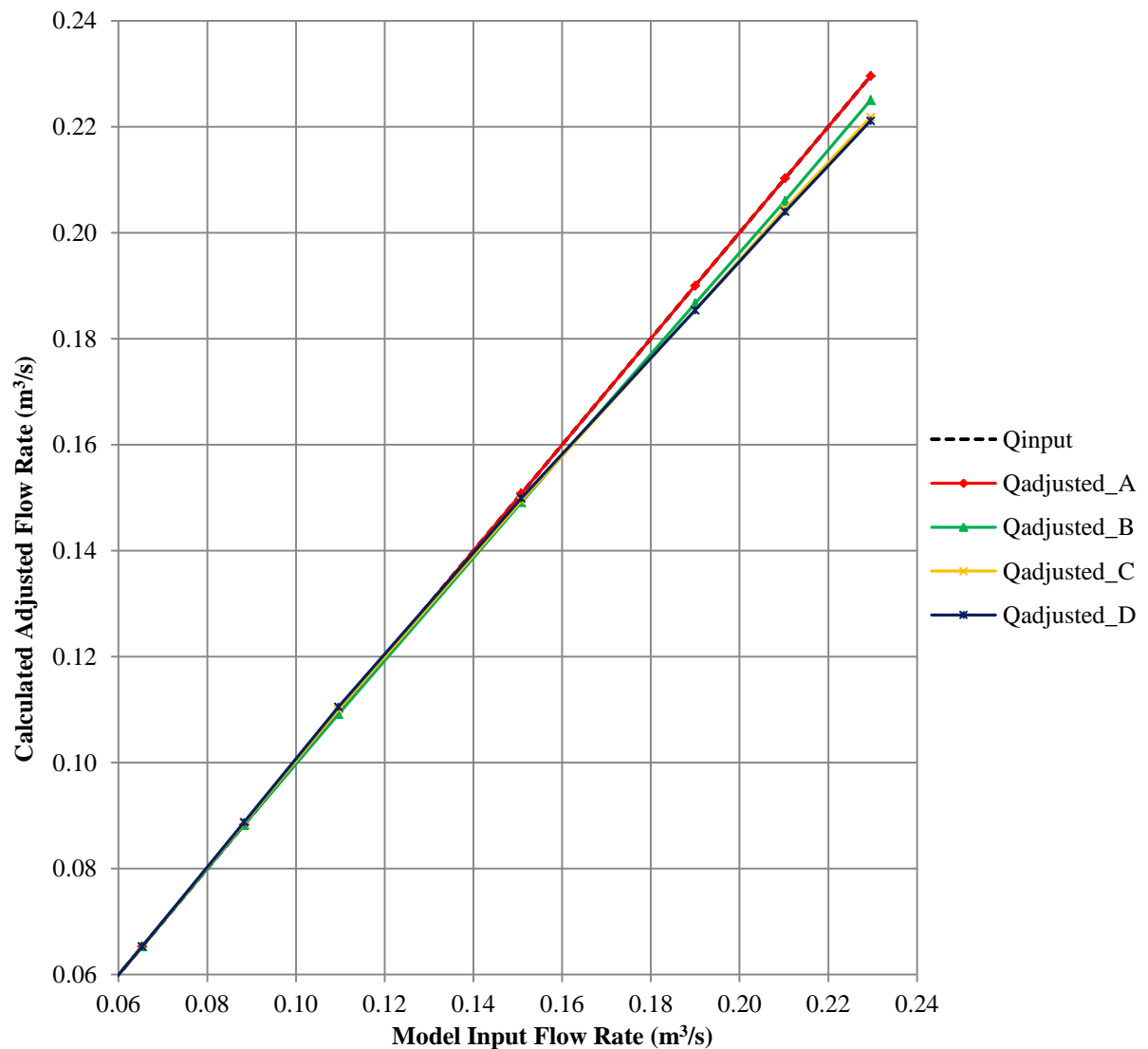


Figure A.16: Flow lines as observed for Ratio 1:1 Layout D

## APPENDIX B

The figures below are to be studied in reference to **Section 4.3.2**. The figures show the results of the physical model study corrected in terms of contraction resulting from the oversized divider and flank walls. For flow rates above the hydraulic capacity, the adjustment values were applied to the results for Layout A until no error was made. These adjustment values were then applied to Layouts B, C and D to illustrate a model with no contraction but with cross-flow.



**Figure B.1:** Graph of adjusted physical model results to account for contraction for Ratio 1:3



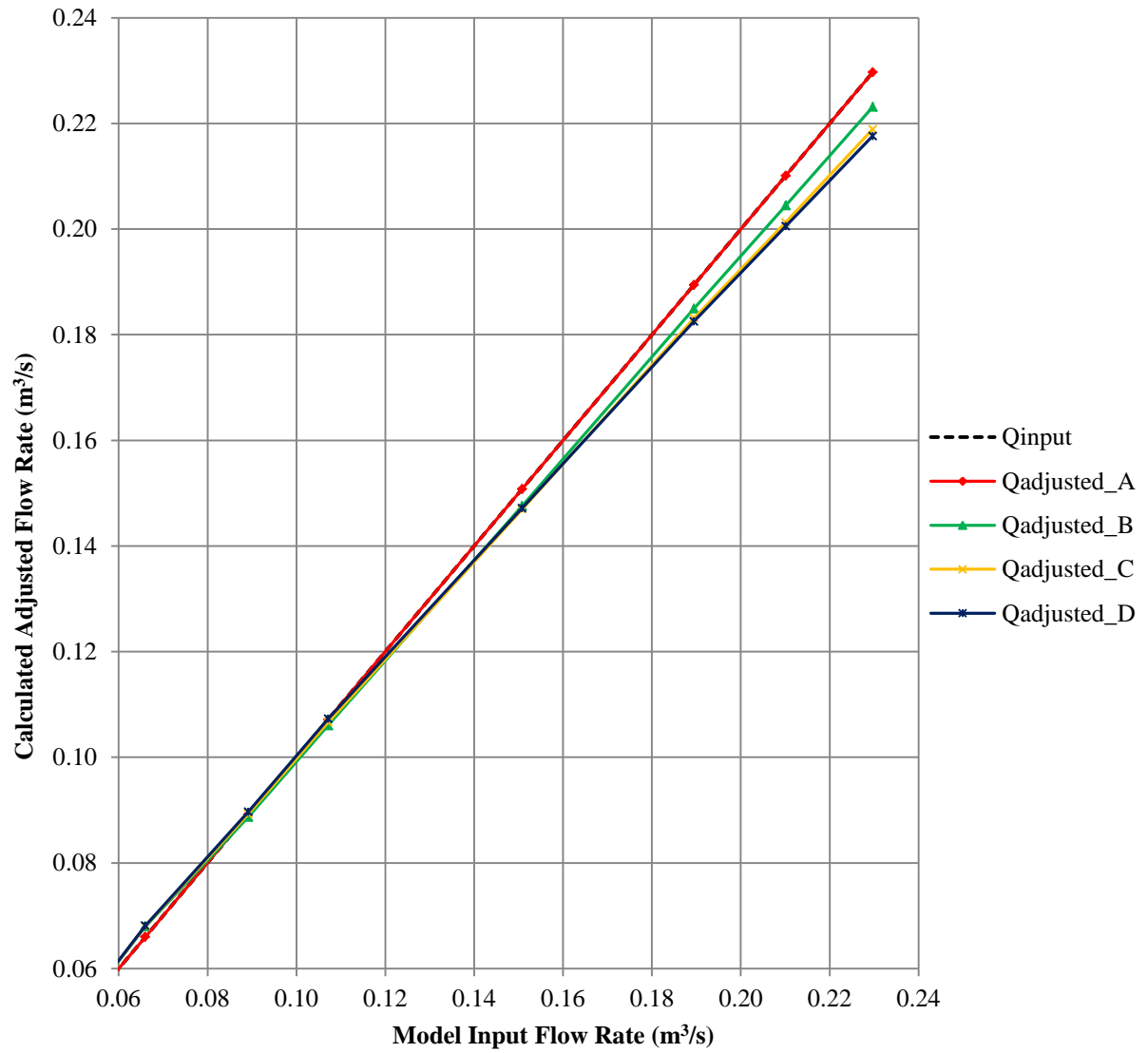


Figure B.2: Graph of adjusted physical model results to account for contraction for Ratio 1:2

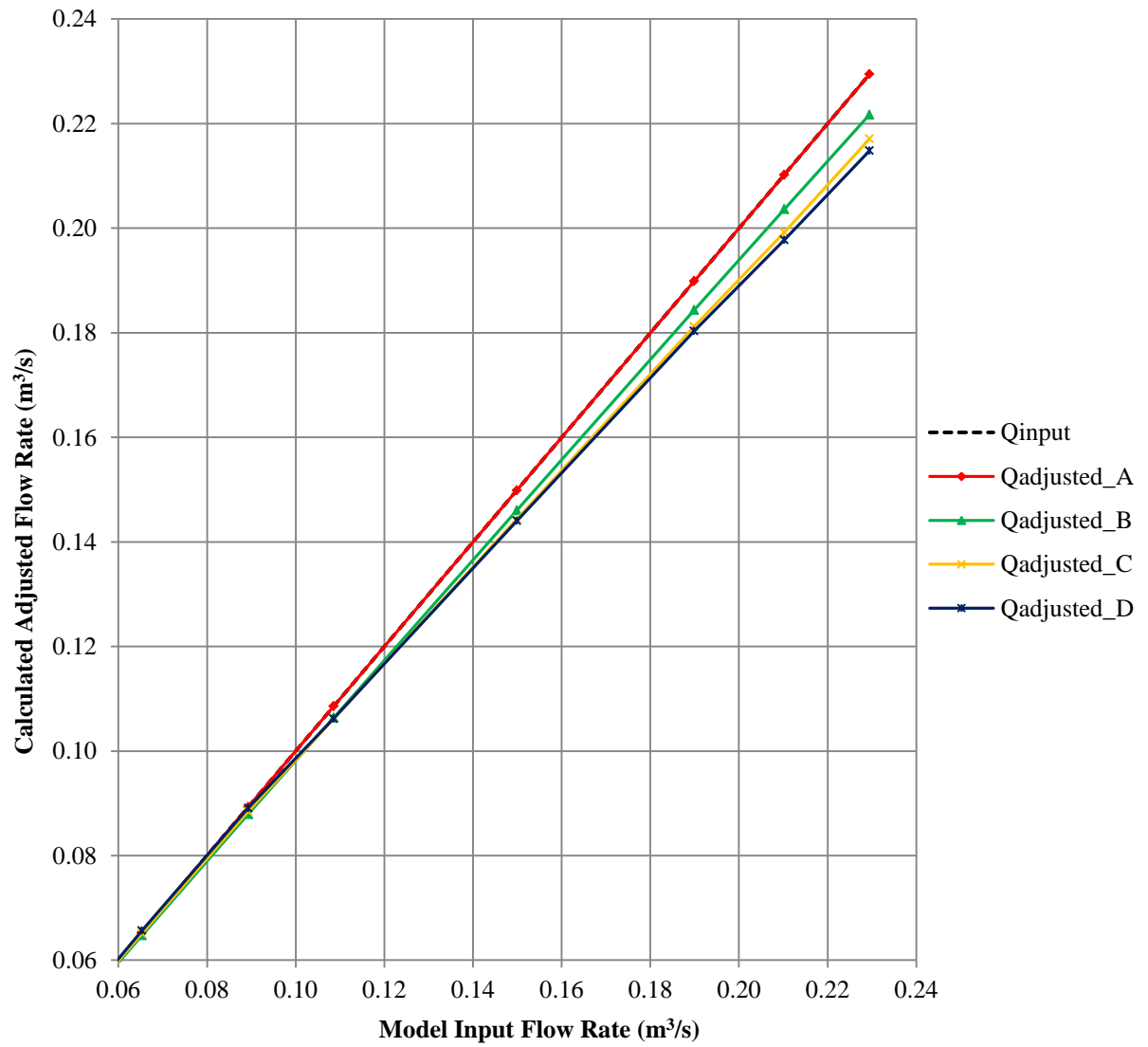


Figure B.3: Graph of adjusted physical model results to account for contraction for Ratio 1:1